Metal complexes of a new polyimido sulfur phosphanyl ligand

Dissertation
zur Erlangung des mathematisch–naturwissenschaftlichen Doktorgrades
„Doctor rerum naturalium“
der Georg–August–Universität Göttingen

Im Promotionsprogramm Catalysis for Sustainable Synthesis (CaSuS)
der Georg–August University School of Science (GAUSS)

vorgelegt von
Elena Carl
aus Höxter

Göttingen, 2014

Betreuungsausschuss

Professor Dr. Dietmar Stalke, Institut für Anorganische Chemie der Georg–August–Universität Göttingen

Professor Dr. Lutz Ackermann, Institut für Organische Chemie der Georg–August–Universität Göttingen

Dr. Regine Herbst–Irmer, Arbeitskreis Stalke, Institut für Anorganische Chemie der Georg–August–Universität Göttingen

Mitglieder der Prüfungskommission

Professor Dr. Dietmar Stalke, Institut für Anorganische Chemie der Georg–August–Universität Göttingen

Professor Dr. Lutz Ackermann, Institut für Organische Chemie der Georg–August–Universität Göttingen

Professor Dr. Konrad Koszinowski, Institut für Organische Chemie der Georg–August–Universität Göttingen

Dr. Inke Siewert, Institut für Anorganische Chemie der Georg–August–Universität Göttingen

Professor Dr. George M. Sheldrick, Institut für Anorganische Chemie der Georg–August–Universität Göttingen

Professor Dr. Guido Clever, Institut für Anorganische Chemie der Georg–August–Universität Göttingen

Tag der mündlichen Prüfung: 27. Juni 2014

Table of contents

List of abbreviations

Å	Ångstrom
ac	alternating current
av.	average
BASF	Batch Scale Factor
CSD	Cambridge Structural Database
CCDC	Cambridge Crystallographic Data Base
dc	direct current
DCM	Dichloromethane
Eq.	Equation
eq.	equivalents
esd	estimated standard deviation
et al.	*et alii*, and others
Et_2O	Diethylether
dipp	Di*iso*propylphenyl
d	distance / doublet
DFT	Density Functional Theory
EI	Electron Ionisation
h	hour
HOMO	Highest Occupied Molecular Orbital
HMBC	Heteronuclear Multiple Bond Correlation
HSAB	Hard and Soft Acids and Bases
IPr	1,3–Bis(2,6–Di*iso*propylphenyl)imidazol–2–yliden
*i*Pr	*iso*–Propyl
LUMO	Lowest Unoccupied Molecular Orbital
M	Molar
Me	Methyl
Me_2cAAC:	$:C(CH_2)(CMe_2)_2N–2,6–iPr_2C_6H_3$
Mes	Mesityl (2,4,6–trimethylphenyl)
$(Mes)_2$DAP	2,4–dimethyl–*N,N*'–bis(mesityl)–1,5–diazapentadienyl
MHz	Megahertz
MS	Mass Spectrometry
*n*BuLi	*n*–Butyllithium

nacnac	1,3–Diketimines
naph	naphtyl
NBO	Natural Bond Orbital
NRT	Natural Resonance Theory
NHC	N–heterocyclic carbene
NMR	Nuclear Magnetic Resonance
Ph	Phenyl
PNN	*N*–(dimethylaminoethyl)–2–diphenylphosphino–aniline)
ppm	parts per million
rt	room temperature
s	singlet
SIM	Single Ion Magnet
SMM	Single Molecular Magnet
sof	site occupation factor
SQUID	Superconducting Quantum Interference Device
*t*Bu	*tertiary* Butyl
*t*butyl	*tertiary* Butyl
THF	Tetrahydrofuran
TMEDA	*N,N,N',N'*–Tetramethylethylenediamine
TMS	Trimethylsilyl
tol	toluene
z	charge

1. Introduction

Focusing on homogenous catalysis every development of a new and efficient catalyst starts with the design of a ligand. The requirements are high since small changes in the periphery of a ligand can dramatically change its chemical properties with the consequence of altering yields, selectivities and turn over numbers.[1] Some relevant attributes for ligands are the ability to coordinate and stabilise metal ions in higher and lower oxidation states but to leave enough space at the active site for a coordination of the substrate. The ligand should also provide coordination sites for hard and soft metal centres[2] targeting for heterobimetallic complexes to accommodate the catalyst and the co–catalyst in close proximity. This means the classical chelating ligand has to be modified by introducing a *Lewis* basic ligand backbone. The resulting Janus head type ligand paves the way for hemilabile systems.[3]

The term hemilability refers to a chelating ligands' ability to partially decoordinate from a metal centre, opening vacant sites for further reactivity while remaining attached to the metal (Scheme 1–1, *left*).[4] Hence, a reversible association /dissociation of one labile function during the catalytic cycle might be feasible (hemilability concept).[4i,5] *Rauchfuss* introduced the concept of hemilable ligands in 1979 and used this term originally for phosphane–amine and phosphane–ether ligands that "*would bind well enough to permit isolation but would readily dissociate the hard end component, thus generating a vacant site for substrate binding*".[4j]

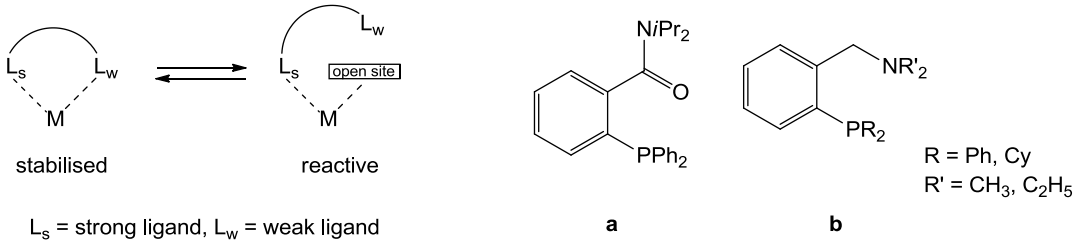

Scheme 1–1: *left*) Dynamic "on/off"–effect of hemilabile ligands. *right*) Two examples of hemilabile *P,O*– and *P,N*–ligands that are applied in catalytic transformations.

Two examples for hemilabile ligands are shown in Scheme 1–1 (*right*). Silver(I) complexes of the ligand **a** were demonstrated to be highly effective in promoting the first examples of homogeneous silver catalysed azide–alkyne cycloaddition

reactions.[6] The *P,N*–type ligand **b** was developed by *Guram* and coworkers for *Suzuki–Miyaura* cross–coupling of aryl chlorides.[7]

Janus head ligands are a type of hemilabile ligands which have at least two different coordination sites with different *Pearson*[2] hardness in opposite directions. Hence, diverse metal ions can be coordinated and thus, two active sites in one molecule can be generated. Some examples are depicted in Figure 1.1. The compound **a** is the iron complex of the *N,P,N*–ligand bis(2–benzothiazolyl)phosphanide. The dual *N,N*–coordinated iron complex is accessible by addition of $[Fe\{N(SiMe_3)\}_2]$ to the pure ligand in Et_2O.[8] The *P* and/or *S* face of the ligand are remaining vacant for a possible coordination of a second metal cation.

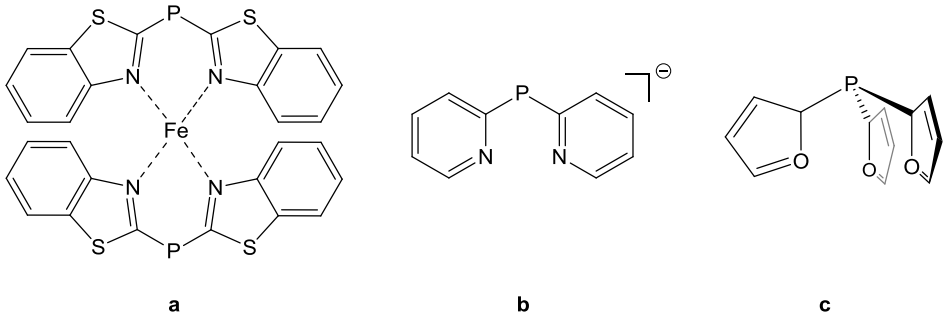

a **b** **c**

Figure 1.1: Three examples of Janus head ligands: **a**) [*N,N*–Bis{bis(2–benzothiazolyl)phosphanide}iron], **b**) di(pyridyl)phosphanide, **c**) tris(2–furyl)phosphine.

The di(pyridyl)phosphanide ligand **b** is also a *N,P,N*–ligand. One face of the Janus head is provided by the divalent P(III) centre while the two ring nitrogen atoms in the heteroaromatic substituents represent the second face.[3a] As an example for ambidentate tripodal ligand systems with a phosphorus as bridgehead atom, the ligand **c** is displayed in (Figure 1.1).[9] The C_3 symmetric tripodal and tridentate ligand is reminiscent of the poly(pyrazolyl)borate ligands, in which the phosphorus atom is replaced by a boron atom (Figure 1.2, **a**).

Poly(pyrazolyl)borate ligands were introduced by *Trofimenko* in 1966 and are another famous example for a successful ligand design.[10] With a *N,N*–chelating claw and the third pyrazolyl ring functioning as the sting, *Trofimenko* described this new class of ligands as scorpionate ligands.[11] Since then, the design has been copied several times. Over 150 different scorpionate ligands have been synthesised until now and they find application in catalysis, bioinorganic model systems, metal extraction and biomedicine.[12]

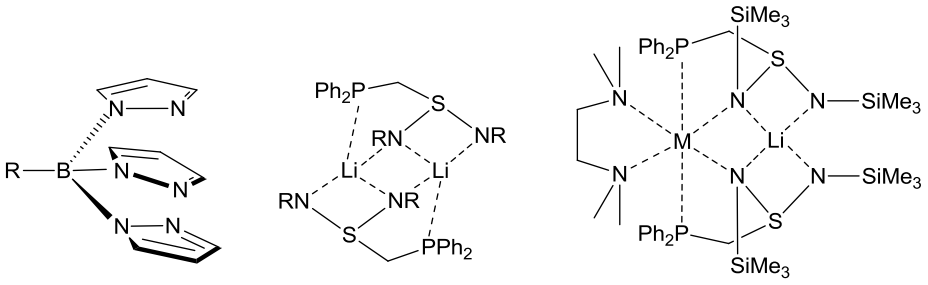

Figure 1.2: **a**) "Classical" scorpionate ligands: tris(pyrazolyl)borates. **b**, **c**) Metal and heterobimetallic complexes of novel scorpionate–like Janus head phosphanyl diimidosulfinate ligands.

In 2011 *Meinholz* succeeded in combining the features of scorpionate and Janus head ligands. By linking sulfur diimides and lithium dialkyl/phenyl phosphanyl–methylides, tridentate and hemilabile phosphanyl diimidosulfinate ligands were synthesised that contain hard nitrogen and soft phosphorus donor sites (Figure 1.2, **b**).[13] The SN_2 moiety chelates the metal cation while the phosphorus–metal interactions are only weak. Hence, the phosphorus sting can close the coordination sphere of the metal ion or swing open to interact with a second metal. This can be observed if the phosphanyl diimidosulfinate ligands are reacted with metal bis(trimethylsilyl)amides. In the obtained alkali mixed metal complexes (Figure 1.2, **c**) the phosphorus coordinates to the softer alkali metal potassium or rubidium.[14]

Over the last years our work group paid much attention to the chemistry of sulfur imides. Sulfur imides are obtained by the isoelectronical replacement of the oxygen atom [O] in sulfur oxides by $[NR]^{2-}$ imido groups. Some examples are given in Table 1.1. The preparation and characterisation of imido analogues of common oxo–anions such as $[CO_3]^{2-}$, $[SO_3]^{2-}$, and $[PO_4]^{3-}$ has been an active area of main–group chemistry research at the beginning of the 21st century.[15]

Table 1.1: Selected examples of polyimido anions with the corresponding oxo–anions.

Polyimido anions of p–block elements[16]	Related oxo–anions
$[C(NR)_3]^{2-}$	carbonate: $[CO_3]^{2-}$
$[Si(NR)_4]^{4-}$	orthosilicate: $[SiO_4]^{4-}$
$[As(NR)_3]^{3-}$	arsenite: $[AsO_3]^{3-}$
$[P(NR)_4]^{3-}$	phosphate: $[PO_4]^{3-}$
$[Se(NR)_3]^{2-}$	selenite: $[SeO_3]^{2-}$

The replacement of one or more oxo ligands by an $[NR]^{2-}$ group generates a new class of p–block polyanions with significantly different chemical and physical properties than those of their parent oxo–anions. The dimeric dilithium trisimidocarbonate complex (**a**)[17] and an imidophosphate trianion (**b**)[16a] are analoga of $[CO_3]^{2-}$ and $[PO_4]^{3-}$ and are illustrated exemplary in Figure 1.3. The organic substituent "R" is often an alkyl or aryl residue that is responsible for the diverse properties of isoelectronic analogues. It provides steric bulk and hinders the molecules from oligomerisation. For example, the lithium sulfate has an infinite solid–state structure while the $[S(NR)_4]^{2-}$ analogue $[(thf)_4Li_2\{(NtBu)_4S\}]$ is present in discrete molecules,[18] Telluriumdioxide $(TeO_2)_\infty$ is a three–dimensional polymer while the tellurium diimide *t*BuNTe(μ–N*t*Bu)$_2$TeN*t*Bu is dimeric (Figure 1.3, **c**), CO_2 and $C(NR)_2$ are both multiply bonded monomers, but carbon dioxide is a gas whereas *N,N'*–dialkyl carbodiimides are liquids.[19]

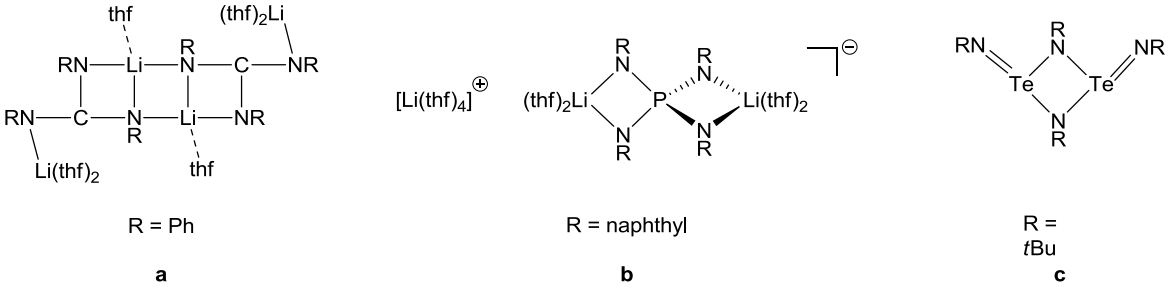

Figure 1.3: **a**) dimeric dilithium trisimidocarbonate, **b**) $[(thf)_4Li][(thf)_4Li_2\{P(Nnaph)_4\}]$ as $[PO_4]^{3-}$ analogue **c**) dimeric tellur diimide.

Lewis diagrams of sulfur imides and the corresponding sulfur oxides, that are relevant for this work, are depicted in Scheme 1–2.[20] Here, the formal charges are shown since theoretical investigations from the mid–1980s indicate that d orbitals cannot participate in the sulfur–nitrogen bonds due to large energy differences between the sulfur p and d orbitals.[21] Recently, the factum was reinforced by an experimental and theoretical charge density analysis of K_2SO_4 published by *Gatti*, *Stalke* and *Iversen* in 2012. Therein, they characterised *"the S–O interactions as highly polarised, covalent bonds with the "single bond" description significantly prevailing over the "double bond" picture*" what clearly rules out the hypervalent description of the sulfur atom.[22]

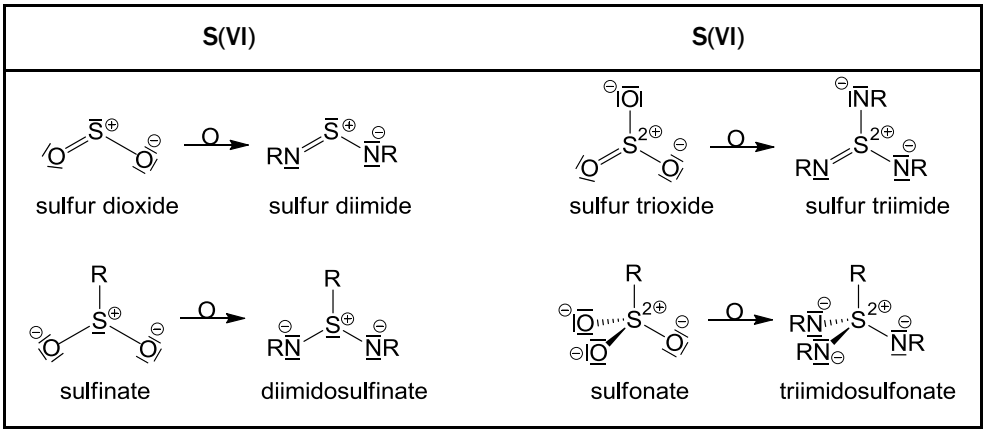

Scheme 1–2: *Lewis* diagrams of selected sulfur imides. Here, the charges of the atoms are written to clarify the bonding situation. In the following, *Lewis* diagrams are depicted without charges for clarity.

Sulfur nitrogen compounds attracted interest in the 1970s with the discovery of the unusual properties of the conducting polymer $(SN)_x$.[23] It was already in 1956 when *Goehring* and *Weiss* synthesised the first sulfur diimide $S(NR)_2$,[24] followed by the Göttinger researchers *Glemser* and *Wegener*. They synthesised the first sulfur triimide $S(NSiMe_3)_3$, starting from $[Li\{N(SiMe_3)_2\}]$ and NSF_3 14 years later (Scheme 1–3, eq. I.).[25] *Lidy* and *Sundermeyer* followed in 1974, publishing the successful synthesis of $S(NSiMe_3)_3$ from OSF_4 and $[Na\{N(NSiMe_3)_2\}]$ (Scheme 1–3, eq. II.).[26]

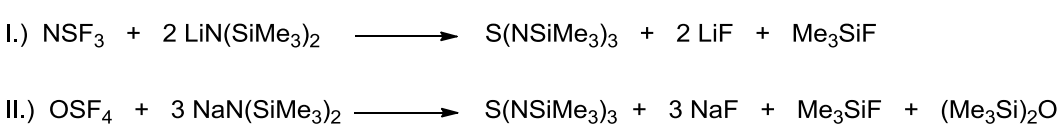

Scheme 1–3: The first reported synthetic routes to $S(NSiMe_3)_3$.

The preparation of $S(NSiMe_3)_3$ marks a milestone in main group chemistry since it was shown for the first time that a sterical demanding group stabilises low coordination numbers.[27] However, for several decades the sulfur triimides have never got the same attention as the sulfur diimides, probably due to the limited synthetic access. Until the end of the last century the only possibilities to obtain $S(NR)_3$ compounds were the quite hazardous reactions starting from NSF_3 or OSF_4 with low yields. Only in 1998 *Fleischer* and *Stalke* reported "*a new route to sulfur triimides*". The new pathway involves the oxidation of the intermediate species $[Li_4\{(NtBu)_3S\}_2]$ with bromine (Scheme 1–4, eq. II.).[28]

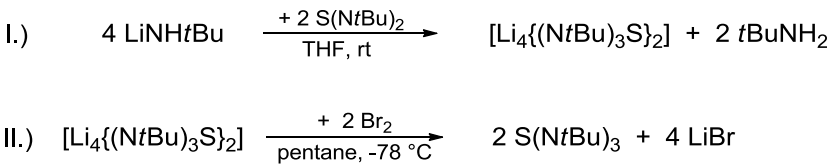

Scheme 1–4: Syntheses of $S(NtBu)_3$: I.) The reaction of $S(NtBu)_2$ with lithiated LiNH*t*Bu gives the intermediate $[Li_4\{(NtBu)_3S\}_2]$. II.) Reduction of $[Li_4\{(NtBu)_3S\}_2]$ with bromine leads to $S(NtBu)_3$.

The intermediate $[Li_4\{(NtBu)_3S\}_2]$ is formed by the reaction of the sulfur diimide $S(NtBu)_2$ with lithiated *t*butylamine. The reactions yields a white powder which turns immediately blue by contact with the slightest amount of an oxidant, indicating the existence of a radical intermediate $[Li_3\{(NtBu)_3S\}_2]^{\cdot}$ confirmed by ESR spectroscopic investigations.[28] This new synthetic pathway opened the door to the chemistry of $S(NtBu)_3$ and a series of metal complexes with versatile coordination motifs were obtained.[18,29]

With the easier synthetic access to $S(NtBu)_3$ and the increased application in synthesis, the interest in the nature of the S–N bonds rose. The S–N bond distances in the planar $S(NtBu)_3$ are with approximately 151.2(2) pm close to the values of S–N double bonds (152 pm). The characterisation as S–N double bonds would imply valence expansion and d orbital participation at the central sulfur atom what can be excluded, as mentioned previously. This was also substantiated by an experimental and theoretical charge density study on $S(NtBu)_3$ done by *Leusser, Engels* and *Stalke* in 2004.[30] They showed that the bonding can be best characterised as a 4–center–6–electron bonding of sp^2 hybridised sulfur and nitrogen atoms with a distinct polarised π–system above and below the SN_3 plane (Figure 1.4). The leading, triply degenerated resonance structure from NBO/NRT analysis, which covers 75% of the distributed electronic structure, is depicted in Figure 1.5. Hence, the short S–N bond lengths are not a result of hypervalency or d orbital participation but of polarised S–N bonds.

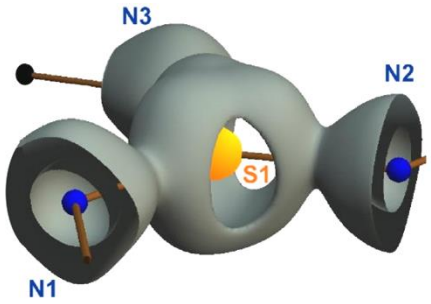

Figure 1.4: Reactive surface around the sulfur atom in $S(NtBu)_3$.

These investigations revealed precious information for the synthetic chemist. The reactive surface of $S(NtBu)_3$ illustrates clearly that small areas of charge depletion are between the bisections of the N–S–N angles. Hence, a nucleophile attracted by

the positively charged central sulfur atom has to approach the positive centre across the bulky N*t*Bu groups. Consequently, the use of sterically undemanding carbanions in the syntheses might be more promising for addition of organometallic reagents to the central sulfur atom of S(N*t*Bu)$_3$.

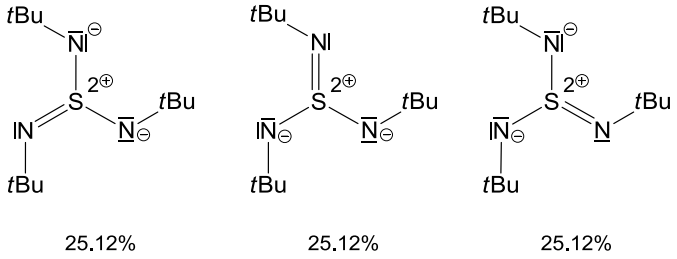

Figure 1.5: Resonance structures of S(N*t*Bu)$_3$ calculated by NBO/NRT analysis.

An overview of the synthesised metal complexes with S(N*t*Bu)$_3$ as a scaffold is shown in Scheme 1–5. A generally approved route is to use organometallic reagents and *via* nucleophilic addition, aromatic heterocylces or alkyls can be connected to the central sulfur atom (reactions **a** and **b**, Scheme 1–5).[29b]

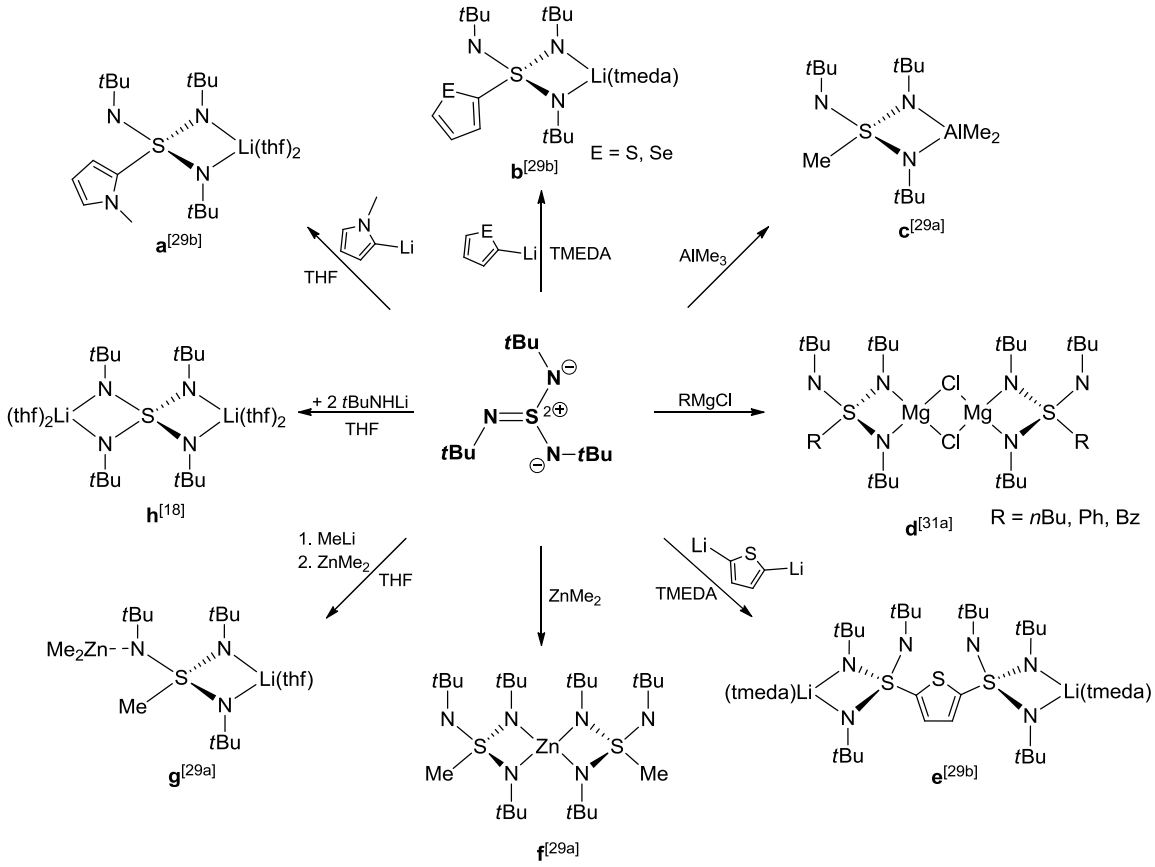

Scheme 1–5: Overview of different metal complexes obtained from sulfur triimides.

In 2010*, Schulz* reported the addition of bulky carbanions to the sulfur triimide despite the assumption that sterically undemanding nucleophiles are favoured (reaction **d**, Scheme 1–5). His approach was to use Grignard reagents in the synthesis, presuming that, according to *Pearson*[2], the soft–soft interactions between the organomagnesium reagent and the sulfur atom would facilitate the addition of sterically more demanding residues in comparison to the less favourable interactions between lithium organic reagents and the sulfur atom.[31]

Reaction **c** and **f** exhibit that the methylation of $S(NtBu)_3$ is also possible by the addition of more covalent bonded organometallic reagents like $ZnMe_2$ and $AlMe_3$. The metal cations are *N,N*–chelated by the imido groups while the methyl groups are added to the electrophilic sulfur atom.

Reaction **g** demonstrates that the pending imido side arm can be employed in the metal coordination as well.[29a] Although the coordination of the lithium cation by the two other nitrogen atoms already caused an additional charge depletion at the sulfur atom, the non–chelating nitrogen atom is still *Lewis* basic enough for a dative binding to a second metal centre.

The $[SO_4]^{2-}$ analoga $[(thf)_4Li_2\{(NtBu)_4\}S]$[18] (reaction **h**) is another example for the ability of sulfur imides to coordinate more than one metal cation. All the presented complexes emphasise that sulfur imides are promising scaffolds for versatile metal and bimetallic complexes.

The functionality of the polyimido sulfur compounds was enhanced by connecting a phosphorus containing side arm to the sulfur atom. *Deuerlein* reported in 2007 that a phosphorus–functionalisation of sulfur diimides is possible by using lithiated phosphanes in the synthesis (Scheme 1–6).[32]

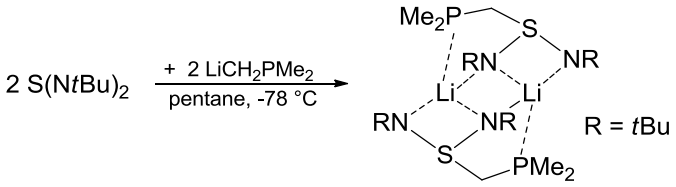

Scheme 1–6: Preparation of $[Li\{Me_2PCH_2S(NtBu)_2\}]_2$.

Based on his results, *Meinholz* continued the investigation in this field and synthesised successfully a series of metal complexes of diimidosulfinates with a phosphorus side arm, as mentioned previously (Figure 1.2, **b** and **c**).[13a,14]

Consequently, the question occurred if the sulfur triimides can be functionalised in the same way and if a *S*–phosphanyl–triimidosulfonate ligand would be a promising starting material for the synthesis of novel metal and bimetallic complexes.

2. Scope

As exemplified in the introduction, it is possible to add various organic residues to the central sulfur atom of the sulfur triimide *via* reaction with organometallic reagents. During my diploma thesis, I have already been successful in enhancing the functionality of $S(NtBu)_3$ by linking a phosphorus side arm to the central sulfur atom.[33] The result was the novel, potentially hemilabile Janus head ligand $[(tmeda)Li\{(NtBu)_3SCH_2PPh_2\}]$ (**1**, Figure 2.1). This ligand seems to be an excellent starting material for the generation of new metal or heterobimetallic complexes since it offers the possibilities to *N,N*–chelate a metal cation and to coordinate a second metal ion by addressing the *P*– or *N*– donor atoms of the pendant side arms. Further coordination motifs for **1** are conceivable, ranging from *P*–coordination, *P,N*–chelation, *P,P*– and *P,N*–bridging of two metal centres what is especially helpful for heterobimetallic complexes because of the different *Lewis* acidity and *Pearson* hardness. The aim of this work was to develop a route for the synthesis of diverse metal complexes starting from the lithiated ligand **1** or the amine ligand $Ph_2PCH_2S(NtBu)_2NHtBu$ (**13**). In this context it had to be investigated which of the conceivable coordination motifs are feasible and if *S*–phosphanyl–triimidosulfonates are suitable ligands for the synthesis of heterobimetallic complexes.

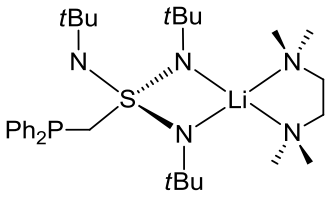

1

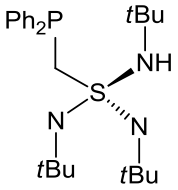

13

Figure 2.1: $[(tmeda)Li\{(NtBu)_3SCH_2PPh_2\}]$ (**1**) and $Ph_2PCH_2S(NtBu)_2NHtBu$ (**13**).

The first priority was to expand the field of metal ions that can be coordinated by the phosphorus functionalised sulfur triimide. Therefore, it was tried to exchange the lithium cation for other metals by transmetalation reactions. Transition and main group metal cations in low oxidation states were applied in the synthesis to test if the ligand can stabilise the low oxidation states since sulfur imides are known to be redox active.[32c,34] The obtained metal complexes were then compared with similar

systems to investigate structural differences and to tell if diverse metal cations have an influence on the properties of the ligand system, like coordination modes, bond lengths and angles.

Furthermore, it had to be tested if the phosphorus atom can be employed in the metal coordination as well in order to obtain heterobimetallic complexes. Therefore, transformations of $Ph_2PCH_2S(NtBu)_2NHtBu$ (**13**) with softer metal ions including the second row transition metals ruthenium(II) and rhodium(II) were investigated. To discuss and compare bond lengths and angles in detail, the analytical method of choice was X–ray crystallography.

3. Results and discussion

3.1. The lithiated ligand [(tmeda)Li{(N*t*Bu)$_3$SCH$_2$PPh$_2$}] (1)

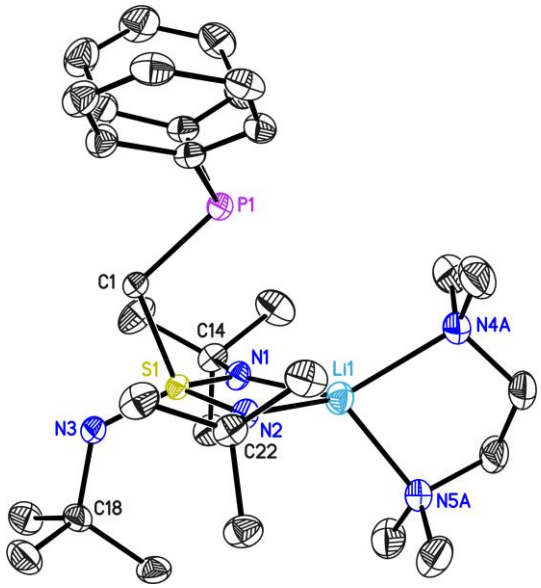

Figure 3.1: Solid state structure of **1**. The anisotropic displacement parameters are shown at the 50% probability level. Hydrogen atoms are omitted for clarity.

The lithiated ligand **1** has already been synthesised during my diploma thesis[33] but is here discussed to represent the complete group of *S*–phosphanyl–triimidosulfonates and because its attributes are important for the following discussions. Further, a detailed comparison with the S(IV) analogue [(tmeda)–Li{(NSiMe$_3$)$_2$SCH$_2$PPh$_2$}] is now possible since it was published by *Meinholz* in 2011.[13a] The linkage between the *N,N',N''*–tris(*tert*–butyl)sulfur triimide S(N*t*Bu)$_3$ and methyldiphenylphosphine Ph$_2$PMe is achieved by an equimolar reaction of [(tmeda)LiCH$_2$PPh$_2$] and S(N*t*Bu)$_3$ in a pentane/THF (2:1) solution at dry ice temperature to give **1** (Scheme 3–1).

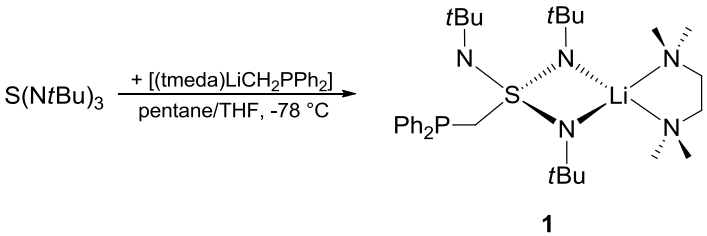

1

Scheme 3–1: Synthesis of [(tmeda)Li{(N*t*Bu)$_3$SCH$_2$PPh$_2$}] (**1**).

The crystal structure of **1** is shown in Figure 3.1. The lithiated complex crystallises in the orthorhombic space group $P2_12_12_1$ with one molecule in the asymmetric unit. In

the monomeric complex the lithium cation is chelated in a distorted tetrahedral manner by only two nitrogen atoms of the three present N*t*Bu groups and by two nitrogen atoms of the chelating TMEDA donor base to saturate the coordination sphere of the lithium cation.

Table 3.1: Selected bond lengths [pm] and angles [°] of **1**.

S1–N1	158.02(13)	P1–C1	185.13(16)
S1–N2	157.06(14)	S1–C1	181.82(16)
S1–N3	153.88(14)	S1–C1–P1	111.76(8)
Li1–N1	197.70(30)	Li1–N1–C14	141.51(13)
Li1–N2	200.50(30)	Li1–N2–C22	136.97(14)
N1–C14	148.19(14)	N1–S1–N2	97.48(7)
N2–C22	148.36(14)	Li1–N1–S1–N2	3.88(11)

A tripodal coordination of the metal ion is prevented due to steric crowding and the pending N*t*Bu group is turned to the vacant site of the complex.[35] The sulfur atom in the oxidation state (VI) is the presumably electronically depleted centre of the ligand. It is also coordinated distorted tetrahedrally by the three nitrogen atoms and the phosphorus side arm. The S–N bond lengths of the nitrogen atoms N1 and N2 (158.02(13) and 157.06(14) pm) are in the middle of the predicted values for a double (152 pm) and a single (170 pm) bond that are reported in the literature (Table 3.1).[36] However, as described in the introduction, it is clear that hypervalency is not an option for sulfur imido compounds and bond shortening is due to electrostatic reinforcement.[30] The coordination of N1 and N2 to the lithium cation causes the elongation of the S–N bonds relatively to the bond lengths in $S(NtBu)_3$ because the electron density of the nitrogen atoms is shifted to the lithium cation. Consequently, the S1–N3 bond has to be the shortest (153.88(14) pm) due to the enhanced electrostatic interaction between the negatively charged pendant nitrogen atom and the positively charged sulfur atom.

In contrast to the S–N bonds, the S1–C1 bond is a rigid system with a typical distance of 181.82(16) pm. The phosphorus atom is pointing to the lithium cation but the distance of 371.8(7) pm is too long for a Li–P–coordination since the mean value of all published Li–P bond lengths in the CSD is around 258 pm.[37] The central

LiN_2S ring is almost perfectly planar (torsion angle: 3.88(11)°) with the phosphorus atom residing above this plane.

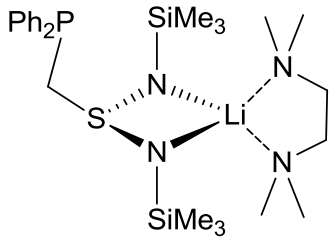

1-S(IV)

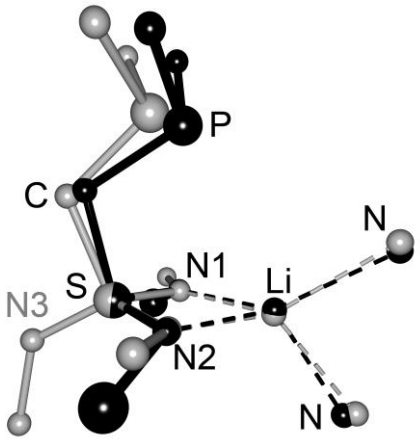

Figure 3.2: *left) Lewis* diagram of **1–S(IV)**. *right)* Superposition plot of **1** (grey) and **1–S(IV)** (black). The atoms S, N2 and N1 are fitted onto each other with a deviation of 6.7 pm. TMEDA is just indicated by the donating nitrogen atoms. The *t*butyl/$SiMe_3$ groups and phenyl rings are also just indicated by the $C_{quart.}$/Si and C_{ipso} atoms.

The complex $[(tmeda)Li\{(NSiMe_3)_2SCH_2PPh_2\}]$[13a] **1–S(IV)** is the sulfur(IV) diimide analogue of **1** in which the third imido side arm is substituted by the free electron pair of the sulfur (IV) atom. A *Lewis* diagram of **1–S(IV)** and a superposition plot of the core of both complexes are depicted in (Figure 3.2). The bond angles and distances of both compounds differ only slightly. The S1–N1/2 distances in **1** are shorter in comparison to **1–S(IV)** (165.20(9) and 171.84(10) pm) because of the higher oxidation state of the sulfur atom.[36] The P1–C1–S1 angle in **1–S(IV)** is a little more acute (108.79(9)°) than in **1** (111.76(8)°), indicating the inclination of the phosphorus atom to the lithium cation resulting in a Li–P distance of 323 pm.

Scheme 3-2: Illustration of the deviation *d*.

Space–filling models of **1** and **1–S(IV)** (Figure 3.3) demonstrate how the *t*butyl groups in **1** hinder the phosphorus atom from coordinating to the lithium cation. Measuring the distances *d* perpendicularly from the virtual N1S1N2 plane to the quaternary carbon or silicon atom, reveals that the $SiMe_3$ groups in **1–S(IV)** deviate significantly from the N1S1N2 plane (*d* = –71.3 and –53.5 pm) while the *t*butyl groups stay more or less in the plane (*d* = +12.5 and –10.1 pm) (Scheme 3-2). Hence, the *t*butyl groups hamper the phosphorus atom from approaching the lithium cation. The reasons for the structural differences are the following:

First, the non–chelating imido side arm in **1** is turned beneath the N1S1N2 plane, impeding the other two *t*butyl groups from bending beneath the N1S1N2 plane by sterical repulsion. Hence, the metal cation coordinating N*t*Bu groups are fixed in the LiN_2S plane, shielding the lithium cation from the phosphorus atom. In contrast, the $SiMe_3$ groups in **1–S(IV)** are not only located beneath the LiN_2S plane but are also bend away from the lithium cation. This is indicated by larger Si–N–Li angles (146.6°) in comparison to the corresponding C–N–Li angles in **1** (141.51(13)° and 136.97(14)°).

Secondly, the average Si–N bonds in **1–S(IV)** are longer $(171.3(1)\ pm)_{av.}$ than the corresponding C14–N1 and C22–N2 bonds in **1** (148.19(14) and 148.36(14) pm), giving the phosphorus side arm more space to approach the lithium cation.

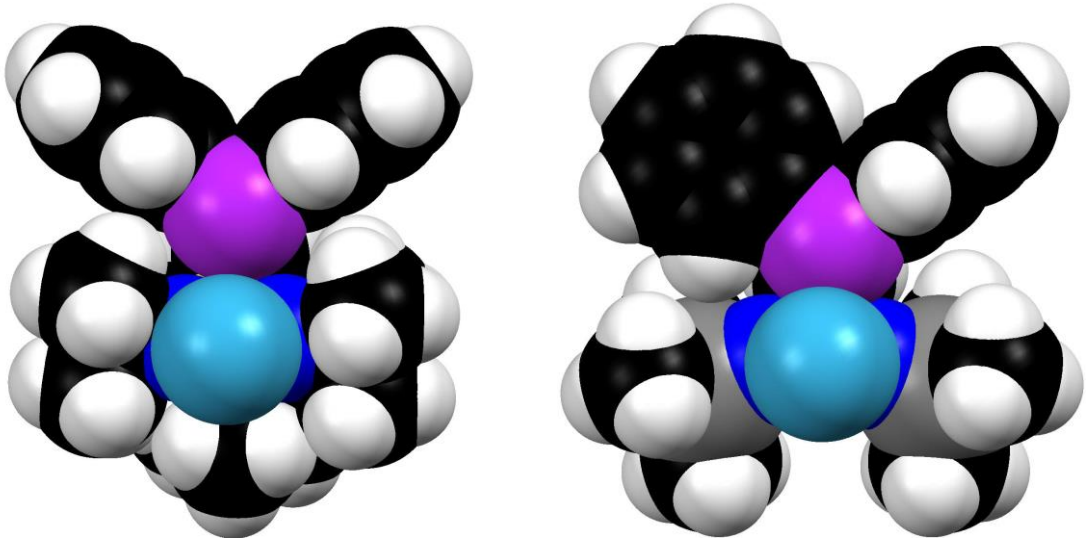

1 **1–S(IV)**

Figure 3.3: Space–filling models of **1** and **1–S(IV)**. The TMEDA donor base that donates to the lithium cation is omitted in both models for clarity.

The ^{1}H–NMR spectrum of **1**, measured in THF–d_8, is displayed in Figure 3.4. Remarkably, there is just one signal for the protons of three N*t*Bu groups (1.28 ppm) although a different shift for the protons of the non–chelating N*t*Bu group would be expected. Probably, the lithium complex is a solvent separated ion pair in the THF solution. The ^{15}N– and ^{13}C–NMR spectra show also just one signal for the N*t*Bu groups, respectively, pointing out the equivalence of the three N*t*Bu groups in the THF solution. Further, the ^{1}H shifts of the TMEDA donor base are similar to the shifts of an uncoordinated TMEDA molecule (2.15 and 2.30 ppm), indicating that the

lithium cation is rather solvated by THF molecules than still coordinated to the ligand.

A ^{1}H–NMR spectrum of **1** was recorded in toluene–d_8 for comparison (Figure 3.4). The detected signals for the protons of the N*t*Bu groups are broad, due to dynamic processes. However, it can be distinguished between the chelating (1.46 ppm) and non–chelating N*t*Bu groups (1.69 ppm). The ^{13}C–NMR spectrum also displays broad but different signals for the CH_3 carbon atoms of the *t*butyl groups (33.80 and 34.78 ppm). Moreover, the ^{1}H signals of the TMEDA moiety are shifted significantly relatively to the uncoordinated signals and the signals measured in THF–d_8 (1.92 ppm for $N(CH_2)_2$ and 2.09 ppm for $N(CH_3)_2$). A ^{15}N–NMR spectrum of **1** in toluene–d_8 could not be detected because the solubility of **1** in toluene is quite poor and consequently the concentration was too low. Interestingly, the ^{1}H signal of the lithium cation chelating N*t*Bu groups is more shifted to the high field than the ^{1}H signal of the non–chelating N*t*Bu group, implying that the latter is more deshielded. For further details regarding the NMR shifts of **1**, see section 5.3.1.

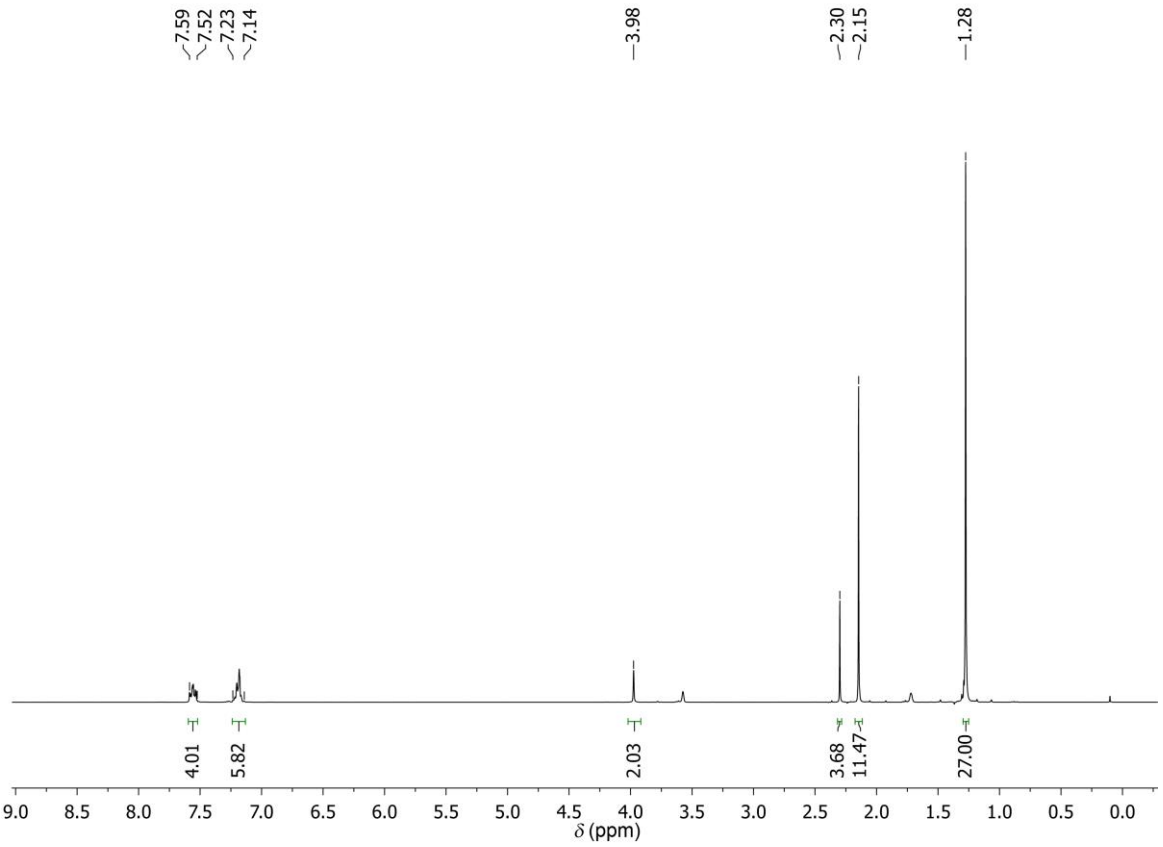

Figure 3.4: ^{1}H–NMR (300 MHz) spectrum of **1** recorded in THF–d_8. Assignment of the signals in [ppm]: 1.28 (C(CH_3)$_3$), 2.16 ((CH_3)$_2$N), 2.30 (N(CH_2)$_2$N), 3.98 (SCH_2P), 7.17 – 7.24 (*o*–H, *p*–H), 7.54 – 7.59 (*m*–H).

To conclude, the compound [(tmeda)Li{(N*t*Bu)$_3$SCH$_2$PPh$_2$}] (**1**) is a novel Janus head ligand that provides coordination sites for hard and soft metal centres. The lithium cation is the hard metal centre and chelated by two strong *σ* donating imido groups. The molecular structure of the S(IV) analogue [(tmeda)Li{(NSiMe$_3$)$_2$SCH$_2$PPh$_2$}] is similar to **1** and shows only slight structural differences. The phosphorus side arm and one of the three imido groups remain in the backbone of the ligand **1**, free for coordinating a further metal centre. The shape of the ligand is reminiscent to a scorpionate ligand but a hemilabile P–Li bond is impeded by the bulky N*t*Bu groups. The free phosphorus and imido side arms are good prerequisites for synthesising bimetallic complexes with **1** as the starting material. Further, the lithium cation might be easily exchangeable for other metal ions by salt–elimination reactions. With these properties the ligand **1** seems to be a promising precursor for the generation of novel and versatile metal complexes.

3.2. Transition metal complexes of [(tmeda)Li{(N*t*Bu)$_3$SCH$_2$PPh$_2$}]

As mentioned before, it was reported that metal metatheses of [Li$_4${(N*t*Bu)$_3$S}$_2$] from reactions with metal(II) halides are hampered by complex redox reactions. It was shown by *Meinholz* that the application of metal bis(trimethylsilyl)amides is in the transformation with S(IV) ligands more promising.[34a] For example, the reaction of [(tmeda)Li{(NSiMe$_3$)$_2$SCH$_2$PPh$_2$}] **1–S(IV)** with [Ca{N(SiMe$_3$)$_2$}$_2$] proceeded with a complete metal exchange and gave the product [Ca{Ph$_2$PCH$_2$S(NSiMe$_3$)$_2$}$_2$].[14] Nonetheless, reactions of **1** with metal halides were investigated to test if the S(VI) ligand **1** is stable enough against redox scrambling or not. The used metal halides had to be treated with care and under exclusion of oxygen and water but they are not as sensitive as transition metal bis(trimethylsilyl)amides and therefore easier to handle.

First row transition metal ions Mn^{2+}, Fe^{2+}, Co^{2+}, Ni^{2+}, Cu^{2+} and Zn^{2+} were utilised for the reaction with **1**. Metal bromides instead of chlorides were used because of the better solubility in organic solvents like pentane. Since compound **1** is very sensitive to oxygen and moisture the metal halides had to be dry *prior to use* and handled in an argon atmosphere. It has been proven to run the syntheses in pentane since LiBr, that is formed during the reaction, is nearly insoluble in pentane and precipitates completely. Thus, it can be filtered off easily when pentane is used as a solvent.

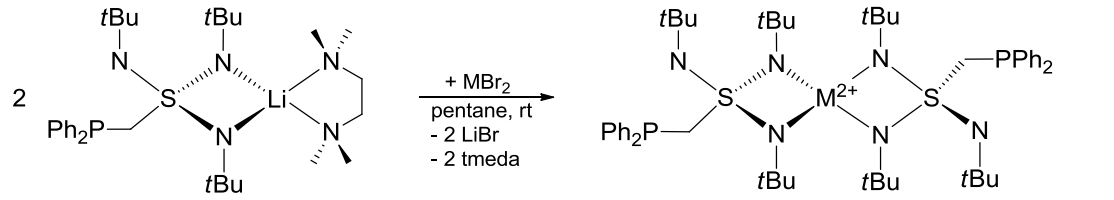

1 M = Mn (**2**), Fe (**3**), Co (**4**), Ni (**7**), Cu (**8**), Zn (**10**)

Scheme 3–3: General preparation route for the first row transition metal complexes of the *S*–phosphanyl–triimidiosulfonate **1**.

A clear drawback is the poor solubility of the reagents in pentane. However, a change of the solvent to toluene or THF turned out to be ineffective because only decomposition of the reagents or formation of a non–crystalline solid was observed. Thus, it is not a suitable option because purification of the products and definite characterisation is only possible by crystallisation. The metal complexes that are presented in this chapter were synthesised according to the general synthetic route

depicted in Scheme 3–3. Variances of the general synthesis are mentioned explicitly.

In the following sections, the obtained metal complexes and their structural properties are presented. The last part of the chapter concludes with a comparison of the different metal complexes.

3.2.1. [Mn{(N*t*Bu)$_3$SCH$_2$PPh$_2$}$_2$] (2)

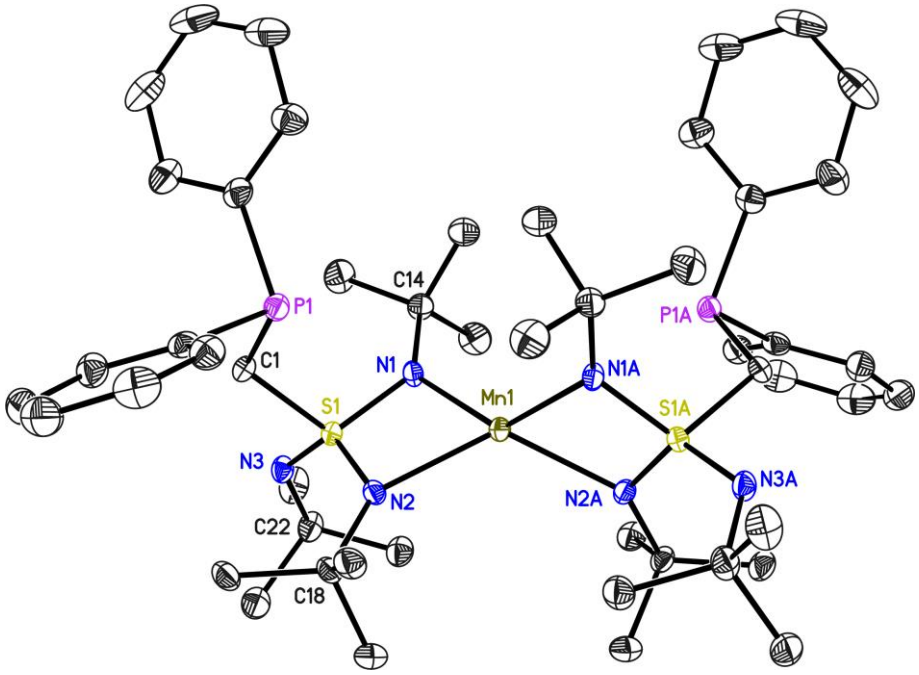

Figure 3.5: Crystal structure of [Mn{(N*t*Bu)$_3$SCH$_2$PPh$_2$}$_2$] (**2**). Anisotropic displacement parameters are depicted at the 50% probability level. Hydrogen atoms are omitted for clarity.

Compound **2** crystallises in the monoclinic space group *C*2/*c* with half a molecule in the asymmetric unit and the other half is generated by a twofold rotation axis. The crystal structure is shown in Figure 3.5. The manganese(II) cation Mn1 is chelated by two N1S1N2 claws in a distorted tetrahedral fashion. The negative charge is delocalised over the N1S1N2 moiety, indicated by the planarity of the SN$_2$– backbone and by the almost equal, symmetry independent S1–N1/N2 bond lengths (Table 3.2). The manganese cation and the N1, S1 and N2 atoms are spanning an almost perfect plane (angle of torsion: Mn1–N1–S1–N2: 0.77(9)°). The homoleptic coordinated manganese atom bridges two SN$_2$ moieties, forming two four–

membered MnN_2S rings which are rotated by 81.78°. The sulfur atom is bound distorted tetrahedrally by the N*t*Bu groups and the phosphorus side arm.

The Mn1–N1/2 distances are in the normal range for tetrahedrally coordinated Mn^{2+} cations in high spin state.[38] The Mn1···S1 distance is 283.51(5) pm and cannot be regarded as a bond although there are reports on Mn–S bonds of the same lengths in the literature and the average Mn–S bond distance found in the CSD is 240.45 pm.[37,39] Here, the short distance is not an indication for a bond or interaction between the sulfur and the manganese atom but more a sign of missing repulsion caused by the arrangement of the ligand.

Table 3.2: Selected bond lengths [pm] and angles [°] of **2**.

S1–N1	159.51(17)	Mn1···S1	283.51(5)
S1–N2	159.66(17)	N1–Mn1–N2	67.61(6)
S1–N3	152.22(17)	N1a–Mn1–N2	137.05(7)
P1–C1	185.8(2)	N1–S1–N2	94.97(9)
Mn1–N1	210.32(17)	Mn1–N1–C14	134.37(13)
Mn1–N2	212.55(17)	Mn1–N2–C18	136.39(13)
S1–C1	180.70(20)	Mn1–N1–S1–N2	0.77(9)

The phosphorus side arm is orientated towards the Mn^{2+} cation but the Mn1···P1 distance (394 pm) is too long to be regarded as a bond. However, this long–range interaction might help to stabilise the Mn^{2+} centre because otherwise the phosphorus atom might have been turned away from the metal.

The non–chelating N*t*Bu groups are bent away to the vacant site of the ligand as observed in **1**. The average S1–N1/2 distances of **2** are in comparison to **1** slightly elongated (159.58(17) pm vs 157.53(14) pm in **1**) due to the coordination of the Mn^{2+} dication. The Mn^{2+} cation is more electron–withdrawing and reduces the electron density at the N1 and N2 atoms more than the TMEDA coordinated Li^+ cation. Consequently, the electrostatic interactions between the S1 atom and the metal coordinating N1 and N2 atoms decrease what leads to an elongation of the S1–N1/2 and a shortening of the S1–N3 bonds relatively to **1** (152.22(17) pm).

The ligand–metal interactions in **2** differentiate from **1** because the manganese d orbitals can interact additionally with the ligand orbitals. An overview of possible orbital interactions is depicted in Scheme 3–4. The N_{sp^2}–M_σ interaction is depicted

only for the Mn^{2+} cation (**a**) but is the same for the Li^{+} cation. The other three models are possible interactions of the ligands N_{sp^2} orbitals with the d orbitals of the manganese atom that result in bonding orbitals. The interaction of both chelating ligands with the metals d_{xy} orbital is shown in **b**. In **c** and **d** the interactions of just one chelating ligand with the d_{xz} and d_{yz} orbitals are displayed because the orbitals of the second ligand would not overlap with the metal orbitals due to the geometry. Interactions between the ligand sp^2 orbitals and metal d_{z^2} and $d_{x^2-y^2}$ orbitals would just lead to non–bonding orbitals. The only significant π–interactions between ligand and metal could be between a N_{pz} lone pair and the $d_{x^2-y^2}$ orbital.

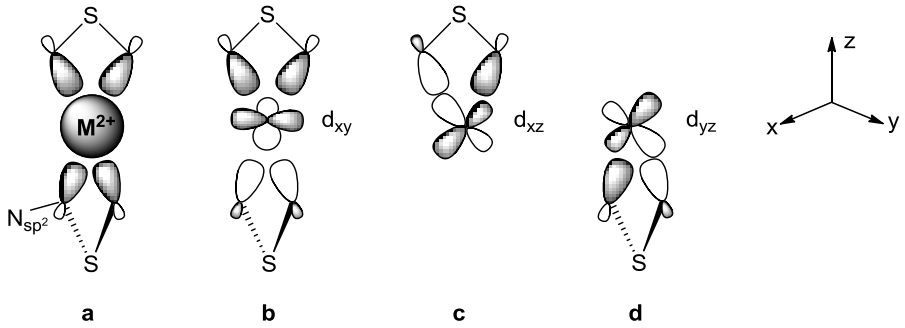

Scheme 3–4: Possible orbital interactions between the N_{sp^2} orbitals of the ligand and the metal orbitals.

The interactions depicted in Scheme 3–4 are just a simplified model that assumes an ideal tetrahedral geometry around the metal centre and neglects mixing of metal p and d orbitals. To know the exact ligand–metal interactions, quantum mechanical calculations are necessary.

3.2.2. [Fe{(N*t*Bu)$_3$SCH$_2$PPh$_2$}$_2$] (3)

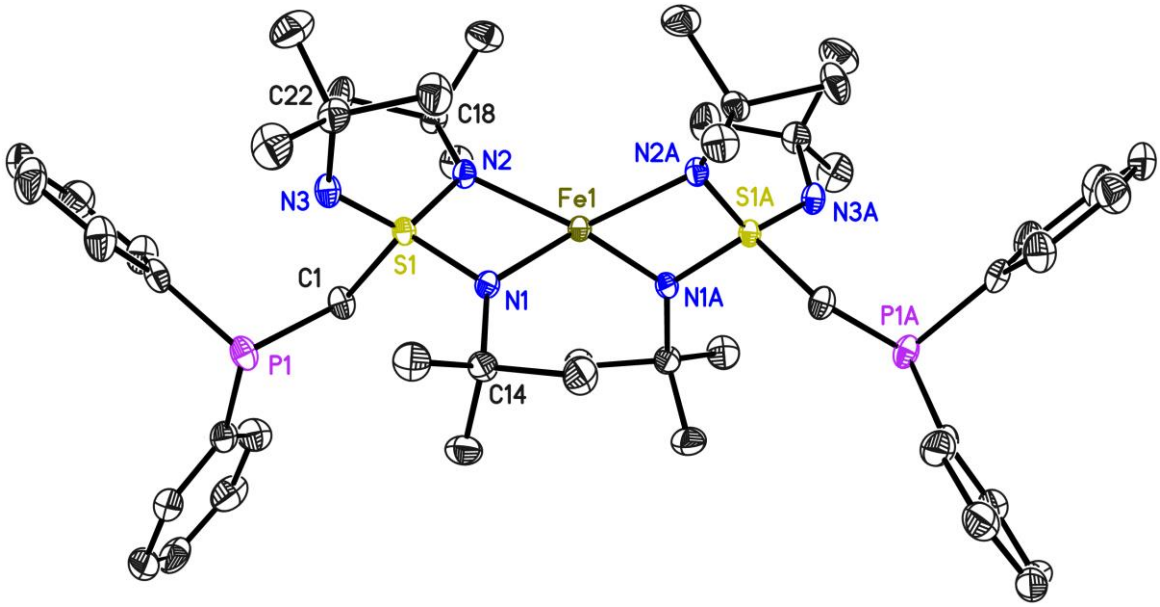

Figure 3.6: Crystal structure of [Fe{(N*t*Bu)$_3$SCH$_2$PPh$_2$}$_2$] (**3**). Anisotropic displacement parameters are depicted at the 50% probability level. Hydrogen atoms are omitted for clarity.

Brown–orange crystals of [Fe{(N*t*Bu)$_3$SCH$_2$PPh$_2$}$_2$] (**3**) were obtained from a reaction of **1** with $FeBr_2$. Compound **3** crystallises in the monoclinic space group *C*2 with half a molecule in the asymmetric unit and the other half is generated by a twofold rotation axis (Figure 3.6). The iron(II) cation and the sulfur atom are coordinated tetrahedrally distorted like in complex **2**, spanning two almost perfectly planar FeN_2S four–membered rings that are twisted by around 85°. The pendant phosphorus and imido side arms are directed to the vacant site of the ligand. Both symmetry independent S–N bond distances in the FeN_2S four–membered ring are almost equal within esds (av. 160.5(3) pm). The S1–N3 bond is shortened due to enhanced electrostatic interaction.

Table 3.3: Selected bond lengths [pm] and angles [°] of **3**.

S1–N1	160.6(3)	Fe1···S1	273.63(7)
S1–N2	160.0(3)	N1–Fe1–N2	71.00(10)
S1–N3	152.0(3)	N1A–Fe1–N2	133.70(10)
P1–C1	184.9(3)	N1–S1–N2	93.72(12)
Fe1–N1	202.3(2)	Fe1–N1–C14	135.50(20)
Fe1–N2	201.0(2)	Fe1–N2–C18	134.13(19)
S1–C1	181.0(3)	Fe1–N1–S1–N2	–3.69(14)

The Fe–N distances (202.3(2) and 201.0(2) pm) as well as the tetrahedral geometry are conforming to a high–spin electron state.[40] A Mössbauer spectrum of a solid sample of **3** was conducted by *S. Demeshko* and is displayed in Figure 3.7. The low signal–to–noise ratio might be due to the fact that the sulfur atom absorbs non–resonantly a large fraction of the incident radiation and produced a high background of scattered radiation, resulting in a low absorption.[41]

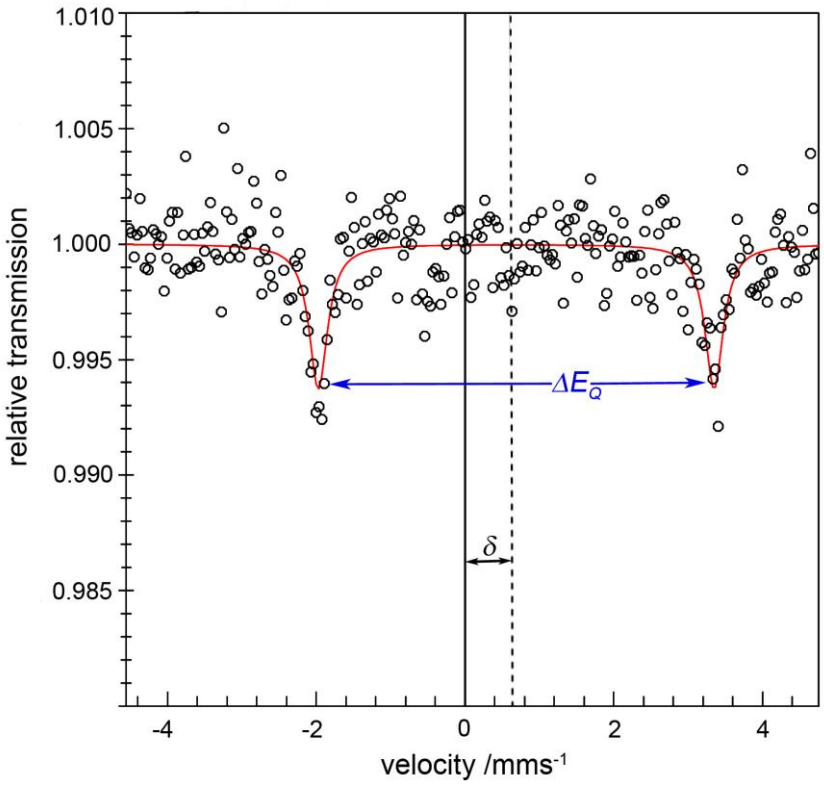

Figure 3.7: Mössbauer spectrum of **3** with the isomer shift δ (0.69 mm/s) and the quadrupole splitting ΔE_Q (5.32 mm/s). The spectrum was recorded at 80 K.

The spectrum of **3** shows an isomer shift of 0.69 mm/s what is consistent with high–spin iron(II). δ values of 0.48 – 0.90 mm/s were observed in other iron(II) diketiminate complexes, for example.[42] A value of δ = 0.55 mm/s has been found in a fourfold coordinated iron(II) complex supported by a tris(phosphino)borate ligand[43] while a larger value of δ = 0.96 mm/s was seen for an iron(II) complex of a tris(thioether)borate.[44] Tetrahedral iron(II) cations in iron–sulfur clusters give δ = 0.60 – 0.70 mm/s. [40b,c,45]

The quadrupole splitting ΔE_Q is the sum of valence–electron contribution and lattice contribution. Values above 4 mm/s may be caused by a significant lattice

contribution to the electric field gradient.[46] The lattice contribution arises from charges on the ligands and distant atoms.

The quadrupole splitting ΔE_Q of 5.32 mm/s in **3** is remarkable since the normal range for tetrahedral high spin iron(II) complexes is 3 – 4 mm/s.[45a,47] The observation of a large quadrupole splitting indicates that the d orbitals of the Fe(II) ion in the crystal field must be split by a distortion of the ion.[41] The d_{z^2}, $d_{x^2-y^2}$ and d_{xy}, d_{xz}, d_{yz} orbitals are degenerated in an ideal tetrahedral crystal field but a distortion of the tetrahedral to a more planar geometry leads to an increase of the energy of the $d_{x^2-y^2}$ and d_{xy} orbitals, for example. Hence, the sixth 3d electron is not distributed equally over the half–filled $3d^5$ shell. Indeed, the N–Fe–N angles in **3** display a tetrahedrally distorted geometry (71.00(10)°, 129.48(15)° and 133.70(10)°). Examples for a quadrupole splitting larger than 4 mm/s can be found in the literature[43,46,48] but examples of similar iron(II) compounds with a quadrupole splitting higher than 5 mm/s are rare. A CSD search for iron(II) complexes with a similar coordination pattern was done to check if a comparably high quadrupole splitting has already been reported for similar compounds. The research revealed that there is one other crystral structure with two iron–bridged FeN_2S rings as a structural motif reported in the literature. In the heteroaromatic S–substituted diimidosulfinates $[Fe\{(NtBu)_2S(C_8H_5S)\}_2]$[49] the Fe^{2+} cation is coordinated in tetrahedrally distorted fashion by two SN_2 claws similar to **3**. Unfortunately, no Mössbauer spectrum of this compound is reported and direct comparison with **3** is impossible.

3.2.3. [Co{(N*t*Bu)$_3$SCH$_2$PPh$_2$}$_2$] (4)

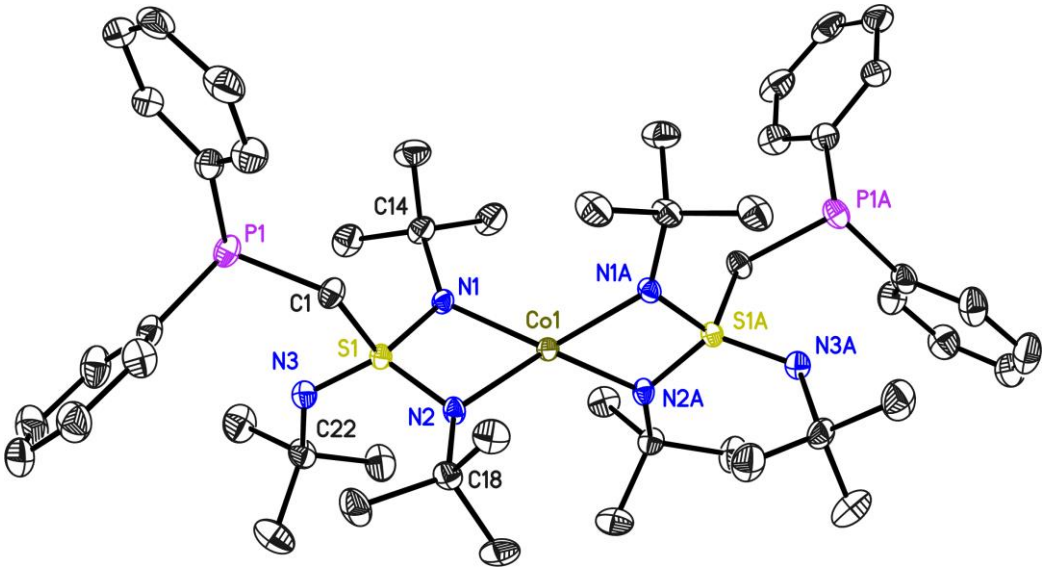

Figure 3.8: Crystal structure of [Co{(N*t*Bu)$_3$SCH$_2$PPh$_2$}$_2$] (**4**). Anisotropic displacement parameters are depicted at the 50% probability level. Hydrogen atoms are omitted for clarity.

The compound **4** is isostructural to the iron complex **3** and crystallises in the monoclinic space group *C*2 with half a molecule in the asymmetric unit (Figure 3.8). The cobalt(II) ion is in a tetrahedrally distorted environment of four nitrogen atoms. A square–planar coordination motif in **4** would be unlikely because of the bulkiness of the ligand and because fourfold coordinated Co(II) compounds containing bidentate nitrogen–based chelating ligands show a clear preference for high–spin tetrahedral geometries (S = 3/2).[50] The majority of low–spin Co(II) (S = 1/2) complexes are square–planar chelates of tetradentate macrocycles, such as porphyrins or *Schiff* base derivatives, which impose this type of geometry at the metal centre due to their intrinsic structural features.[51] SQUID susceptometric measurements were done by *S. Demeshko* to confirm the assumption of a high–spin configuration in **4**. The magnetic moment at room temperature is 5.17 μ_B what corresponds to a S = 3/2 ground state and indicates high–spin configuration Co(II) (Figure 3.9).[52] The best simulation parameters are g = 2.671 and $|D|$ = 15.572 cm^{-1}. The g value deviates from the value for a free electron (g_e = 2.0) because of additional orbital contributions. The D value indicates a large zero–field splitting.

The Co–N bond distances of 201.0(2) pm and 197.7(2) pm are in the expected range of tetrahedral, high–spin cobalt complexes (Table 3.4).[50c,53]

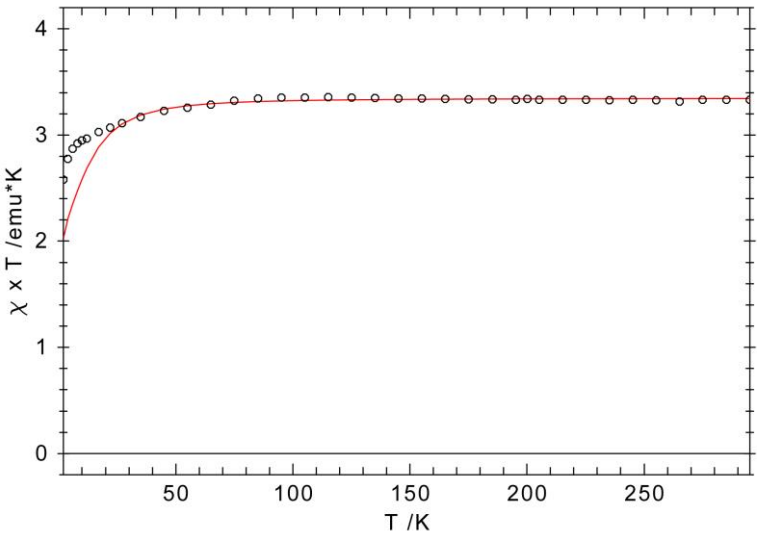

Figure 3.9: Plot of the magnetic susceptibility ($\chi \times T$) vs T for **4** in the range 45 – 295 K; the solid line represents the calculated curve fit. The best simulation parameters are g = 2.671, $|D|$ = 15.572 cm^{-1}.

The complex $[Co\{Ph_2PCH_2S(NSiMe_3)_2\}_2]$ (**4–S(IV)**) is the S(IV) analogue of **4** and was obtained from a reaction of **1–S(IV)** with $[Co\{N(SiMe_3)_2\}_2]$. The central cobalt(II) cation is sixfold coordinated in a (*N*,*N*,*P*)–tridentate manner (Figure 3.10, *left*).[54]

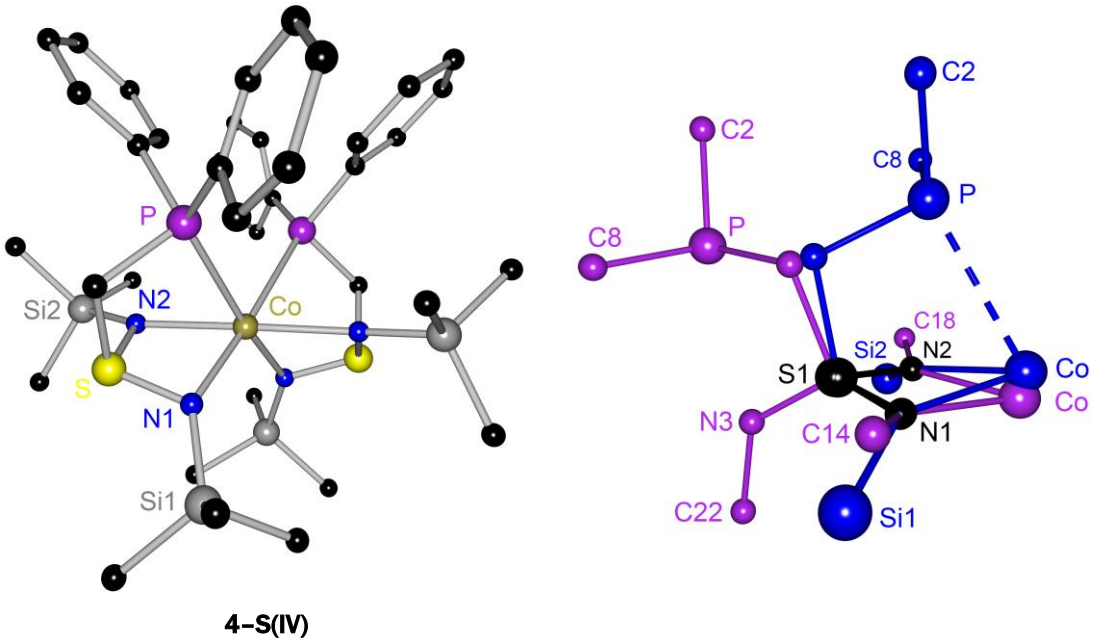

4–S(IV)

Figure 3.10: *left*) Molecular structure of $[Co\{Ph_2PCH_2S(NSiMe_3)_2\}_2]$ (**4–S(IV)**). *right*) Superposition plot of the symmetry independent part of the molecules **4** (pink coloured) and **4–S(IV)** (blue coloured). The black coloured atoms S1, N1 and N2 are fitted onto each other with a deviation of 6.3 pm. For clarity, the phenyl rings and *t*butyl groups are just indicated by the C_{ipso} or $C_{quart.}$ atoms and the $SiMe_3$ groups just by the Si atoms.

A detailed comparison of **4** and **4–S(IV)** revealed that the N*t*Bu groups shield the cobalt(II) cation and prevent a P1 · · · Co1 interaction in **4**. The Co1–N1–C14 and Co1–N2–C18 angles (135.48(19)° and 132.98(18)°) in **4** are sharper in comparison to the corresponding average Co–N–Si angles (143.50(13)°) in **4–S(IV)**, because the non–chelating N*t*Bu group hinders the *t*butyl groups of the N1 and N2 atoms from turning away from the metal cation. A superposition plot of both structures is displayed in Figure 3.10, illustrating nicely that the cobalt(II) cation in **4–S(IV)** deviates significantly out of the N1S1N2 plane to interact with the phosphorus atom. The Co–N bond lengths in **4–S(IV)** are elongated due to the distorted octahedral coordination (Co–$N_{av.}$ = 213.3(2) pm). The magnetic moment at room temperature is 5.11 μ_B and indicates high–spin configuration Co(II) like in **4**.

Table 3.4: Selected bond lengths [pm] and angles [°] of **4**.

S1–N1	161.3(2)	Co1 · · · S1	271.70(7)
S1–N2	159.5(2)	N1–Co1–N2	71.53(10)
S1–N3	151.8(2)	N2A–Co1–N1	133.12(10)
P1–C1	185.2(3)	N1–S1–N2	93.19(12)
Co1–N1	201.0(2)	Co1–N1–C14	135.48(19)
Co1–N2	197.7(2)	Co1–N2–C18	132.98(18)
S1–C1	181.0(3)	Co1–N1–S1–N2	–4.02(13)

Complex **4** was synthesised according to the general reaction procedure depicted in Scheme 3–3. To improve the solubility and increase the yield, a small amount of THF was added to the reaction mixture so that the reaction was run in a 5:1 ration of pentane and THF (Scheme 3–5).

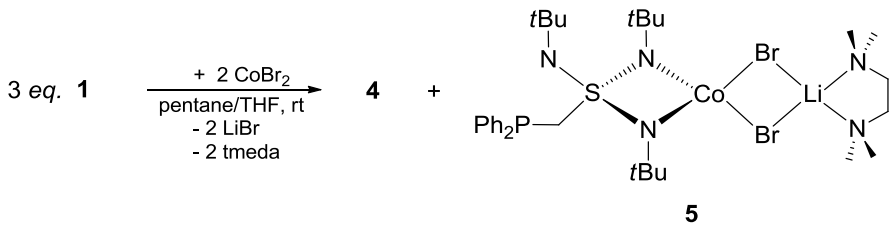

5

Scheme 3–5: Reaction of **1** with $CoBr_2$ in a pentane/THF mixture yielding **4** and the side product **5**.

After LiBr was filtered off, the pink solution was stored at 4 °C and after one day pink crystals of **4** and a small amount of blue crystals were visible. The two different

kinds of crystals were separated under a polarised microscope and the crystal structure of the blue compound was determined *via* X–ray structure analysis (Figure 3.11).

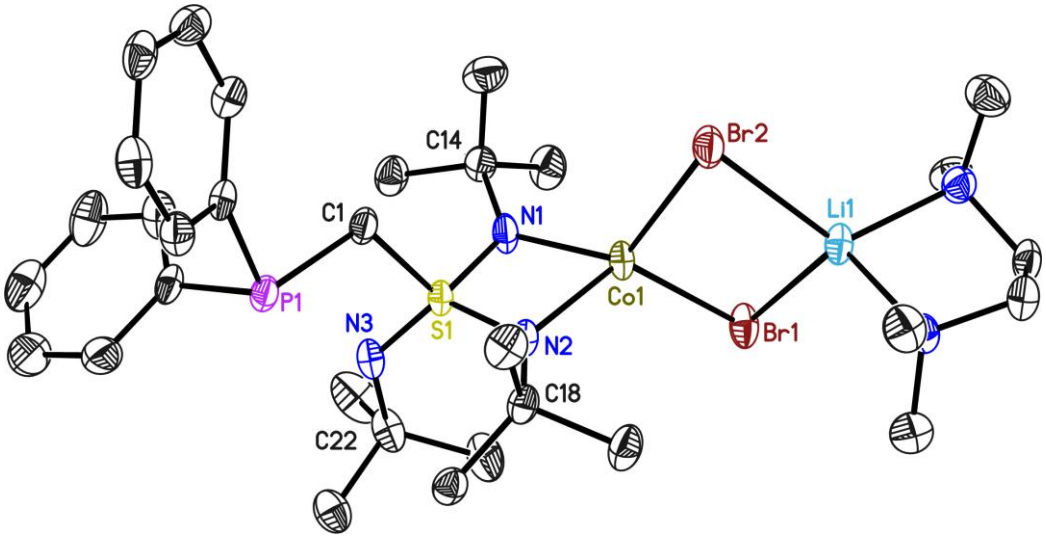

Figure 3.11: Crystal structure of [(tmeda)Li(μ–Br)$_2$Co{(N*t*Bu)$_3$SCH$_2$PPh$_2$}] (**5**). Anisotropic displacement parameters are depicted at the 50% probability level. Hydrogen atoms and disordered moieties with the lower site occupation factors (*t*butyl group (C14) and (tmeda)LiBr$_2$) are omitted for clarity.

5 crystallises in the triclinic space group $P\bar{1}$ with one molecule in the asymmetric unit. The resulted structure is a mixed metal cobalt–lithium complex that seems like an intermediate of a salt–elimination reaction between the lithiated complex **1** and $CoBr_2$. $CoBr_2$ inserts into the Li1–N1/2 bonds forming a $LiBr_2Co$ and CoN_2S ring with the cobalt(II) cation as the bridging centre. The bromine atoms are already coordinated by the lithium cation, ready to leave the complex as a [(tmeda)LiBr]$_2$ adduct if a second lithium cation would inserted to the Co–Br bonds.

5 exhibits a distorted tetrahedral geometry at the cobalt, sulfur and lithium atoms. The cobalt and lithium cations are connected by two bromine bridges what is a quite rare coordination motif. Eleven halide–bridged lithium–cobalt complexes are reported in the CSD and two of them are bromine bridged.[37,55] In none of the reported structures the $LiBr_2Co$ ring is coordinated by an *N,N*–chelating ligand. Hence, with the synthesis of **5** a novel structure motif is presented. Unfortunately, the $LiBr_2Co$ ring is highly disordered and therefore the bond distances cannot be discussed in detail. Nonetheless, the bond lengths and angles are listed in Table 3.6 and for the disordered moieties the parts with the higher site occupation factor are

chosen. The Co1–Br1 and Co1–Br2 distances are close to the average Co–Br distances of fourfold coordinated cobalt(II) cations found in the CSD (238.55 pm). The Li1–Br1 and Li1–Br2 bond lengths are within the expected range and close to the average values of the Li–Br bonds in $[(tmeda)LiBr]_2$ (249.4 pm).[56] The bond distances and angles of the sulfur triimide moiety of **5** are similar to **4**. Due to the fact that **5** is just a byproduct and could not be isolated from the main product **4**, the magnetic moment of **5** could not be measured. Nonetheless, from the tetrahedral coordination and the Co–N bond distances a high spin state can be concluded.

Table 3.5: Selected bond lengths [pm] and angles [°] of **5**.

S1–N1	160.14(17)	Li1–Br1	249.6(3)
S1–N2	159.79(16)	Li1–Br2	250.4(3)
S1–N3	151.59(17)	N1–Co1–N2	72.06(7)
Co1–N1	197.32(17)	S1–C1–P1	113.52(11)
Co1–N2	197.13(16)	Co1–N1–C14	132.10(13)
S1–C1	179.8(2)	Co1–N2–C18	132.90(12)
P1–C1	185.7(2)	N1–S1–N2	92.97(9)
Co1···S1	269.52(7)	Br1–Co1–Br2	100.93(3)
Co1–Br1	242.66(10)	Co1–N1–S1–N2	–2.94(9)
Co1–Br2	245.80(6)		

In a 1:1 ratio of the reagents in pure pentane only the formation of **4** is observed. Hence, the formation of **5** is depending on the addition of THF to the reaction mixture. THF increases the solubility not only of the reagents but also of the formed $[(tmeda)LiBr]_2$ and if $[(tmeda)LiBr]_2$ does not precipitate completely a total salt–elimination might be inhibited.

A solution of **1** in THF was also added to a suspension of $CoBr_2$ in pentane at –78 °C to test if the formation of **5** is temperature dependent. But also from this reaction just a mixture of **4** and **5** was obtained.

It was tried to activate the free *P,N*–donor functionality at the backbone of the ligand by treating **4** with $ZnMe_2$ and $[(arene)RuCl_2]_2$ in THF to generate bimetallic complexes. $ZnMe_2$ was used because a dative coordination of the pending imido

group to $ZnMe_2$ has been observed already in $[(thf)_2Li\{(NtBu)_3SMe\}\cdot ZnMe_2]$.[29a] By adding $[(arene)RuCl_2]_2$ in THF to a solution of **4** in toluene, it was attempted to achieve a coordination of the ruthenium(II) by the phosphorus side arm since many *P*–coordinated $[(arene)RuCl_2]_2$ complexes can be found in the literature. Unfortunately, no crystals were obtained from the reaction mixtures and the obtained crude powders could not be identified.

3.2.4. $[Co\{(NtBu)_3SMe\}_2]$ (6)

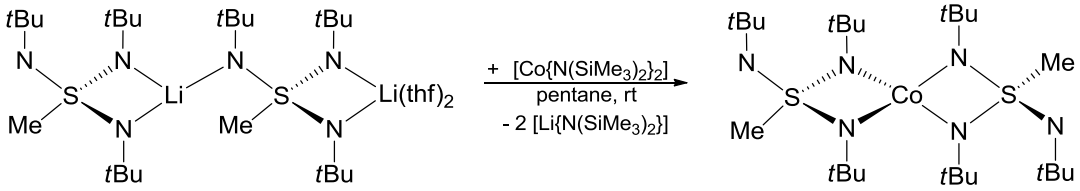

6

Scheme 3–6: Reaction of $[(thf)_2Li_2\{(NtBu)_3SMe\}_2]$ with $[Co\{N(SiMe_3)_2\}_2]$.

The complex $[Co\{(NtBu)_3SMe\}_2]$ (**6**) was synthesised to test if the phosphorus side arm influences the coordination behaviour of the sulfur triimide moiety. The starting material $[(thf)_2Li_2\{(NtBu)_3SMe\}_2]$ was prepared according to the literature known procedure from a reaction of MeLi and $S(NtBu)_3$.[18] Since a salt–elimination reaction with $CoBr_2$ failed, $[Co\{N(SiMe_3)_2\}_2]$ was used in the synthesis and the complex **6** was obtained as pink crystals (Scheme 3–6).

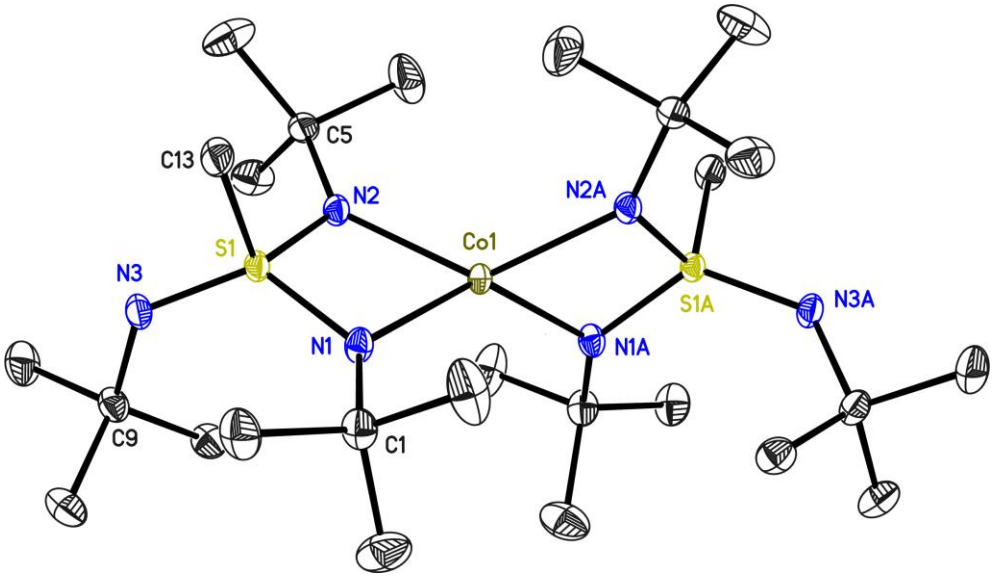

Figure 3.12: Crystal structure of $[Co\{(NtBu)_3SMe\}_2]$ (**6**). Anisotropic displacement parameters are depicted at the 50% probability level. Hydrogen atoms are omitted for clarity.

Compound **6** crystallises in the monoclinic space group *C*2/*c* with half a molecule in the asymmetric unit and the other half is generated by a twofold rotation axis. **6** is isotypical to $[Co\{(NtBu)_3SCH_2PPh_2\}_2]$ and as in **4** the cobalt(II) cation is coordinated in a tetrahedral fashion by the *N,N*–chelating ligand. The bond distances and angles are similar to those in **4**. The analogousness of both structures is illustrated by a superposition plot in Figure 3.13 (*left*).

Table 3.6: Selected bond lengths [pm] and angles [°] of **6**.

S1–N1	160.84(11)	N1–Co1–N2	71.46(4)
S1–N2	159.89(10)	N1A–Co1–N2	130.02(4)
S1–N3	152.67(10)	N3–S1–C13	99.43(6)
Co1–N1	198.73(11)	Co1–N1–C1	132.83(8)
Co1–N2	199.39(10)	Co1–N2–C5	135.81(8)
S1–C13	178.67(13)	N1–S1–N2	92.92(5)
Co1···S1	271.59(7)	Co1–N1–S1–N2	–5.59(5)

The symmetry independent Co1–N1/2 bond lengths of **4** display a considerable divergence (201.0(2) pm and 197.7(2) pm) in comparison to the Co1–N1/2 distances of compound **6** (Table 3.6). The slight structural difference is probably related to the presence of the phosphorus side arm. There are short intramolecular P1 ··· H contacts (297.1 and 284.2 pm) to the *t*butyl group of the N1 atom which also shows the longer Co1–N distance (Figure 3.13, *right*). The phosphanyl arm is directed to one site of the ligand relatively to the *N,N*–chelating claw. Hence, the different Co–N bond lengths are caused by a different sterical environment. Apart from that, the structures do not show significant differences which on the other hand demonstrates that the phosphorus side arm has just a slight effect on the sulfur triimide core and the *N,N*–donor functionality of the ligand.

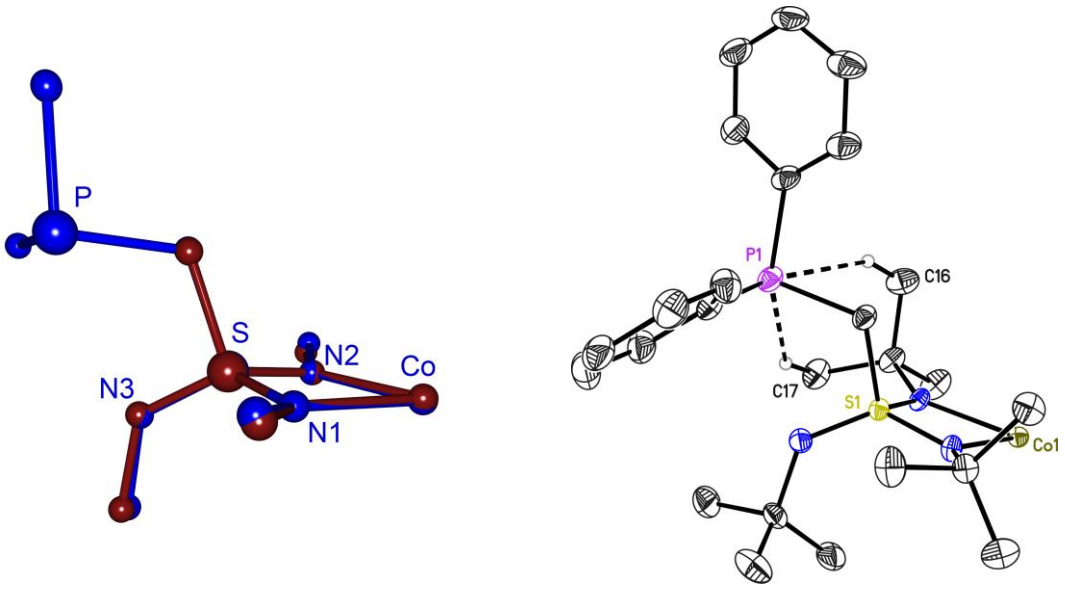

Figure 3.13: *left*) Superposition plot of **4** (blue) and **6** (scarlet). The phenyl rings and *t*butyl groups are just indicated by C_{ipso} or $C_{quart.}$ atoms. The S, N1 and N2 atoms are fitted onto each other with a deviation of 2.21 pm. *right*) Asymmetric unit of compound **4** with short P1 ··· H contacts.

$[Zn\{Me(SNtBu)_3\}_2]$ is the only other transition metal complex of the $[MeS(NtBu)_3]^-$ ligand reported in the literature.[29a] It was synthesised in a reaction of sulfur triimide with $ZnMe_2$ and not by salt–elimination reaction. The geometry and bond lengths are similar to those in **6**.

The ^1H–NMR spectrum of the paramagnetic, high–spin Co^{2+} complex **6** displays a substantial peak–broadening effect with three broad peaks at δ = –45.95, 23.04 and 119.67 ppm (measured in THF–d_8). An exact determination of the integrals is not possible due to the large peak–broadening. Nonetheless, the peaks can be assigned with the approximated integrals because they show an obvious tendency. Thus, the signal at –45.95 ppm belongs to 36 protons of the four metal coordinating N*t*Bu groups. The peak at 23.04 ppm can be assigned to 18 protons of the two non–chelating N*t*Bu groups and the last peak at 199.67 ppm to six protons of the two methyl groups.

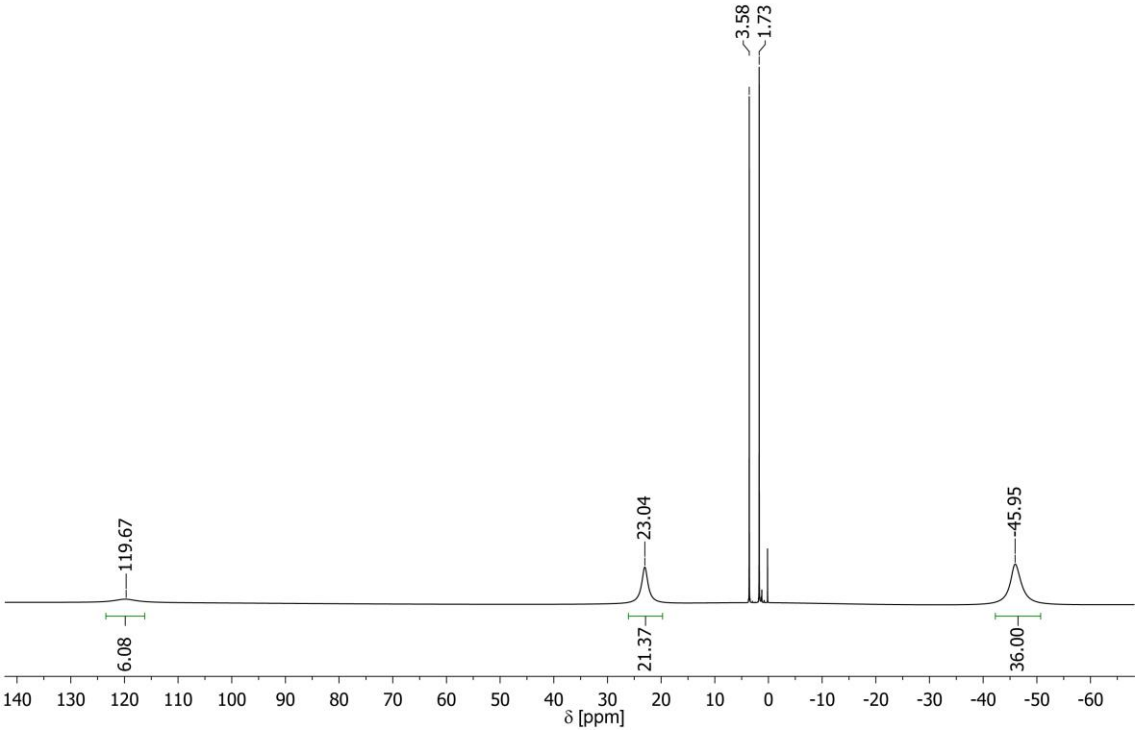

Figure 3.14: ^{1}H–NMR spectrum (500.26 MHz) of **6** recorded in THF–d_8.

Magnetic susceptibility data were collected by *S. Demeshko* and the observed $\mu_M T$ value at rt is 3.11 $cm^3mol^{-1}K$, corresponding to an $S = 3/2$ spin centre in **6** with the best simulation parameters $g = 2.578$ and $|D| = 10.257$ cm^{-1}, indicating some orbital angular momentum contribution (Figure 3.15). It remains roughly constant between 16 and 296 K and begins to drop at lower temperatures due to zero field splitting.

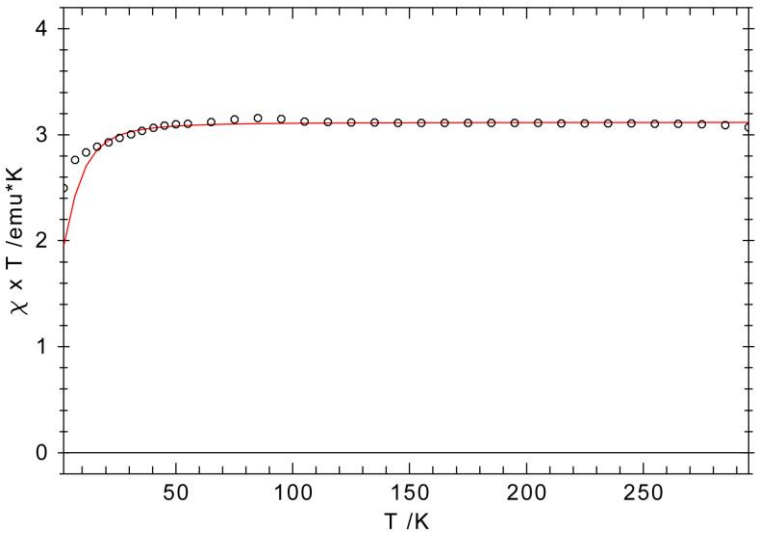

Figure 3.15: Plot of the magnetic susceptibility ($\chi \times T$) vs T for **6** in the range 16 – 295 K; the solid line represents the calculated curve fit. The best simulation parameters for the values above 20 K are

g = 2.578 and $|D|$ = 10.257 cm^{-1}.

Variable temperature–variable field magnetisation (VTVH) data were collected and the best fit to the data afforded D = –108.856 cm^{-1} (Figure 3.16). The large negative D value indicates a large magnetic axial anisotropy what is one of the crucial properties of single molecular magnets (SMM).

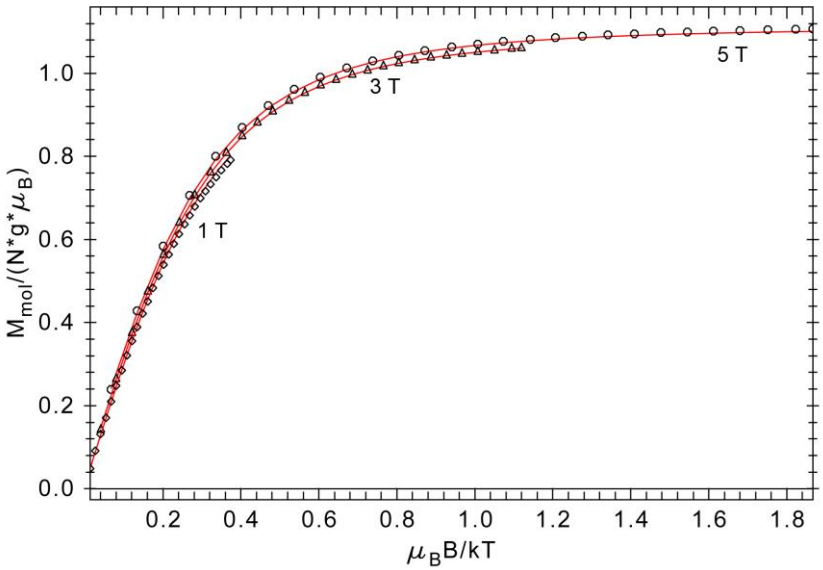

Figure 3.16: Variable temperature–variable field (VTVH) magnetisation measurements as M_{mol} vs B/T for **6**. The symbols display the measured values under different magnetic fields. Solid lines represent the calculated curve fits.

Another specific characteristic of SMM behaviour is the frequency dependence of the imaginary part of the magnetic susceptibility (χ'') using alternating current (*ac*) magnetic fields. The *ac* magnetic susceptibility of **6** at various frequencies in the absence of a direct current (*dc*) magnetic field and with an applied *dc* field (H_{DC} = 3000 Oe) were measured at low temperatures (1 –20 K) (Figure 3.17). Interestingly, the imaginery component of the susceptibility (χ'') shows significant frequency dependence within a broad temperature range in both cases (with and without an applied *dc* field), indicating single molecule magnet (SMM) behaviour of **6**. Slow magnetic relaxation has been observed in tetrahedrally coordinated Co(II) complexes under an applied field with D > 0[57] or at zero field with D < 0.[58] Comparable compounds showing SMM behaviour with and without an applied field and with D < 0 are rare.

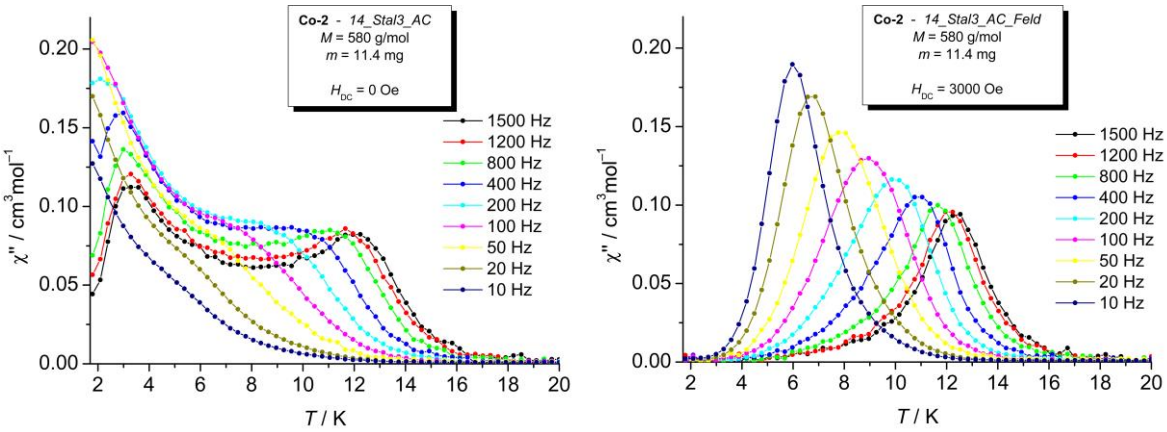

Figure 3.17: Temperature dependence of χ''_M at various frequencies in the absence of a *dc* fields (*left*) and with an applied *dc* field of H_{DC} = 3000 Oe (*right*).

The $\chi''(\upsilon)$ data allow relaxation time, τ, to be determined from $\tau = 1/(2\pi\upsilon)$, where the values of υ are the peak maxima in the plot depicted in Figure 3.17, *right*. The relaxation dynamics are characterised by a relaxation time as $\tau = \tau_0$ exp(U_{eff}/k_BT). The experimental relaxation barrier U_{eff} can then be extracted from the linear section of the Arrhenius plot of ln τ vs 1/T, which describes a regime in which the relaxation is thermally activated (Figure 3.18, *left*). The relaxation energy barrier of **6** is U_{eff} = 74 cm^{-1} and the relaxation time is τ_0 = 1.66 × 10^{-8} s with H_{DC} = 3000 Oe. These values can be classified in the normal range for single molecular magnets and higher values can be found for polymetallic transition metal cages or dimetallic organolanthanide complexes.[59] A more important measure of the success of a single magnet molecule is whether or not the field dependence of the magnetisation shows hysteresis. The hysteresis loops recorded for **6** are depicted in Figure 3.18, *right*.

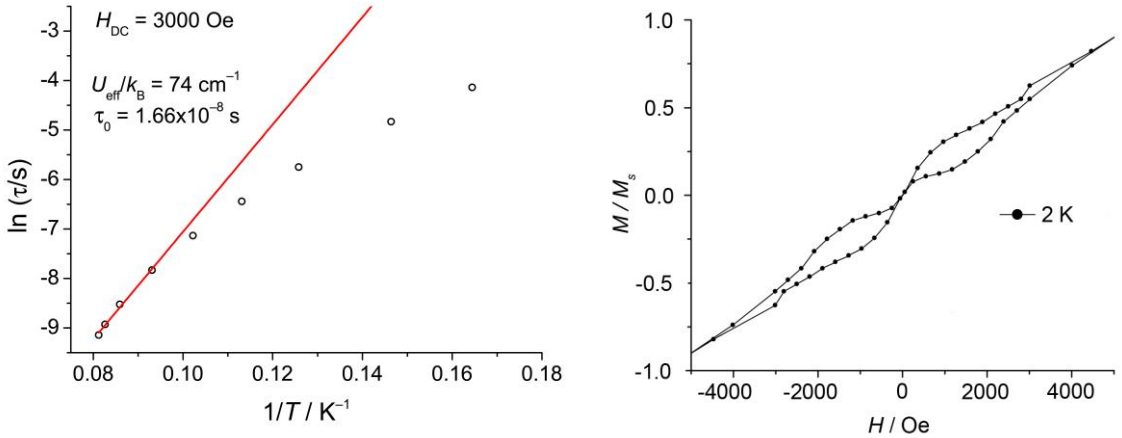

Figure 3.18: *left*) Arrhenius analysis of the relaxation process. *right*) Field dependence of the magnetisation at T = 2 K.

In summary, the foregoing results of the magnetic studies demonstrate conclusively that **6** is a rare example of a mononuclear complex that displays slow magnetic relaxation in the absence as well as in the presence of an applied field originating from the individual tetrahedrally coordinated Co(II) ion. Hence, compound **6** is a transition metal single ion magnet (SIM) and besides several SIMs containing single lanthanide or actinide ions that have been reported it is an extraordinary example for a designed SIM from a single transition metal ion.[58b]

3.2.5. [Ni{(N*t*Bu)$_3$SCH$_2$PPh$_2$}$_2$] (7)

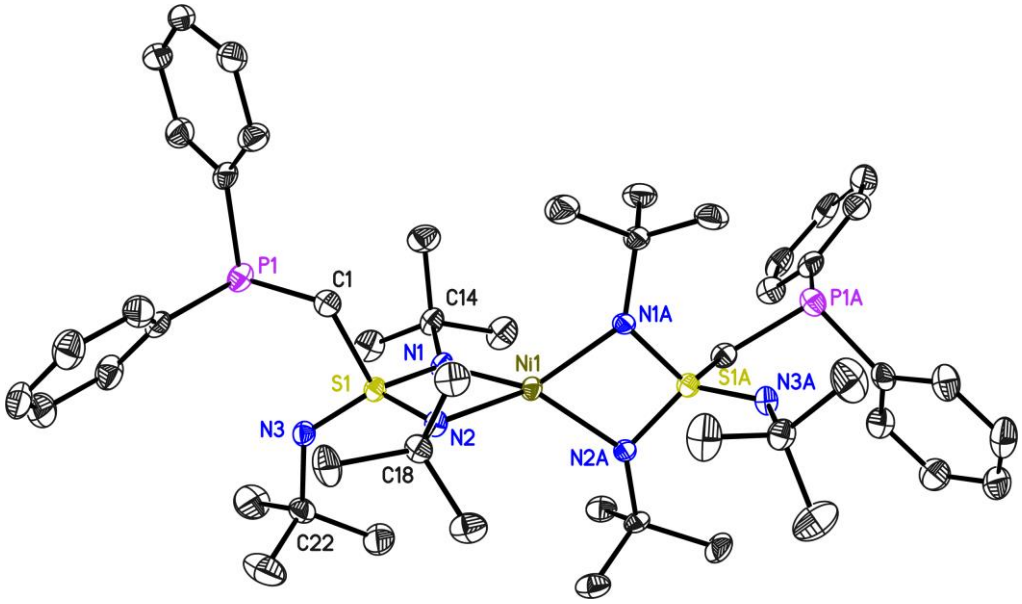

Figure 3.19: Crystal structure of [Ni{(N*t*Bu)$_3$SCH$_2$PPh$_2$}$_2$] (**7**). Anisotropic displacement parameters are depicted at the 50% probability level. Hydrogen atoms are omitted for clarity.

The metal complex **7** was obtained by a reaction of **1** with $NiBr_2$ in pentane according to Scheme 3–3. It was also obtained by a reaction of **1** with $NiCl_2$ but in lower yields due to the low solubility of $NiCl_2$ in pentane. The compound **7** crystallises in the monoclinic space group *C*2 with half a molecule in the asymmetric unit and the other half is generated by a twofold rotation axis. Selected bond lengths and angles are listed in Table 3.7.

Table 3.7: Selected bond lengths [pm] and angles [°] of **7**.

S1–N1	160.4(3)	Ni1···S1	269.84(8)
S1–N2	159.3(3)	N1–Ni1–N2	71.65(11)
S1–N3	152.0(3)	N1A–Ni1–N2	133.84(11)
Ni1–N1	198.5(3)	Ni1–N1–C14	134.3(2)
Ni1–N2	196.4(3)	Ni1–N2–C18	132.1(2)
P1–C1	184.7(4)	N1–S1–N2	92.64(14)
S1–C1	179.9(4)	Ni1–N1–S1–N2	–6.47(16)

In the crystal structure of **7** the central nickel(II) cation is located in a tetrahedral environment defined by the four nitrogen atoms from the two bidentate ligands. One would expect a square–planar geometry for a nickel(II) cation because for 16

valence electron complexes (eight metal electrons plus eight electrons from the two ligands) a square–planar geometry is more attractive since all bonded orbitals and no anti– bonded orbitals are occupied. However, the tetrahedrally distorted geometry in **7** is favoured because the bulky *t*butyl groups prevent planar coordination geometry at the nickel cation. The Ni1–N1/2 distances (198.5(3) and 196.4(3) pm) are in the normal range for fourfold coordinated high–spin nickel(II) complexes.[60] A search in the CSD for fourfold *N*–coordinated nickel complexes with an N–N–N–N torsion angle between 45° and 135° revealed an average Ni–N distance of 195.1 pm. A similar search for a torsion angle between 0° and 45° resulted in an average Ni–N distance of 190.2 pm. This shows clearly that the distances in tetrahedral and presumably high spin nickel(II) complexes are longer than in square–planar, low–spin complexes. Unfortunately, the magnetic moment of **7** could not be measured since the yields are poor and the compound does not crystallise purely. A recorded ^{1}H–NMR spectrum displays very diversely shifted broad signals that are typical for paramagnetic compounds. Hence, a low spin diamagnetic d^8 configuration can be excluded.

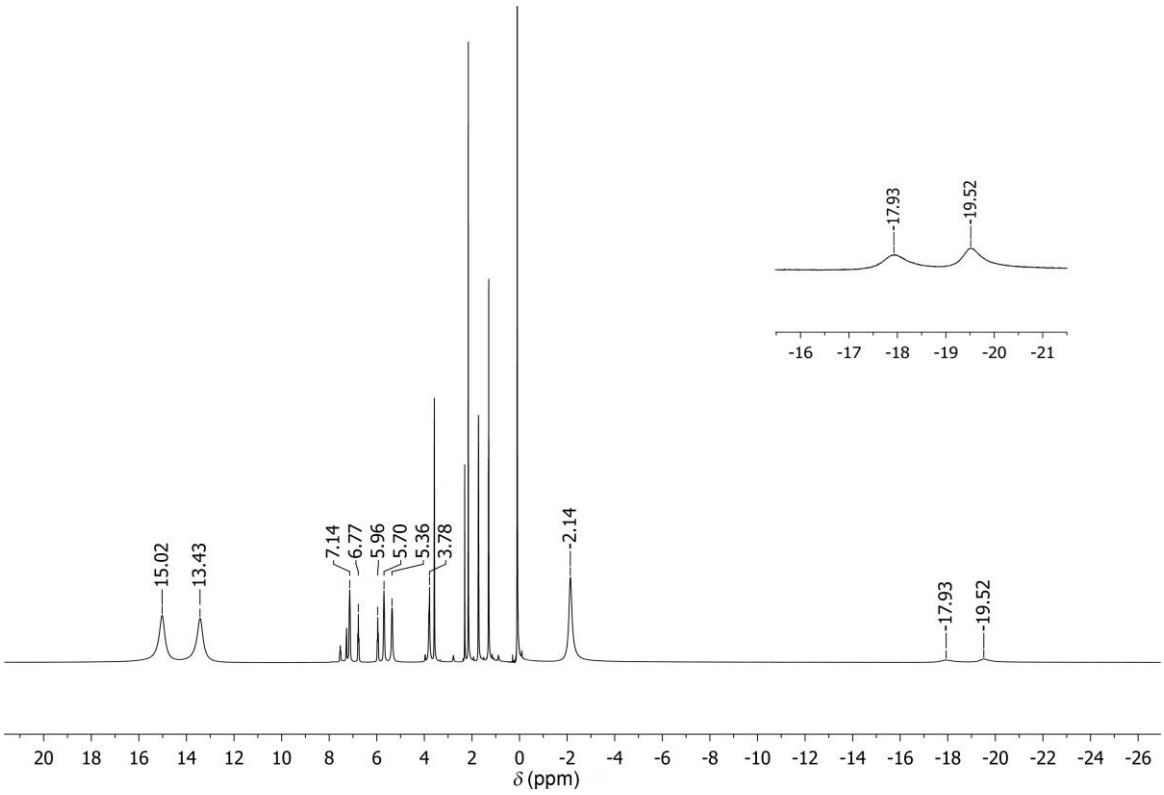

Figure 3.20: ^{1}H–NMR spectrum (300 MHz) of **7** recorded in THF–d_8. Peaks not marked with a shift are impurities of grease and small amounts of starting material.

A CSD search revealed that the coordination motif found in **7** is pretty rare. In fact, there is just one other crystal structure listed in the CSD which displays a *N,N*–chelated nickel(II) cation as a bridging atom between two four–membered rings.[37] The mononuclear nickel(II) amide, $[Ni(C_{12}H_{21}N_2Si)_2]$, has the Ni(II) atom *N,N'*–chelated by the *N*–silylated anilinide ligands, whereas the two ends of the NSiN chelating unit exhibit different affinities for the metal atom: the Ni–$N_{anilinide}$ and Ni–N_{amine} bond lengths are 191.3(3) pm and 218.7(3) pm, respectively (Figure 3.21).[61]

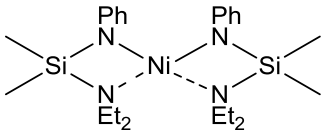

Figure 3.21: Bis{*N*–[(diethylamino)dimethylsilyl]–anilinido–κ^2*N,N'*}nickel(II).

Hence, the first molecular structure with a NiN_2S ring as a central structure motif could be obtained by synthesising compound **7** what underlines the potential of the ligand **1** to form unusual and novel coordination motifs.

3.2.6. [Cu{(NtBu)$_3$SCH$_2$PPh$_2$}$_2$] (8)

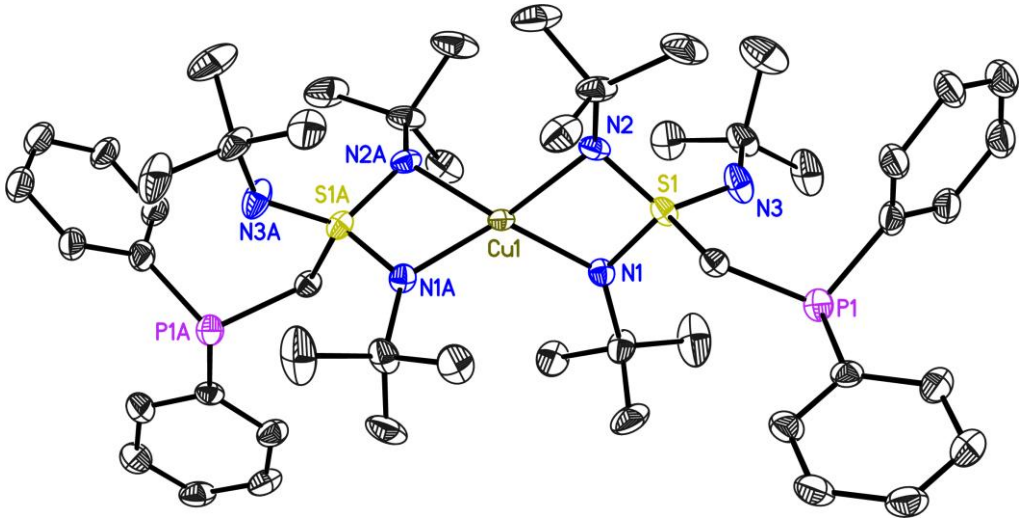

Figure 3.22: Crystal structure of [Cu{(N*t*Bu)$_3$SCH$_2$PPh$_2$}$_2$] (**8**). Anisotropic displacement parameters are depicted at the 50% probability level. Hydrogen atoms and disordered parts with the lower *sof* (the non–chelating N*t*Bu group and one phenyl ring) are omitted for clarity.

The reaction of ligand **1** with CuBr$_2$ in a 2:1 ratio in pentane led to a dark orange solution, from which dark orange crystals were obtained. The crystals are very sensitive and decomposition is observed even in the mother liquor after a couple of days, indicated by the formation of a green or black powder probably due to complex redox reaction between the copper and the sulfur atom. The complex of [Cu{(N*t*Bu)$_3$SCH$_2$PPh$_2$}$_2$] (**8**) crystallises in the monoclinic space group *C*2/*c* with half a molecule in the unit cell (Figure 3.22).

Table 3.8: Selected bond lengths [pm] and angles [°] of **8**.

S1–N1	160.42(16)	Cu1···S1	269.33(5)
S1–N2	159.78(18)	N1–Cu1–N2	72.01(7)
S1–N3	151.30(18)	N1A–Cu1–N2	144.05(7)
Cu1–N1	196.59(16)	Cu1–N1–C14	135.47(13)
Cu1–N2	200.52(16)	Cu1–N2–C22	125.44(14)
P–C1	186.1(2)	N1–S1–N2	93.62(8)
S1–C1	181.2(2)	Cu1–N1–S1–N2	–7.71(9)

8 is isostructural to the manganese complex **2** and the copper as well as the sulfur atom have a tetrahedral coordination sphere which displays a remarkable distortion for the copper(II) cation. This is indicated by the largest Cu1–N1–S–N2 torsion– and

N1A–Cu1–N2 angle of all here discussed structures (Table 3.8). The Cu1–N1/2 bond lengths (196.59(16) and 200.52(16) pm) are in the range of the average value (197.8 pm) that can be found in the CSD for fourfold coordinated tetrahedral copper(II) complexes and are in total agreement with values that are found in the literature.[60c,62]

3.2.7. [(tmeda)$Li_{0.79}$/$Cu_{2.21}$(μ–$Cl_{1.96}Br_{0.04}$){$Ph_2PCH_2S(NtBu)_3$}] (9)

It was reported that the reaction of the lithiated polyimido sulfur(IV) phosphanyl ligand [Li{$Me_2PCH_2S(NSiMe_3)_2$}]$_2$ and [Cu{$N(SiMe_3)_2$}] gave the copper(I) complex [{$Me_2PCH_2S(NSiMe_3)_2$}$_4$$Cu_8${CuS}$_4$].[13c] The formation of the {CuS}$_4$ cube is either due to ligand scrambling or to impurities in the starting material. To investigate if the ligand **1** is redox stable enough to stabilise a redox sensitive salt like CuCl, the ligand **1** was reacted with CuCl in a 1:1 ratio in pentane at room temperature (Scheme 3–7).

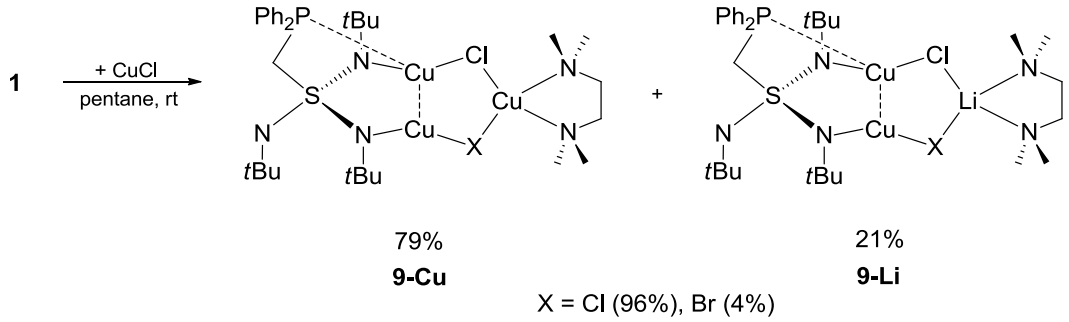

Scheme 3–7: Reaction of **1** with CuCl. There are two different complexes **9–Cu** and **9–Li** present due to a Cu/Li position disorder (*sof* 0.791(2)). Additionally, there is a Cl/Br disorder.

The reaction mixture turned dark red almost immediately and after one day dark red crystals were obtained suitable for X–ray analysis. The refinement of the high quality data–set revealed a quite astonishing structure (Figure 3.23).

First, the expected ligand scrambling due to the redox sensitive reagents was not observed.

Secondly, this is the first metal complex obtained from the lithiated ligand **1** in which both a *P*– and an *N*–donating side arm are active. Two imido groups coordinate to different copper(I) centres leading to an enlargement of the N1–S1–N3 bite angle (108.24(11)). The bulky *t*butyl group of the N3 atom is even twisted

out of the N1S1N3 plane, giving the phosphorus sting enough space to approach the Cu(I) cation.

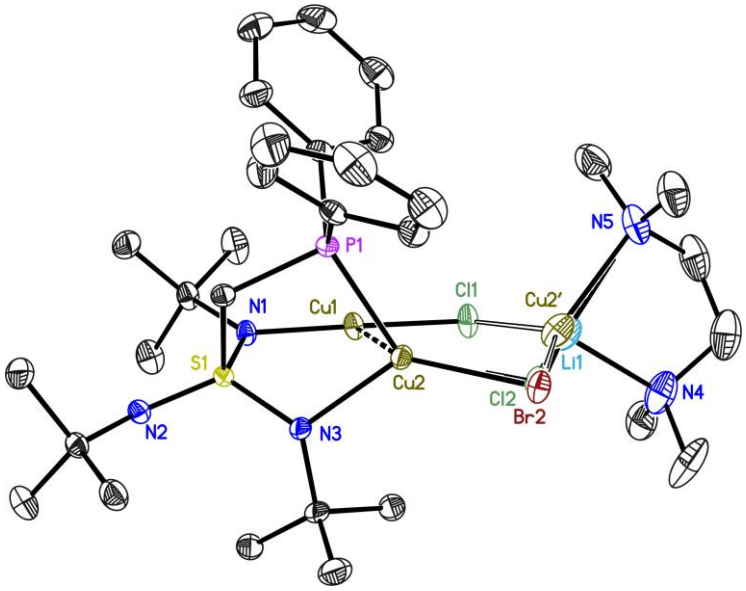

Figure 3.23: Crystal structure of compound **9**. The anisotropic displacement parameters are shown at the 50% probability level. Hydrogen atoms are omitted for clarity. The Li1 and Cu2' atoms are disordered with a *sof* of 0.791(2) and the Cl2 and Br2 atoms with a *sof* of 0.957(2). The TMEDA moiety is disordered on two positions (*sof*: 0.667(6)) which is not shown here for clarity.

Thirdly, instead of the expected salt–elimination a five–membered Cu_3Cl_2 ring was formed in which two copper(I) ions (Cu1 and Cu2) are coordinated by different imido donor groups of the ligand and the third copper(I) ion (Cu2') is connected *via* two chlorine bridges to the other copper cations (see Scheme 3–7, **9–Cu**). Only a few examples of comparable structural motifs are known from the literature.[63]

Fourthly, the lithium cation was not completely eliminated during the synthesis. The refinement of the high quality X–ray data revealed that there are two position disorders in the compound. The first position disorder is a Cu/Li disorder with a site occupation factor of 0.791(2). The second disorder is a Cl/Br disorder with a site occupation factor of 0.957(2) what is quite surprising since CuCl and not CuBr was used in the synthesis. An explanation might be that either the ligand **1** was contaminated with LiBr or the CuCl salt with CuBr. Lithium bromide is formed during the synthesis of $S(NtBu)_3$ and is filtered off. Moreover, $S(NtBu)_3$ as well as the following product $[(tmeda)Li\{(NtBu)_3SCH_2PPh_2\}]$ (**1**) are purified by crystallisation. Still, the presence of LiBr cannot be excluded for sure.

Selected bond lengths and angles of the not disordered parts are listed in Table 3.9. The Cu1 atom is coordinated in a trigonal planar fashion by the N1, Cl1 and Cu2

atoms. The Cu1–Cu2 distance is 277.10(7) pm long and above the average Cu–Cu distances found in the CSD (Figure 3.24). Shorter Cu–Cu distances were characterised as d^{10}–d^{10} metallophilic bonding, comparable to aurophilic Au(I)–Au(I) interactions and were even found in unsupported Cu(I)–Cu(I) dimers.[63a,64] However, it should be pointed out, that the close proximity of the metal centres in **9** is a consequence of the small bite angle of the ligand that brings the Cu1 and Cu2 atoms close together, leading to an intermetal distance that may be a phenomenon of a lack of antibonding rather than due to a significant attractive interaction.[65]

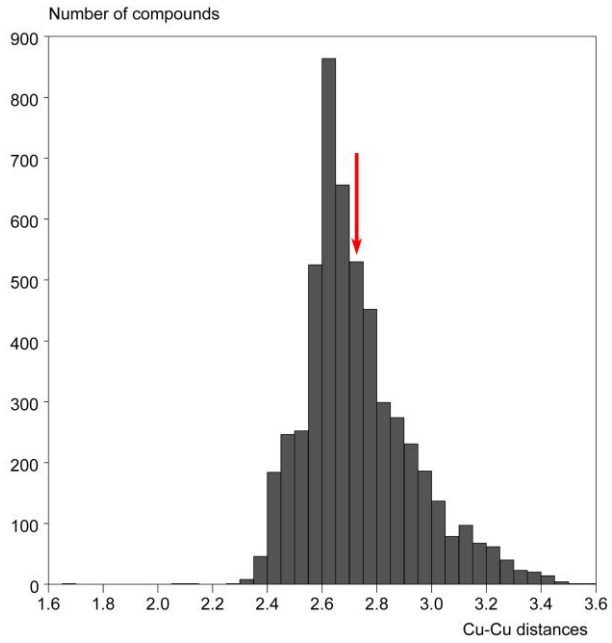

Figure 3.24: Cu–Cu distances reported in the CSD. The minimum and maximum values are 1.677 and 3.575 Å. The mean value is 2.732 Å.

The Cu1–Cl1 (212.57(8) pm) and Cu1–N1 (188.23(19) pm) distances are another hint for the absence of a Cu1–Cu2 interaction because they are closer to the average values for twofold coordinated than threefold coordinated copper chlorine compounds. The average Cu–Cl and Cu–N distances for twofold coordinated copper complexes are 210.8 pm and 188.0 pm in comparison to 233.8 pm and 197.5 pm for threefold coordinated copper complexes.[37] The Cu1–N1 distance (188.23(19) pm) is shorter in comparison to the Cu2–N3 distance (204.8(2) pm) due to the lower coordination number of the Cu1 atom. The Cu2–N3 as well as the Cu2–P1 distances are in the normal range and comparable to the distances in other copper compounds. The S–N distances do not differ significantly from the distances

described in the previous structures and the geometry at the sulfur atom is still tetrahedrally distorted.

Table 3.9: Selected bond lengths [pm] and angles [°] of **9**.

S1–N1	159.80(19)	Cu1···Cu2	277.10(7)
S1–N3	158.7(2)	Cu1–Cl1	212.57(8)
S1–N2	151.18(19)	N1–S1–N3	108.24(11)
Cu1–N1	188.23(19)	N2–S1–N3	123.24(11)
Cu2–N3	204.8(2)	N2–S1–N1	107.93(10)
P1–Cu2	220.59(7)	S1–C1–P1	112.53(13)

To conclude, with the synthesis of complex **9** a new coordination pattern of the polyimido sulfur phosphanyl ligand was discovered. Principally, it is possible to activate more donor atoms of the ligand than just the *N,N*–chelating claw as in the previously described structures **2** to **8**. A complete salt–elimination reaction as observed for the reaction with $CuBr_2$ is not preferred for CuCl. A clear drawbrack are the Cu/Li and Cl/Br disorders. Attempts to remove the lithium completely by using CuCl or CuBr in access or refluxing the reaction mixture ended either in complete decomposition of the ligand or in co–crystallisation of CuS. Hence, resynthesis of the compound is challenging and further reactions with **9** could not be investigated.

3.2.8. [Zn{(N*t*Bu)$_3$SCH$_2$PPh$_2$}$_2$] (10)

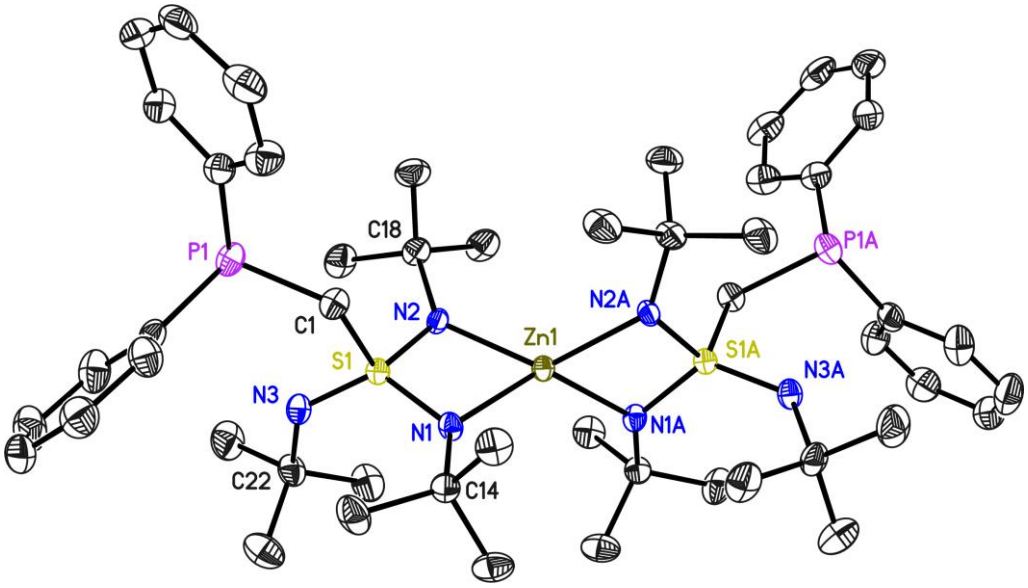

Figure 3.25: Crystal structure of [Zn{(N*t*Bu)$_3$SCH$_2$PPh$_2$}$_2$] (**10**). Anisotropic displacement parameters are depicted at the 50% probability level. Hydrogen atoms are omitted for clarity.

The latest transition metal of the first row is zinc that differs from the other transition metals because of its filled d shell. A reaction of **1** with $ZnBr_2$ gives the metal complex **10** (Scheme 3–3) that is isotypical to the structures **2**, **3**, **4**, **7** and **8** (Figure 3.25). **10** crystallises in the monoclinic space group *C*2. In the crystal structure, two ZnN_2S four–membered rings are connected *via* the zinc(II) cation with a torsion angle of 85.69°. The zinc(II) ion as well as the sulfur atom display tetrahedral coordination. A tetrahedral environment is clearly preferred by d^{10} cations, in agreement with the 18–electron rule, although there are also numerous square–planar Zn^{2+} complexes with porphyrin or other macrocyclic ligands.[66] The symmetry independent Zn–N distances (200.5(2) and 201.3(2) pm) are comparable with similar coordinated zinc complexes like [Zn{(N*t*Bu)$_3$SMe}$_2$] (Figure 3.26) and [Zn{*p*–MeC$_6$H$_4$S(O)N(*t*Bu)$_2$}$_2$].[67] They can be classified between covalent bonds as in [Zn{NSiMe$_3$}$_2$] (182 pm, determined by gas electron diffraction) analysed by *Power et al.*[68] and dative bonds (212–216 pm) as, for example in bis(1,4–dihydropyridin–

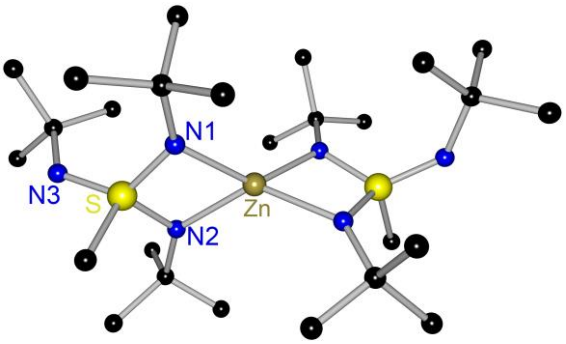

Figure 3.26: Molecular structure of [Zn{(N*t*Bu)$_3$SMe}$_2$].

1–yl)bis(pyridine)zinc.[69] Further, the bond lengths and angles of the sulfur–nitrogen moiety in the zinc complex **10** and of the previously mentioned methyl substituted analoga [Zn{(N*t*Bu)$_3$SMe}$_2$] do not differ significantly from each other.

Among the here presented transition metal complexes of the *S*–phosphanly–triimidosulfonate ligand, the zinc compound **10** is the only compound that shows a sharp signal in the ^{31}P–NMR spectrum. Due to the paramagnetic character of **2**, **3**, **4**, **7** and **8**, no ^{31}P signal or just broad and highly shifted signals could be detected. The ^{31}P signal of **10** (–24.87 ppm) does not differ significantly from the signal of the lithiated compound **1** (–24.18 ppm). The ^{1}H signals of the bridging methylene group (S–C*H*$_2$–P) in the ^{1}H–NMR spectrum are the best indicator to differentiate between both structures because they show significantly different shifts (3.98 ppm for **1** and 4.22 ppm for **10**). The ^{1}H–NMR spectrum of **10** also displays different signals for the chelating and non–chelating N*t*Bu groups (1.26 and 1.40 ppm; for details, see section 5.3.10.).

Table 3.10: Selected bond lengths [pm] and angles [°] of **10**.

S1–N1	159.5(2)	Zn1···S1	271.73(7)
S1–N2	160.4(3)	N1–Zn1–N2	71.35(9)
S1–N3	152.2(3)	N1A–Zn1–N2	133.25(9)
Zn1–N1	200.5(2)	Zn1–N1–C14	133.63(19)
Zn1–N2	201.3(2)	Zn1–N2–C22	134.63(19)
P1–C1	184.9(3)	N1–S1–N2	94.20(12)
S1–C1	180.7(3)	Zn1–N1–S1–N2	–4.72(13)

3.2.9. Structural comparison of 2, 3, 4, 7, 8 and 10

First row transition metals were used to obtain the isotypical metal complexes [M{(N*t*Bu)$_3$SCH$_2$PPh$_2$}$_2$] (M = Mn (**2**), Fe (**3**), Co (**4**), Ni (**7**), Cu (**8**), Zn (**10**)). The S–N, M···S and N–M distances as well as the N–M–N bond angles are listed in Table 3.11 to compare the structural features and to investigate the influence of the coordinated metal cation on the geometry of the ligand. Further, the included angle *φ* between the two NMN planes and the distance *d* from the metal cation to the N1S1N2 plane are given and compared (Scheme 3–8). The parameters are also illustrated in Diagram 1 and 2 for a better overview.

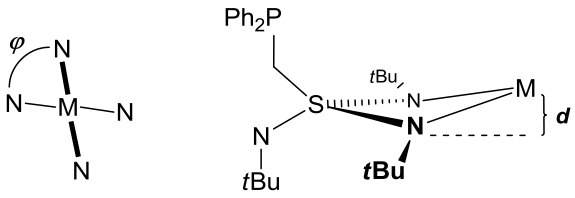

Scheme 3–8: Illustration of the angle *φ* and the distance *d*. The angle *φ* has to be 90° for an ideal tetrahedral environment of the metal ion.

Based on these parameters the following observations and conclusion can be made:

First, the choice of the metal cation does not have an effect on the ligands sphere since the S–N distances and N–S–N angles do not differ significantly within the row. Secondly, the M–N and M–S distances are shortened from **2** (Mn) to **3** (Fe) and the N1–M–N2 bite angle increases, reflecting the differing ionic radii of Mn(II) and Fe(II).[70] The slight variances of the bond lengths from **3** (Fe) to **10** (Zn) go also hand in hand with the radii, respectively.

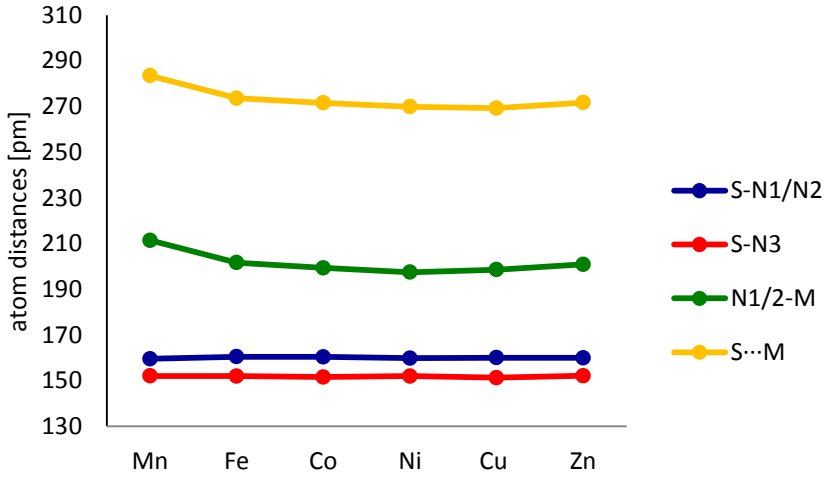

Diagram 1: A summarised overview of selected distances of **2** (Mn), **3** (Fe), **4** (Co), **7** (Cu), **8** (Ni) and **10** (Zn). For detailed values see also Table 3.11.

Thirdly, the drift of the included angle *φ* from the ideal tetrahedral value of 90° reflects the distortion of the complexes from a tetrahedral to a square–planar geometry at the metal centre. While in the compounds **2** (Mn), **3** (Fe), **4** (Co), **7** (Ni) and **10** (Zn) the included angle *φ* does not differ dramatically from 90° the deviation in the copper complex **8** is obvious (φ = 62°), indicating a change from tetrahedral into a more planar coordination sphere.

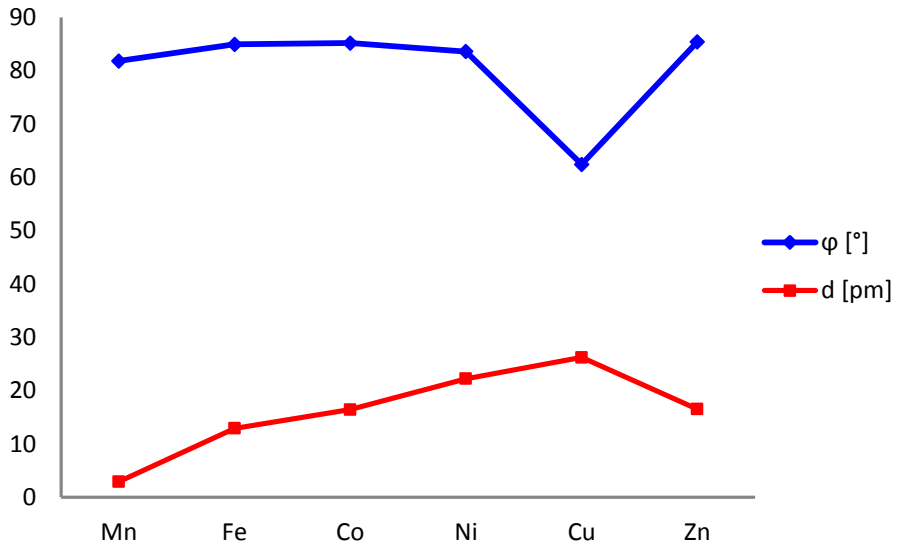

Diagram 2: Course of the angle *φ* and distance *d* within the row of **2** (Mn), **3** (Fe), **4** (Co), **7** (Ni), **8** (Cu) and **10** (Zn). For more precise values see also Table 3.11.

Copper(II) complexes with octahedral and tetrahedral geometries are well known to be *Jahn–Teller* active since the copper(II) cation is a d^9 metal with one single occupied d orbital.[71] While octrahedral copper(II) complexes exhibit the well–known *trans*–elongation, in tetrahedral examples the *Jahn–Teller* distortion and splitting of the t_2 orbital manifold is reflected in the bond angles about the metal ion, rather than its bond lengths.[71b,72] The splitting of the d energy levels in a tetrahedral ligand field (T_d symmetry) relatively to a tetrahedrally compressed ligand field (D_{2d} symmetry) is depicted in Scheme 3–9. The distortion of the tetrahedral geometry causes a stabilisation of the d_{z^2}, d_{xz} and d_{yz} orbitals of the metal

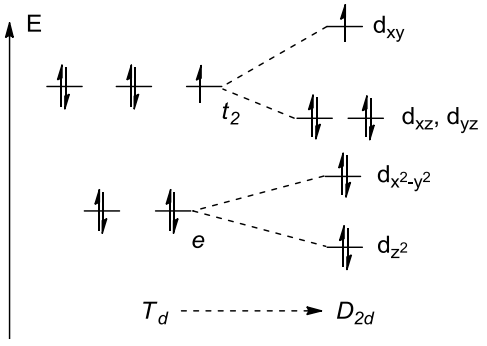

Scheme 3–9: Splitting of the d energy levels in a tetrahedrally compressed ligand field. The splittings between the energy levels are indicative only, and are not drawn on scale.

with respect to the tetrahedral t_2 and e state. The $d_{x^2-y^2}$ and d_{xy} orbitals instead are destabilised by a more planar coordination. An overall stabilisation energy results from this geometrical arrangement because the higher energy orbital d_{xy} houses just on electron while the stabilised orbitals are occupied with two electrons. The total square–planar geometry (D_{4h} symmetry) is not achieved because of the steric and electronical repulsion between the ligands and the metal cation.[72b,73]

Table 3.11: Selected parameters of the complexes **2**, **3**, **4**, **7**, **8** and **10**. Distances are given in [pm] and angles in [°].

	$r(M^{2+})^a$	S–N1/2[b]	S–N3	M–N1/2[b]	M···S	N–M–N	φ	d
2 (Mn)	80	159.58(17)	152.22(17)	211.44(17)	283.51(5)	67.61(6)	81.78	2.9
3 (Fe)	77	160.5(3)	152.0(3)	201.65(20)	273.63(7)	71.00(10)	84.91	12.9
4 (Co)	72	160.4(2)	151.6(2)	199.35(2)	271.70(7)	71.53(10)	85.16	16.4
7 (Ni)	69	159.9(3)	152.0(3)	197.45(3)	269.84(8)	71.65(11)	83.57	22.2
8 (Cu)	71	160.10(18)	151.30(18)	198.56(10)	269.33(5)	72.01(7)	62.39	26.2
10 (Zn)	74	160.0(3)	152.2(3)	200.9(2)	271.73(7)	71.35(9)	85.38	16.5

a) The radii $r(M^{2+})$ refer to tetrahedrally coordinated metal cations in the high–spin state.[74]
b) The average values are given.

Fourthly, it can be seen from the Table 3.11 and Diagram 2 that the distance d between the N1S1N2 plane and the metal cation has a maximum of 26.2 pm for the copper complex, too. A superposition plot of the complexes **2**, **8** and **10** is displayed in Figure 3.27 to illustrate the deviation. The dislocation of the metal ion from the N1S1N2 plane is unusual because it moves two positively charged centres (the sulfur atom and the metal(II) cation) in closer proximity. The Cu · · · S distance is indeed the shortest one in the row (269.33(5) pm).

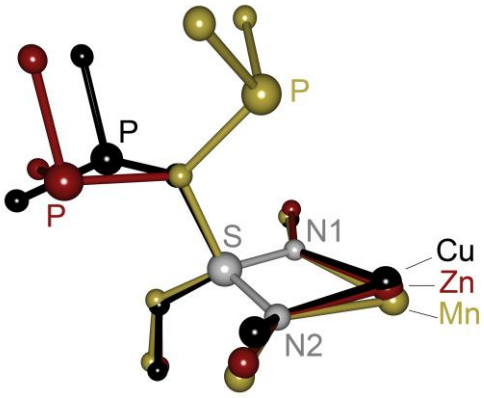

Figure 3.27: Superposition plot of the **2**, **8** and **10**. The atoms N2, S1 and N1 are fitted onto each other.

The phenomenon of the out of plane coordination has been observed in heavier alkaline earth metal complexes of benzamidinates, aminoiminodiphenylphosphinates and triazasulfite and was interpreted as an indication of increasing π–interactions between the soft and easy to polarise metal ions and the ligand.[75] Here, the deviation is not as pronounced as in the heavier

alkaline earth metals and is more a steric effect what is indicated by the M–N distances and the angle φ. The copper complex **8** displays not only the smallest included angle and one of the shortest M–N distances but also the most pronounced deviation. The compounds **4** (Co) and **10** (Zn) have nearly the same M–N distances and angle φ and show nearly the same deviation from the N1S1N2 plane. The included angle φ of **3** (Fe) is comparable to **4** and **10** and the M–N distances are slightly longer, what reduces the steric strain. Therefore, the deviation is a little less pronounced. The nickel complex **7** displays a similar angle φ but the shortest M–N distances within the row, causing a steric strain that pushes the Ni^{2+} cation relatively far out of the N1S1N2 plane. In contrast to that, the Mn^{2+} cation lies almost perfectly in the plane although the included angle φ is smaller than in **3**, **4**, **7** and **10**. The steric strain is reduced by the longest M–N distances within the row.

Nonetheless, interactions between the metal ions and the delocalised π–system of the N1S1N2 moiety cannot be excluded. Possible arrangements of the ligand and metal d orbitals are depicted in Scheme 3–4, p. 21. These interactions would involve a contribution of the 4s and 4p orbitals since the zinc(II) cation has a filled d shell but also shows the deviation out of the N1S1N2 plane. Another possibility would be some kind of π backbonding from the filled d orbitals of the metal to vacant ligand orbitals.

To summarise, starting from **1** different first row transition metal complexes were synthesised. The complexes **2**, **3**, **4**, **7**, **8** and **10** are isotypical and show only marginal differences in their geometry. The copper complex **8** differs from the geometry of the other transition metal complexes more significant because of its d^9 electron configuration and the implied *Jahn Teller* distortion. Further, the choice of the first row transition metal halide does not have an influence on the coordination pattern of the ligand. The copper(I) complex **9** proved that metals in other oxidation states can yield in a diverse and unique coordination motif. Also a variation of the solvent can make a difference as it was shown for the transformation of **1** with $CoBr_2$ in a mixture of pentane and THF.

3.3. Main group metal complexes of 1

After reactions of [(tmeda)Li{(N*t*Bu)$_3$SCH$_2$PPh$_2$}] (**1**) with first row transition metals were studied, the horizon of the periodic table of elements was expanded to main group elements. $MgCl_2$ was the first reagent which was tried to react with **1** because of the diagonal relationship between lithium and magnesium in the periodic table of elements. However, a reaction of **1** with neither $MgCl_2$ nor $MgBr_2$ in different solvents (pentane, THF and toluene) was successful, yielding in hydrolyses of the ligand or crystallisation of starting material. Probably, the magnesium salts are too hygroscopic, although they were stored under inert gas conditions and used with extensive care.

Reactions of **1** with $AlClMe_2$ or $AlMe_3$ were also tried to afford a monomeric dimethyl or chloromethyl aluminium compound like [$AlMe_2${(N*t*Bu)$_3$SCH$_2$PPh$_2$}] or [AlClMe–{(N*t*Bu)$_3$SCH$_2$PPh$_2$}]. Even a *P,N,N*–coordination motif as in the aluminium dimethyl complex [PNN]$AlMe_2$ published by *Liang et al*.[76] was conceivable (Figure 3.28, **a**).

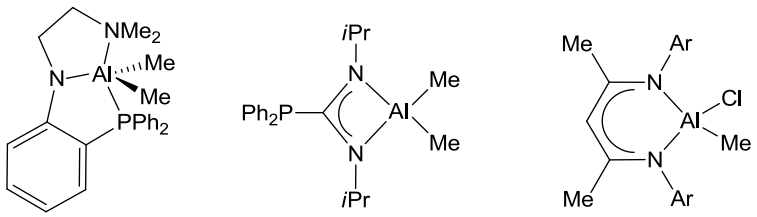

a **b** **c**

Figure 3.28: a) Example for an aluminium complex with a *P,N,N*–ligand. **b**, **c**) Aluminium complexes obtained *via* salt–elimination of LiCl.

$AlClMe_2$ has already been applied successfully in salt–elimination reactions like, for example, in the synthesis of aluminium phosphaguanidinate compounds [$AlMe_2$(Ph_2PC{N*i*Pr}$_2$)][77] and *β*–diketiminate methylaluminum chloride (Figure 3.28, **b** and **c**).[78] Unfortunately, the transformations of **1** with $AlMe_3$ and $AlClMe_2$ turned out to be not fruitful, yielding in decomposition of the ligand, indicated by numerous peaks in the ^{31}P–NMR spectra.

Finally, the application of group 14 metal halides $GeCl_2$ and $SnBr_2$ was successful, even though *Fleischer* investigated similar reactions of [Li$_4${(N*t*Bu)$_3$S}$_2$] with group 14 metal(II) halides that resulted in decomposition of the [S(N*t*Bu)$_3$]$^{2-}$ dianion.[34a]

The preparation of the desired complexes *via* salt–elimination reactions from the lithiated ligand **1** with $GeCl_2 \cdot$dioxane and $SnBr_2$, respectively, in molar ratio 1 : 1 has been performed according to Scheme 3–10 in rather good yields. The reactions were conducted in pentane, yielding pure and colourless crystals after a crystallisation time between one and two weeks. The formation of a heteroleptic metal(II) halide compound is also observed when the reagents are used in a 2:1 ratio.

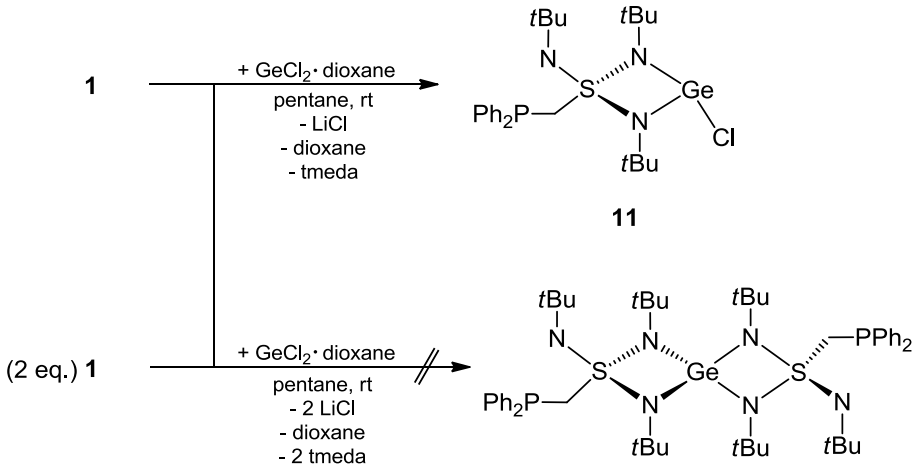

Scheme 3–10: Synthesis of $[GeCl\{(NtBu)_3SCH_2PPh_2\}]$ (**11**). The preparation of $[SnBr\{(NtBu)_3SCH_2PPh_2\}]$ (**12**) is similar, with $SnBr_2$ instead of $GeCl_2$ as a reagent.

Metal halide complexes of heavier group 14 elements with the metal atom in a lower oxidation state are of fundamental interest in main group chemistry. They can be seen as *Lewis* amphoters as they are equipped with nucleophilic (lone pair of the metal(II) cation) and electrophilic (vacant p orbital) reactive sites at the metal(II) atom. Further, they are important precursors for a variety of promising compounds. To stabilise the metal ion in a low oxidation state, *β*–diketiminate ligands and ligands based on amidinates and guanidinates were mainly used as backbones.[79]

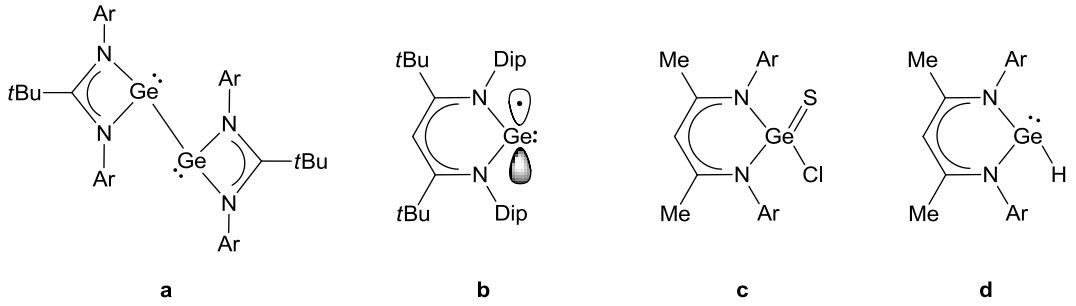

Figure 3.29: a) Neutral germanium(I) dimer, **b**) neutral, monomeric germanium(I) radical, **c**) sulfur oxidized germylene mono chloride, and **d**) germylene hydride.

The germanium(II) chloride [GeCl(Piso)] (Piso = $[(ArN)_2Ctert Bu]^-$), for example, is the precursor to the neutral germanium(I) dimer $[\{Ge(Piso)\}_2]$ (Figure 3.29, **a**) and salt–elimination reactions have yielded the monomeric complexes $[Ge(Piso)(NiPr_2)]$ and $[\{Ge(Piso)\}FeCp(CO)_2]$.[80] *Jones et al.* also reported the synthesis of a neutral, monomeric germanium(I) radical (Figure 3.29, **b**) by the reduction of a bulky *β*–diketiminato germanium(II) chloride complex with either sodium naphthalenide or the magnesium(I) dimer $[\{Mg(Mesnacnac)\}_2]$.[81] The metathesis reaction between $[(Mes)_2DAP]MCl$ and sodium azide affords the azido compounds $[(Mes)_2DAP]MN_3$ (with M = Ge or Sn).[82] The monomeric threefold coordinated (amidinato)tin chloride $[SnCl\{PhC(NtBu)_2\}]$ was treated with $Fe_2(CO)_9$ to afford the *Lewis* acid–base adduct $[SnCl\{PhC(NtBu)_2\}]Fe(CO)_4$.[83]

The oxidation of germylene mono chlorides with elemental sulfur and selenium gave germanethioacid chloride and germaneselenoacid chloride, respectively (Figure 3.29, **c**).[84] The reduction of *β*–diketiminato germylene monochloride to stable terminal germylene hydride is possible by the addition of 1 molar equivalent of $AlH_3 \cdot NMe_3$ (Figure 3.29, **d**).[85]

These are just a few examples for a variety of reactions which use halides of group 14 metal complexes as starting material. The group of germanium(II) and tin(II) halides stabilising ligands is expanded by two new complexes $[GeCl\{(NtBu)_3SCH_2PPh_2\}]$ (**11**) and $[SnBr\{(NtBu)_3SCH_2PPh_2\}]$ (**12**) that are presented in the following chapter.

3.3.1. [GeCl{(NtBu)$_3$SCH$_2$PPh$_2$}] (11)

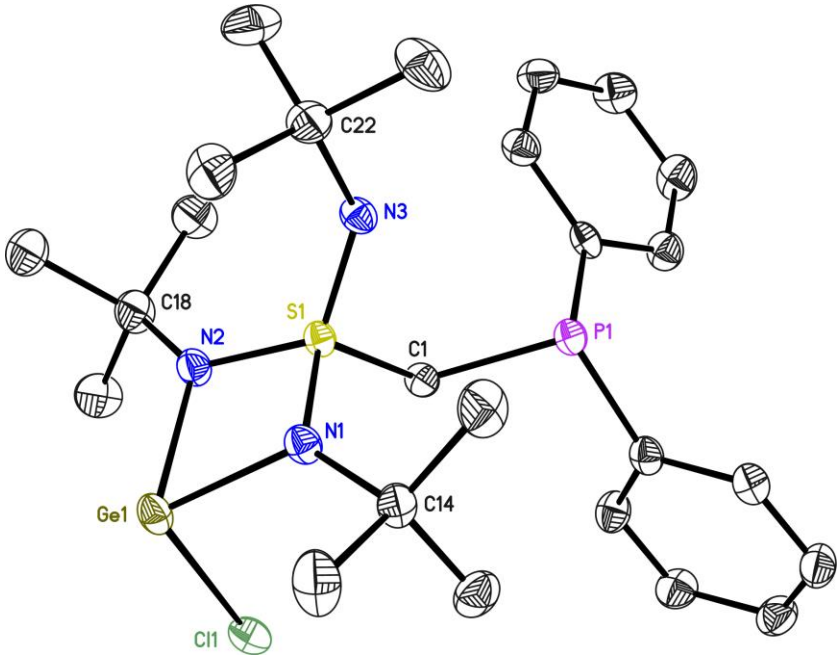

Figure 3.30: Crystal structure of [GeCl{(N*t*Bu)$_3$SCH$_2$PPh$_2$}] (**11**). Anisotropic displacement parameters are depicted at the 50% probability level. Hydrogen atoms and the disordered part of the *t*butyl group (C18) with the lower *sof* are omitted for clarity.

The germanium complex **11** crystallises in the monoclinic space group $P2_1/n$ with one molecule in the asymmetric unit (Figure 3.30). Its molecular structure consists of a four–membered GeN$_2$S ring with a distorted trigonal pyramidal coordinated germanium(II) cation and a Ge1–Cl1 bond almost orthogonal to the GeN$_2$S ring. The *N,N*–chelating mode of **1** is maintained and the phosphorus atom does not interact with the metal(II) cation. The germanium atom is displaced from the N1S1N2 plane by about 29.1 pm what has been observed previously for other germanium complexes.[82,86]

Table 3.12: Selected bond lengths [pm] and angles [°] of **11**.

S1–N1	161.5(2)	Ge1–Cl1	236.33(7)
S1–N2	161.2(2)	Ge1···S1	272.49(7)
S1–N3	149.7(2)	N1–Ge1–N2	71.15(8)
Ge1–N1	197.0(2)	N1–S1–N2	90.18(10)
Ge1–N2	195.7(2)	Ge1–N1–C14	128.12(15)
P1–C1	186.5(2)	Ge1–N2–C18	130.9(3)
S1–C1	180.3(2)	N2–S1–N1–Ge1	8.58(10)

The Ge1–N1/2 bond lengths are slightly shorter than the mean Ge–N distances (198.9 pm) found for threefold coordinated, *N,N*–chelated germanium compounds in the CSD (Table 3.12).[37] Together with the N1–Ge1–N2 angle they are similar to those reported for Ge(II) complexes of *β*–diketiminate, amidinate, guanidinate or phenylamidinate, for example.[79b,80a,84a,86a,87] The Ge1–Cl1 distance of 236.33(77) pm is longer than the average Ge–Cl distance (222.3 pm) found in the CSD but still within the normal range (Figure 3.31).[37]

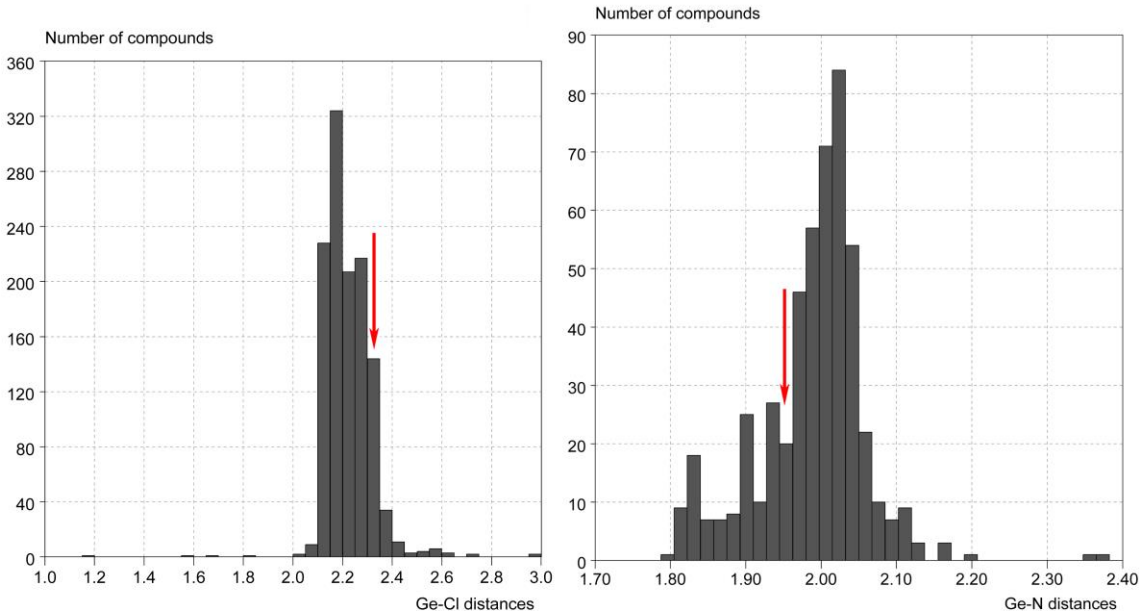

Figure 3.31: *left*) Ge–Cl distances [Å] of all germanium containing crystal structures reported in the CSD. The minimum and maximum values are 1.170 and 2.985 Å. *right*) Ge–N distances [Å] of all threefold coordinated, *N,N*–chelated germanium crystal structures reported in the CSD. The minimum and maximum values are 1.795 and 2.371 Å. The red arrow marks the values of **11**.

The S1–N1/2 distances are slightly elongated and the N1–S1–N2 angle is more acute in **11** relatively to the already discussed metal complexes of sulfur triimide. Moreover, the S1–N3 bond length of 149.7(2) pm is shorter than in the previously reported transition metal complexes and in the lithiated ligand **1**. This is probably due to the electron–withdrawing GeCl moiety. The chlorine atom has a fairly high electronegativity and its electron withdrawing property lowers the electron density at the N1 and N2 atoms and consequently also at the sulfur atom. Since the N1 and N2 atoms are sp^2 hybridised, the geometry would allow an interaction between the N_{pz} and the antibonding σ^*(Ge1–Cl1) orbital (Figure 3.32). This interaction would shorten the Ge1–N1/N2 and elongate the Ge1–Cl1 bond lengths. Further, the S1–N1/2 distances would be elongated because the electrostatic interactions between

the sulfur atom and the metal cation chelating nitrogen atoms would decrease. Consequently, this would lead to an increase of the electrostatic interactions between the S1 and the N3 atom and hence, to a shorter S–N3 bond distance. The plot displayed in Figure 3.31 illustrates that the Ge1–N and Ge1–Cl1 bond lengths in **11** are under and above the average distances found in the CSD. Nevertheless, quantum mechanical calculations would be necessary to prove this assumption and to estimate the influence of such an interaction.

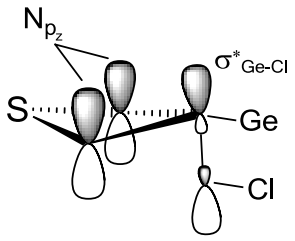

Figure 3.32: Interaction between the N_{pz} and the antibonding σ^*(Ge–Cl) orbital.

Attempts to oxidise **11** with sulfur or reduce it with K–selectride were not successful. No crystals could be isolated of the reaction mixture and the ^{31}P–NMR spectra showed several signals that could not be assigned to a product. Reactions with $[(arene)RuCl_2]_2$ and $[Rh(OAc)_2]_2$ were tried to activate the *P*–donor functionality of the ligand, but just a brownish powder was obtained that could not be characterised.

3.3.2. [SnBr{(N*t*Bu)$_3$SCH$_2$PPh$_2$}] (12)

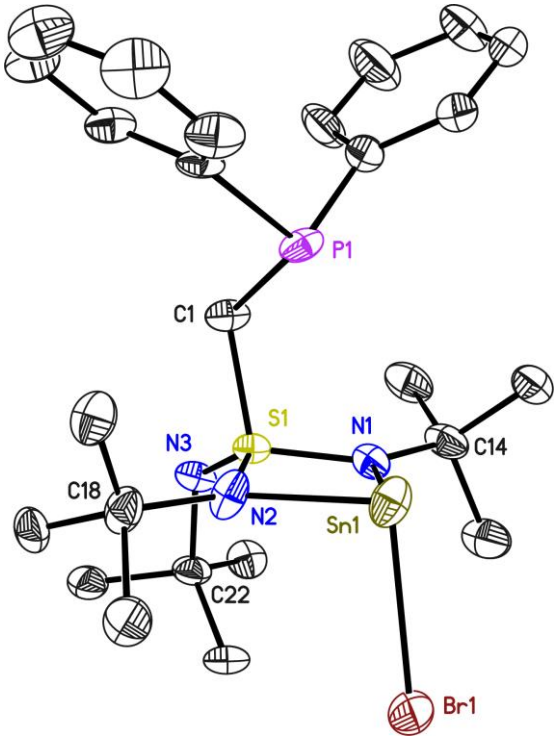

Figure 3.33: Crystal structure of [SnBr{(N*t*Bu)$_3$SCH$_2$PPh$_2$}] (**12**). Anisotropic displacement parameters are depicted at the 50% probability level. The phosphorus side arm and the *t*butyl groups of the carbon atoms C18 and C22 are disordered on two positions. Hydrogen atoms and disordered parts with the lower *sof* are omitted for clarity.

The tin complex **12** shown in Figure 3.33 was prepared according to the reaction depicted in Scheme 3–10. First, it was tried to synthesise a tin(II) halide complex, starting from $SnCl_2$ similar to the reaction with $GeCl_2 \cdot$ dioxane. Unfortunately, it turned out to be challenging. $SnCl_2$ is nearly insoluble in pentane and a change of the solvent to toluene or the addition of a small amount of THF resulted in crystallisation of a [(tmeda)$SnCl_2$] complex or led to the formation of an oily product. It could not be analysed by NMR spectroscopy because it precipitated in THF–d_8 and $CDCl_3$ and was not soluble enough in toluene–d_8. Hence, $SnBr_2$ was used instead because it is more soluble in pentane and after a crystallisation time of two weeks compound **12** could be isolated as colourless crystals in good yields. Both compounds show one signal with similar shifts in the ^{31}P–NMR spectrum (–23.92 ppm (**11**) and –27.45 ppm (**12**)). A shift for a ^{119}Sn signal cannot be given because the detected signal is too broad.

As it has already been indicated at the beginning of the chapter, there are numerous reports known on the synthesis of chloro derivatives of compounds with low valent

group 14 elements but the reports on tin(II) bromides compounds are limited. In fact, only two comparable structures were found in the CSD, reported by *Lappert et al.* in 2004[88] and *Roesky et al.* in 2010.[89] In both tin(II) bromides complexes the *β*–diketiminate ligand is used as a backbone (Figure 3.34).

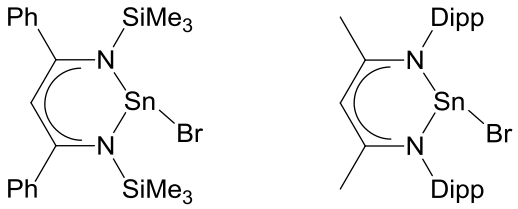

Figure 3.34: Two tin(II) bromides containing nacnac complexes reported by *Lappert* (**a**) and *Roesky* (**b**).

The compound **12** crystallises in the monoclinic space group $P2_1/n$ with one molecule in the asymmetric unit. The central structural motif is similar to **11**. The four–membered SnN_2S ring with bromine almost perpendicular to the ring is a novel structural motif. The S–N distances differ only marginally from the distances in **11**. The N1–Sn1–N2 angle (64.65(9)°) is smaller than the corresponding angle in **11** (71.15(8)°) and, as expected, the Ge1–N1/2 bond lengths (197.0(2) and 195.7(2) pm) in **11** are slightly shorter than the corresponding Sn1–N1/2 bond lengths in **12** (216.9(2) and 216.5(3) pm). This reflects the different atomic radii of the two elements (Ge(II) 93 pm, Sn(II) 112 pm) and the decreasing ionic interactions of the central metal atom with the ligand.[89]

Table 3.13: Selected bond lengths [pm] and angles [°] of **12**.

S1–N1	160.2(3)	Sn1–Br1	267.41(6)
S1–N2	160.2(2)	Sn1···S1	292.34(9)
S1–N3	150.2(2)	N1–Sn1–N2	64.65(9)
Sn1–N1	216.9(2)	N1–S1–N2	92.68(13)
Sn1–N2	216.5(3)	Sn1–N1–C14	129.6(2)
P1–C1	disordered	Sn1–N2–C18	129.97(18)
S1–C1	disordered	Sn1–N1–S1–N2	–9.90(13)

In contrast to **11**, the phosphorus side arm is orientated to the tin(II) cation but the Sn1–P1 distance cannot be determined exactly because the phosphorus side arm is disordered on two positions. For the two different positions the distances are

361(1) pm and 354(1) pm (*sof*: 0.579(6)) what is too long to be regarded as a bond and can be interpreted as not more than a weak intramolecular interaction. Nonetheless, this weak interaction can be responsible for the different arrangement of the phosphorus side arm in **12** because in **11**, where definitely no Ge···P interaction is present, the phosphorus side arm is turned away from the metal. The structural differences of both structures are illustrated by a superposition plot of the central structure motif of **11** and **12** in Figure 3.35. Beside the orientations of the phosphorus side arms, the opposite positions of the halides are obvious. While the chlorine atom is orientated to the same site of the ligand as the phosphorus side arm, the bromine atom is directed to the same site of the ligand as the pending imido group, probably due to the weak Sn···P interaction.

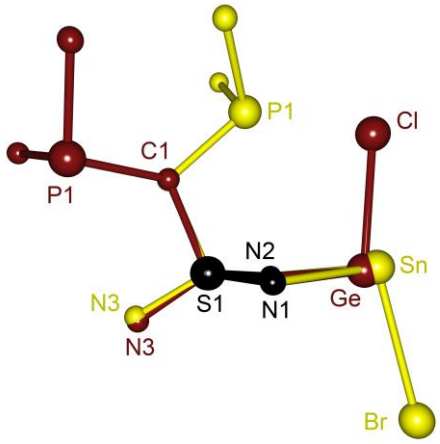

Figure 3.35: Superposition plot of the central core of **11** (dark–red) and **12** (yellow). The black coloured atoms are fitted onto each other with a deviation of 2.06 pm. The *t*butyl groups are omitted for clarity and the phenyl rings are just indicated by the C_{ipso} atoms.

Further, a space filling model of **11** shows an intramolecular interaction between the Cl1 atom and the proton H1B of the C1 atom. The Cl1–H1B distance of 288.1 pm and Cl1–C1 distance of 365.1 pm are in the range of other reported C–H···Cl interactions (Figure 3.36).[90] A comparable proton–halide interaction is not found in **12**. Therefore, the weak Sn1···P1 intramolecular interactions might be one factor that drags the tin atom out of the N1S1N2 plane (Figure 3.36). The Sn(II) atom is shifted slightly more from the best N1S1N2 plane in **12** (36.7 pm) than the Ge(II) atom in **11** (29.1 pm). These intramolecular interactions are probably not strong enough to be the only geometry determining factor but they have an influence which dimension cannot be quantified.

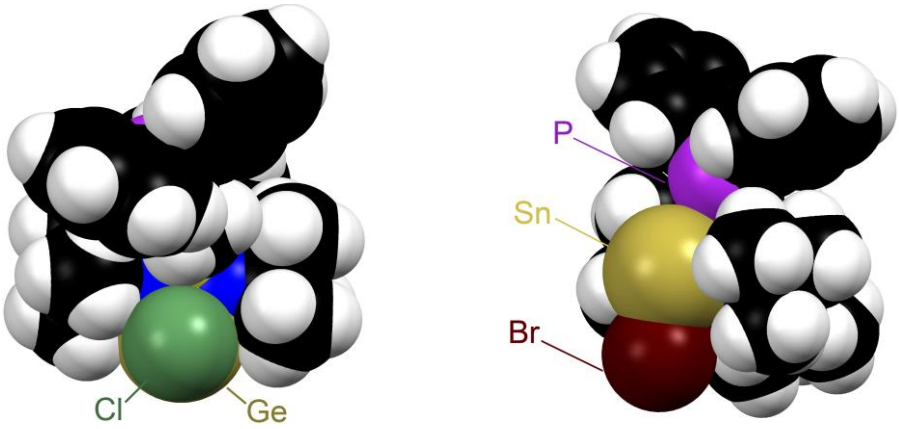

Figure 3.36: Space–filling model of **11** *(left)* and **12** *(right)*.

Further, the geometry at the metal centre is affected by the stereochemically active lone pair that occupies the fourth coordination site of the metal ion causing the pyramidal arrangement (Figure 3.37, *left*).

Another explanation for the deviation of the metal centre form the N1S1N2 plane is that the ligand coordinates in an η^3–fashion to the metal centre. These kind of metal ligand interactions have been observed in β–diketiminate complexes of heavier alkaline earth elements, rare–earth metals as well as Group 4 metal centres.[91] Figure 3.37 (*right*) displays the molecular structure of $[ZrCl_3(nacnac)]$ as an example for such a binding mode. A look at the bond lengths and the geometry shows clearly that the deviation in $[ZrCl_3(nacnac)]$ is much more pronounced than in **12** and that the dimensions are not comparable. Hence, these are extreme examples which involve direct interaction of the ligand backbone with the coordinatively unsaturated metal centre.

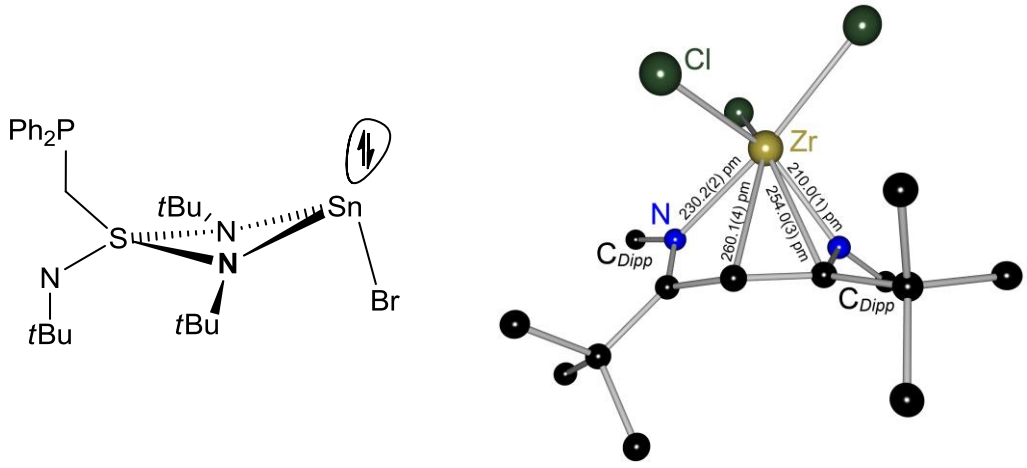

Figure 3.37: *left*) Position of the stereochemically active lone pair in **12**. *right*) Molecular structure of $[ZrCl_3(nacnac)]$ with a sandwich–like coordination motif.

Lappert and *Fulton* synthesised a series of rare *β*–diketiminate lead halide complexes and observed a pyramidal arrangement at the Pb(II) centre that implies a displacement by at least 40.8 pm from the plane spanned by the ligand (Figure 3.38).[92] They have investigated the influence of the lone pair on the geometry of the lead(II) halide *β*–diketiminate complexes, as well as the isostructural germanium and tin complexes using DFT calculations and NBO analyses. The calculations revealed little mixing between the 6s and 6p orbitals in the lone pair of the lead complexes, especially compared to the isotypical germanium(II) and tin(II) compounds. Further, the lone pair in the lead(II) complexes appears to contribute to more than one molecular orbital of the *β*–diketiminate ligand backbone while the lone pair in the germanium and tin complexes are more distinct. They concluded that the deviation from planarity can be attributed to a combination of steric and electronic factors.[92]

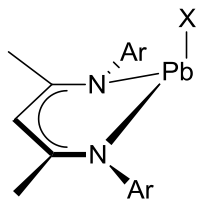

X = Cl, Br, I

Figure 3.38: *β*–Diketiminate lead halide complexes published by *Lappert.*

The questions arose if a lead(II) complex analogue to **11** and **12** would show a more pronounced pyramidal geometry and if a Pb · · · P interaction could be observed because of the increasing size of the cation relatively to germanium(II) and tin(II) cations. It was tried to synthesise an analogue Pb(II) complex by the reaction of $PbCl_2$ with **1** in toluene and a crystalline solid could be obtained. Unfortunately, the crystal quality was very poor and the collected data were not good enough to result in a reliable structure.

To summarise, two group 14 metal halide complexes with the polyimido sulfur phosphanyl ligand as a backbone were synthesised successfully, including a rare example of a threefold coordinated tin bromine complex. The central structure motif is a four–membered MN_2S ring (M = Ge or Sn) with a halide almost perpendicular to the plane. The metal(II) cation is coordinated in a distorted trigonal pyramidal fashion and deviates from an ideal N1S1N2 plane due to intramolecular interactions and a stereochemically active lone pair. To decide if electronic factors play a significant role, it is necessary to do DFT calculations.

3.4. The amine ligand $Ph_2PCH_2S(NtBu)_2NHtBu$ (13)

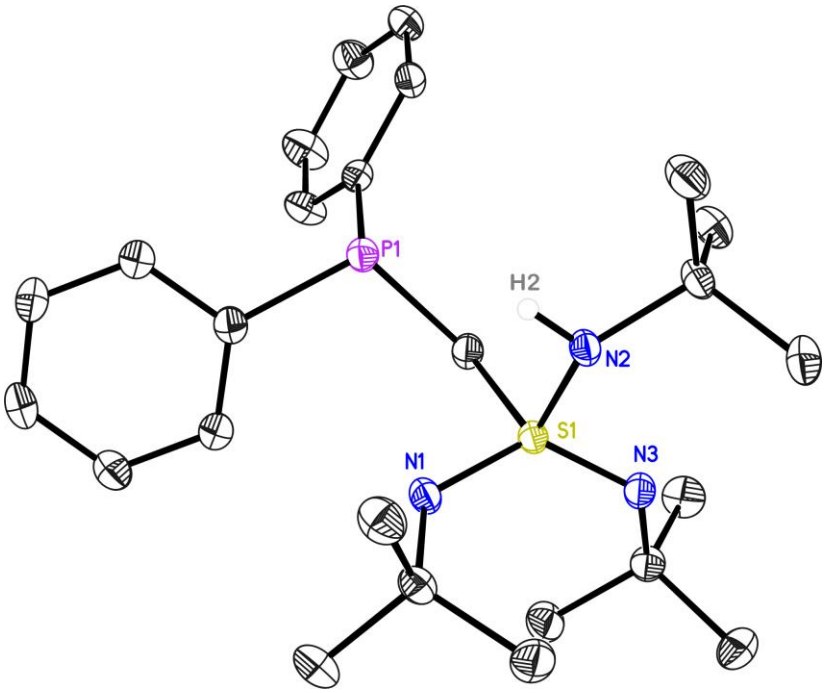

Figure 3.39: Crystal structure of $Ph_2PCH_2S(NtBu)_2NHtBu$ (**13**). Anisotropic displacement parameters are depicted at the 50% probability level. Not freely refined hydrogen atoms and a second molecule in the asymmetric unit are omitted for clarity.

The preliminary crystal structure of the amine ligand **13** has already been presented in my diploma thesis but is here presented again for completeness.[33] Moreover, the reaction was optimised and the product completely characterised during this work. The first crystal structure of **13** was measured from crystals that were obtained as a side–product of the protonated ligand **1**. In comparison to **1**, the amine ligand **13** is easier to handle because it is less sensitive to moisture and it is also more soluble in common organic solvents like pentane, THF or toluene than its lithiated precursor **1**. Further, halogenated reagents and solvents like DCM can be used in the synthesis without inducing a salt–elimination reaction.

A drawback is the longer crystallisation time relatively to **1** and the additional synthetic step. Nonetheless, **13** was used as a precursor for metal complexes since the phosphorus side arm with its π–acceptor character is predestinated as a coordination site for soft metal ions while the nitrogen claws' σ–donor ability is most suited for hard metal ions. First, it had to be investigated how to obtain the ligand **13** directly as a main product. This was achieved successfully in a straightforward one–step synthesis of **1** with tBuNH$_3$Cl in pentane (Scheme 3–11).

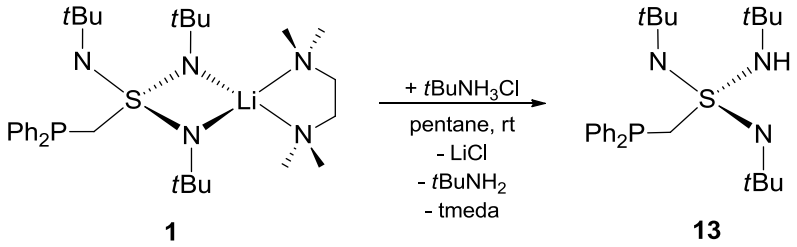

1 13

Scheme 3–11: Preparation of the amine ligand **13**.

Compound **13** was crystallised from pentane, yielding colourless crystals in the triclinic space group $P\bar{1}$ with two molecules in the asymmetric unit (Figure 3.39). The distorted tetrahedrally bonded sulfur atom remains in the oxidation state (VI). The S1–N2(H) distance (165.25(12) pm) is longer than in **1**, quite close to the predicted values for a single bond (169 pm) and close to the S–N(H) distance in the *S*–methyl–tri(*tert*–butylimido)sulfonic acid MeS(N*t*Bu)$_2$NH*t*Bu.[29a] The protonated nitrogen atom N2 does not have a negative charge that could stabilise the positively charged central sulfur atom by electrostatic interactions. In contrast to that, the S1–N1 and S1–N3 bond distances (152.34(12) and 152.34(12) pm) are shorter relatively to the S–N distances of the Li$^+$ chelating N*t*Bu groups in **1** (158.02(13) and 157.06(14) pm) (Table 3.14). The two nitrogen atoms are still negatively charged so that the S1–N2 and S1–N3 bonds can be characterised as single, electrostatically shortened bonds.

Table 3.14: Selected bond lengths [pm] and angles [°] of **13**. Since there are two molecules in the asymmetric unit, the values are averaged.

S1–N1	152.34(12)	N3–C22	148.37(18)
S1–N2	165.25(12)	S1–C1	181.30(14)
S1–N3	151.16(12)	S1–C1–P1	113.49(7)
P1–C1	185.22(14)	N1–S1–N2	109.14(6)
P1–C2	183.56(15)	C1–S1–N2	105.97(6)
P1–C8	184.27(14)	S1–N2–C18	129.06(10)
N1–C14	148.50(18)	S1–N1–C14	125.16(10)
N2–C18	149.80(17)	S1–N3–C22	127.05(10)

To clarify the bonding situation in **13**, charge density studies would be necessary like they were done for MeS(N*t*Bu)$_2$NH*t*Bu by *Leusser*, *Engels* and *Stalke* in 2004. The molecular structure of MeS(N*t*Bu)$_2$NH*t*Bu is shown in Figure 3.40 (*left*) and

NBO/NRT analysis of MeS(N*t*Bu)$_2$NH*t*Bu revealed a bonding situation that is illustrated by *Lewis* diagrams in Scheme 3–12. Just the three leading *Lewis* structures which cover 75% of the electron distribution are displayed. The investigations elucidated a sp^3 hybridisation of S and all N atoms so that consequently the long S–N(H) bonds can be best described as polar single bonds and the shorter S–N are not double bonds but shortened due to ionic contributions.[30a]

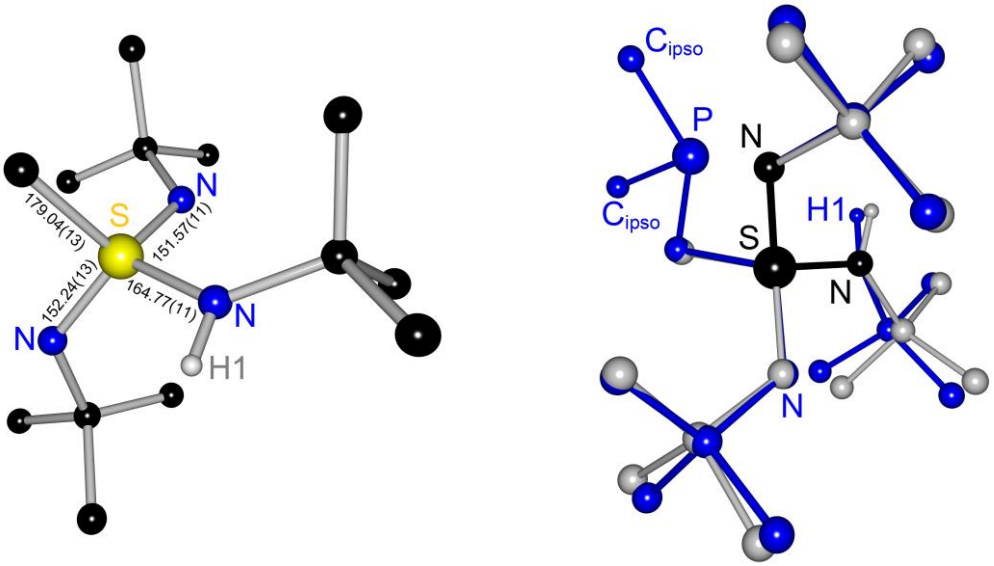

Figure 3.40: *left*) Solid state structure of MeS(N*t*Bu)$_2$NH*t*Bu with the bond lengths given in [pm]. *right*) Superposition plot of of MeS(N*t*Bu)$_2$NH*t*Bu (grey) and **13** (blue). The black coloured S and N atoms are fitted onto each other with a deviation of 0.25 pm.

A superposition plot of MeS(N*t*Bu)$_2$NH*t*Bu and **13** demonstrates nicely that bond lengths and geometry in both structures do not differ significantly (Figure 3.40, *right*). Due to the structural similarity of MeS(N*t*Bu)$_2$NH*t*Bu and Ph$_2$PCH$_2$S(N*t*Bu)$_2$NH*t*Bu, it can be presumed that the bonding situations in **13** are similar.

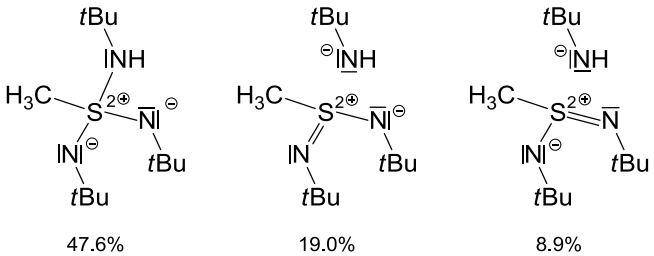

Scheme 3–12: The bonding situation in MeS(N*t*Bu)$_2$NH*t*Bu elucidated

by NBO/NRT analysis and illustrated by *Lewis* diagrams.

An overlay of two ^{1}H–NMR spectra of **13** recorded in THF–d_8 (red) and toluene–d_8 (green) is shown in Figure 3.41. As in the lithiated ligand **1**, it cannot be distinguished between the ^{1}H signals of the protonated and unprotonated N*t*Bu groups in the THF–d_8 solution but the ^{1}H–NMR spectrum of **13** measured in toluene–d_8 displays significantly different ^{1}H shifts (1.43 and 1.28 ppm). However, in the ^{15}N and ^{13}C spectra the N*t*Bu groups show differently shifted signals in both solvents, respectively (for further details, see section 5.3.2).

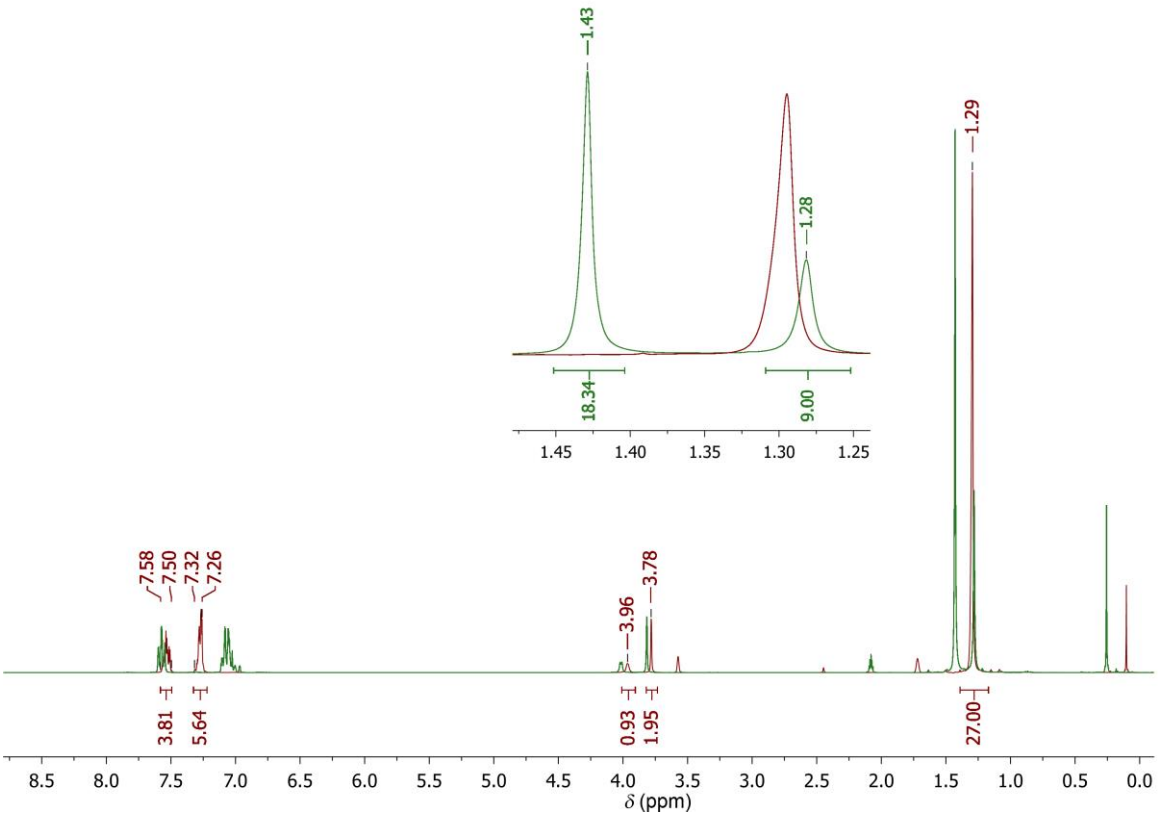

Figure 3.41: ^{1}H–NMR (300 MHz) spectra of **13** recorded in THF–d_8 (red) and toluene–d_8 (green). Assignment of the red signals in [ppm]: 1.29 (C(CH_3)$_3$), 3.78 (PCH_2S), 3.96 (NH), 7.25 – 7.31 (*o*–H, *p*–H), 7.50 – 7.58 (4 H, *m*–H).

3.5. Metal complexes of $Ph_2PCH_2S(NtBu)_2NHtBu$ (13)

Starting from amine **13**, it should be much easier to obtain mono– or even heterobimetallic complexes directly without salt–elimination. First, it was tried to deprotonated the NH*t*Bu group again to obtain *N,N*–chelated metal complexes. Therefore, **13** dissolved in THF was added to a suspension of $[K\{N(SiMe_3)_2\}]$, $[Ti\{N(SiMe_3)_2\}_3]$ or $ZnMe_2$ in pentane at room temperature, respectively. Unfortunately, only the starting materials were crystallised from the reaction mixture. Regarding the just mentioned results of the charge density investigations of $MeS(NtBu)_2NHtBu$, it is probable that the amine **13** is not acidic enough to be deprotonated.

Hence, the generation of *N,N*–chelated metal complexes is more promising by salt–elimination starting from the lithiated ligand **1**. Since an activation of the phosphanyl side arm could not be achieved in the previously described metal complexes of the polyimdio sulfur phosphanyl ligand, it was focused on addressing the phosphorus donor functionality in **13**. In comparison to nitrogen, the phosphorus is the softer donor atom and therefore, softer metal cations, known to be coordinated by *P*–donors, were chosen. $[(benzene)RuCl_2]_2$ and $[(p\text{–cymene})RuCl_2]_2$ are widely used ruthenium complexes and ruthenium(II) *P,N*–complexes are effective catalysts for transfer hydrogenation and also homocoupling of terminal alkynes, for example.[93] To investigate the coordination chemistry of **13** with $[(benzene)RuCl_2]_2$ and $[(p\text{–cymene})RuCl_2]_2$, reactions according to the synthetic route displayed in Scheme 3–13 were performed.

The neutral ruthenium(II) complexes $[(benzene)RuCl_2\{Ph_2PCH_2S(NtBu)_2NHtBu\}]$ (**14**) with a *P*–coordinated Ru(II) atom could be isolated by crystallisation from a THF solution at –24 °C (Scheme 3–13).

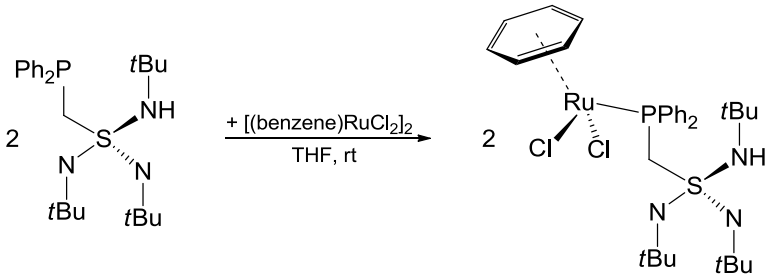

13 **14**

Scheme 3–13: Synthesis of compound **14**.

The crystal structure of **14** revealed a new coordination motif for polyimido sulfur phosphanyl ligands since it is the first neutral sulfur centered *P,N,N*–ligand that shows only a *P*–donating coordination mode (Figure 3.42). **14** crystallises in the triclinic space group $P\bar{1}$ with one molecule in the asymmetric unit.

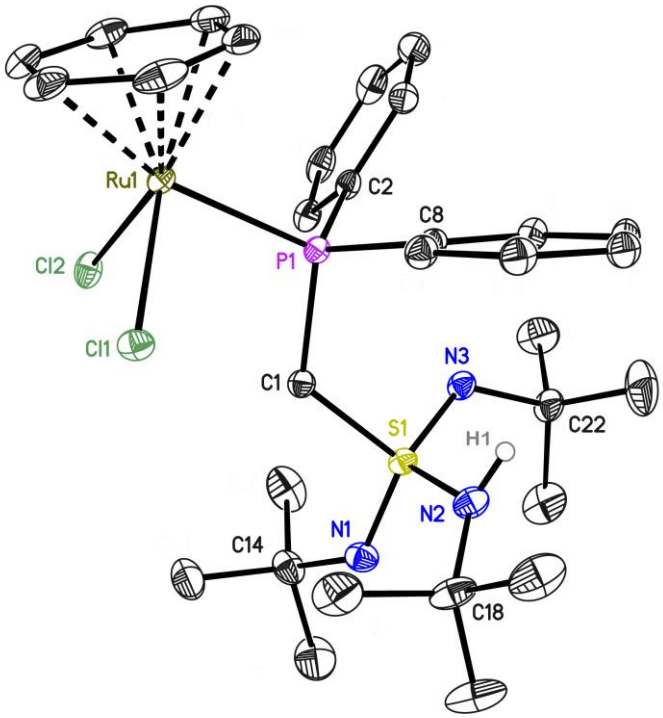

Figure 3.42: Crystal structure of [(benzene)$RuCl_2${$Ph_2PCH_2S(NtBu)_2NHtBu$}] (**14**). Anisotropic dis–placement parameters are depicted at the 50% probability level. Not freely refined hydrogen atoms are omitted for clarity.

The S1 and P1 atoms display a tetrahedrally distorted geometry. The S–N distances and angles are comparable to those of the free ligand **13** but the P–C distances in **14** deviate from the corresponding bond lengths in **13** (Table 3.15). For example, the P1–C1 distance in **14** is 182.84(14) pm in comparison to 185.22(14) pm in **13**. The electron density at the phosphorus atom is reduced by coordinating the ruthenium(II) ion. Consequently, the phosphorus atom is positively polarised what leads to shorter carbon distances and increasing electrostatic interactions. The Ru1–P1 and Ru1–Cl1/2 bond lengths of 235.02(6) pm and $241.12(7)_{av.}$ pm are close to the mean value of all Ru–P and Ru–Cl distances found in the CSD (233.2 pm and 243.6 pm).

Table 3.15: Selected bond lengths [pm] and angles [°] of **14** and **15**.

	14	15		14	15
S1–N1	151.21(13)	152.5(3)	N2–C18	149.3(2)	149.4(5)
S1–N2	164.74(14)	163.6(3)	N3–C22	148.96(19)	149.5(4)
S1–N3	152.07(13)	152.2(3)	S1–N2–C18	130.68(12)	131.9(3)
S1–C1	181.17(14)	179.4(4)	S1–N1–C14	127.71(11)	127.5(3)
P1–C1	182.84(14)	183.6(3)	S1–N3–C22	125.53(10)	124.9(2)
P1–C2	181.99(15)	181.9(4)	Ru1–P1–C1	111.28(5)	108.89(12)
P1–C8	182.15(15)	183.0(4)	Ru1–Cl1	240.90(6)	242.36(9)
P1–Ru1	235.02(6)	235.98(10)	Ru1–Cl2	241.34(7)	242.60(9)
N1–C14	148.6(2)	148.3(4)			

Arene ruthenium(II) half–sandwich complexes are very useful catalysts or catalyst precursors for a wide range of reactions such as alkene hydrogenation and enantioselective transfer hydrogenation of ketones and imines. Hence, it is useful to introduce an asymmetric environment at the metal centre.[94] Therefore, [(*p*–cymene)$_2$RuCl$_2$]$_2$ was used in the synthesis according to Scheme 3–13.

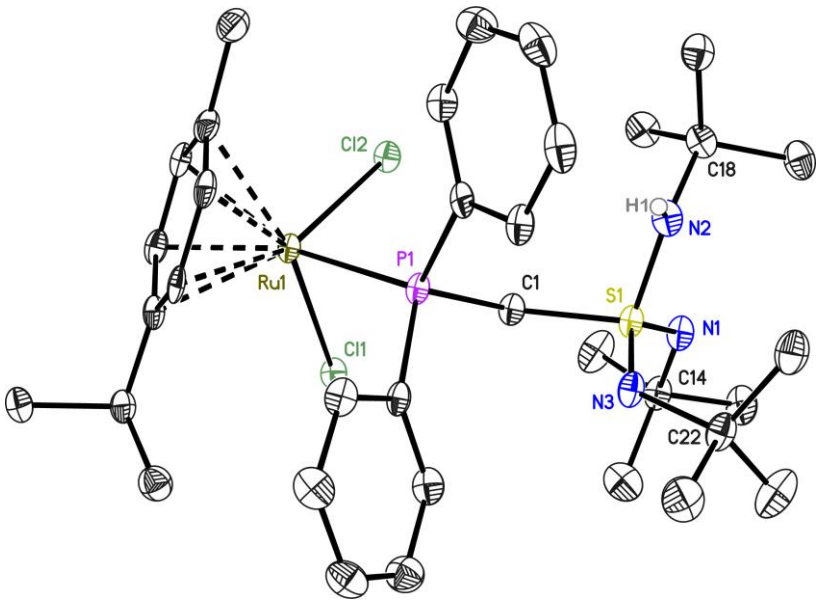

Figure 3.43: Crystal structure of **15**. Anisotropic displacement parameters are depicted at the 50% probability level. Not freely refined hydrogen atoms are omitted for clarity.

After a crystallisation time of two weeks at –24 °C, red–orange needles of [(*p*–cymene)RuCl$_2${Ph$_2$PCH$_2$S(N*t*Bu)$_2$NH*t*Bu}] (**15**) were obtained from the reaction

mixture. **15** crystallises in the monoclinic space group $P2_1/c$ with one molecule in the asymmetric unit. The bond lengths and angles are comparable to those in compound **14** (Table 3.15).

The Ru–C distances in *cis* position to the chlorine atoms are elongated in comparison to the Ru–C bond lengths in *trans* position to the phosphorus atom in both complexes (Figure 3.44). The elongation is more pronounced in the benzene complex **14** and is due to the *trans*–bond–lengthening influence of the tertiary phosphane ligand.[95]

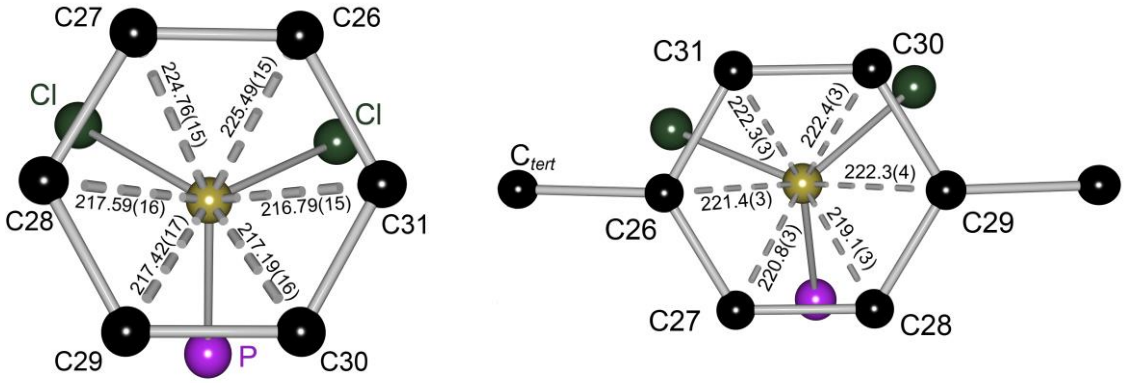

14 **15**

Figure 3.44: (arene)$RuCl_2$ moiety of **14** and **15** with Ru–C bond lengths given in [pm].

Both compounds show one signal in the ^{31}P–NMR spectrum with similar shifts (21.19 ppm (**14**) and 22.47 ppm (**15**)). While the proton resonances of **14** appear as sharp singlets, the signals for the aryl (4.65 and 5.11 ppm), N*t*Bu group (1.15 ppm) and methyl protons of the *i*propyl group (0.81 ppm) in **15** are broad, indicating dynamic intramolecular processes in solution (Figure 3.45). However, the characteristic *septett* of the C*H*$(CH_3)_3$ signal and a sharp signal of the methyl group are resonate at 2.40 and 1.82 ppm, respectivley. The ^1H signals for the aromatic protons of the phenyl rings are at 7.46 and 8.22 ppm. Further, a recorded ^{15}N–^1H–HMBC spectrum proves that the signal at 0.87 ppm can be assigned to the NH*t*Bu group. The ^{15}N signal can be detected at –262.45 ppm and is in the region of the ^{15}NH*t*Bu signal measured for compound **13** (for further details, see section 5.3.15).

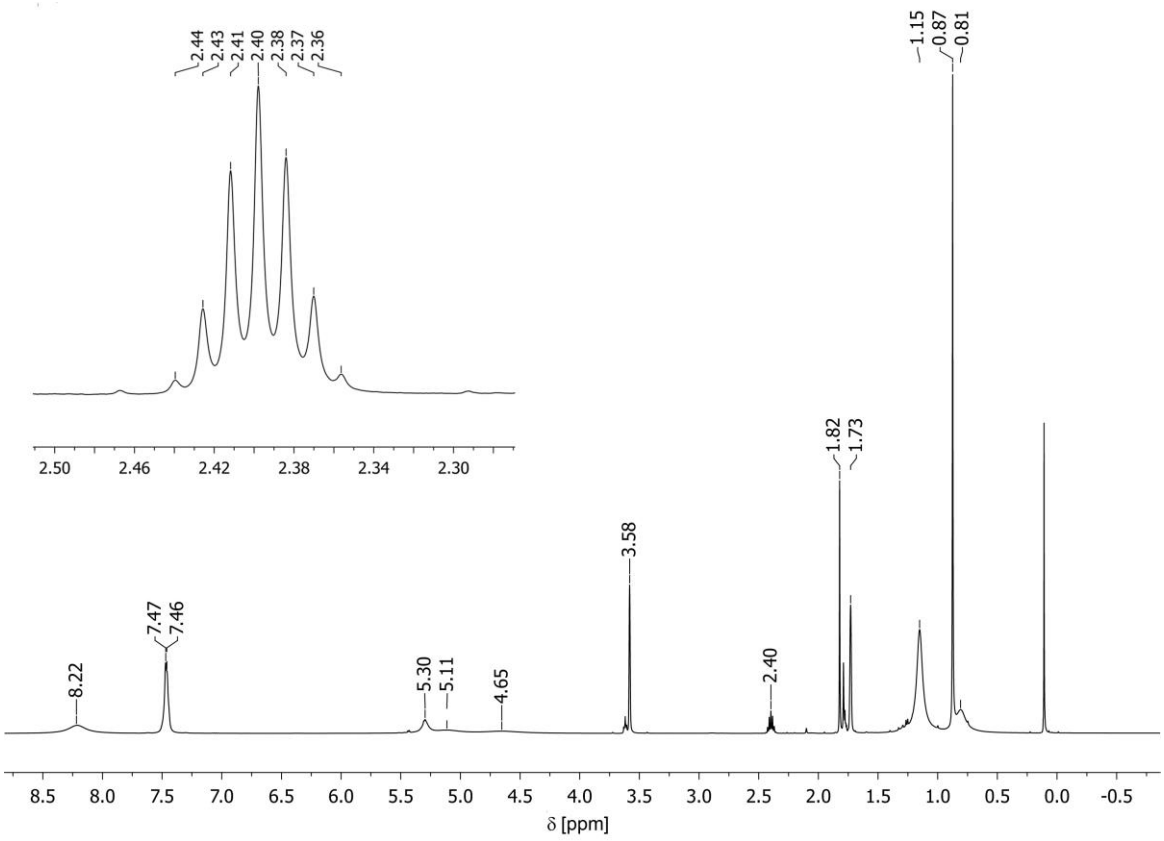

Figure 3.45: ^{1}H–NMR (500.26 MHz) spectrum of **15** recorded in THF–d_8. Integrals are not given because of the broadened signals.

As already mentioned, the imido side arms do not participate in the coordination. In other *P,N*–ligands in which the ruthenium(II) is also just coordinated by the phosphorus atom an additional activation of the nitrogen donor functionality was achieved by refluxing the reaction mixture.[96] To investigate if a similar effect can be observed for compound **14** and **15**, the reaction mixture was refluxed for three hours in THF. Unfortunately, just crystals from the starting material and decomposition products were obtained. Probably, the steric hindrance is too large and changing to another solvent and higher temperature is not recommendable since decomposition of the reagents has already been observed in THF.

A bridging coordination motif was found when **13** was reacted with $[Rh(OAc)_2]_2$ in THF. The molecular structure of $[Rh(OAc)_2\{Ph_2PCH_2S(NtBu)_2NHtBu\}]_2$ is depicted in Figure 3.46 but is not discussed in detail because the data quality was poor. There is high residual electron density (highest difference peak 1.937 e·Å^{-3}, deepest hole –0.885 e·Å^{-3}) that cannot be identified, and that is not close to the rhodium atom what would be an indication for absorption. Nevertheless, the structural motif of $[Rh(OAc)_2\{Ph_2PCH_2S(NtBu)_2NHtBu\}]_2$ is new for sulfur triimide ligands and it proves

that the polyimido sulfur phosphanyl ligand offers versatile coordination modes. It was tried to resynthesise the rhodium(II) complex because just a few crystals were obtained from the first synthesis but recrystallisation was not successful and a characterisation by NMR spectroscopy is not straightforward. Since the reaction mixture changed its colour from green to red after the addition of **13**, it is probable that the compound is formed in solution because also the measured crystal was red coloured. To achieve a crystallisation, it was tried to deprotonate the amine functionality of $[Rh(OAc)_2\{Ph_2PCH_2S(NtBu)_2NHtBu\}]_2$ again by adding $[Li\{N(SiMe_3)_2\}]$ to a reaction mixture in THF at dry ice temperature. Unfortunately, no further crystals could be obtained and it cannot be said if the compound is not formed again or if it just does not crystallise. However, there are too many by–products formed in the synthesis and a definite characterisation is not possible without purification by crystallisation.

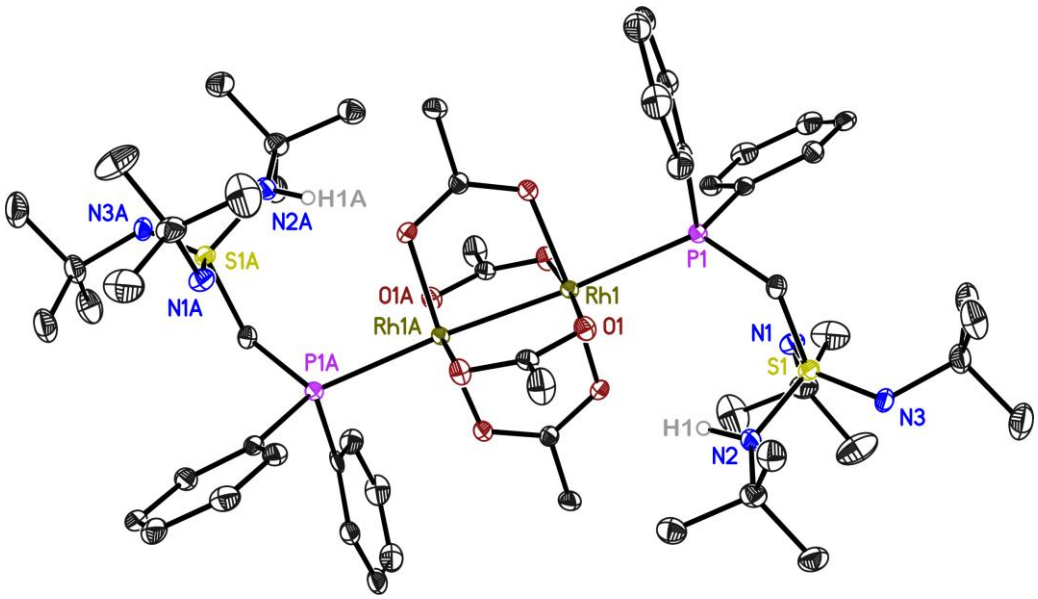

Figure 3.46: Molecular structure of $[Rh(OAc)_2\{Ph_2PCH_2S(NtBu)_2NHtBu\}]_2$. Anisotropic displacement parameters are depicted at the 50% probability level. Not freely refined hydrogen atoms are omitted for clarity.

Hence, it can be summarised that – starting from the protonated ligand **13** – a selective activation of the *P*–donor functionality is possible. The ligand **13** coordinates the rather soft transition metal ions ruthenium(II) and rhodium(II) in a *P*–donating or bridging fashion. The compounds **14**, **15** and $[Rh(OAc)_2\{Ph_2PCH_2$–$S(NtBu)_2NHtBu\}]_2$ are unprecedented for polyimido sulfur phosphanyl ligands because no metal complexes without an *N,N*–chelated metal cation has been

synthesised so far. Starting from the lithiated complex **1**, a specific activation of the *P*–donor functionality with [(benzene)$RuCl_2$]$_2$ and [(*p*–cymene)$RuCl_2$]$_2$ is not feasible. The ligand decomposes due to salt–elimination reactions. Thus, **13** is an excellent precursor for the synthesize of a *P*–coordinated Ru(II) complexes. Further, the compounds **14** and **15** are excellent starting materials for the generation of bimetallic compounds because the imido groups offer a further coordination site for a second metal centre.

4. Conclusion and outlook

Within this thesis, a new synthetic access to diverse metal complexes of polyimido sulfur phosphanyl ligands was developed. The coordination behaviour of either the lithiated ligand [(tmeda)Li{(N*t*Bu)$_3$SCH_2PPh_2}] (**1**) or the protonated ligand Ph_2PCH_2–S(N*t*Bu)$_2$N*H*tBu (**13**) with metal halides was investigated.

An effective synthetic route was found to synthesise first row transition metal and main group metal halide complexes by transmetalation reactions with metal halides starting from **1**. It could be shown that the ligand coordinates the transition metals Mn^{2+}, Fe^{2+}, Co^{2+}, Ni^{2+}, Cu^{2+} and Zn^{2+} in a bidentate fashion and that a tripodal *N,N,N*– or *N,N,P*– coordination is excluded due to steric hindrance. Main group metal halide complexes of germanium(II) and tin(II) could be obtained with a monomeric coordination motif. The sulfur triimide scaffold of the ligand appears as a rigid system in all synthesised metal complexes. The S–N distances of the metal chelating N*t*Bu groups are elongated relative to the S–N distances in S(N*t*Bu)$_3$ because the electropositive sulfur and the metal cation compete for the negative charge of the ligand. Consequently, the S–N distance of the pending N*t*Bu group is shortened by electrostatic interactions. Remarkably, the sum of all three S–N distances in each metal complexes presented herein lays in the range of 468.96 to 473.40 pm, demonstrating nicely that within the rigid SN_3 system the ligand scaffold reacts flexible to different metal cations and different electronic environments by varying the position of the central sulfur atom. This is achieved by concentrating the negative charge either towards the metal ion or in the non–chelating backbone, resulting in shortened or lengthened S–N bonds.

A clear drawback of the ligand is the passivity of the phosphorus side arm. However, employment of the *P*–donor functionality in coordination was achieved by using the amine ligand Ph_2PCH_2S(N*t*Bu)$_2$N*H*tBu (**13**) in combination with soft metal centres like ruthenium(II) and rhodium(II). The Cu(I) compound **9–Cu/Li** may be an example that coordination motifs other than *N,N*–chelating and *P*–donation are possible but the LiBr impurities and the instability of the compound indicate the limits of the ligand. Hence, the application of ligands **1** and **13** as Janus head ligands and precursors for heterobimetallic complexes is questionable since the obtained metal

complexes are often too instable for a reaction with further metals. Also hemilabile coordination could not be observed so far.

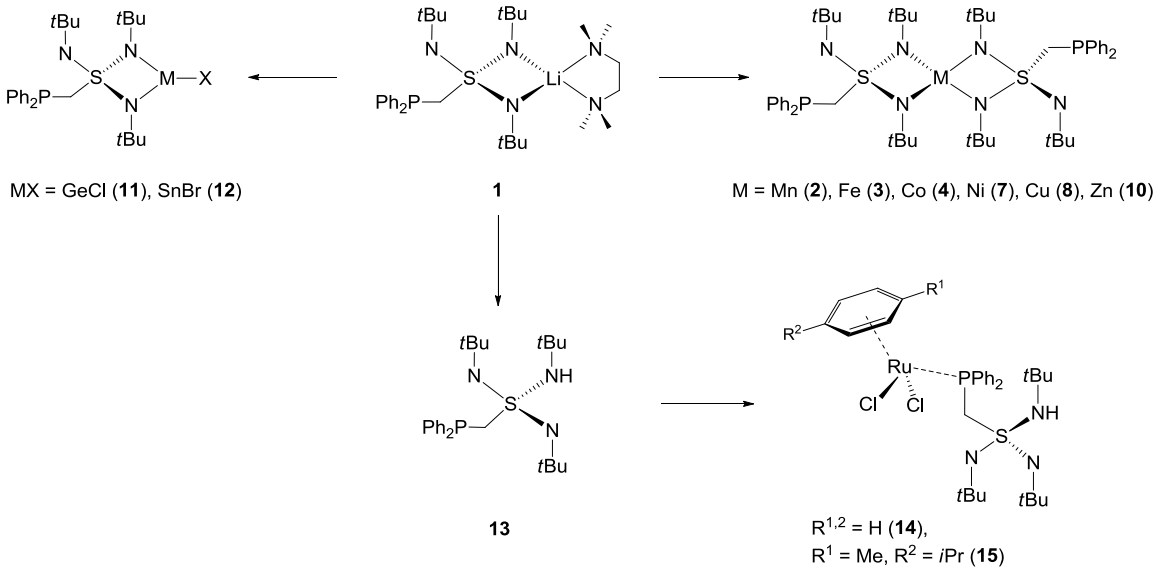

Figure 4.1: Overview of the metal complexes synthesised within this thesis, starting from **1**.

Nonetheless, within this work the variety of metal complexes of polyimido sulfur ligands was expanded appreciably (Figure 4.1) and unprecedented coordination motifs like in **14** and **15** were found.

For future prospect the focus should be on metal halide complexes (**11**, **12**) and the ruthenium complexes (**14**, **15**) because their synthesis is straight forward and they are relatively stable. For the synthesis of heterobimetallic complexes, the next step would be to combine the *N,N*–chelating and *P*–donating properties of the ligand. Other metal cations, for example, palladium or gold could be applied in the synthesis to address the *P*–donor functionality. Further, it might be interesting to modify the ligand by changing from $S(NtBu)_3$ to $S(NSiMe)_3$ as a scaffold to investigate if the $SiMe_3$ groups have an influence on the coordination geometry.

Since the magnetic measurements of compound **6** revealed an exceptional SIM behaviour, it should be investigated if the phosphorus functionalised analogue **4** displays also slow relaxation of the magnetisation in the absence of an applied magnetic field. More afford should be paid in synthesising analogue transition metal complexes of the *S*–methyl–triimidosulfonates ligand $[Me\{(NtBu)_3S\}]^-$ to test if they also behave as single ion magnets.

5. Experimental section

5.1. General procedures

All reactions were carried out with strict exclusion of air and moisture under nitrogen or argon atmosphere using modified *Schlenk*–techniques or in an argon dry box.[97] All solvents were dried using standard laboratory procedures and were freshly distilled from sodium/potassium alloy (Et_2O, *n*pentane), potassium (THF) or sodium (*n*hexane, toluene) prior to use. Solvents used for the synthesis were degassed according to standard laboratory procedures. All employed reactants were commercially available or reproduced according to the given literature procedure.

5.2. Analytical methods

5.2.1. Mass spectrometry

EI–spectra were recorded with a *MAT 95* device (EI–MS: 70 eV). Peaks are given as a mass to charge ratio (*m/z*) of the fragment ions, based on the molecular mass of the isotopes with the highest natural abundance.

5.2.2. NMR spectroscopy

All samples were prepared and filled into *Schlenk*–NMR–tubes inside an argon dry box. The NMR–tube was sealed–off to exclude any impurities. Solvents were dried with potassium. Spectra were recorded at variable temperatures at a *Bruker Avance 300*, *Bruker Avance 400,* or a *Bruker Avance 500* NMR spectrometer. All chemical shifts *δ* are given in ppm, relative to the residual proton signal of the deuterated solvent. Assignments of the shifts were checked by two–dimensional correlation spectra. The shifts of the ^{15}N signals were recorded in a $^{15}N,^{1}H$–HMBC experiment.

5.2.3. Elemental analysis

Elemental analysis was performed as a combustion analysis by the *Analytischen Labor des Institutes für Anorganische Chemie* at the Georg–August–Universität Göttingen with an elementar vario EL III device. The inclusion of argon, from canning in an argon drybox, led to systematic errors.

5.2.4. Magnetic susceptibility measurements

Temperature–dependent magnetic susceptibility measurements of **4** and **6** were carried out with a *Quantum–Design* MPMS–XL–5 SQUID magnetometer equipped with a 5 Tesla magnet in the range from 295 to 2.0 K at a magnetic field of 0.5 T. The powdered sample was contained in a gel bucket and fixed in a non–magnetic sample holder. Each raw data file for the measured magnetic moment was corrected for the diamagnetic contribution of the sample holder and the gel bucket. The molar susceptibility data were corrected for the diamagnetic contribution.
Magnetic parameters were determined using a fitting procedure to the spin Hamiltonian for zero–field splitting and Zeeman interaction

$$\hat{H} = D(\hat{S}_z^2 - \frac{1}{3}S(S+1)) + g_{iso}\mu_B\vec{B}\vec{S}\,.$$

Temperature–independent paramagnetism (*TIP*) was included according to $\chi_{calc} = \chi + TIP$. Simulation of the experimental magnetic data with a full–matrix diagonalisation of exchange coupling and Zeeman splitting was performed with the *julX* program.

5.2.5. Mössbauer spectroscopy

The Mössbauer spectrum for compound **3** was recorded with a ^{57}Co source in a Rh matrix using an alternating constant acceleration *Wissel* Mössbauer spectrometer operated in the transmission mode and equipped with a *Janis* closed–cycle helium cryostat. Isomer shift is given relative to iron metal at ambient temperature. Simulation of the experimental data was performed with the *Mfit* program.[98]

5.3. Syntheses and characterisation

5.3.1. [(tmeda)Li{(N*t*Bu)$_3$SCH$_2$PPh$_2$}] (1)

S(N*t*Bu)$_3$ (1.47 g, 6.00 mmol, 1.0 eq) in THF (10 mL) was slowly added to a slurry of [(tmeda)LiCH$_2$PPh$_2$] (1.93 g, 6.00 mmol, 1.0 eq.) in *n*pentane (30 mL) at –78 °C. After stirring at room temperature overnight, the solution was filtered over celite, reduced in volume and stored at –25 °C, yielding colourless crystals after 5 days. The crystals were washed with *n*pentane and dried *in vacuo* before storage in an argon box.

Empirical formula: $C_{31}H_{55}LiN_5PS$ **Molecular weight:** 567.77 g/mol

Yield: 4.44 g, 8.40 mmol, 90%.

^{1}H–NMR (300.13 MHz, THF–*d*$_8$): δ = 1.28 (s, 27 H, C(C*H*$_3$)$_3$), 2.16 (s, 12 H, (C*H*$_3$)$_2$N), 2.30 (s br, 12 H, N(C*H*$_2$)$_2$N), 3.98 (s br, 2 H, SC*H*$_2$P), 7.17 – 7.24 (m, 6 H, *o*–H, *p*–H), 7.54 – 7.59 (m, 4 H, *m*–H).

^{13}C{^{1}H}–NMR (75.47 MHz, THF–*d*$_8$): δ = 34.07 (C(*C*H$_3$)$_3$), 46.01 ((*C*H$_3$)$_2$N), 52.19 (*C*(CH$_3$)$_3$), 58.72 (N(*C*H$_2$)$_2$), 64.54 (d, $^1J_{P-C}$ = 26.80 Hz, P*C*H$_2$S), 128.16 – 128.28 (m, *o*–*C, p*–C), 134.25 (d, $^3J_{P-C}$ = 19.74 Hz, *m*–C), 142.70 (d, $^1J_{P-C}$ = 16.9 Hz, *ipso*–C).

^{31}P{^{1}H}–NMR (121.49 MHz, THF–*d*$_8$): δ = –24.18.

^{7}Li–NMR (116.64 MHz, THF–*d*$_8$): δ = 0.528.

^{15}N–NMR (30.42 MHz, THF–*d*$_8$): δ = –254.76 (*N*tBu).

^{1}H–NMR (300.13 MHz, tol–*d*$_8$): δ = 1.46 (s br, 18 H, C(C*H*$_3$)$_3$), 1. 69 (s br,9 H, C(C*H*$_3$)$_3$), 1.92 (s br, 12 H, (C*H*$_3$)$_2$N), 2.09 (s, 4 H, N(C*H*$_2$)$_2$N), 4.49 (s br, 2 H, SC*H*$_2$P), 6.99 – 7.10 (m, *o*–H, *p*–H), 7.68 – 7.74 (m, 4 H, *m*–H).

^{13}C{^{1}H}–NMR (75.47 MHz, tol–*d*$_8$): δ = 33.80 (C(*C*H$_3$)$_3$), 34.78 (C(*C*H$_3$)$_3$), 46.64 (N(*C*H$_2$)$_2$), 51.69 (*C*(CH$_3$)$_3$), 53.32 (*C*(CH$_3$)$_3$), 57.43 ((C*H*$_3$)$_2$N), 64.16 (d, $^1J_{P-C}$ = 24.20 Hz, P*C*H$_2$S), 127.65 – 129.20 (m, *o*–*C, p*–C), 134.22 (d, $^3J_{P-C}$ = 21.00 Hz, *m*–C), 142.64 (d, $^1J_{P-C}$ = 17.6 Hz, *ipso*–C).

Elemental analysis (found (calc.) [%]): C 65.58 (65.57), H 9.52 (9.76), N 12.00 (12.33), S 5.99 (5.65).

5.3.2. $Ph_2PCH_2S(NtBu)_2NHtBu$ (13)

*t*BuNH$_3$Cl (0.33 g, 3.00 mmol, 1.0 eq.) and **1** (1.70 g, 3.00 mmol, 1.0 eq.) were combined in an argon dry box and dissolved in *n*pentane (50 mL) at room temperature. After stirring overnight, the suspension was filtered over celite and the volume of the filtrate was reduced. Colourless crystals were obtained after storing the colourless solution at least for seven days at –25 °C.

Empirical formula: $C_{25}H_{40}N_3PS$ **Molecular weight:** 445.66 g/mol

Yield: 1.07 g, 2.40 mmol, 80%.

^{1}H–NMR (300.13 MHz, THF–*d*$_8$): δ = 1.30 (s, 27 H, C(C*H*$_3$)$_3$), 3.79 (s, 2 H, PC*H*$_2$S), 3.98 (s br, 1 H, N*H*), 7.25 – 7.33 (m, 6 H, *o*–H, *p*–H), 7.50 – 7.58 (m, 4 H, *m*–H).

^{13}C{^{1}H}–NMR (75.47 MHz, THF–*d*$_8$): δ = 30.63 (N(H)C(*C*H$_3$)$_3$), 33.54 (C(*C*H$_3$)$_3$), 53.63 (N*C*(CH$_3$)$_3$), 55.09 (NH*C*(CH$_3$)$_3$), 65.56 (d, $^1J_{P,C}$ = 30.1 Hz, P*C*H$_2$S), 128.93 – 129.15 (m, *p*–C, *o*–C), 134.00 (d, $^3J_{P,C}$ = 19.5 Hz, *m*–C), 140.53 (d, $^1J_{P,C}$ = 14.4 Hz, *ipso*–C).

^{31}P{^{1}H}–NMR (121.49 MHz, THF–*d*$_8$): δ = –17.06.

^{15}N–NMR (30.42 MHz, THF–*d*$_8$): δ = –269.7 (*N*H*t*Bu), –250.3 (N*t*Bu).

^{1}H–NMR (300.13 MHz, tol–*d*$_8$): δ = 1.28 (s, 9 H, NHC(C*H*$_3$)$_3$), 1.43 (s, 18 H, C(C*H*$_3$)$_3$), 3.82 (s, 2 H, PC*H*$_2$S), 4.02 (s, 1 H, N*H*), 7.00 – 7.11 (m, *o*–H, *p*–H), 7.54 – 7.60 (m, 4 H, *m*–H).

^{13}C{^{1}H}–NMR (75.47 MHz, tol–*d*$_8$): δ = 29.00 (C(*C*H$_3$)$_3$), 32.06 (C(*C*H$_3$)$_3$), 51.92 (N*C*(CH$_3$)$_3$), 53.17 (NH*C*(CH$_3$)$_3$), 64.03 (d, $^1J_{P,C}$ = 30.5 Hz, P*C*H$_2$S), 126.26 – 127.80 (m, *p*–C, *o*–C), 132.15 (d, $^3J_{P,C}$ = 19.3 Hz, *m*–C), 138.66 (d, $^1J_{P,C}$ = 14.4 Hz, *ipso*–C).

^{1}H NMR (500.26 MHz, C$_6$D$_6$): δ = 1.28 (s, 9 H, NHC(C*H*$_3$)$_3$), 1.46 (s, 18 H, C(C*H*$_3$)$_3$), 3.85 (s br, 1 H, N*H*), 4.03 (d, 2 H, $^2J_{P-H}$ = 3.0 Hz, PC*H*$_2$S), 7.00 – 7.13 (m, 6 H, *o*–H, *p*–H), 7.59 – 7.65 (m, 4 H, *m*–H).

^{13}C{^{1}H}–NMR (125.76 MHz, C$_6$D$_6$): δ = 30.33 (C(*C*H$_3$)$_3$), 33.41 (C(*C*H$_3$)$_3$), 53.24 (N*C*(CH$_3$)$_3$), 54.39 (NH*C*(CH$_3$)$_3$), 65.14 (d, $^1J_{P,C}$ = 50.30 Hz, P*C*H$_2$S), 128.59 (d, $^2J_{P,C}$ = 11.32 Hz, *o*–C), 128.68 (*p*–C), 133.50 (d, $^3J_{P,C}$ = 37.70 Hz, *m*–C), 140.00 (d, $^1J_{P,C}$ = 23.89 Hz, *ipso*–C).

^{31}P{^{1}H}–NMR (202.46 MHz, C$_6$D$_6$): δ = –17.07.

^{15}N–NMR (50.71 MHz, C_6D_6): δ = –269.5 (*N*H*t*Bu), –249.9 (N*t*Bu).

Elemental analysis (found (calc.) [%]): C 67.27 (67.37), H 8.91 (8.97), N 9.57 (9.43), S 7.53 (7.20).

EI–MS m/z [%]: 446 [{M}, 1]$^+$, 317 [{M – NH*t*Bu, – *t*Bu}, 1]$^+$, 302 [{M –NH*t*Bu, – N*t*Bu}, 2]$^+$, 199 [{Ph_2PCH_2}, 56]$^+$.

5.3.3. [Mn{(N*t*Bu)$_3$SCH$_2$PPh$_2$}$_2$] (2)

$MnBr_2$ (0.21 g, 1.00 mmol, 0.5 eq.) and **1** (1.14 g, 2.00 mmol, 1.0 eq.) were combined in an argon dry box and dissolved in *n*pentane (100 mL) at room temperature. After stirring overnight, the suspension was filtered over celite, reduced in volume and stored at 4 °C. Colourless crystals were obtained after three days.

Empirical formula: $C_{50}H_{78}MnN_6P_2S_2$ **Molecular weight:** 943.59 g/mol

Yield: 0.47 g, 0.50 mmol, 25%.

^{1}H–NMR (500.13 MHz, THF–d_8): δ = 7.10 (s br), 7.70 (s br).

^{13}C{^{1}H}–NMR (125.76 MHz, THF–d_8): 130.47 (s br), 131.47 (s br), 131.61 (s br), 142.71 (s br), 143.75 (s br).

^{31}P{^{1}H}–NMR (202.46 MHz, THF–d_8): δ = No signal could be detect due to the paramagnetic character of the compound.

Elemental analysis (found (calc.) [%]): C 62.38 (63.64), H 8.08 (8.35), N 9.25 (8.91), S 7.18 (6.80)

EI–MS m/z [%]: 943.4 [{M}, 100]$^+$, 673.2 [{M – N*t*Bu, –CH_2PPh_2}, 66]$^+$, 570 [{M – 4 N*t*Bu, –SCH_2PPh_2,}, 10]$^+$, 428 [{M – 2 N*t*Bu, –SCH_2PPh_2 }, 5]$^+$.

5.3.4. [Fe{(N*t*Bu)$_3$SCH$_2$PPh$_2$}$_2$] (3)

$FeBr_2$ (0.05 g, 0.25 mmol, 0.5 eq.) and **1** (0.28 g, 0.50 mmol, 1.0 eq.) were combined in an argon dry box and dissolved in *n*pentane (40 mL) at room temperature. After stirring overnight, the suspension was filtered over celite,

reduced in volume and stored at 4 °C. Orange–brown crystals were obtained after three days.

Empirical formula: $C_{50}H_{78}FeN_6P_2S_2$ **Molecular weight:** 945.09 g/mol

Yield: 0.34 g, 0.36 mmol, 71%.

^{1}H–NMR (500.13 MHz, THF–*d*$_8$): δ = 4.40 (s br,), 6.66 (s br), 7.76 (s br), 8.00 (s br), 8.27 (s br), 22.86 (s br), 45.97 (s br).

^{13}C{^{1}H}–NMR (125.76 MHz, THF–*d*$_8$): δ = 110.50, 164.97, 211.70, 297.27, 363.05.

^{31}P{^{1}H}–NMR (202.46 MHz, THF–*d*$_8$): δ = 356.46.

Elemental analysis (found (calc.) [%]): Due to co–crystallisation of the protonated ligand **13** and residue of starting material, no CHN analysis is given.

EI–MS m/z [%]: 944.3 [{M}, 5]$^+$.

5.3.5. [Co{(N*t*Bu)$_3$SCH$_2$PPh$_2$}$_2$] (4)

$CoBr_2$ (0.11 g, 0.50 mmol, 0.5 eq.) and **1** (0.57 g, 1.00 mmol, 1.0 eq.) were combined in an argon dry box and dissolved in *n*pentane (80 mL) at room temperature. After stirring overnight, the suspension was filtered over celite, reduced in volume and stored at 4 °C. Pink crystals were obtained after one day.

Empirical formula: $C_{50}H_{78}CoN_6P_2S_2$ **Molecular weight:** 948.17 g/mol

Yield: 0.76 g, 0.80 mmol, 79%.

^{1}H–NMR (500.26 MHz, THF–*d*$_8$): δ = –45.933 (s br, C(C*H*$_3$)$_3$), 9.63 (s br), 11.06 (s br), 15.72 (s br), 17.94 (s br), 21.99 (s br), 24.15 (s br), 35.55 (s br), 113.0 (s br).

^{31}P{^{1}H}–NMR (202.46 MHz, THF–*d*$_8$): δ = No signal could be detect due to the paramagnetic character of the compound.

^{13}C{^{1}H}–NMR (125.76 MHz, THF–*d*$_8$): δ = 72.30, 131.23, 137.66, 141.81, 144.87, 153.273, 161.26, 193.17, 231.51, 325.89, 379.44.

Elemental analysis (found (calc.) [%]): C 62.08 (63.33), H 7.73 (8.31), N 9.25 (8.87), S 8.34 (6.76).

EI–MS m/z [%]: 947.5 [{M}, 1]$^+$, 677.3 [{M – N*t*Bu, – CH_2PPh_2}, 100]$^+$, 574.3 [{M – 2 N*t*Bu, – SCH_2PPh_2}, 4]$^+$, 503.2 [{M – 3 N*t*Bu, – SCH_2PPh_2}, 11]$^+$, 432.1 [{M – 4 N*t*Bu, – SCH_2PPh_2}, 11]$^+$, 407.2 [{M – 2 N*t*Bu, – 2 CH_2PPh_2}, 20]$^+$, 199 [{Ph_2PCH_2} 36]$^+$, 57.1 [{*t*Bu}, 12}]$^+$.

5.3.6. [(tmeda)Li(μ–Br)$_2$Co{(N*t*Bu)$_3$SCH_2PPh_2}] (5)

$CoBr_2$ (0.05 g, 0.25 mmol, 0.5 eq.) and **1** (0.28 g, 0.50 mmol, 1.0 eq.) were combined in an argon dry box and dissolved in a mixture of *n*pentane (20 mL) and THF (5 mL) at room temperature. After stirring overnight, the suspension was filtered over celite, reduced in volume and stored at 4 °C. Pink crystals of compound **4** and blue crystals of **5** were obtained after one day.

Empirical formula: $C_{31}H_{55}Br_2CoLiN_5PS$ **Molecular weight:** 786.52 g/mol

The compound was only a side–product of the reaction and the yield very low. A separation of the two different kinds of crystals was not possible for further analytical methods.

5.3.7. [Co{(N*t*Bu)$_3$SMe}$_2$] (6)

[Co{N($SiMe_3$)$_2$}$_2$] (0.19 g, 0.50 mmol, 1.0 eq.) and [(thf)Li{(N*t*Bu)$_3$SMe}]$_2$ (0.26 g, 0.50 mmol, 1.0 eq.) were combined in an argon dry box and dissolved in *n*pentane (40 mL) at room temperature. After stirring overnight, the suspension was filtered over celite, reduced in volume and stored at –24 °C. Pink crystals were obtained after one day.

Empirical formula: $C_{26}H_{60}CoN_6S_2$ **Molecular weight:** 579.85 g/mol

Yield: 0.23 g, 0.40 mmol, 80%.

^{1}H–NMR (500.26 MHz, THF–*d*$_8$): δ = –45.95 (s br, 4 C(CH_3)$_3$), 23.03 (s br, 2 C(CH_3)$_3$), 119.92 (s br, 2 CH_3).

^{13}C{^{1}H}–NMR (125.76 MHz, THF–*d*$_8$): δ = 76.85, 126.68, 328.30, 367.62, 650.00 (s br), 689.00 (s br).

Elemental analysis (found (calc.) [%]): C 53.81 (53.85), H 10.24 (10.45), N 14.64 (14.50), S 11.15 (11.06).

EI–MS m/z [%]: 579.2 [{M}, 100]$^+$, 493.1 [{M – CH_3, – N*t*Bu$_3$}, 38]$^+$, 390 [{M – SCH_3, – 2 N*t*Bu$_3$}, 36]$^+$, 375.1 [{M – SCH_3, – 2 N*t*Bu$_3$, – CH_3}, 18]$^+$, 304.1 [{M – SCH_3, – 3 N*t*Bu$_3$, –CH_3}, 8]$^+$, 233 [{M – SCH_3, – 4 N*t*Bu$_3$, – CH_3}, 20]$^+$.

5.3.8. [Ni{(N*t*Bu)$_3$SCH$_2$PPh$_2$}$_2$] (7)

$NiCl_2$ (0.03 g, 0.25 mmol, 0.5 eq.) and **1** (0.28 g, 0.50 mmol, 1.0 eq.) were combined in an argon dry box and dissolved in *n*pentane (40 mL) at room temperature. After stirring overnight, the suspension was filtered over celite, reduced in volume and stored at –24 °C. Blue crystals were obtained after one month.

Empirical formula: $C_{50}H_{78}NiN_6P_2S_2$ **Molecular weight:** 947.95 g/mol

Yield: 0.05. g, 0.05 mmol, 10%.

The ^{1}H NMR displays are mixture of two compounds. One compound is the paramagnetic nickel complex **7**. The other compound is the protonated ligand **13**.

^{1}H–NMR (300.13 MHz, THF–*d*$_8$): δ = –19.51 (s), –17.97 (s), –2.13 (s), 3.81 (s), 5.37 (s), 5.70 (s), 5.96 (s), 6.77 (s), 714 (s), 13.42 (s), 15.01 (s).

^{31}P{^{1}H}–NMR (121.49 MHz, THF–*d*$_8$): δ = 224.73.

Elemental analysis (found (calc.) [%]): C 61.76 (63.35), H 8.31 (8.29), N 8.71 (6.53), S 7.24 (6.77).

EI–MS m/z [%]: 946.4 [{M}, 8]$^+$, 901.3 [{M – 3 CH_3}, 14]$^+$, 869.4 [{M –Ph}, 6]$^+$, 798.4 [{M – N*t*Bu$_3$, – Ph}, 18]$^+$, 830.3 [{M – N*t*Bu$_3$, – 3 CH_3}, 22]$^+$, 777.2 [{M – 2 Ph, – CH_3}, 38]$^+$, 759.2 [{M – N*t*Bu, – 2 *t*Bu, – 4 CH_3}, 100]$^+$.

5.3.9. [Cu{(N*t*Bu)$_3$SCH$_2$PPh$_2$}$_2$] (8)

$CuBr_2$ (0.22 g, 1.00 mmol, 0.5 eq.) and **1** (1.13 g, 2.00 mmol, 1.0 eq.) were combined in an argon dry box and dissolved in *n*pentane (100 mL) at room temperature. After stirring overnight, the suspension was filtered over celite, reduced in volume and stored at 4 °C. Dark orange crystals were obtained after two days.

Empirical formula: $C_{50}H_{78}CuN_6P_2S_2$ **Molecular weight:** 952.78 g/mol

Yield: 0.47 g, 0.66 mmol, 33%.

No further analyses of the compound were made because the crystals are highly unstable and their colour turned from dark orange to green after a short time.

5.3.10. [(tmeda)$Li_{0.79}$/$Cu_{2.21}$(μ–$Cl_{1.96}Br_{0.04}$){$Ph_2PCH_2S(NtBu)_3$}] (9)

CuCl (0.10 g, 1.00 mmol, 0.5 eq.) and **1** (0.57 g, 1.00 mmol, 1.0 eq.) were combined in an argon dry box and dissolved in *n*pentane (40 mL) at room temperature. After stirring overnight, the suspension was filtered over celite, reduced in volume and stored at room temperature. Dark red crystals were obtained after one day.

Empirical formula: $C_{31}H_{55}Br_{0.04}Cl_{1.96}Cu_{2.21}Li_{0.79}N_5PS$

Molecular weight: 779.5 g/mol

No further analyses are given because just a few crystals were obtained from the solution before the unstable compound decomposed and resynthesis was not successful.

5.3.11. [Zn{$(NtBu)_3SCH_2PPh_2$}$_2$] (10)

$ZnBr_2$ (0.23 g, 1.00 mmol, 0.5 eq.) and **1** (1.13 g, 2.00 mmol, 1.0 eq.) were combined in an argon dry box and dissolved in *n*pentane (100 mL) at room temperature. After stirring overnight, the suspension was filtered over celite, reduced in volume and stored at –24 °C. Colourless crystals were obtained after two days.

Empirical formula: $C_{50}H_{78}ZnN_6P_2S_2$ **Molecular weight:** 954.61 g/mol

Yield: 0.40 g, 0.42 mmol, 21%.

^{1}H–NMR (300.13 MHz, THF–*d*$_8$): δ = 1.26 (s, 18 H, C(CH_3)$_3$), 1.40 (s, 36 H, C(CH_3)$_2$), 4.22 (s br, 4 H, SCH_2P), 7.17–7.29 (m, 12 H, *o*–H, *p*–H), 7.51–7.56 (m, 10 H, *m*–H).

^{13}C{^{1}H}–NMR (75.47 MHz, THF– *d*$_8$): δ = 30.62 (C(CH_3)$_3$), 33.53 (C(CH_3)$_3$), 53.64 (C(CH$_3$)$_3$), 57.50 (C(CH$_3$)$_3$), 62.99 (s, PCH_2S), 129.10 (d, $^2J_{P-C}$ = 18.84 Hz, *o*–C), 132.87 (d, $^4J_{P-C}$ = 32.70 Hz, *p*–C), 133.00 (d, $^2J_{P-C}$ = 32.69 Hz, *m*–C).

$^{31}P\{^{1}H\}$–NMR (121.49 MHz, THF–d_8): δ = –24.87.

Elemental analysis (found (calc.) [%]): C 60.10 (62.91), H 7.78 (8.24), N 9.14 (8.80), S 6.49 (6.72).

5.3.12. [GeCl{(N*t*Bu)$_3$SCH$_2$PPh$_2$}] (11)

$GeCl_2 \cdot$dioxane (0.12 g, 0.50 mmol, 1.0 eq.) and [(tmeda)Li{(N*t*Bu)$_3$SCH$_2$PPh$_2$}] (**1**) (0.28 g, 0.50 mmol, 1.0 eq.) were combined in an argon dry box and dissolved in *n*pentane (40 mL) at room temperature. After stirring overnight, the suspension was filtered over celite, reduced in volume and stored at –24 °C. Colourless crystals were obtained after ten days.

Empirical formula: $C_{25}H_{39}N_3ClGePS$ **Molecular weight:** 552.66 g/mol

Yield: 0.19 g, 0.34 mmol, 68%.

^{1}H–NMR (300.13 MHz, tol–d_8): δ = 1.16 (s, 9 H, C(CH_3)$_3$), 1.46 (s, 18 H, C(CH_3)$_3$), 4.79 (s, 2 H, PCH_2S), 6.99 – 7.06 (m, 6 H, *o*–H, *p*–H), 7.42 – 7.52 (m, 4 H, *m*–H).

$^{13}C\{^{1}H\}$–NMR (75.47 MHz, tol–d_8): δ = 31.38 (C(*C*H$_3$)$_3$), 32.29 (C(*C*H$_3$)$_3$), 56.06 (N*C*(CH$_3$)$_3$), 64.03 (P*C*H$_2$S), 128.23 (*o*–C), 128.51 (*p*–*C*), 133.47 (d, $^{3}J_{P-C}$ = 31.44 Hz, *m*–*C*), 137.44 (*ipso*–*C*).

$^{31}P\{^{1}H\}$–NMR (121.49 MHz, tol–d_8): δ = –23.92.

Elemental analysis (found (calc.) [%]): C 54.12 (54.32), H 6.96 (7.11), N 7.96 (7.60), S 6.70 (5.80).

EI–MS m/z [%]: 553 [{M}, 2]$^+$, 518 [{M – Cl}, 13]$^+$, 496 [{M – *t*Bu}, 8]$^+$, 440 [{M – 2 *t*Bu}, 3]$^+$, 382 [{M – 3 *t*Bu}, 8]$^+$, 302 [{Ph$_2$PCH$_2$SN*t*Bu}, 16]$^+$.

5.3.13. [SnBr{(N*t*Bu)$_3$SCH$_2$PPh$_2$}] (12)

$SnBr_2$ (0.14 g, 0.50 mmol, 1.0 eq.) and [(tmeda)Li{(N*t*Bu)$_3$SCH$_2$PPh$_2$}] (**1**) (0.28 g, 0.50 mmol, 1.0 eq.) were combined in an argon dry box and dissolved in *n*pentane (40 mL) at room temperature. After stirring overnight, the suspension was filtered over celite, reduced in volume and stored at –24 °C. Colourless crystals were obtained after 14 days.

Empirical formula: $C_{25}H_{39}N_3BrSnPS$ **Molecular weight:** 643.22 g/mol

Yield: 0.23 g, 0.35 mmol, 70%.

^{1}H–NMR (500.26 MHz, THF–*d*$_8$): δ = 1.34 (s, 9 H, C(C*H*$_3$)$_3$), 1.42 (s, 18 H, C(C*H*$_3$)$_3$), 4.58 (s, 2 H, PC*H*$_2$S), 7.27 – 7.35 (m, 6 H, *o*–H, *p*–H), 7.58 – 7.63 (m, 4 H, *m*–H).

^{13}C{^{1}H}–NMR (125.76 MHz, THF–*d*$_8$): δ = 32.53 (C(*C*H$_3$)$_3$), 33.63 (C(*C*H$_3$)$_3$), 55.92 (N*C*(CH$_3$)$_3$), 56.79 (N*C*(CH$_3$)$_3$), 64.95 (d, $^1J_{P-C}$ = 24.40 Hz, PCH$_2$S), 129.74 (d, $^3J_{P-C}$ = 7.55 Hz, *o*–C), 129.90 (*p*–C), 134.54 (d, $^2J_{P-C}$ = 10.57 Hz, *m*–C), 139,84 (d, $^1J_{P-C}$ = 12.83 Hz, *ipso*–C).

^{31}P{^{1}H}–NMR (202.45 MHz, THF–*d*$_8$): δ = –27.45.

^{15}N–NMR (50.71 MHz, *d*$_8$–THF): δ = –249.5 (Sn–N*t*Bu), –223.71 (N*t*Bu).

Elemental analysis (found (calc.) [%]): C 46.85 (46.68), H 6.29 (6.11), N 6.51 (6.53), S 5.24 (4.98).

EI–MS m/z [%]: 643 [{M}, 3]$^+$, 628 [{M – CH$_3$}, 5]$^+$, 586 [{M – *t*Bu}, 3]$^+$, 564 [{M – Br}, 100]$^+$, 473 [{M – 3 *t*Bu}, 16]$^+$, 444 [{M – Ph$_2$PCH$_2$}, 8]$^+$.

5.3.14. [(benzene)RuCl$_2${Ph$_2$PCH$_2$S(N*t*Bu)$_2$NH*t*Bu}] (14)

[(benzene)RuCl$_2$]$_2$ (0.11 g, 0.20 mmol, 0.5 eq.) and Ph$_2$PCH$_2$S(N*t*Bu)$_2$NH*t*Bu (**13**) (0.18 g, 0.40 mmol, 1.0 eq.) were combined in an argon dry box and dissolved in THF (50 mL) at room temperature. After stirring overnight, the insoluble residue was filtered off and the red filtrate was reduced in volume and stored at –24 °C. Orange crystals were obtained after 14 days.

Empirical formula: $C_{31}H_{46}Cl_2N_3PRuS$ **Molecular weight:** 695.16 g/mol

Yield: 0.106 g, 0.16 mmol, 40%.

^{1}H–NMR (300.13 MHz, THF–*d*$_8$): δ = 0.86 (s, 9 H, N(H)C(C*H*$_3$)$_3$), 1.16 (s, 18 H, NC(C*H*$_3$)$_3$), 4.69 (s br, 2 H, PC*H*$_2$S), 5.26 (s br, 6 H, H$_{benzene}$), 7.39 – 7.55 (m, 6 H, *o*–H, *p*–H), 8.16 – 8.35 (m, 4 H, *m*–H).

^{13}C{^{1}H}–NMR (75.47 MHz, THF–*d*$_8$): δ = 29.00 (C(*C*H$_3$)$_3$), 32.01 (2 C(*C*H$_3$)$_3$), 52.65 (N*C*(CH$_3$)$_3$), 53.20 (N*C*(CH$_3$)$_3$), 87.97 (C$_{benzene}$), 126.93 (*o*–C$_{Ph}$), 130.27 (*m*, *p*–C$_{Ph}$), *ipso*–C$_{Ph}$ is not detected.

$^{31}P\{^{1}H\}$–NMR (121.49 MHz, THF–d_8): δ = 21.19.

Elemental analysis (found (calc.) [%]): C 55.06 (53.52), H 6.12 (6.65), N 5.56 (6.04), S 4.95 (4.61).

Deviations of the found values from the calculated values are due to traces of starting material in the product.

5.3.15. [(*p*–cymene)$RuCl_2${$Ph_2PCH_2S(NtBu)_2NHtBu$}] (15)

[(*p*–cymene)$RuCl_2]_2$ (0.13 g, 0.10 mmol, 0.5 eq.) and $Ph_2PCH_2S(NtBu)_2NHtBu$ (**13**) (0.18 g, 0.40 mmol, 1.0 eq.) were combined in an argon dry box and dissolved in THF (35 mL) at room temperature. After stirring overnight, the insoluble residue was filtered off and the red filtrate was reduced in volume and stored at –24 °C. Red–orange crystals were obtained after 21 days.

Empirical formula: $C_{35}H_{54}Cl_2N_3PRuS$ **Molecular weight:** 751.87 g/mol

Yield: 0.110 g, 0.14 mmol, 70%.

^{1}H–NMR (500.26 MHz, THF–d_8): δ = 0.81 (s br, 6 H, $CH(CH_3)_2$), 0.87 (s, 9 H, $N(H)C(CH_3)_3$), 1.15 (s, 18 H, $C(CH_3)_3$), 1.81 (s, 3 H, CH_3), 2.40 (hept, $^{3}J_{H,H}$ = 6.9 Hz, 1 H, $CH(CH_3)_2$),4.66 (s br, 2 H, PCH_2S), 5.90 (s br, 2 H, H_{arene}), 5.41 (s br, 2 H, H_{arene}), 7.46 – 7.47 (m, 6 H, *o*–H, *p*–H), 8.21 (s br, 4 H, *m*–H).

$^{13}C\{^{1}H\}$–NMR (125.76 MHz, THF–d_8): δ = 17.51 (CH_3), 21.27 ($CH(CH_3)_2$), 30.47 ($N(H)C(CH_3)_3$), 30.74($CH(CH_3)_2$)), 33.45 ($C(CH_3)_3$), 51.56 (d, $^{1}J_{P-C}$ = 8.30 Hz, SCH_2P), 53.98 ($NC(CH_3)_3$), 54.54 ($N(H)C(CH_3)_3$), 87.05 (s br, C_{arene}), 94.73 (*ipso*–C_{arene}), 108.15 (*ipso*–C_{arene}), 126.32 (*o*–C_{Ph}), 131.26 (*p*–C_{Ph}), 135.58 (*m*–C_{Ph}), *ipso*–C_{Ph} is not detected.

$^{31}P\{^{1}H\}$–NMR (202.46 MHz, THF–d_8): δ = 22.47.

^{15}N–NMR (50.71 MHz, THF–d_8): δ = –262.5 (*N*HtBu).

Elemental analysis (found (calc.) [%]): C 55.15 (55.91), H 7.25 (7.24), N 5.46 (5.59), S 4.69 (4.26).

6. Crystallographic section

6.1. Crystal selection and manipulation

Single crystals were selected from a Schlenk flask under argon atmosphere and covered with perfluorated polyether oil on a microscope slide, which was cooled with an inert gas flow (nitrogen, +25 °C – −100 °C) using the *X–TEMP2* device.[99] An appropriate crystal was selected using a microscope equipped with polarization filter, mounted on the tip of a MiTeGen©MicroMount or glass fiber, fixed to a goniometer head and shock cooled by the crystal cooling device.

6.2. Data collection and processing

The compounds were measured using either an Incoatec microfocus source with mirror optics or on a rotating anode turbo X–ray source.[100] Both are equipped with an APEX II CCD detector, mounted on a three–circle D8 goniometer, and mirrors as monochromator optics, which supplies very intense and brilliant MoK_α radiation (λ = 0.71073 Å). Compound **12** was measured on a similar machine with a Ag–K_α (λ = 0.56086 Å) microfocus source. All crystals were centred optically using a video camera after being placed on the diffractometer.

The data collection strategy was calculated with the APEX plugin *COSMO*[101] or entered by hand. Therefore, a test run (*matrix scan*) was recorded prior to each experiment to check the crystal quality, to get a rough estimate of the cell parameters, and to determine the optimum exposure time. All scans of the data collections were performed in an ω–scan mode with a step–width of 0.3° or 0.5° at fixed ϕ–angles.

The unit cell was indexed with the tools in the Bruker *APEX2* software suite.[102] The intensities on the raw frames were integrated with *SAINT* 7.68a.[102b] The orientation matrix was refined in several integration runs and the maximum resolution was adjusted so that only useable data with a maximum R_{int} of 0.20 were integrated.

The software *SADABS* 2012/1[103] was used for absorption correction and scaling. *TWINABS*[104] was utilised in the cases of non–merohedral twins or split crystals. Both programs refine an empirical error function by symmetry–equivalent

reflections. ***XPREP*** in various version up to 2013/1[105] was used for the examination of data statistics and preliminary space group determination prior to the absorption correction, as this is crucial for a correct treatment. Finally, ***XPREP*** was used to setup the files for structure solution and refinement.

6.3. Structure solution and refinement

The structures were solved with direct methods using ***SHELXS***.[106] All refinements were performed on F^2 with ***SHELXL–2012***[107] implemented in the ***SHELXLE–GUI***.[108] All non–hydrogen–atoms were refined with anisotropic displacement parameters. The C–bonded hydrogen atoms were set on calculated positions and refined isotropically using a riding model with their U_{iso} values constrained equal to 1.5 times the U_{eq} of their pivot atoms for methyl carbon atoms and 1.2 times for all other carbon atoms. The N–bonded hydrogen atom coordinates were refined freely from the residual density map and constrained to 1.5 U_{eq} of their pivot nitrogen atom. If not stated otherwise, the hydrogen bond lengths were restrained to a sensible value and the U_{iso} were constrained as mentioned above.

In the absence of restraints, the only data the structural model is refined against are the measured intensities in the form of squared structure factors. Structure factors are calculated from the atomic model and the so–calculated intensities are then compared with the measured intensities, and the best model is the one that minimises $M(p_i, k)$ (Eq. 6–1) using the weights w defined in Eq. 6–2.

Eq. 6–1 $$M\left(p_i,k\right) = \sum w[k|F_{obs}|^2 - |F_{calc}|^2]^2 = min$$

(p_i: structural parameters; k: scale factor)

Eq. 6–2 $$w^{-1} = \sigma^2(F_{obs}^2) + (g1 \times P)^2 + g2 \times P \qquad \text{with} \quad P = \left(\frac{Max\,(F_{obs}^2, 0 + 2F_{calc}^2}{3}\right)$$

The results of the refinements were verified by comparison of the calculated and the observed structure factors. Commonly used criteria are the residuals ***R1*** (Eq. 6–3) and ***wR2*** (Eq. 6–4).

Eq. 6–3 $$R1 = \frac{\sum||F_{obs}|-|F_{calc}||}{\sum|F_{obs}|}$$

Eq. 6–4 $$wR2 = \sqrt{\frac{\sum w\left(F_{obs}^2 - F_{calc}^2\right)^2}{\sum w\left(F_{obs}^2\right)^2}}$$

Additionally, the goodness of fit (***GoF, S***), a figure or merit showing the relation between deviation of F_{calc} from F_{obs} and the over–determination of refined parameters is calculated (Eq. 6–5).

Eq. 6–5 $$S = \sqrt{\frac{\sum\left(w\left(F_{obs}^2 - F_{calc}^2\right)^2\right)}{n-p}}$$

(*n*: number of reflections; *p*: number of parameters)

The residual densities from difference *Fourier* analysis should be low. Due to the model restrictions the residuals are normally found in the bonding regions. Higher residuals for heavy scatterers are acceptable as they arise mainly from absorption effects and *Fourier* truncation errors due to the limited recorded resolution range. The highest peak and deepest hole from difference *Fourier* analysis are listed in the crystallographic tables.

Additionally, the orientation, size and ellipticity of the ADPs show the quality of the model. Ideally, the ADPs should be oriented perpendicular to the bonds, be equal in size and show little ellipticity. All graphics were generated and plotted with the *xp*[109] program at the 50 % probability level.

6.4. Treatment of disorder

Structures containing disordered fragments were refined using constraints and restraints. Constraints used within this work are, for example, the site occupation factor and the AFIX instruction, which defines and constrains rigid groups.

Mathematically, restraints are treated as additional experimental observations, thus increasing the number of data to refine against. In the presence of restraints the minimization function changes as follows:

Eq. 6–6 $$M = \sum w\left(F_{obs}^2 - F_{calc}^2\right)^2 + \sum w_r\left(R_{target} - R_{calc}\right)^2$$

The geometries of chemically equivalent but crystallographically independent fragments can be fitted to each other by distance restraints. Especially the 1,2

distances (bond lengths) and 1,3 distances (bond angles) are set to be equal within their effective standard deviations. This is helpful for refining disordered positions as the averaging of equivalent fragments implements chemical information and stabilises the refinement. Within this work, disordered moieties were refined using distance restraints (***SADI*** and ***SAME***) and anisotropic displacement parameter restraints (***SIMU, DELU*** and ***RIGU***).[110]

6.5. Determined structures

6.5.1. [(tmeda)Li{(N*t*Bu)$_3$SCH$_2$PPh$_2$}] (1)

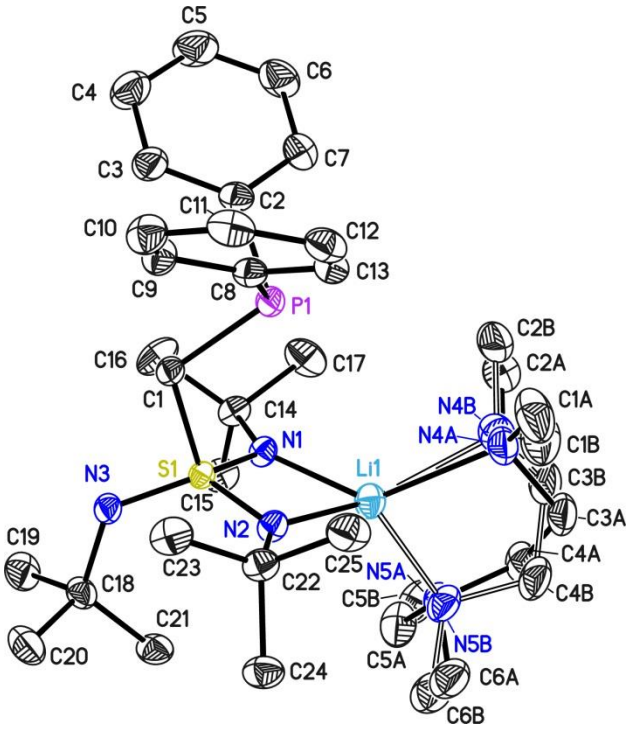

Figure 6.1: Asymmetric unit of compound **1**. The anisotropic displacement parameters are shown at the 50% probability level. Hydrogen atoms are omitted for clarity. The TMEDA moiety is disordered on two positions (*sof*: 0.668(7)).

Structure code		EC50	Z	4
Empirical formula		$C_{31}H_{55}LiN_5PS$	Crystal dimensions [mm]	0.10 × 0.05 × 0.05
Formula weight [g/mol]		567.77	$\rho_{calcd.}$ [g/cm^3]	1.116
Sample temperature [K]		100(2)	μ[mm^{-1}]	0.170
Wavelength [Å]		0.71073	*F* (000)	1240
Crystal system		Orthorhombic	Θ range [°]	1.574 to 26.394
Space group		$P2_12_12_1$	Reflections collected	136236
Unit cell dimensions [Å]			Unique reflections	6921
	a =	9.959(2)	R_{int}	0.0309
	b =	16.962(3)	Completeness to θ_{max}	100%
	c =	20.007(3)	restraints/parameters	434 / 434
	α =	90°	GooF	1.073
	β =	90°	$R1(I > 2\sigma(I))$	0.0249
	γ =	90°	*wR*2 (all data)	0.0682
Volume [Å^3]		3379.7(10)	max. diff. peak/hole [e·Å^{-3}]	0.236 and −0.242
Extinction coefficient		–	Absolute structure parameter[111]	0.007(7)

6.5.2. [Mn{(N*t*Bu)$_3$SCH$_2$PPh$_2$}$_2$] (2)

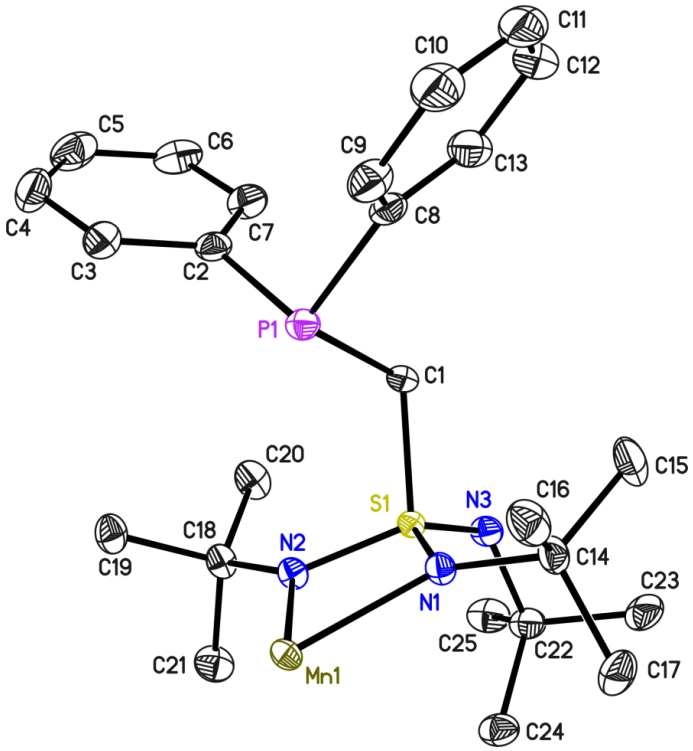

Figure 6.2: Asymmetric unit of compound **2**. The anisotropic displacement parameters are shown at the 50% probability level. Hydrogen atoms are omitted for clarity.

Structure code		EC61_Mn	Z	4
Empirical formula		$C_{50}H_{78}MnN_6P_2S_2$	Crystal dimensions [mm]	0.09 × 0.05 × 0.05
Formula weight [g/mol]		944.18	$\rho_{calcd.}$ [g/cm^3]	1.218
Sample temperature [K]		100(2)	μ[mm^{-1}]	0.438
Wavelength [Å]		0.71073	*F* (000)	2028
Crystal system		Monoclinic	Θ range [°]	1.732 to 25.344
Space group		*C* 2/*c*	Reflections collected	50751
Unit cell dimensions [Å]			Unique reflections	4717
	a =	16.805(2)	R_{int}	0. 0644
	b =	13.033(2)	Completeness to θ_{max}	99.9%
	c =	24.084(2)	restraints/parameters	0 / 285
	α =	90°	GooF	1.059
	β =	102.44(2)°.	*R*1(I > 2σ(I))	0.0351
	γ =	90°	*wR*2 (all data)	0.0814
Volume [Å^3]		5151.0(12)	max. diff. peak/hole [e·Å^{-3}]	0.316 and –0.302
Extinction coefficient		–	Absolute structure parameter[111]	–

6.5.3. [Fe{(N*t*Bu)$_3$SCH$_2$PPh$_2$}$_2$] (3)

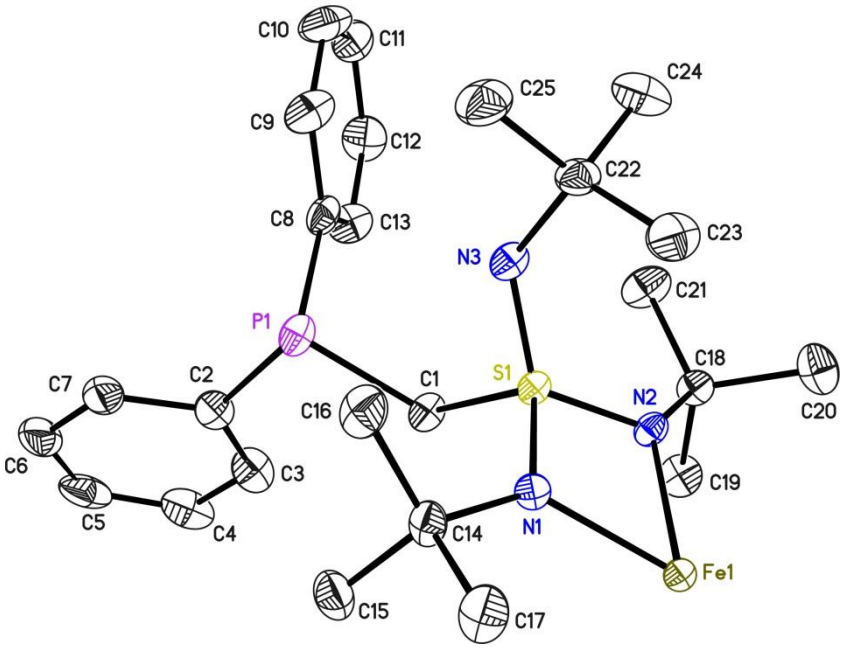

Figure 6.3: Asymmetric unit of compound **3**. The anisotropic displacement parameters are shown at the 50% probability level. Hydrogen atoms are omitted for clarity.

Structure code		EC77_Fe	Z	2
Empirical formula		$C_{50}H_{78}FeN_6P_2S_2$	Crystal dimensions [mm]	0.10 × 0.09 × 0.05
Formula weight [g/mol]		945.09	$\rho_{calcd.}$ [g/cm^3]	1.190
Sample temperature [K]		100(2)	μ[mm^{-1}]	0.464
Wavelength [Å]		0.71073	*F* (000)	1016
Crystal system		Monoclinic	Θ range [°]	1.585 to 26.791
Space group		*C* 2	Reflections collected	24770
Unit cell dimensions [Å]			Unique reflections	5619
	a =	26.068(2)	R_{int}	0.0463
	b =	9.389(2)	Completeness to θ_{max}	99.9%
	c =	10.929(2)	restraints/parameters	1 / 285
	α =	90°	GooF	1.056
	β =	99.68(2)°	*R*1(I > 2σ(I))	0.0333
	γ =	90°	*wR*2 (all data)	0.0920
Volume [Å^3]		2636.8(8)	max. diff. peak/hole [e·Å^{-3}]	0.905 and –0.421
Extinction coefficient		–	Absolute structure parameter[111]	0.024(8)

6.5.4. [Co{(N*t*Bu)$_3$SCH$_2$PPh$_2$}$_2$] (4)

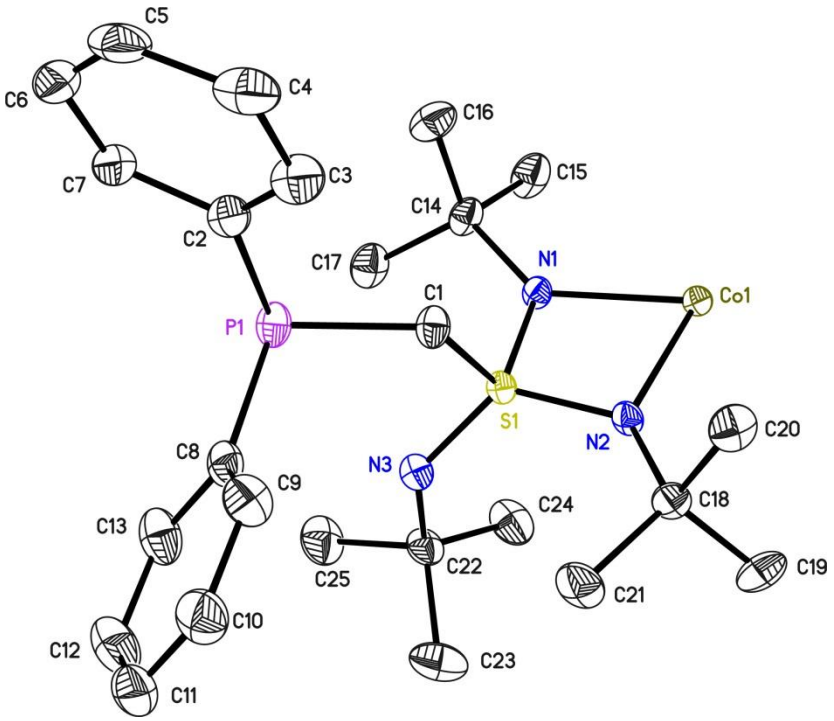

Figure 6.4: Asymmetric unit of compound **4**. The anisotropic displacement parameters are shown at the 50% probability level. Hydrogen atoms are omitted for clarity. The crystal is a non–merohedral twin. The structure was refined against HKLF5 data, including two domains, with a batch scale factor of 0.096(2).

Structure code		ECP63	Z	2
Empirical formula		$C_{50}H_{78}CoN_6P_2S_2$	Crystal dimensions [mm]	0.1 × 0.08 × 0.05
Formula weight [g/mol]		947.95	$\rho_{calcd.}$ [g/cm^3]	1.198
Sample temperature [K]		99(2)	μ[mm^{-1}]	0.505
Wavelength [Å]		0.71073	*F* (000)	1018
Crystal system		Monoclinic	Θ range [°]	1.583 to 26.034
Space group		*C* 2	Reflections collected	11821
Unit cell dimensions [Å]			Unique reflections	2763
	a =	26.085(2)	R_{int}	0.0485
	b =	9.382(2)	Completeness to θ_{max}	99.8%
	c =	10.892(2)	restraints/parameters	256 / 286
	α =	90°	GooF	1.044
	β =	99.47(2)°	*R*1(I > 2σ(I))	0.0278
	γ =	90°	*wR*2 (all data)	0.0687
Volume [Å^3]		2629.3(8)	max. diff. peak/hole [e·Å^{-3}]	0.351 and –0.525
Extinction coefficient		–	Absolute structure parameter[111]	0.093(8)

6.5.5. [(tmeda)Li(*μ*–Br)$_2$Co{(N*t*Bu)$_3$SCH$_2$PPh$_2$}] (5)

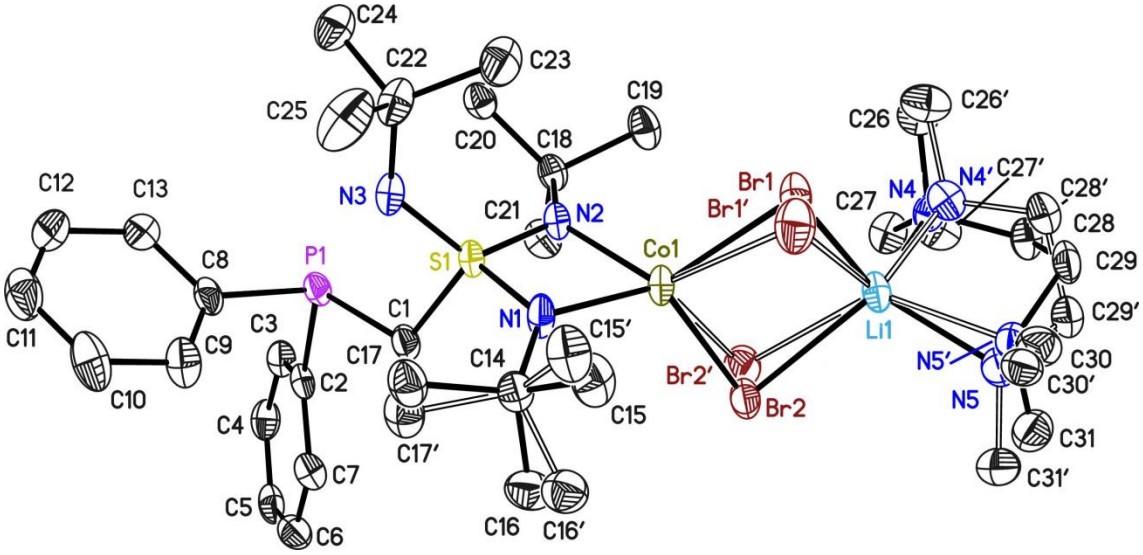

Figure 6.5: Asymmetric unit of compound **5**. The anisotropic displacement parameters are shown at the 50% probability level. The bromine atoms, the *t*butyl group C15 to C16 and the TMEDA moiety are disordered on two positions, respectively (*sof*s: 0.939(4), 0.722(4) and 0.604(19)). Hydrogen atoms are omitted for clarity.

Structure code		ECP162	Z	2
Empirical formula		$C_{31}H_{55}Br_2CoLiN_5PS$	Crystal dimensions [mm]	0.08 × 0.07 × 0.02
Formula weight [g/mol]		786.52	$\rho_{calcd.}$ [g/cm^3]	1.357
Sample temperature [K]		100(2)	μ[mm^{-1}]	2.643
Wavelength [Å]		0.71073	*F* (000)	814
Crystal system		Triclinic	Θ range [°]	1.268 to 25.382
Space group		$P\bar{1}$	Reflections collected	42381
Unit cell dimensions [Å]			Unique reflections	7054
	a =	9.094(2)	R_{int}	0.0329
	b =	13.259(2)	Completeness to θ_{max}	100%
	c =	16.882(2)	restraints/parameters	546/513
	α =	106.73(2)°	GooF	1.032
	β =	94.37(2)°	*R*1(I > 2σ(I))	0.0251
	γ =	24(2)°	*wR*2 (all data)	0.0598
Volume [Å^3]		1925.5(6)	max. diff. peak/hole [e·Å^{-3}]	0.444 and –0.246
Extinction coefficient		–	Absolute structure parameter[111]	–

6.5.6. [Co{(NtBu)$_3$SMe}$_2$] (6)

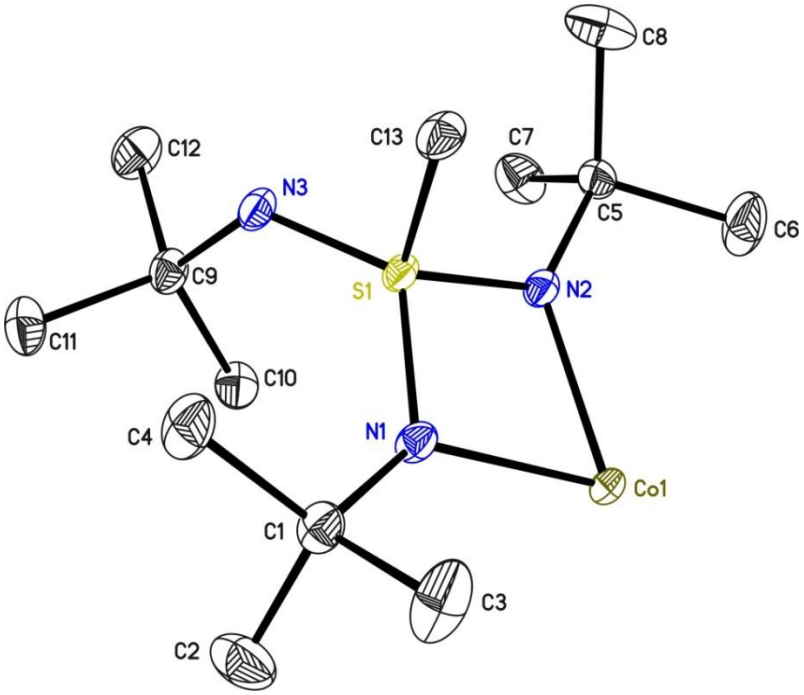

Figure 6.6: Asymmetric unit of compound **6**. The anisotropic displacement parameters are shown at the 50% probability level. Hydrogen atoms are omitted for clarity.

Structure code		ECP11	Z	4
Empirical formula		$C_{26}H_{60}CoN_6S_2$	Crystal dimensions [mm]	0.10 × 0.10 × 0.05
Formula weight [g/mol]		579.85	$\rho_{calcd.}$ [g/cm^3]	1.186
Sample temperature [K]		100(2)	μ[mm^{-1}]	0.681
Wavelength [Å]		0.71073	*F* (000)	1268
Crystal system		Monoclinic	Θ range [°]	1.959 to 27.121
Space group		*C* 2/*c*	Reflections collected	46244
Unit cell dimensions [Å]			Unique reflections	3585
	a =	25.274(2)	R_{int}	0.0263
	b =	8.809(2)	Completeness to θ_{max}	99.8%
	c =	17.735(2)	restraints/parameters	0 / 169
	α =	90°	GooF	1.089
	β =	124.67(2)°	*R*1(I > 2σ(I))	0.0231
	γ =	90°	*wR*2 (all data)	0.0635
Volume [Å^3]		3247.4(11)	max. diff. peak/hole [e·Å^{-3}]	0.410 and –0.303
Extinction coefficient		–	Absolute structure parameter[111]	–

6.5.7. [Ni{(N*t*Bu)$_3$SCH$_2$PPh$_2$}$_2$] (7)

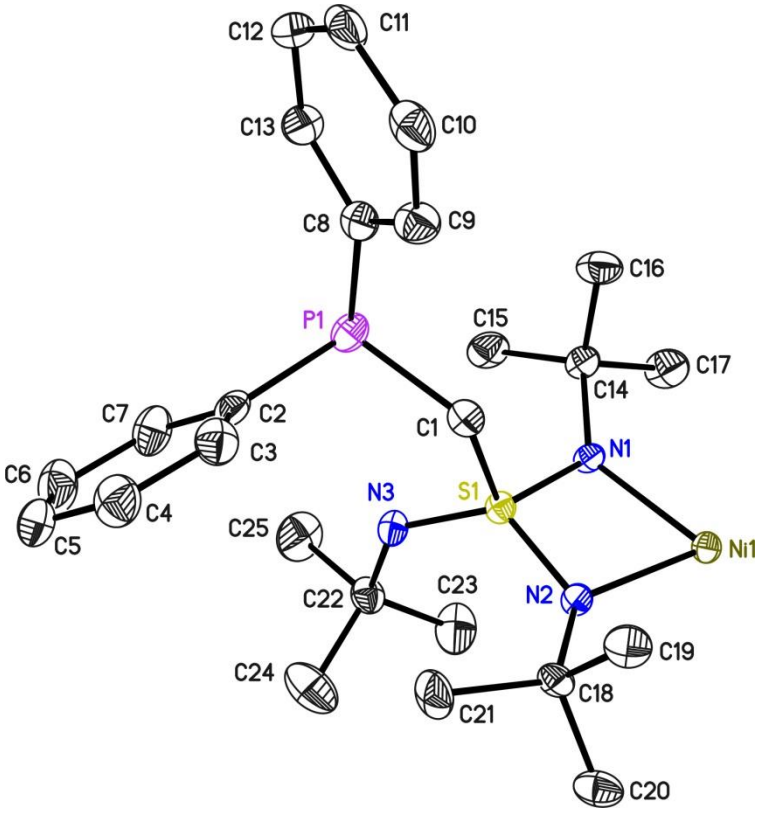

Figure 6.7: Asymmetric unit of compound **7**. The anisotropic displacement parameters are shown at the 50% probability level. Hydrogen atoms are omitted for clarity.

Structure code		ECP113	Z	2
Empirical formula		$C_{50}H_{78}NiN_6P_2S_2$	Crystal dimensions [mm]	0.05 × 0.04 × 0.01
Formula weight [g/mol]		947.95	$\rho_{calcd.}$ [g/cm^3]	1.205
Sample temperature [K]		100(2)	μ[mm^{-1}]	0.551
Wavelength [Å]		0.71073	*F* (000)	1020
Crystal system		Monoclinic	Θ range [°]	1.586 to 25.387
Space group		*C* 2	Reflections collected	20228
Unit cell dimensions [Å]			Unique reflections	4803
	a =	26.033(2)	R_{int}	0.0522
	b =	9.369(2)	Completeness to θ_{max}	100%
	c =	10.858(2)	restraints/parameters	1 / 285
	α =	90°	GooF	0.988
	β =	99.50(2)°	*R*1(I > 2σ(I))	0.0332
	γ =	90°	*wR*2 (all data)	0.0646
Volume [Å^3]		2612.0(8)	max. diff. peak/hole [e·Å^{-3}]	0.267 and –0.234
Extinction coefficient		–	Absolute structure parameter[111]	0.038(8)

6.5.8. [Cu{(NtBu)$_3$SCH$_2$PPh$_2$}$_2$] (8)

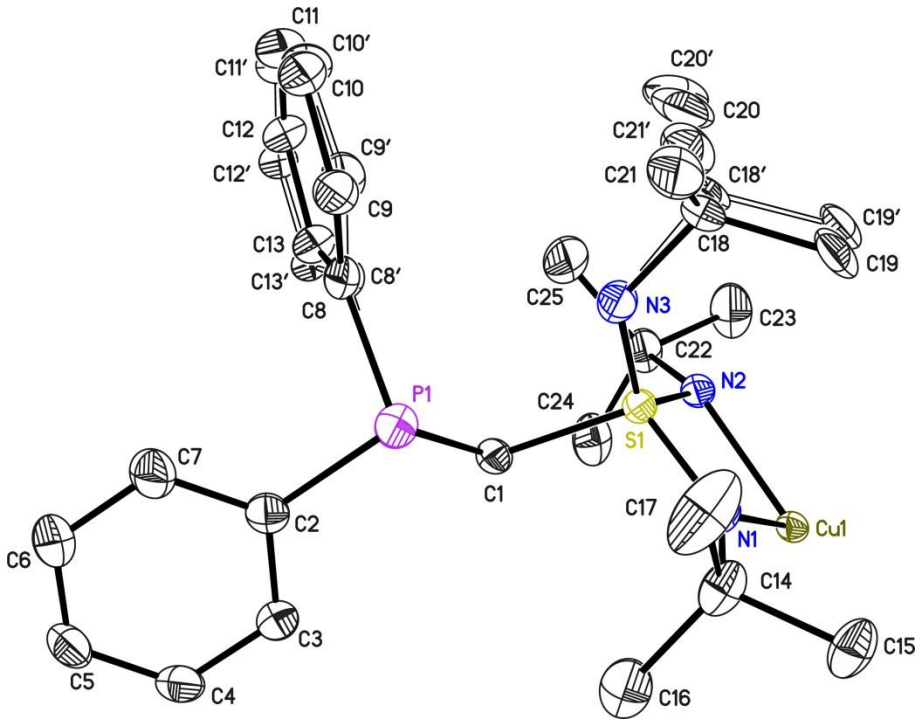

Figure 6.8: Asymmetric unit of compound **8**. The anisotropic displacement parameters are shown at the 50% probability level. Hydrogen atoms are omitted for clarity. The phenyl ring (C8) and the *t*butyl group C18 are disordered on two positions (*sof*s: 0.57(1) and 0.60(3)).

Structure code		ECP_Cu	Z	4
Empirical formula		$C_{50}H_{78}CuN_6P_2S_2$	Crystal dimensions [mm]	0.10 × 0.05 × 0.05
Formula weight [g/mol]		952.78	$\rho_{calcd.}$ [g/cm^3]	1.197
Sample temperature [K]		100(2)	μ[mm^{-1}]	0.590
Wavelength [Å]		0.71073	*F* (000)	2044
Crystal system		Monoclinic	Θ range [°]	1.34 to 26.04
Space group		*C* 2/*c*	Reflections collected	45222
Unit cell dimensions [Å]			Unique reflections	5221
	a =	30.529(2)	R_{int}	0.0520
	b =	9.545(2)	Completeness to θ_{max}	99.9%
	c =	18.223(2)	restraints/parameters	351 / 380
	α =	90°	GooF	1.064
	β =	95.17(2)°	*R*1(I > 2σ(I))	0.0333
	γ =	90°	*wR*2 (all data)	0.0897
Volume [Å^3]		5288.6(13)	max. diff. peak/hole [e·Å^{-3}]	0.375 and –0.277
Extinction coefficient		–	Absolute structure parameter[111]	–

6.5.9. [(tmeda)$Li_{0.79}/Cu_{2.21}(\mu$-$Cl_{1.96}Br_{0.04})\{Ph_2PCH_2S(NtBu)_3\}$] (9)

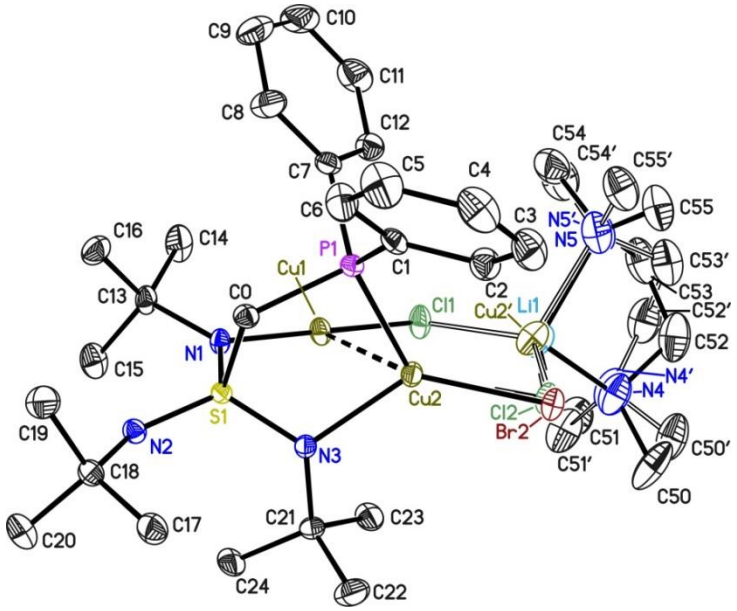

Figure 6.9: Asymmetric unit of compound **9**. The anisotropic displacement parameters are shown at the 50% probability level. Hydrogen atoms are omitted for clarity. The non–integer numbers in the formula sum results from two position disorders. The Li1 and Cu2' atoms are disordered with a site occupation factor of 0.791(2) and the Cl2 and Br2 atom with a site occupation factor of 0.957(2). The TMEDA moiety is disordered on two positions (*sof:* 0.667(6)).

Structure code		EC105	Z	2
Empirical formula		$C_{31}H_{55}Br_{0.04}Cl_{1.96}Cu_{2.21}Li_{0.79}N_5PS$	Crystal dimensions [mm]	0.10 × 0.10 × 0.08
Formula weight [g/mol]		779.50	$\rho_{calcd.}$ [g/cm³]	1.325
Sample temperature [K]		100(2)	μ[mm⁻¹]	1.498
Wavelength [Å]		0.71073	*F* (000)	816
Crystal system		Monoclinic	Θ range [°]	1.746 to 28.296
Space group		$P\,2_1$	Reflections collected	59343
Unit cell dimensions [Å]			Unique reflections	9709
	a =	9.952(2)	R_{int}	0.0326
	b =	16.830(2)	Completeness to θ_{max}	99.9%
	c =	11.666(2)	restraints/parameters	395 / 478
	α =	90°	GooF	1.028
	β =	90.91(2)°	*R*1(I > 2σ(I))	0.0236
	γ =	90°	*wR*2 (all data)	0.0532
Volume [Å³]		1953.7(6)	max. diff. peak/hole [e·Å⁻³]	0.351 and –0.215
Extinction coefficient		–	Absolute structure parameter[111]	0.010(3)

6.5.10. [Zn{(N*t*Bu)$_3$SCH$_2$PPh$_2$}$_2$] (10)

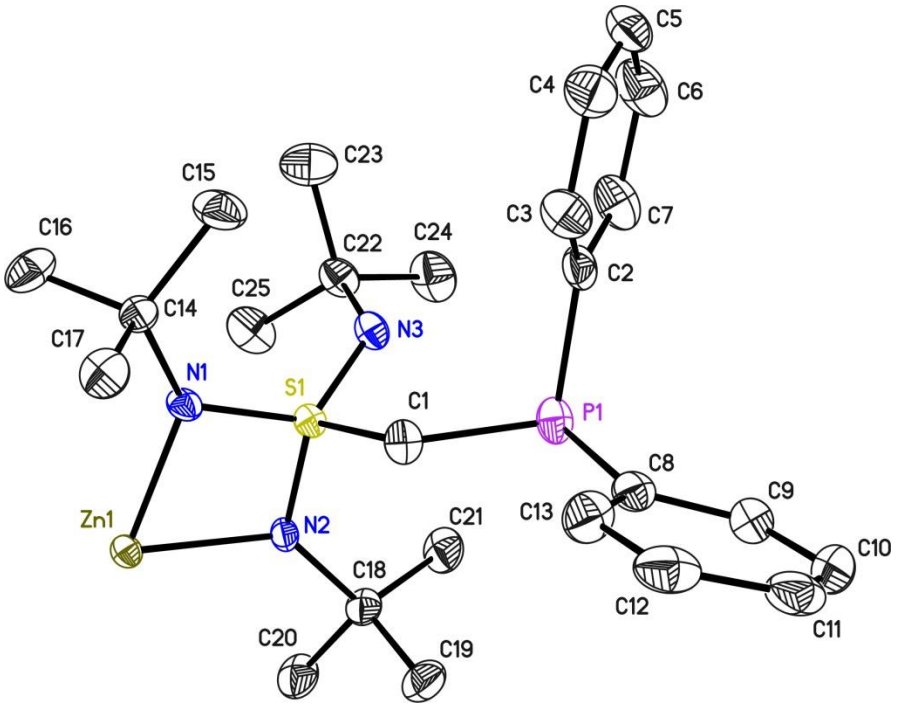

Figure 6.10: Asymmetric unit of compound **10**. The anisotropic displacement parameters are shown at the 50% probability level. Hydrogen atoms are omitted for clarity.

Structure code		ECP143	Z	2
Empirical formula		$C_{50}H_{78}ZnN_6P_2S_2$	Crystal dimensions [mm]	0.1 × 0.08 × 0.06
Formula weight [g/mol]		954.61	$\rho_{calcd.}$ [g/cm^3]	1.207
Sample temperature [K]		100(2)	μ[mm^{-1}]	0.646
Wavelength [Å]		0.71073	*F* (000)	1024
Crystal system		Monoclinic	Θ range [°]	1.585 to 26.378
Space group		*C* 2	Reflections collected	21432
Unit cell dimensions [Å]			Unique reflections	5362
	a =	26.054(2)	R_{int}	0.0295
	b =	9.375(2)	Completeness to θ_{max}	100%
	c =	10.907(2)	restraints/parameters	1 / 285
	α =	90°	GooF	1.035
	β =	99.56(2)°	*R*1(I > 2σ(I))	0.0290
	γ =	90°	*wR*2 (all data)	0.0654
Volume [Å^3]		2627.0(4)	max. diff. peak/hole [e·Å^{-3}]	0.410 and –0.182
Extinction coefficient		–	Absolute structure parameter[111]	0.028(5)

6.5.11. [GeCl{(N*t*Bu)$_3$SCH$_2$PPh$_2$}] (11)

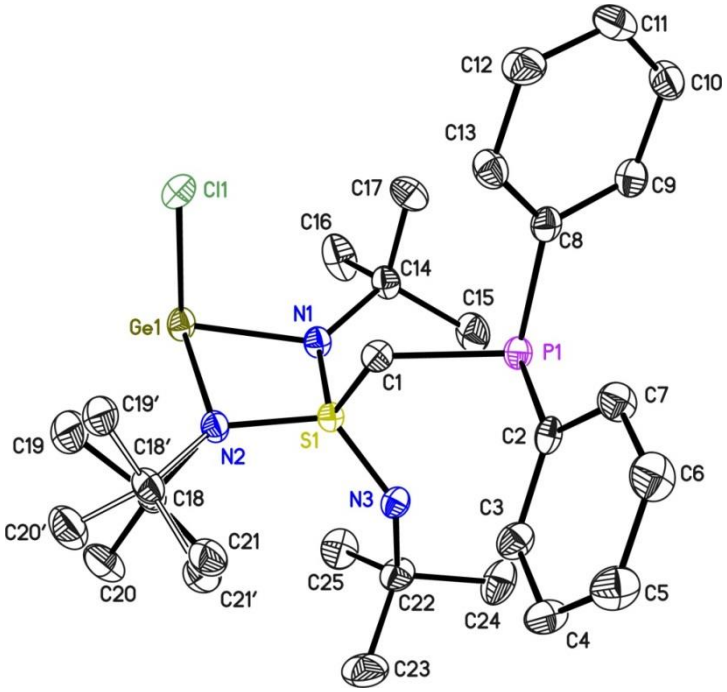

Figure 6.11: Asymmetric unit of compound **11**. The anisotropic displacement parameters are shown at the 50% probability level. Hydrogen atoms are omitted for clarity. The C18 *t*butyl group is disordered on two positions (*sof*: 0.724(11)).

Structure code		EC_LK14	Z	4
Empirical formula		$C_{25}H_{39}ClGeN_3PS$	Crystal dimensions [mm]	0.10 × 0.08 × 0.06
Formula weight [g/mol]		552.66	$\rho_{calcd.}$ [g/cm^3]	1.312
Sample temperature [K]		105(2)	μ[mm^{-1}]	1.340
Wavelength [Å]		0.71073	*F* (000)	1160
Crystal system		Monoclinic	Θ range [°]	1.407 to 25.679
Space group		*P* 2$_1$/*n*	Reflections collected	30668
Unit cell dimensions [Å]			Unique reflections	5303
	a =	10.136(1)	R_{int}	0.0511
	b =	9.535(1)	Completeness to θ_{max}	100%
	c =	29.385(2)	restraints/parameters	184 / 332
	α =	90°	GooF	1.026
	β =	99.89(2)°	*R*1(I > 2σ(I))	0.0325
	γ =	90°	*wR*2 (all data)	0.0714
Volume [Å^3]		2797.8(5)	max. diff. peak/hole [e·Å^{-3}]	0.311 and –0.350
Extinction coefficient		–	Absolute structure parameter[111]	–

6.5.12. [SnBr{(N*t*Bu)$_3$SCH$_2$PPh$_2$}] (12)

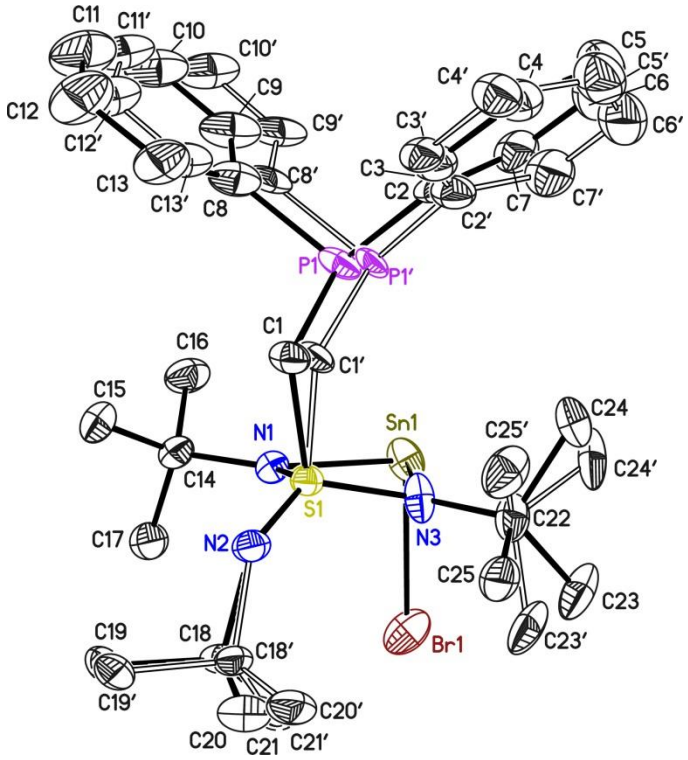

Figure 6.12: Asymmetric unit of compound **12**. Hydrogen atoms are omitted for clarity. The CH_2PPh_2 moiety is disordered on two positions (*sof*: 0.579(6)). The *t*butyl groups (C18 and C22) are also disordered on two positions (*sof*s: 0.776(17) and 0.488(5)).

Structure code		EC_LK_07	Z	4
Empirical formula		$C_{25}H_{39}BrSnN_3PS$	Crystal dimensions [mm]	0.1 × 0.09 × 0.05
Formula weight [g/mol]		643.22	$\rho_{calcd.}$ [g/cm^3]	1.504
Sample temperature [K]		100(2)	μ[mm^{-1}]	1.309
Wavelength [Å]		0.56085	*F* (000)	1304
Crystal system		Monoclinic	Θ range [°]	1.395 to 21.974
Space group		*P* 2$_1$/*n*	Reflections collected	30356
Unit cell dimensions [Å]			Unique reflections	7060
	a =	10.645(2)	R_{int}	0.0409
	b =	15.489(3)	Completeness to θ_{max}	100 %
	c =	17.754(3)	restraints/parameters	1519 / 484
	α =	90°	GooF	1.093
	β =	103.91(2)°	*R*1(I > 2σ(I))	0.0386
	γ =	90°	*wR*2 (all data)	0.0770
Volume [Å^3]		2841.5(9)	max. diff. peak/hole [e·Å^{-3}]	1.032 and –0.928[a]
Extinction coefficient		–	Absolute structure parameter[111]	–

[a] There is a high residual electron density at the tin(II) atom due to absorption.

6.5.13. [(benzene)$RuCl_2${$Ph_2PCH_2S(NtBu)_2NHtBu$}] (14)

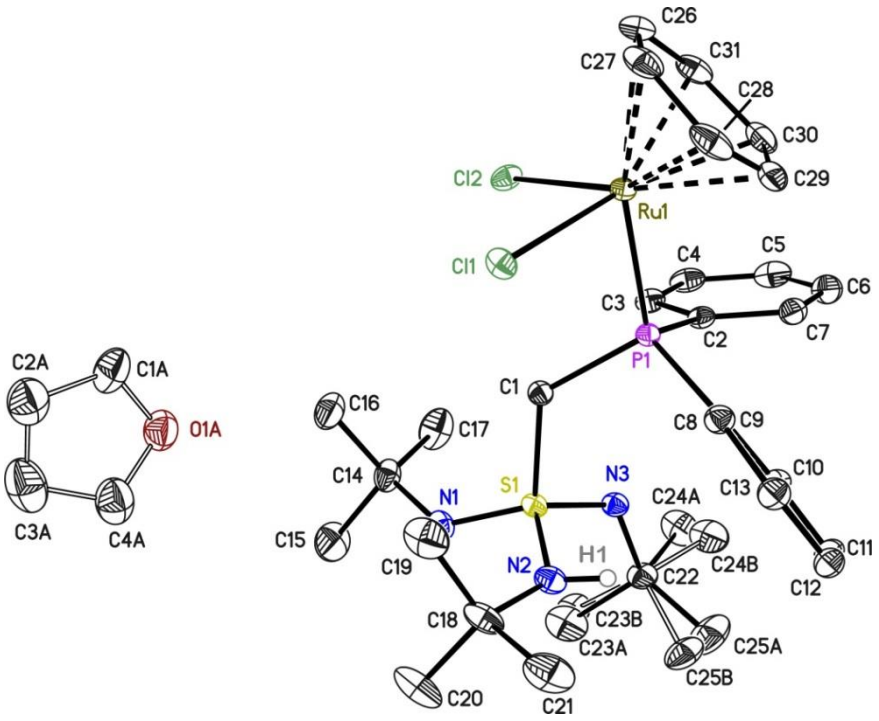

Figure 6.13: Asymmetric unit of compound **14**. The anisotropic displacement parameters are shown at the 50% probability level. Not freely refined hydrogen atoms are omitted for clarity. One *t*butyl group is disordered with a site occupation factor of 0.193(16). The THF solvent molecule is disordered on a special position and just with one half in the unit cell.

Structure code		EC_FB_08	Z	2
Empirical formula		$C_{33}H_{50}Cl_2N_3O_{0.50}PRuS$	Crystal dimensions [mm]	0.10 × 0.09 × 0.05
Formula weight [g/mol]		731.76	$\rho_{calcd.}$ [g/cm^3]	1.396
Sample temperature [K]		100(2)	μ[mm^{-1}]	0.738
Wavelength [Å]		0.71073	*F* (000)	764
Crystal system		Triclinic	Θ range [°]	2.080 to 30.038
Space group		$P\bar{1}$	Reflections collected	40630
Unit cell dimensions [Å]			Unique reflections	10203
	a =	9.518(2)	R_{int}	0.0349
	b =	9.790(2)	Completeness to θ_{max}	100%
	c =	18.740(2)	restraints/parameters	123 / 441
	α =	89.53(2)°	GooF	1.054
	β =	85.65(2)°	*R*1(I > 2σ(I))	0.0255
	γ =	89.18(2)°	*wR*2 (all data)	0.0589
Volume [Å^3]		1741.0(5)	max. diff. peak/hole [e·Å^{-3}]	0.461 and –0.493
Extinction coefficient		–	Absolute structure parameter	–

6.5.14. [(*p*–cymene)$RuCl_2${$Ph_2PCH_2S(NtBu)_2NHtBu$}] (15)

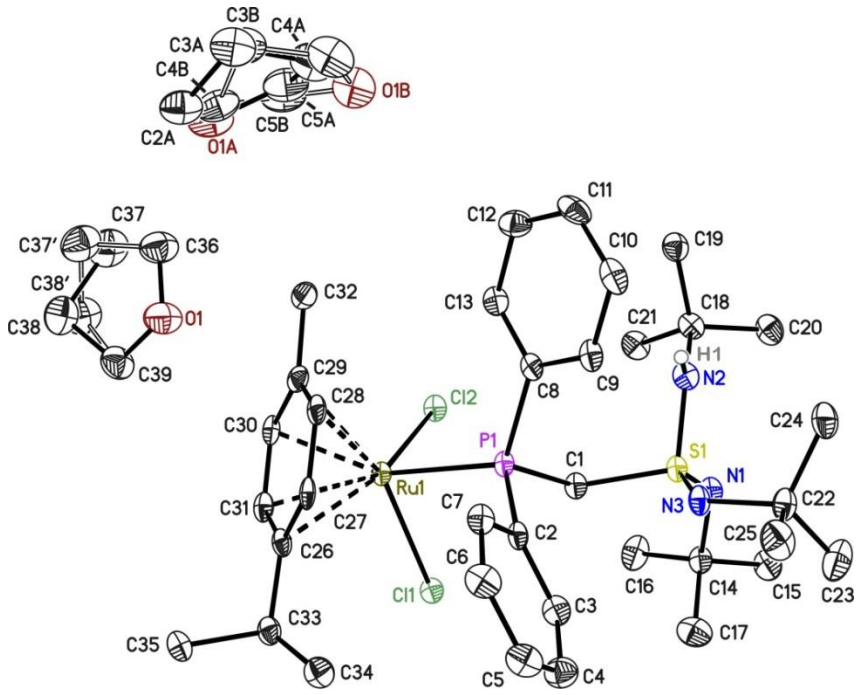

Figure 6.14: Asymmetric unit of compound **15**. The anisotropic displacement parameters are shown at the 50% probability level. Not freely refined hydrogen atoms are omitted for clarity. The THF molecules are disordered with site occupation factors of 0.437(7) (for O1A to C5B) and 0.599(12) (for O1 to C39).

Structure code		ECP150	Z	4
Empirical formula		$C_{43}H_{70}Cl_2N_3O_2PRuS$	Crystal dimensions [mm]	0.10 × 0.05 × 0.01
Formula weight [g/mol]		896.02	$\rho_{calcd.}$ [g/cm³]	1.307
Sample temperature [K]		100(2)	μ[mm⁻¹]	0.58
Wavelength [Å]		0.71073	*F* (000)	1896
Crystal system		Monoclinic	Θ range [°]	1.381 to 26.022
Space group		*P* $2_1/c$	Reflections collected	52733
Unit cell dimensions [Å]			Unique reflections	8955
	a =	15.048(2)	R_{int}	0.0457
	b =	13.442(2)	Completeness to θ_{max}	99.9%
	c =	22.974(2)	restraints/parameters	368 / 583
	α =	90°	GooF	1.172
	β =	101.48(2)°	*R*1(I > 2σ(I))	0.0468
	γ =	90°	*wR*2 (all data)	0.1028
Volume [Å³]		4554.1(10)	max. diff. peak/hole [e·Å⁻³]	1.249 and –1.335[a]
Extinction coefficient		–	Absolute structure parameter	–

[a] There is a high residual electron density at the ruthenium(II) atom due to absorption.

7. Crystal structure determination in collaborations

7.1. Structures determined for Kartik Chandra Mondal

7.1.1. $(Me_2–cAACH)[(Me_2–cAAC:)Co(\mu–Cl)_2Cl(Li)_{0.5}]_2$

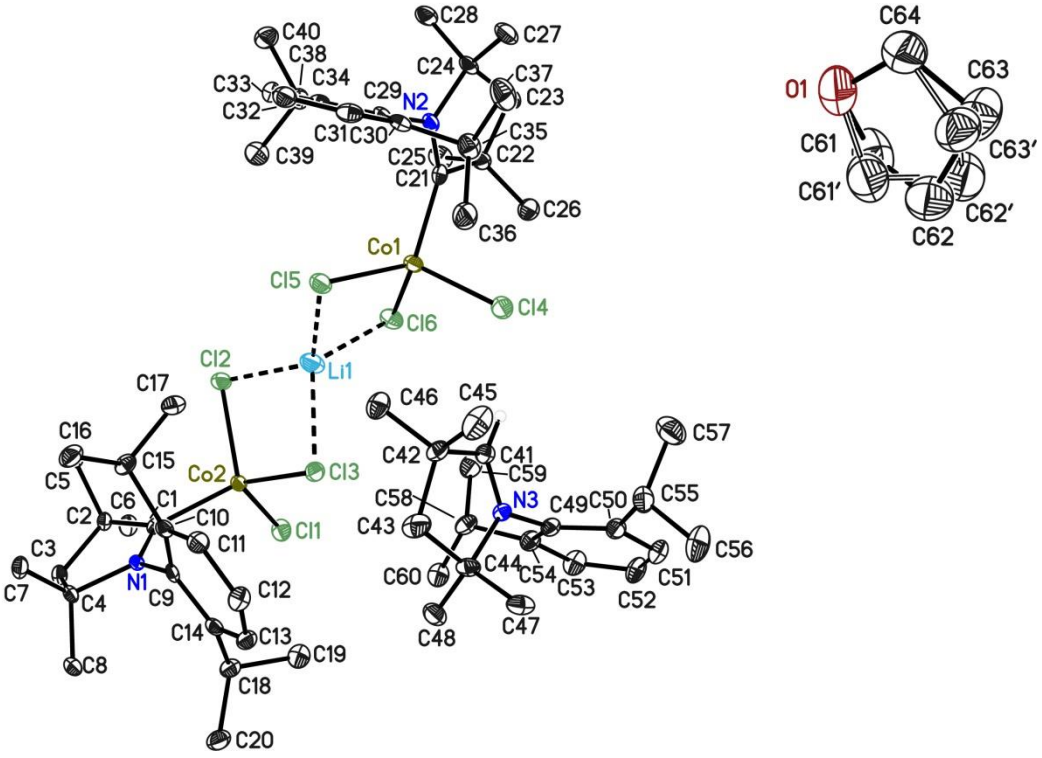

Figure 7.1 Asymmetric unit of $(Me_2–cAACH)[(Me_2–cAAC:)Co(\mu–Cl)_2Cl(Li)_{0.5}]_2$ ($Me_2–cAAC$: = $:C(CH_2)(CMe_2)_2N–2,6–iPr_2C_6H_3$) with one THF solvent molecule in the unit cell. Anisotropic displacement parameters are depicted at the 50% probability level. Hydrogen atoms are omitted for clarity. The THF molecule shows a disorder (*sof*: 0.682(14)).

Published in *"Stabilisation of a Cobalt–Cobalt Bond by Two Cyclic Alkyl Amino Carbenes."* K. C. Mondal, P. P. Samuel, H. W. Roesky, E. Carl, R. Herbst–Irmer, D. Stalke, B. Schwederski, W. Kaim, L.Ungur, L. F. Chibotaru, M.Hermann, and G. Frenking: *J. Am. Chem. Soc*. **2014**, *136*, 1770–1773.

CCDC number		969776		
Structure code		EC_Kartik155	Z	4
Empirical formula		$C_{64}H_{102}Cl_6Co_2LiN_3O$	Crystal dimensions [mm]	0.10 × 0.05 × 0.04
Formula weight [g/mol]		1266.98	$\rho_{calcd.}$ [g/cm^3]	1.244
Sample temperature [K]		100(2)	μ[mm^{-1}]	0.767
Wavelength [Å]		0.71073	F (000)	0.767
Crystal system		Tetragonal	Θ range [°]	1.137 to 25.365
Space group		$P\bar{4}$	Reflections collected	101142
Unit cell dimensions [Å]			Unique reflections	12397
	a =	25.322(2)	R_{int}	0.0912
	b =	25.322(2)	Completeness to θ_{max}	100%
	c =	10.553(2)	restraints/parameters	176 / 746
	α =	90°	GooF	1.022
	β =	90°	$R1(I > 2\sigma(I))$	0.0330
	γ =	90°	$wR2$ (all data)	0.0643
Volume [Å^3]		6766.6(17)	max. diff. peak/hole [e·Å^{-3}]	0.324 and –0.269
Extinction coefficient		–	Absolute structure parameter	–

7.1.2. (Me_2-cAACH$^+$) [(thf)$CoCl_3$]$^-$

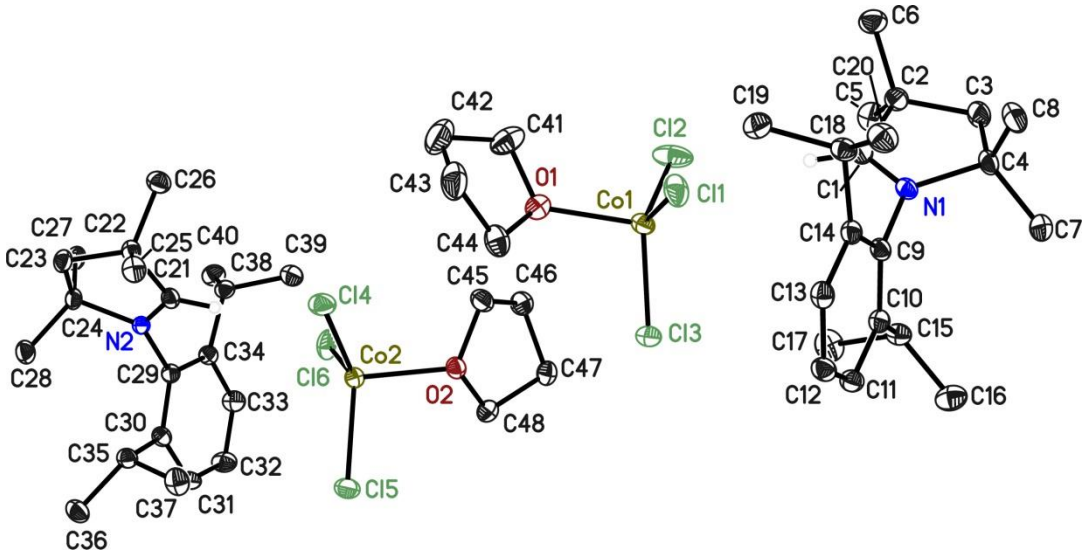

Figure 7.2: Molecular structure of (Me_2–cAACH$^+$) [(thf)$CoCl_3$]$^-$ (Me_2–cAAC: = :C(CH_2)(CMe_2)$_2$N–2,6–$iPr_2C_6H_3$) with two THF solvent molecules in the crystal. Anisotropic displacement parameters are depicted at the 50% probability level. Not freely refined hydrogen atoms are omitted for clarity.

Published in *"Stabilisation of a Cobalt–Cobalt Bond by Two Cyclic Alkyl Amino Carbenes."* K. C. Mondal, P. P. Samuel, H. W. Roesky, E. Carl, R. Herbst–Irmer, D. Stalke, B. Schwederski, W. Kaim, L.Ungur, L. F. Chibotaru, M.Hermann, and G. Frenking: *J. Am. Chem. Soc.* **2014**, *136*, 1770–1773.

CCDC number		969777		
Structure code		EC_KartikCoCl$_3$	Z	4
Empirical formula		$C_{24}H_{40}Cl_3CoNO$	Crystal dimensions [mm]	0.10 × 0.10 × 0.10
Formula weight [g/mol]		523.85	$\rho_{calcd.}$ [g/cm^3]	1.285
Sample temperature [K]		100(2)	μ[mm^{-1}]	0.945
Wavelength [Å]		0.71073	F (000)	1108
Crystal system		Triclinic	Θ range [°]	1.306 to 25.684
Space group		$P\bar{1}$	Reflections collected	61259
Unit cell dimensions [Å]			Unique reflections	10296
	a =	12.818(1)	R_{int}	0.0391
	b =	14.301(1)	Completeness to θ_{max}	100%
	c =	15.849(1)	restraints/parameters	0 / 557
	α =	90.11(2)°	GooF	1.047
	β =	99.65(2)°	$R1$(I > 2σ(I))	0.0282
	γ =	108.68(2)°	$wR2$ (all data)	0.0713
Volume [Å^3]		6766.6(17)	max. diff. peak/hole [e·Å^{-3}]	0.500 and –0.315
Extinction coefficient		–	Absolute structure parameter	–

7.1.3. $(Me_2–cAACH^+)_2[CoCl_4]^{2-}$

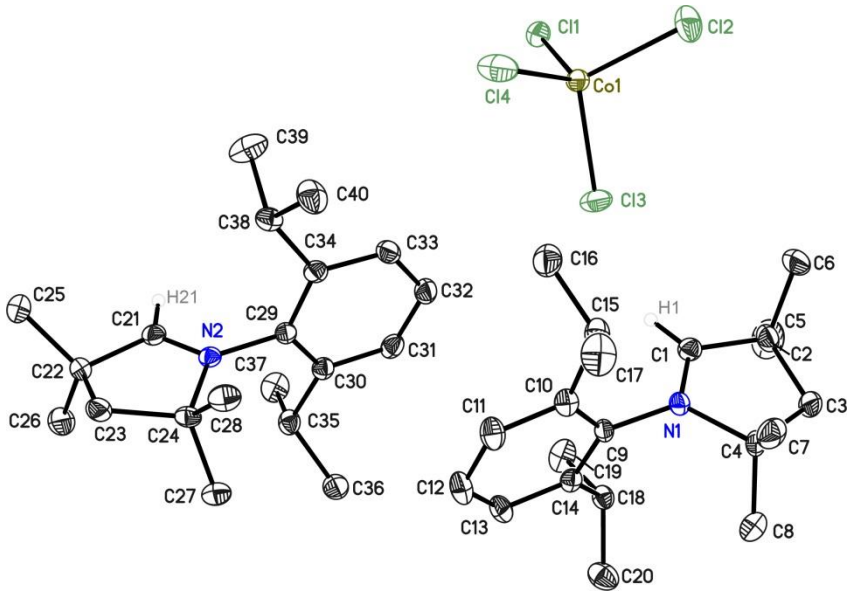

Figure 7.3: Asymmetric unit of $(Me_2–cAACH^+)_2[CoCl_4]^{2-}$ ($Me_2–cAAC$: = $:C(CH_2)(CMe_2)_2N–2,6–iPr_2C_6H_3$) in the crystal. Anisotropic displacement parameters are depicted at the 50% probability level. The $CoCl_4^-$ anion and the C3, C5 and C6 atoms are disordered (*sof*: 0.926(5), 0.709(22) and 0.718(29)). These disorders are not shown for clarity.

Published in *"Stabilisation of a Cobalt–Cobalt Bond by Two Cyclic Alkyl Amino Carbenes."* K. C. Mondal, P. P. Samuel, H. W. Roesky, E. Carl, R. Herbst–Irmer, D. Stalke, B. Schwederski, W. Kaim, L.Ungur, L. F. Chibotaru, M.Hermann, and G. Frenking: *J. Am. Chem. Soc.* **2014**, *136*, 1770–1773.

CCDC number		969779		
Structure code		EC_Kartik142	Z	4
Empirical formula		$C_{40}H_{64}Cl_4CoN_2$	Crystal dimensions [mm]	0.10 × 0.08 × 0.06
Formula weight [g/mol]		773.66	$\rho_{calcd.}$ [g/cm^3]	1.231
Sample temperature [K]		100(2)	μ[mm^{-1}]	0.696
Wavelength [Å]		0.71073	*F* (000)	1652
Crystal system		Orthorhombic	Θ range [°]	1.440 to 26.031
Space group		$P\,2_1\,2_1\,2_1$	Reflections collected	78210
Unit cell dimensions [Å]			Unique reflections	8149
	a =	10.020(2)	R_{int}	0.0509
	b =	14.726(2)	Completeness to θ_{max}	99.9%
	c =	28.284(2)	restraints/parameters	244 / 505
	α =	90°	GooF	1.030
	β =	90°	*R*1(I > 2σ(I))	0.0270
	γ =	90°	*wR*2 (all data)	0.0594
Volume [Å^3]		4173.4(10)	max. diff. peak/hole [e·Å^{-3}]	0.247 and –0.241
Extinction coefficient		–	Absolute structure parameter[111]	0.005(5)

7.1.4. $(Me_2–cAAC:)_2Co_2$

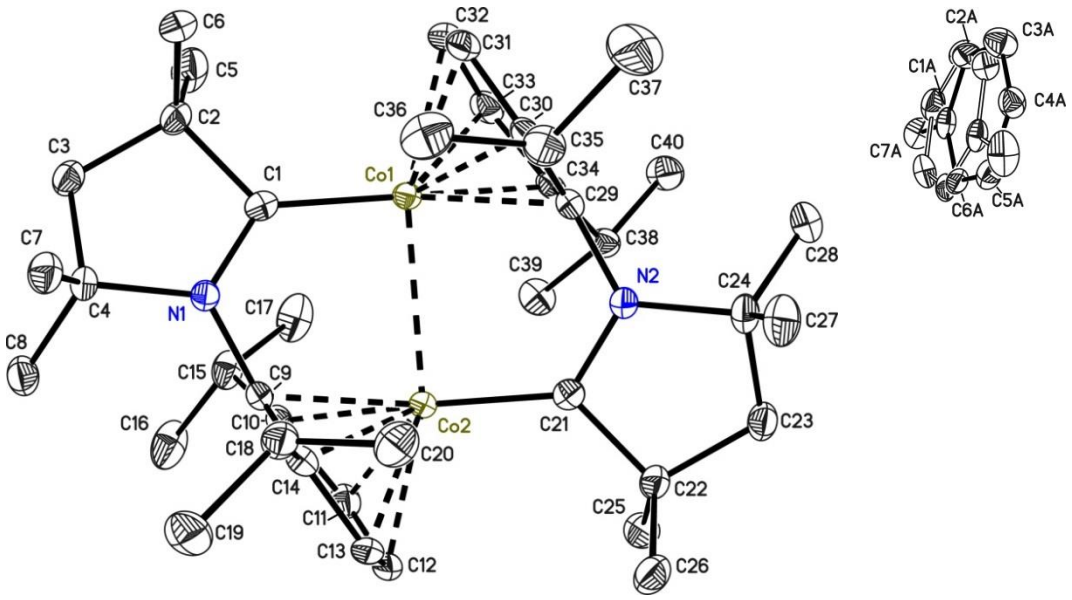

Figure 7.4: Molecular structure of $(Me_2–cAAC:)_2Co_2$ ($Me_2–cAAC:$ = $:C(CH_2)(CMe_2)_2N–2,6–iPr_2C_6H_3$) with one toluene solvent molecule in the unit cell. Anisotropic displacement parameters are depicted at the 50% probability level. Hydrogen atoms are omitted for clarity. The toluene molecule is disordered on two positions (*sof*: 0.452(5)).

Published in *"Stabilisation of a Cobalt–Cobalt Bond by Two Cyclic Alkyl Amino Carbenes."* K. C. Mondal, P. P. Samuel, H. W. Roesky, E. Carl, R. Herbst–Irmer, D. Stalke, B. Schwederski, W. Kaim, L.Ungur, L. F. Chibotaru, M.Hermann, and G. Frenking: *J. Am. Chem. Soc*. **2014**, *136*, 1770–1773.

CCDC number		969778		
Structure code		EC_Kartik135	Z	4
Empirical formula		$C_{47}H_{70}Co_2N_2$	Crystal dimensions [mm]	0.05 × 0.01 × 0.01
Formula weight [g/mol]		780.91	$\rho_{calcd.}$ [g/cm^3]	1.264
Sample temperature [K]		100(2)	μ[mm^{-1}]	0.843
Wavelength [Å]		0.71073	*F* (000)	1680
Crystal system		Orthorhombic	Θ range [°]	1.788 to 27.497
Space group		$Pna2_1$	Reflections collected	117899
Unit cell dimensions [Å]			Unique reflections	9411
	a =	22.773(2)	R_{int}	0.0614
	b =	10.794(2)	Completeness to θ_{max}	99.9%
	c =	16.689(2)	restraints/parameters	352 / 542
	α =	90°	GooF	1.080
	β =	90°	*R*1(I > 2σ(I))	0.0249
	γ =	90°	*wR*2 (all data)	0.0560
Volume [Å^3]		4102.4(10)	max. diff. peak/hole [e·Å^{-3}]	0.211 and –0.270
Extinction coefficient		–	Absolute structure parameter[111]	0.001(4)

7.1.5. $[(Me_2–cAAC:)_2Co_2]^+$ OTf^-

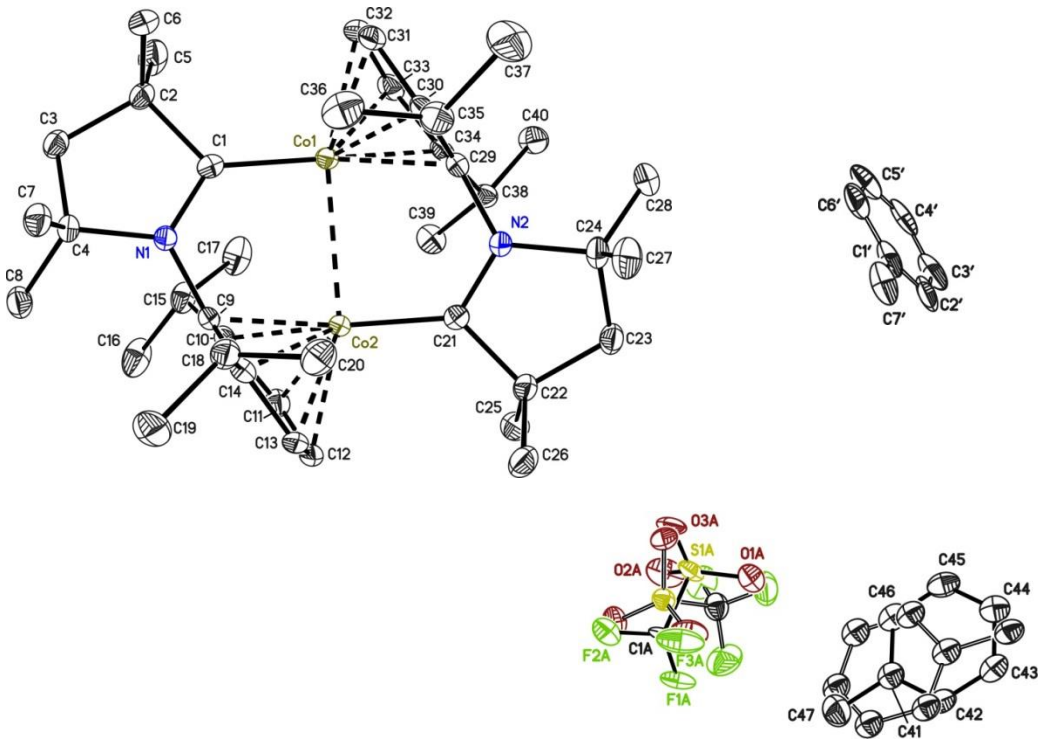

Figure 7.5: Molecular structure of $[(Me_2–cAAC:)_2Co_2]^+$ OTf^- ($Me_2–cAAC:$ = $:C(CH_2)(CMe_2)_2N–2,6–iPr_2C_6H_3$) with 1.5 toluene solvent molecules in the crystal. Anisotropic displacement parameters are depicted at the 50% probability level. The toluene molecule (C41 to C47) is disordered on two positions (*sof*: 0.938(3)). The toluene molecule C1' to C7' is on a special position. The triflate moiety shows a positional disorder with a site occupation factor of 0.605(2).

Published in *"Stabilisation of a Cobalt–Cobalt Bond by Two Cyclic Alkyl Amino Carbenes."* K. C. Mondal, P. P. Samuel, H. W. Roesky, E. Carl, R. Herbst–Irmer, D. Stalke, B. Schwederski, W. Kaim, L.Ungur, L. F. Chibotaru, M.Hermann, and G. Frenking: *J. Am. Chem. Soc.* **2014**, *136*, 1770–1773.

CCDC number		969775		
Structure code		EC_Kartik150	Z	4
Empirical formula		$C_{51.50}H_{74}Co_2F_3N_2O_3S$	Crystal dimensions [mm]	0.09 × 0.07 × 0.03
Formula weight [g/mol]		976.04	$\rho_{calcd.}$ [g/cm^3]	1.343
Sample temperature [K]		100(2)	μ[mm^{-1}]	0.785
Wavelength [Å]		0.71073	*F* (000)	2072
Crystal system		Monoclinic	Θ range [°]	1.151 to 26.423
Space group		$P2_1/n$	Reflections collected	90157
Unit cell dimensions [Å]			Unique reflections	9987
	a =	21.385(1)	R_{int}	0.0554
	b =	10.513(1)	Completeness to θ_{max}	99.9%
	c =	22.532(1)	restraints/parameters	1129 / 751
	α =	90°	GooF	1.127
	β =	107.59(2)°	*R*1(I > 2σ(I))	0.0441
	γ =	90°	*wR*2 (all data)	0.0911
Volume [Å^3]		4828.8(8)	max. diff. peak/hole [e·Å^{-3}]	0.346 and –0.357
Extinction coefficient		–	Absolute structure parameter	–

7.1.6. $(Me_2–cAAC:)_2CoCl$

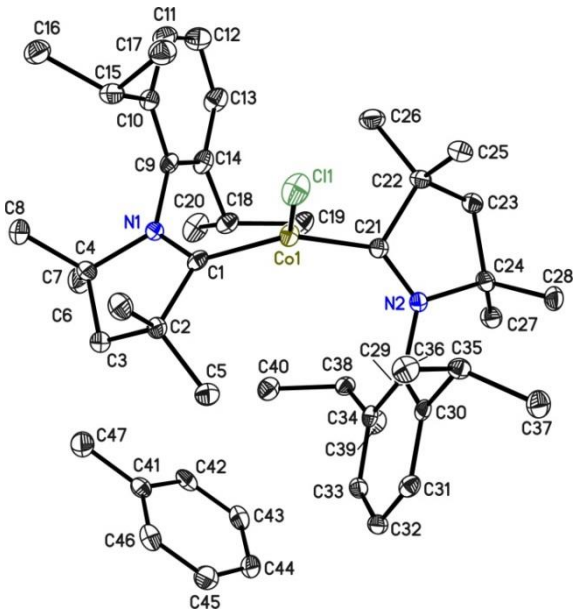

Figure 7.6: Asymmetric unit of $(Me_2–cAAC:)_2Co^{I}Cl$ ($Me_2–cAAC:$ = $:C(CH_2)(CMe_2)_2N–2,6–iPr_2C_6H_3$) with one toluene solvent molecule. Anisotropic displacement parameters are depicted at the 50% probability level. Hydrogen atoms are omitted for clarity. The data were collected on a twinned crystal. The twin law is (–1 0 0 0 –1 0 0 0.7 0.99). The fractional contribution of the minor component refined to 0.2842.

Published in *"Stabilisation of a Cobalt–Cobalt Bond by Two Cyclic Alkyl Amino Carbenes."* K. C. Mondal, P. P. Samuel, H. W. Roesky, E. Carl, R. Herbst–Irmer, D. Stalke, B. Schwederski, W. Kaim, L.Ungur, L. F. Chibotaru, M.Hermann, and G. Frenking: *J. Am. Chem. Soc.* **2014**, *136*, 1770–1773.

CCDC number		969780		
Structure code		Kartik142_CoCl	Z	2
Empirical formula		$C_{47}H_{70}ClCoN_2$	Crystal dimensions [mm]	0.07 × 0.05 × 0.04
Formula weight [g/mol]		757.43	$\rho_{calcd.}$ [g/cm^3]	1.201
Sample temperature [K]		100(2)	μ[mm^{-1}]	0.507
Wavelength [Å]		0.71073	F (000)	820
Crystal system		Triclinic	Θ range [°]	1.070 to 25.390
Space group		$P\bar{1}$	Reflections collected	49119
Unit cell dimensions [Å]			Unique reflections	7693
	a =	9.683(2)	R_{int}	0.0368
	b =	11.794(2)	Completeness to θ_{max}	99.9%
	c =	19.932(2)	restraints/parameters	0 / 478
	α =	104.34(2)°	GooF	1.065
	β =	95.28(2)°	$R1$(I > 2σ(I))	0.0392
	γ =	105.55(2)°	$wR2$ (all data)	0.0736
Volume [Å^3]		2093.8(7)	max. diff. peak/hole [e·Å^{-3}]	0.298 and –0.334
Extinction coefficient		–	Absolute structure parameter	–

7.1.7. $(Me_2cAAC:)_2NiCl_2$

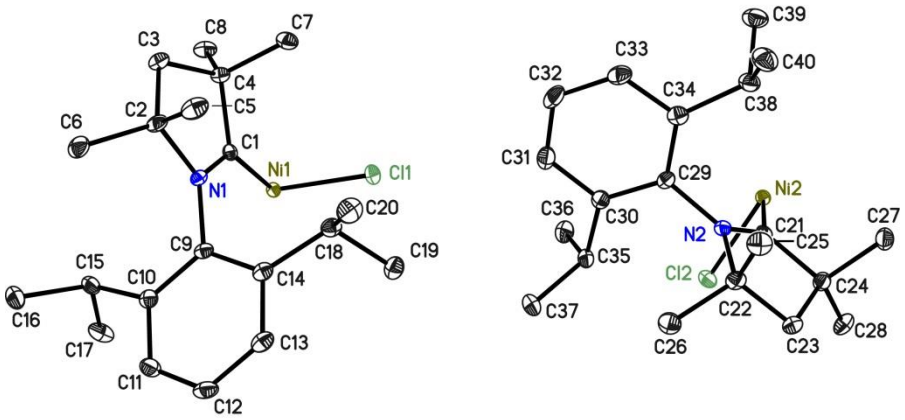

Figure 7.7: Asymmetric unit of $(Me_2–cAAC:)_2NiCl_2$ ($Me_2–cAAC:$ = $:C(CH_2)(CMe_2)_2N–2,6–iPr_2C_6H_3$). Anisotropic displacement parameters are depicted at the 50% probability level. Hydrogen atoms are omitted for clarity.

CCDC number		956915		
Structure code		EC_KM173	Z	2
Empirical formula		$C_{40}H_{62}Cl_2N_2Ni$	Crystal dimensions [mm]	0.20 × 0.10 × 0.09
Formula weight [g/mol]		757.43	$\rho_{calcd.}$ [g/cm^3]	1.229
Sample temperature [K]		100(2)	μ[mm^{-1}]	0.683
Wavelength [Å]		0.71073	F (000)	756
Crystal system		Triclinic	Θ range [°]	1.155 to 26.738°
Space group		$P\bar{1}$	Reflections collected	57070
Unit cell dimensions [Å]			Unique reflections	8018
	a =	9.434(1)	R_{int}	0.0375
	b =	11.493(1)	Completeness to θ_{max}	100%
	c =	18.017(1)	restraints/parameters	0 / 425
	α =	101.53(2)°	GooF	1.016
	β =	91.47(2)°	$R1(I > 2\sigma(I))$	0.0277
	γ =	98.01(2)°	$wR2$ (all data)	0.0695
Volume [Å^3]		1892.5(3)	max. diff. peak/hole [e·Å^{-3}]	0.439 and –0.281
Extinction coefficient		–	Absolute structure parameter	–

7.1.8. (cAAC:)$_2$NiCl$_2$

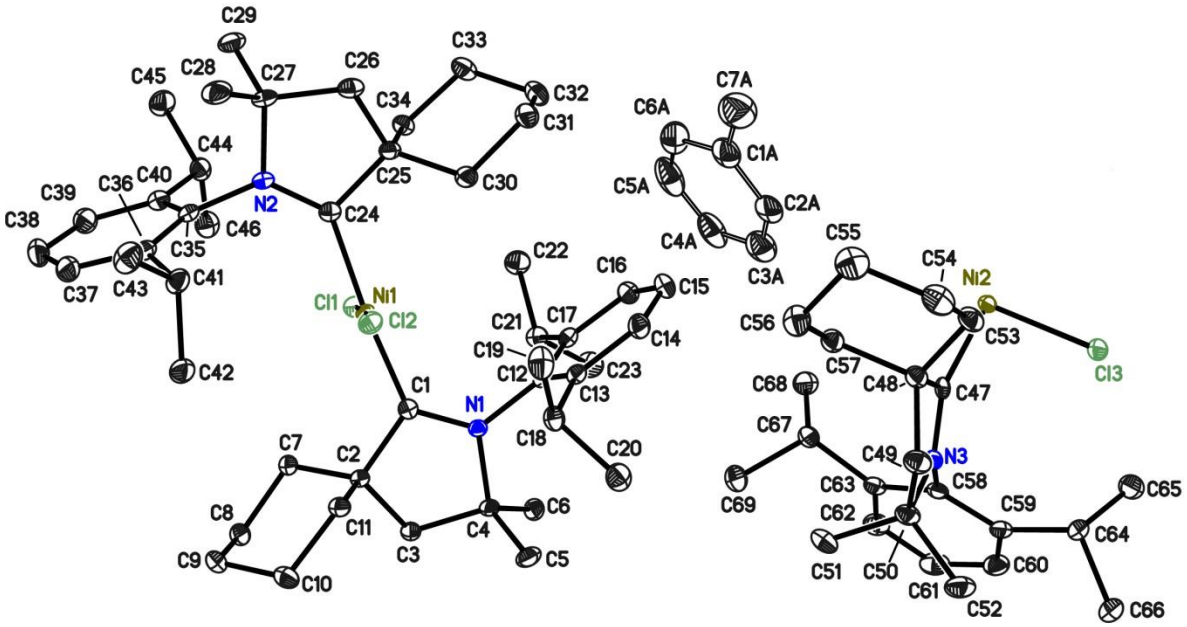

Figure 7.8: Asymmetric unit of (cAAC:)$_2$NiCl$_2$ (cAAC: = :C(CH$_2$)(CMe$_2$)(CCy)N–2,6–*i*Pr$_2$C$_6$H$_3$) with one toluene solvent molecule. Anisotropic displacement parameters are depicted at the 50% probability level. Hydrogen atoms are omitted for clarity.

Structure code		EC_KM181	Z	1
Empirical formula		$C_{145}H_{218}Cl_6N_6Ni_3$	Crystal dimensions [mm]	0.15 × 0.10 × 0.09
Formula weight [g/mol]		2434.07	$\rho_{calcd.}$ [g/cm^3]	1.230
Sample temperature [K]		100(2)	μ[mm^{-1}]	0.599
Wavelength [Å]		0.71073	*F* (000)	1316
Crystal system		Triclinic	Θ range [°]	1.121 to 27.877
Space group		$P\bar{1}$	Reflections collected	76014
Unit cell dimensions [Å]			Unique reflections	15028
	a =	12.888(2)	R_{int}	0.0470
	b =	14.378(2)	Completeness to θ_{max}	100%
	c =	18.417(2)	restraints/parameters	714 / 773
	α =	82.85(2)°	GooF	1.046
	β =	82.46(2)°	*R*1(I > 2σ(I))	0.0333
	γ =	77.49(2)°	*wR*2 (all data)	0.0848
Volume [Å^3]		3286.6(8)	max. diff. peak/hole [e·Å^{-3}]	0.379 and –0.443
Extinction coefficient		–	Absolute structure parameter	–

7.1.9. (cAAC:)$_2$NiBr$_2$

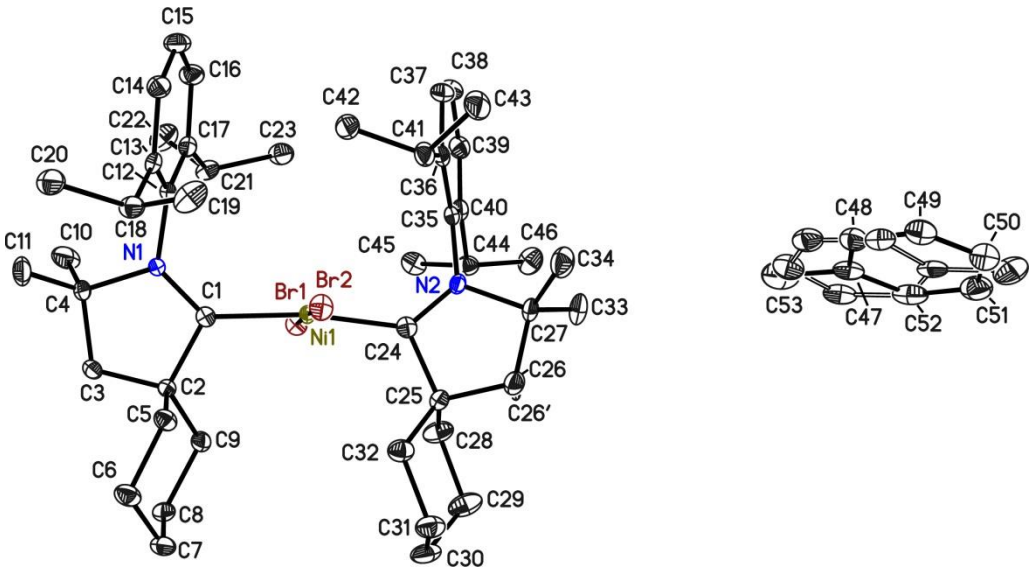

Figure 7.9: Molecular structure of (cAAC:)$_2$NiBr$_2$ (cAAC: = :C(CH$_2$)(CMe$_2$)(CCy)N–2,6–*i*Pr$_2$C$_6$H$_3$) with one toluene solvent molecule, lying on a special position. Anisotropic displacement parameters are depicted at the 50% probability level. Hydrogen atoms are omitted for clarity.

Structure code		EC_KM183	Z	2
Empirical formula		$C_{53}H_{78}Br_2N_2Ni$	Crystal dimensions [mm]	0.1 × 0.08 × 0.05
Formula weight [g/mol]		961.70	$\rho_{calcd.}$ [g/cm^3]	1.355
Sample temperature [K]		100(2)	μ[mm^{-1}]	2.145
Wavelength [Å]		0.71073	*F* (000)	1016
Crystal system		Triclinic	Θ range [°]	1.160 to 26.037
Space group		$P\bar{1}$	Reflections collected	51460
Unit cell dimensions [Å]			Unique reflections	9295
	a =	11.875(1)	R_{int}	0.0381
	b =	11.909(1)	Completeness to θ_{max}	99.9%
	c =	18.819(1)	restraints/parameters	465 / 611
	α =	72.30(2)°	GooF	1.030
	β =	73.73(2)°	*R*1(I > 2σ(I))	0.0259
	γ =	71.70(2)°	*wR*2 (all data)	0.0601
Volume [Å^3]		2356.4(5)	max. diff. peak/hole [e·Å^{-3}]	0.555 and –0.326
Extinction coefficient		–	Absolute structure parameter	–

7.1.10. $(Me_2cAAC:)_2NiBr_2$

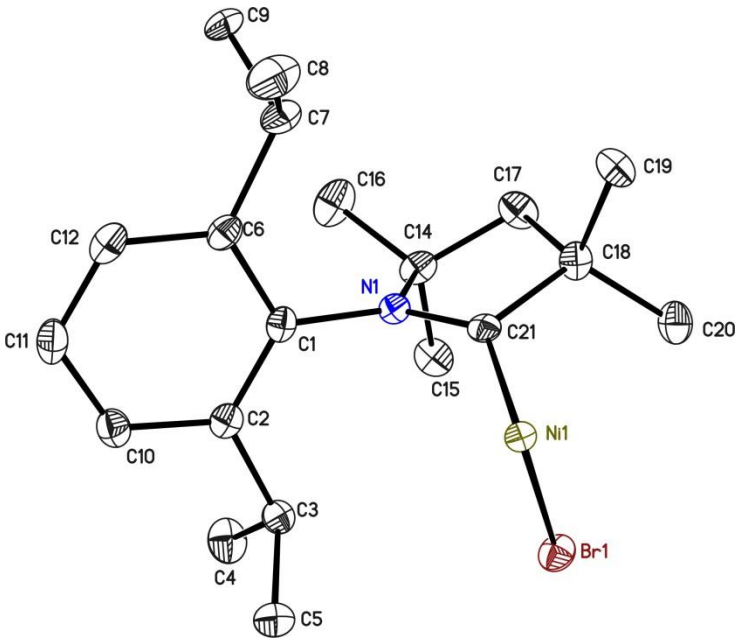

Figure 7.10: Asymmetric unit of $(cAAC:)_2NiBr_2$ (cAAC: = $:C(CH_2)(CMe_2)_2N–2,6–iPr_2C_6H_3$). Anisotropic displacement parameters are depicted at the 50% probability level. Hydrogen atoms are omitted for clarity. The atoms C15 to C20 are disordered with a site occupation factor of 0.644(7). The *i*propyl group C7 to C9 is also disordered (*sof*: 0.606(32)). These disordered groups are not shown for clarity.

Structure code		EC_Kartik176	Z	4
Empirical formula		$C_{40}H_{62}Br_2N_2Ni$	Crystal dimensions [mm]	0.1 × 0.08 × 0.07
Formula weight [g/mol]		789.44	$\rho_{calcd.}$ [g/cm^3]	1.358
Sample temperature [K]		100(2)	μ[mm^{-1}]	2.601
Wavelength [Å]		0.71073	*F* (000)	1656
Crystal system		Monoclinic	Θ range [°]	2.054 to 27.487
Space group		*C*2/*c*	Reflections collected	57333
Unit cell dimensions [Å]			Unique reflections	4437
	a =	15.003(2)	R_{int}	0.0397
	b =	14.173(2)	Completeness to θ_{max}	99.8%
	c =	19.640(2)	restraints/parameters	322 / 292
	α =	90°	GooF	1.033
	β =	112.41(2)°	*R*1(I > 2σ(I))	0.0219
	γ =	90°	*wR*2 (all data)	0.0542
Volume [Å^3]		3860.8(10)	max. diff. peak/hole [e·Å^{-3}]	0.419 and –0.302
Extinction coefficient		–	Absolute structure parameter	–

7.1.11. (cAAC:)$SiCl_2$

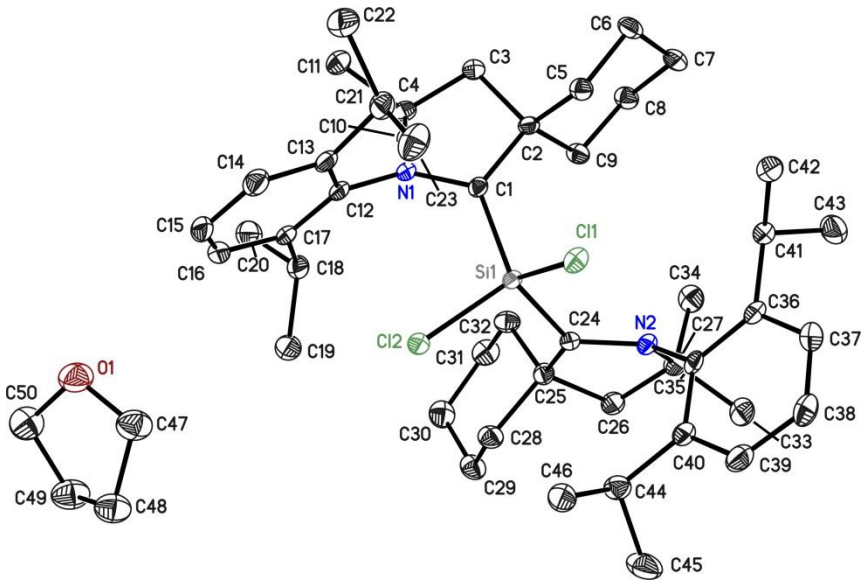

Figure 7.11: Molecular structure of (cAAC:)$_2SiCl_2$ (cAAC: = :C(CH_2)(CMe_2)(CCy)N–2,6–*i*$Pr_2C_6H_3$) with one THF solvent molecule in the asymmetric unit. Anisotropic displacement parameters are depicted at the 50% probability level. Hydrogen atoms are omitted for clarity. The atoms C26, C33 and c34 are disordered with a site occupation factor of 0.917(4). The hexyl ring is also disordered on two positions (atoms C5, C6, C8, C9, *sof*: 0.898(190)).

Published in "*Easy Access to Silicon(0) and Silicon(II) Compounds*." K. C. Mondal, P. P Samuel, M. Tretiakov, A.P. Singh, H. W. Roesky, . C. A. Stueckl, B. Niepoetter, E. Carl, H. Wolf; R. Herbst–Irmer, D. Stalke: *Inorg. Chem.* **2013**, *52*, 4736–4743.

Structure code		EC_APS505	Z	4
Empirical formula		$C_{50}H_{78}Cl_2N_2OSi$	Crystal dimensions [mm]	0.10 × 0.08 × 0.05
Formula weight [g/mol]		822.13	$\rho_{calcd.}$ [g/cm^3]	1.179
Sample temperature [K]		100(2)	μ[mm^{-1}]	0.204
Wavelength [Å]		0.71073	*F* (000)	1792
Crystal system		Monoclinic	Θ range [°]	1.546 to 25.693
Space group		$P2_1/n$	Reflections collected	36248
Unit cell dimensions [Å]			Unique reflections	8780
	a =	13.159(1)	R_{int}	0.0589
	b =	17.21(1)	Completeness to θ_{max}	99.8%
	c =	20.494(1)	restraints/parameters	210 / 582
	α =	90°	GooF	1.047
	β =	94.11(2)	*R*1(I > 2σ(I))	0.0471
	γ =	90°	*wR*2 (all data)	0.1163
Volume [Å^3]		4631.4(5)	max. diff. peak/hole [e·Å^{-3}]	0.316 / –0.329
Extinction coefficient		–	Absolute structure parameter	–

7.2. Structures determined for Prinson Samuel

7.2.1. $(Me_2cAAC:)_2FeCl_2$

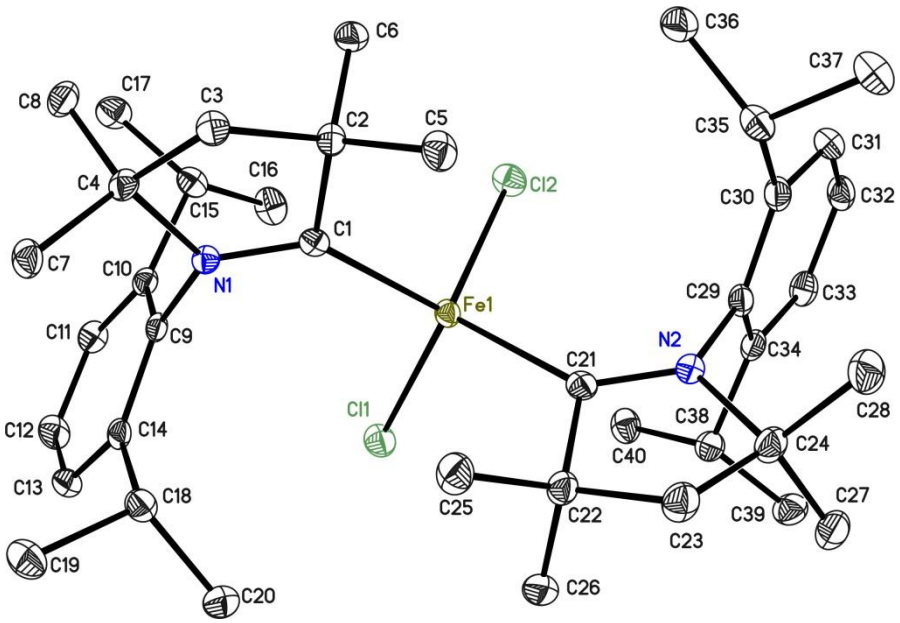

Figure 7.12: Asymmetric unit of $(Me_2–cAAC:)_2FeCl_2$ ($Me_2–cAAC:$ = $:C(CH_2)(CMe_2)_2N–2,6–iPr_2C_6H_3$). Anisotropic displacement parameters are depicted at the 50% probability level. Hydrogen atoms are omitted for clarity.

Structure code		EC_PS_$FeCl_2$	Z	4
Empirical formula		$C_{40}H_{62}Cl_2FeN_2$	Crystal dimensions [mm]	0.10 × 0.08 × 0.06
Formula weight [g/mol]		697.66	$\rho_{calcd.}$ [g/cm³]	1.237
Sample temperature [K]		100(2)	μ[mm⁻¹]	0.575
Wavelength [Å]		0.71073	F (000)	1504
Crystal system		Monoclinic	Θ range [°]	1.631 to 26.029
Space group		$P2_1/c$	Reflections collected	107288
Unit cell dimensions [Å]			Unique reflections	7385
	a =	13.173(2)	R_{int}	0.0622
	b =	17.403(2)	Completeness to θ_{max}	100%
	c =	17.237(2)	restraints/parameters	0 / 422
	α =	90°	GooF	1.033
	β =	108.58(2)°	$R1(I > 2\sigma(I))$	0.0317
	γ =	90°	$wR2$ (all data)	0.0764
Volume [Å³]		3745.6(9)	max. diff. peak/hole [e·Å⁻³]	0.373 and –0.325
Extinction coefficient		–	Absolute structure parameter	–

7.2.2. $(Me_2cAAC:)_2CrCl_2$

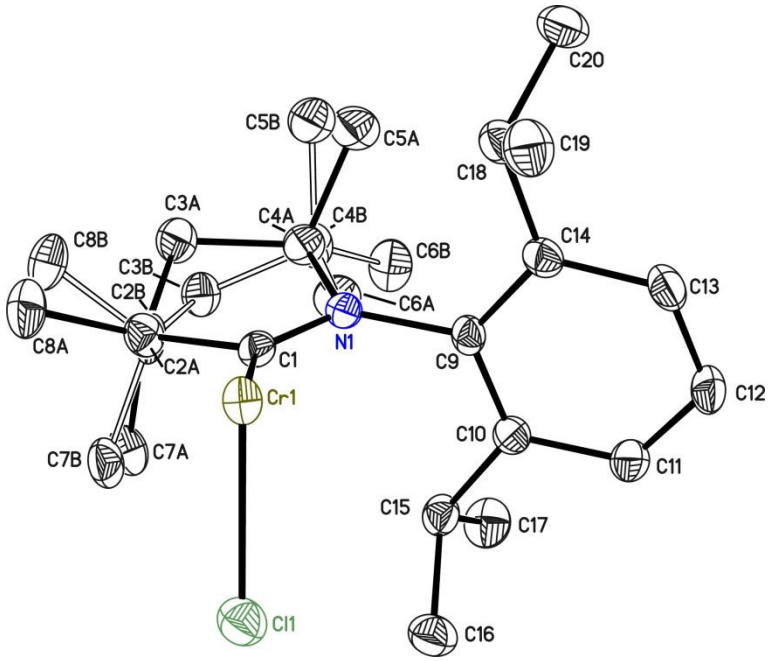

Figure 7.13: Asymmetric unit of $(Me_2–cAAC:)_2CrCl_2$ ($Me_2–cAAC:$ = $:C(CH_2)(CMe_2)_2N–2,6–iPr_2C_6H_3$). Anisotropic displacement parameters are depicted at the 50% probability level. Hydrogen atoms are omitted for clarity. The atoms C2A to C8A are disordered on two positions (*sof*: 0.604(6)).

Structure code		EC_APSCrCl$_2$	Z	4
Empirical formula		$C_{40}H_{62}Cl_2CrN_2$	Crystal dimensions [mm]	0.10 × 0.07 × 0.05
Formula weight [g/mol]		693.81	$\rho_{calcd.}$ [g/cm^3]	1.192
Sample temperature [K]		100(2)	μ[mm^{-1}]	0.463
Wavelength [Å]		0.71073	*F* (000)	1495
Crystal system		Monoclinic	Θ range [°]	1.963 to 25.362
Space group		*C* 2/*c*	Reflections collected	49869
Unit cell dimensions [Å]			Unique reflections	3543
	a =	17.012(2)	R_{int}	0.0459
	b =	10.952(2)	Completeness to θ_{max}	100%
	c =	21.915(2)	restraints/parameters	357 / 280
	α =	90°	GooF	1.035
	β =	108.77(2)°	*R*1(I > 2σ(I))	0.0360
	γ =	90°	*wR*2 (all data)	0.0974
Volume [Å^3]		3866.0(10)	max. diff. peak/hole [e·Å^{-3}]	0.759 and –0.551
Extinction coefficient		–	Absolute structure parameter	–

7.2.3. $(Me_2cAAC:)_2FeCl$

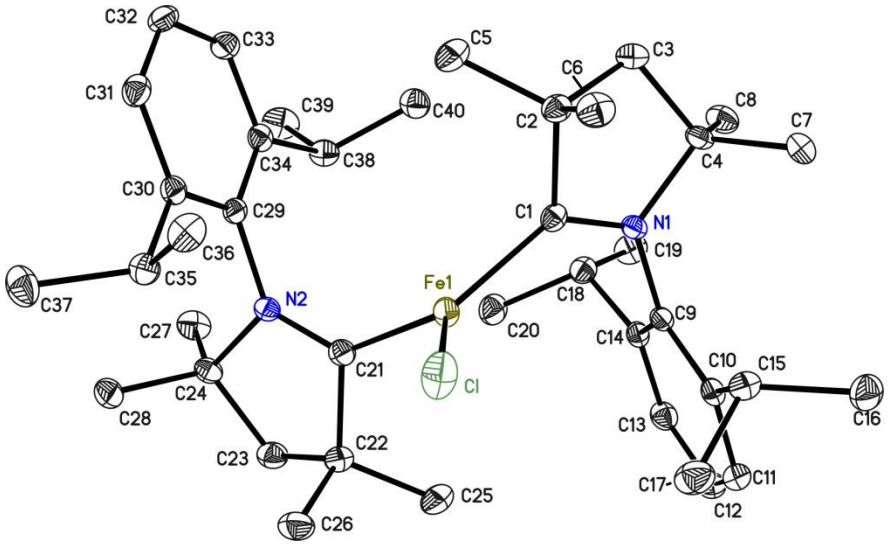

Figure 7.14: Asymmetric unit of $(Me_2–cAAC:)_2FeCl$ ($Me_2–cAAC:$ = $:C(CH_2)(CMe_2)_2N–2,6–iPr_2C_6H_3$). Anisotropic displacement parameters are depicted at the 50% probability level. Hydrogen atoms are omitted for clarity.

Structure code		EC_APFeCl	Z	4
Empirical formula		$C_{40}H_{62}ClFeN_2$	Crystal dimensions [mm]	0.10 × 0.09 × 0.05
Formula weight [g/mol]		662.21	$\rho_{calcd.}$ [g/cm^3]	1.197
Sample temperature [K]		100(2)	μ[mm^{-1}]	0.512
Wavelength [Å]		0.71073	F (000)	1436
Crystal system		Monoclinic	Θ range [°]	1.601 to 27.491
Space group		$P2_1/c$	Reflections collected	110950
Unit cell dimensions [Å]			Unique reflections	8434
	a =	11.224(2)	R_{int}	0.0377
	b =	19.524(3)	Completeness to θ_{max}	99.9%
	c =	16.903(2)	restraints/parameters	124 / 413
	α =	90°	GooF	1.031
	β =	97.29(2)°	$R1(I > 2\sigma(I))$	0.0300
	γ =	90°	$wR2$ (all data)	0.0733
Volume [Å^3]		3674.1(10)	max. diff. peak/hole [e·Å^{-3}]	0.367 and –0.288
Extinction coefficient		–	Absolute structure parameter	–

7.3. Structures determined for Amit Pratap Singh

7.3.1. $[(LB)GeCl]^+[GeCl_3]^-$

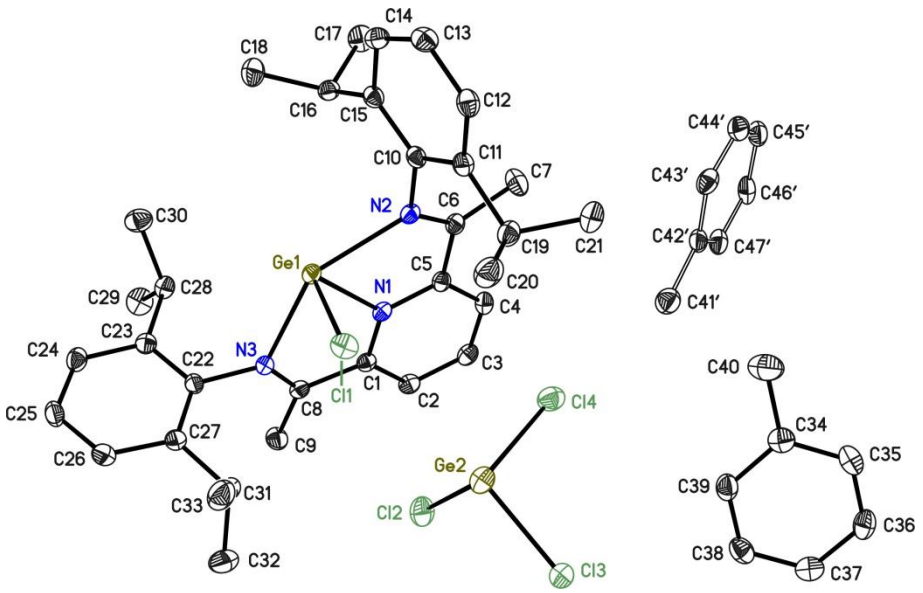

Figure 7.15: Asymmetric unit of $[(LB)Ge^{II}Cl]^+[Ge^{II}Cl_3]^-$ (LB=2,6–bis(imino)pyridyl). Anisotropic displacement parameters are depicted at the 50% probability level. Hydrogen atoms are omitted for clarity. The crystal was a split crystal and the structure was refined against HKLF4 data. The non–integer number of atoms in the formula sum is caused by the toluene molecule C41' to C47' lying on a special position.

Published in *"Lewis Base (LB) initiated inherent Dissociation of $GeCl_2$ to $[(LB)Ge^{II}Cl]^+$ $[Ge^{II}Cl_3]^-$ and the corresponding reaction with $SnCl_2$."* A. P. Singh, H. W. Roesky, E. Carl, D. Stalke, J.–P. Demers, A. Lange: *J. Am Chem. Soc*. **2012**, *134*, 4998–5003.

CCDC number		862039		
Structure code		EC_AP202	Z	2
Empirical formula		$C_{43.5}H_{55}Cl_4Ge_2N_3$	Crystal dimensions [mm]	0.10 × 0.05 × 0.05
Formula weight [g/mol]		906.89	$\rho_{calcd.}$ [g/cm³]	1.382
Sample temperature [K]		100(2)	μ[mm⁻¹]	1.658
Wavelength [Å]		0.71073	F (000)	938
Crystal system		Triclinic	Θ range [°]	1.22 to 26.83
Space group		$P\bar{1}$	Reflections collected	33183
Unit cell dimensions [Å]			Unique reflections	9181
	a =	10.330(3)	R_{int}	0.0398
	b =	13.013(3)	Completeness to θ_{max}	98.2%
	c =	16.873(7)	restraints/parameters	96 / 517
	α =	93.66(2)°	GooF	1.045
	β =	97.33(2)°	$R1(I > 2\sigma(I))$	0.0253
	γ =	103.26(2)°	$wR2$ (all data)	0.0569
Volume [Å³]		2179.4(12)	max. diff. peak/hole [e·Å⁻³]	0.357 and –0.291
Extinction coefficient		–	Absolute structure parameter	–

7.3.2. $[(LB)SnCl]^+[SnCl_3]^-$

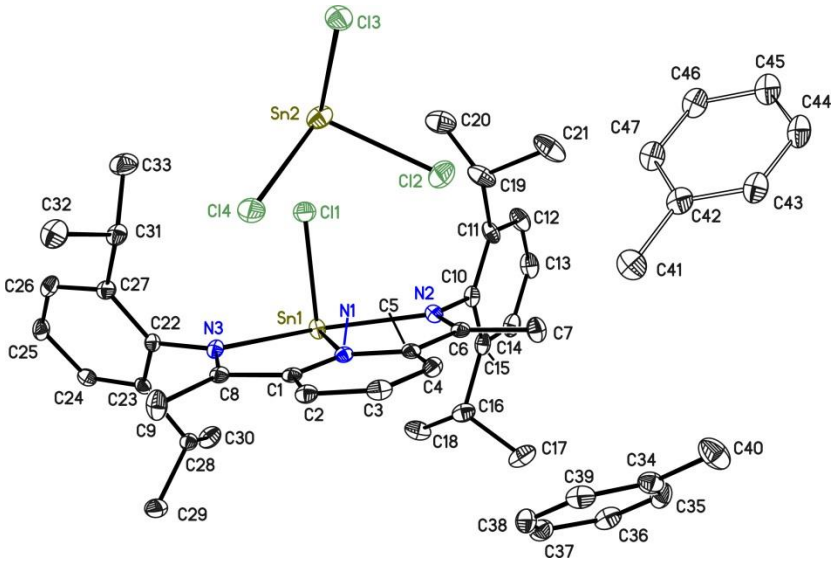

Figure 7.16: Asymmetric unit of $[(LB)Sn^{II}Cl]^+[Sn^{II}Cl_3]^-$ (LB=2,6–bis(imino)pyridyl). Anisotropic displacement parameters are depicted at the 50% probability level. Hydrogen atoms are omitted for clarity. There are two toluene solvent molecules in the unit cell. The non–integer number of atoms in the formula sum is caused by the toluene molecule C41' to C47' lying on a special position.

Published in *"Lewis Base (LB) initiated inherent Dissociation of $GeCl_2$ to $[(LB)Ge^{II}Cl]^+$ $[Ge^{II}Cl_3]^-$ and the corresponding reaction with $SnCl_2$."* A. P. Singh, H. W. Roesky, E. Carl, D. Stalke, J.–P. Demers, A. Lange: *J. Am Chem. Soc*. **2012**, *134*, 4998–5003.

CCDC number		862038		
Structure code		EC_AP205	Z	2
Empirical formula		$C_{43.5}H_{55}Cl_4Sn_2N_3$	Crystal dimensions [mm]	0.10 × 0.05 × 0.05
Formula weight [g/mol]		999.09	$\rho_{calcd.}$ [g/cm^3]	1.490
Sample temperature [K]		100(2)	μ[mm^{-1}]	0.738
Wavelength [Å]		0.71073	F (000)	1010
Crystal system		Triclinic	Θ range [°]	0.97 to 20.60
Space group		$P\bar{1}$	Reflections collected	53144
Unit cell dimensions [Å]			Unique reflections	9045
	a =	10.438 (2)	R_{int}	0.0628
	b =	13.174 (2)	Completeness to θ_{max}	98.1%
	c =	16.908 (4)	restraints/parameters	96 / 513
	α =	90.68 (1)°	GooF	1.030
	β =	99.080(1)°	$R1(I > 2\sigma(I))$	0.0306
	γ =	103.21(1)°	$wR2$ (all data)	0.0684
Volume [Å^3]		2226.8 (8)	max. diff. peak/hole [e·Å^{-3}]	0.939 and –1.124
Extinction coefficient		–	Absolute structure parameter	–

7.4. Structure determined for Markus Scheibel

[Rh(N$_2$){N(CHCHP*t*Bu$_2$)$_2$}]

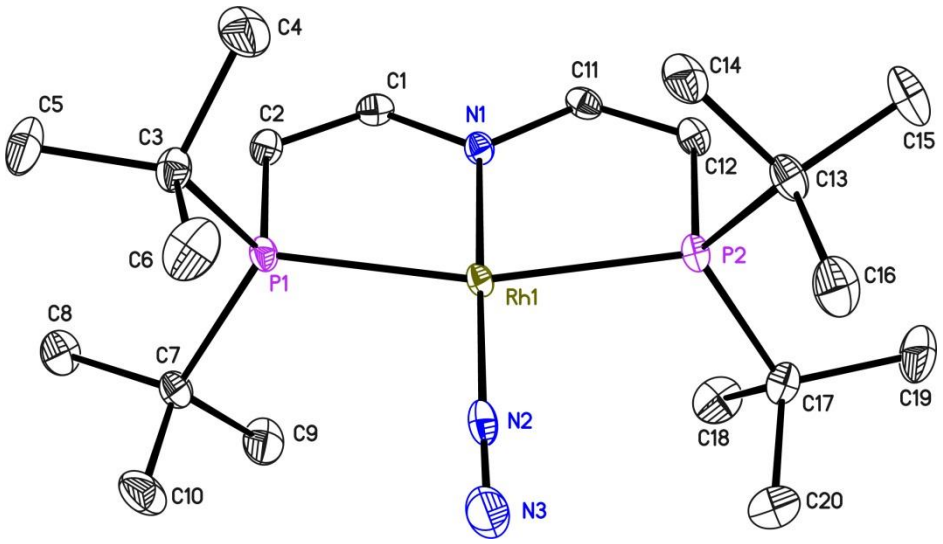

Figure 7.17: Asymmetric unit of [Rh(N$_2$){N(CHCHP*t*Bu$_2$)$_2$}]. Anisotropic displacement parameters are depicted at the 50% probability level. Hydrogen atoms are omitted for clarity.

Published in "*Synthesis and Reactivity of a Transient, Terminal Nitrido Complex of Rhodium*". M.G. Scheibel, Y. Wu, A. C. Stückl, L. Krause, E. Carl, D. Stalke, B. de Bruin, and S. Schneider: *J. Am. Chem. Soc.* **2013**, *135*, 17719–17722.

CCDC number		960651		
Structure code		MS_HS_RhN2	Z	4
Empirical formula		$C_{20}H_{40}N_3P_2Rh_1$	Crystal dimensions [mm]	0.10 × 0.05 × 0.01
Formula weight [g/mol]		487.4	$\rho_{calcd.}$ [g/cm^3]	1.337
Sample temperature [K]		100(2)	μ[mm^{-1}]	0.450
Wavelength [Å]		0.56085	*F* (000)	1024
Crystal system		Monoclinic	Θ range [°]	1.188 to 20.943
Space group		$P2_1/c$	Reflections collected	22081
Unit cell dimensions [Å]			Unique reflections	5218
	a =	7.867(2)	R_{int}	0.0552
	b =	27.050(6)	Completeness to θ_{max}	100%
	c =	11.866(2)	restraints/parameters	0 / 247
	α =	90°	GooF	1.070
	β =	106.53(2)°	*R*1(I > 2σ(I))	0.0445
	γ =	90°	*wR*2 (all data)	0.0967
Volume [Å^3]		2420.8(9)	max. diff. peak/hole [e·Å^{-3}]	1.041 and –1.091
Extinction coefficient		–	Absolute structure parameter	–

7.5. Structures determined for Sven Ole Reichmann

7.5.1. (IPr)–$SiPh_2Cl$

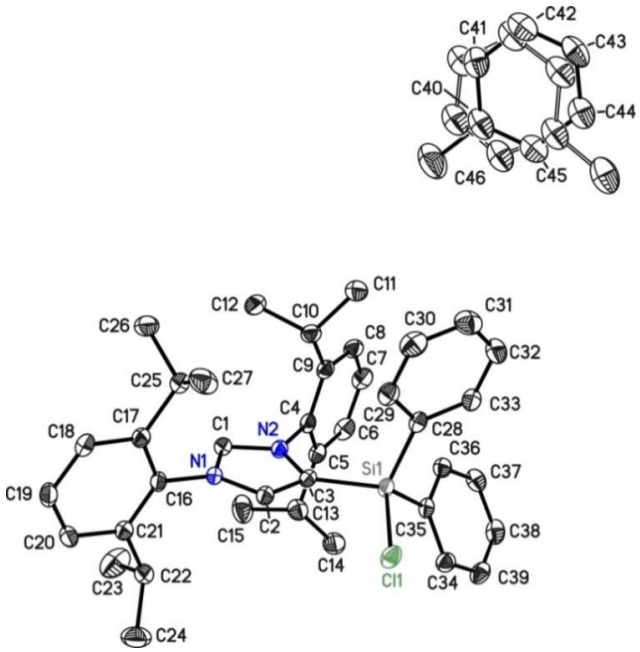

Figure 7.18: Asymmetric unit of (IPr)–$SiPh_2Cl$ (IPr: 1,3–Bis(2,6–Di*iso*propylphenyl)imidazol–2–yliden). Anisotropic displacement parameters are depicted at the 50% probability level. Hydrogen atoms are omitted for clarity. The toluene molecule in the unit cell is disordered with a site occupation factor of 0.798(3).

Published in "*A Facile Route to Bis–NHC Scaffolds".* R. S. Ghadwal, S. O. Reichmann, E. Carl, and R. Herbst–Irmer: submitted to *Inorganic Chemistry,* **2014**.

CCDC number		982103		
Structure code		SR_045	Z	2
Empirical formula		$C_{46}H_{53}ClN_2Si$	Crystal dimensions [mm]	0.19 × 0.13 × 0.09
Formula weight [g/mol]		697.44	$\rho_{calcd.}$ [g/cm³]	1.152
Sample temperature [K]		100(2)	μ[mm⁻¹]	0.158
Wavelength [Å]		0.71073	*F* (000)	748
Crystal system		Triclinic	Θ range [°]	1.125 to 27.483
Space group		$P\bar{1}$	Reflections collected	55303
Unit cell dimensions [Å]			Unique reflections	9200
	a =	10.900 (1)	R_{int}	0.0418
	b =	11.161(1)	Completeness to θ_{max}	99.9%
	c =	18.612(2)	restraints/parameters	346 / 525
	α =	78.13(2)°	GooF	1.049
	β =	79.30(2)°	*R*1(I > 2σ(I))	0.0417
	γ =	65.94(2)°	*wR*2 (all data)	0.1053
Volume [Å³]		2010.1(3)	max. diff. peak/hole [e·Å⁻³]	0.356 and –0.341
Extinction coefficient		–	Absolute structure parameter	–

7.5.2. (IPr)–NLi

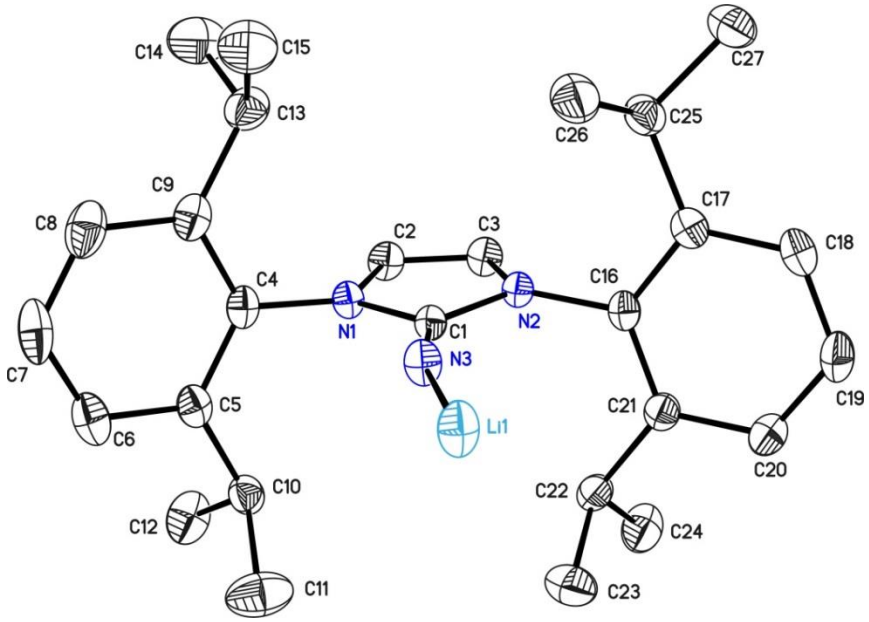

Figure 7.19: Asymmetric unit of (IPr)–NLi (IPr: 1,3–Bis(2,6–Di*iso*propylphenyl)imidazol–2–yliden). Anisotropic displacement parameters are depicted at the 50% probability level. Hydrogen atoms are omitted for clarity.

Structure code		SR_043	Z	2
Empirical formula		$C_{54}H_{72}Li_2N_6$	Crystal dimensions [mm]	0.08 × 0.06 × 0.05
Formula weight [g/mol]		819.06	$\rho_{calcd.}$ [g/cm^3]	1.116
Sample temperature [K]		100(2)	μ[mm^{-1}]	0.065
Wavelength [Å]		0.71073	F (000)	888
Crystal system		Monoclinic	Θ range [°]	2.158 to 25.104
Space group		$P2_1/n$	Reflections collected	36376
Unit cell dimensions [Å]			Unique reflections	4307
	a =	10.971(2)	R_{int}	0.0407
	b =	18.637(2)	Completeness to θ_{max}	97.8%
	c =	11.953(2)	restraints/parameters	0 / 288
	α =	90°	GooF	1.032
	β =	94.22(1)°	$R1$(I > 2σ(I))	0.0395
	γ =	90°	$wR2$ (all data)	0.0944
Volume [Å^3]		2437.4(7)	max. diff. peak/hole [e·Å^{-3}]	0.148 and –0.187
Extinction coefficient		–	Absolute structure parameter	–

7.5.3. IPr–$NPCl_2$

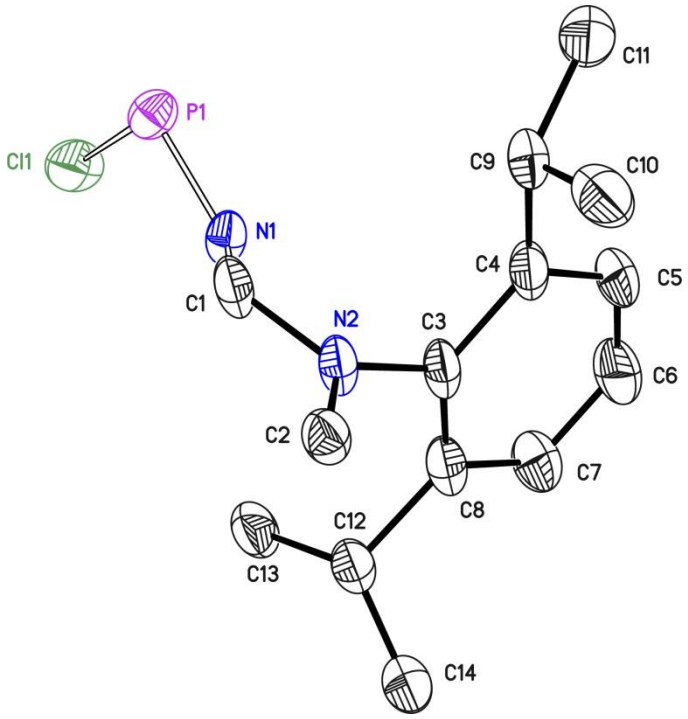

Figure 7.20: One half of (IPr)–$NPCl_2$ (IPr: 1,3–Bis(2,6–Di*iso*propylphenyl)imidazol–2–yliden) in the asymmetric unit. The molecule lies on a special position, generating the other half of the molecule by a mirror plane. The $NPCl_2$ moiety is disordered on a special position. The anisotropic displacement parameters are depicted at the 50% probability level. Hydrogen atoms are omitted for clarity.

Structure code		SR_033	Z	4
Empirical formula		$C_{27}H_{36}Cl_2N_3P$	Crystal dimensions [mm]	0.10 × 0.09 × 0.05
Formula weight [g/mol]		504.46	$\rho_{calcd.}$ [g/cm³]	1.254
Sample temperature [K]		100(2)	μ[mm⁻¹]	0.323
Wavelength [Å]		0.71073	*F* (000)	1072
Crystal system		Monoclinic	Θ range [°]	2.341 to 25.032
Space group		*C*2/*c*	Reflections collected	29657
Unit cell dimensions [Å]			Unique reflections	2369
	a =	16.721(2)	R_{int}	0.0735
	b =	9.185(2)	Completeness to θ_{max}	99.9%
	c =	17.409(3)	restraints/parameters	2 / 173
	α =	90°	GooF	1.062
	β =	91.87(2)°	*R*1(I > 2σ(I))	0.0408
	γ =	90°	*wR*2 (all data)	0.1075
Volume [Å³]		2672.3(8)	max. diff. peak/hole [e·Å⁻³]	0.206 and –0.287
Extinction coefficient		0.0011(3)	Absolute structure parameter	–

7.5.4. $(IPr)_2$–$SiPh_2$

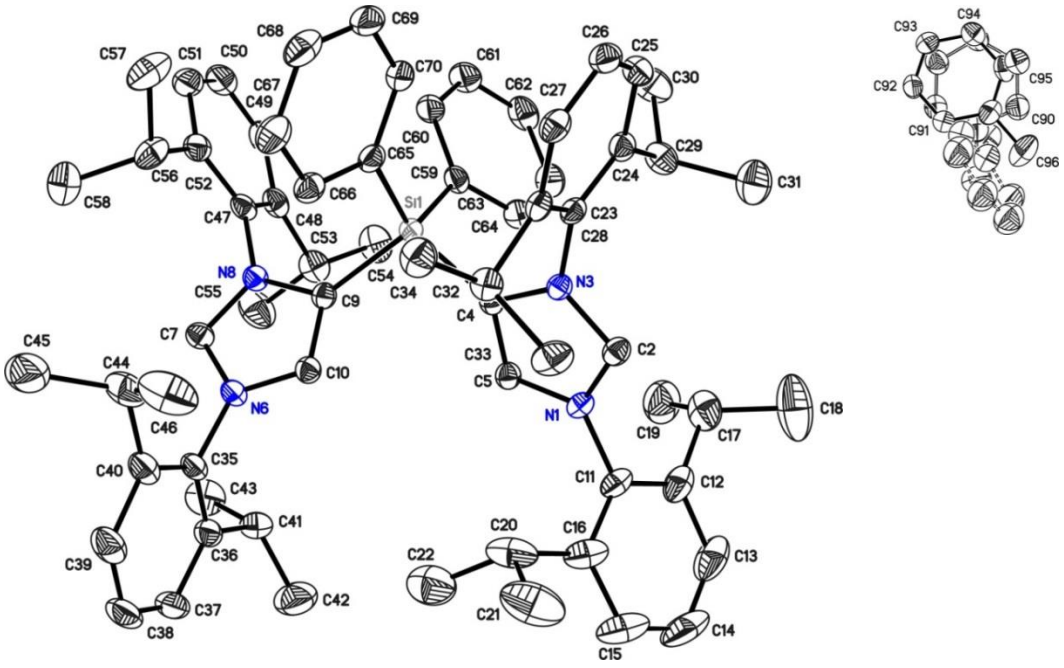

Figure 7.21: Molecular structure of (IPr)–$SiPh_2$ (IPr: 1,3–Bis(2,6–Di*iso*propylphenyl)imidazol–2–yliden). The anisotropic displacement parameters are depicted at the 50% probability level. Hydrogen atoms are omitted for clarity. There is one toluene molecule in the asymmetric unit that is disordered on three different positions. One of these disordered toluenes is also disordered on a special position. The command *sump* was used to sum the three free variables up to 1.0000(1). The site occupation factors are 0.688(2), 0.152(2) and 0.160(2).

Published in "*A Facile Route to Bis–NHC Scaffolds*". R. S. Ghadwal, S. O. Reichmann, E. Carl, and R. Herbst–Irmer: submitted to *Inorganic Chemistry,* **2014.**

CCDC number		982101		
Structure code		EC_Raj	Z	4
Empirical formula		$C_{72.45}H_{87.35}N_4Si$	Crystal dimensions [mm]	0.10 × 0.10 × 0.07
Formula weight [g/mol]		1042.30	$\rho_{calcd.}$ [g/cm³]	1.098
Sample temperature [K]		100(2)	μ[mm⁻¹]	0.081
Wavelength [Å]		0.71073	F (000)	2256
Crystal system		Monoclinic	Θ range [°]	1.343 to 26.029°
Space group		$P2_1/c$	Reflections collected	102837
Unit cell dimensions [Å]			Unique reflections	12433
	a =	13.646(2)	R_{int}	0.0485
	b =	20.372(2)	Completeness to θ_{max}	100%
	c =	22.809(2)	restraints/parameters	840 / 850
	α =	90°	GooF	1.029
	β =	95.89(2)°	$R1(I > 2\sigma(I))$	0.0408
	γ =	90°	$wR2$ (all data)	0.1170
Volume [Å³]		6307.3(13)	max. diff. peak/hole [e·Å⁻³]	0.343 and –0.259
Extinction coefficient		0.00062(15)	Absolute structure parameter	–

8. References

[1] B. Cornils, W. A. Herrmann, M. Muhler, C.-H. Wong, *Catalysis from A to Z: A Concise Encyclopedia, Vol. 3*, Wiley-VCH, Weinheim, **2007**.

[2] R. G. Pearson, *J. Am. Chem. Soc.* **1963**, *85*, 3533-3539.

[3] a) F. Baier, Z. Fei, H. Gornitzka, A. Murso, S. Neufeld, M. Pfeiffer, I. Rüdenauer, A. Steiner, T. Stey, D. Stalke, *J. Organomet. Chem.* **2002**, *661*, 111-127; b) F. Armbruster, I. Fernández, F. Breher, *Dalton Trans.* **2009**, 5612-5626; c) I. Kuzu, I. Krummenacher, J. Meyer, F. Armbruster, F. Breher, *Dalton Trans.* **2008**, 5836-5865; d) M. Viciano, M. Sanaú, E. Peris, *Organometallics* **2007**, *26*, 6050-6054; e) T. Stey, M. Pfeiffer, J. Henn, S. K. Pandey, D. Stalke, *Chem. Eur. J.* **2007**, *13*, 3636-3642; f) T. Stey, J. Henn, D. Stalke, *Chem. Commun.* **2007**, 413-415; g) M. Veith, *Chem. Rev.* **1990**, *90*, 3-16; h) M. Knorr, E. Hallauer, V. Huch, M. Veith, P. Braunstein, *Organometallics* **1996**, *15*, 3868-3875.

[4] a) A. R. Shaffer, J. A. R. Schmidt, *Organometallics* **2009**, *28*, 2494-2504; b) A. Marson, J. E. Ernsting, M. Lutz, A. L. Spek, P. W. N. M. van Leeuwen, P. C. J. Kamer, *Dalton Trans.* **2009**, 621-633; c) J. Pfeiffer, G. Kickelbick, U. Schubert, *Organometallics* **1999**, *19*, 62-71; d) C. Wetzel, P. C. Kunz, I. Thiel, B. Spingler, *Inorg. Chem.* **2011**, *50*, 7863-7870; e) I. Hyder, M. Jiménez-Tenorio, M. C. Puerta, P. Valerga, *Organometallics* **2011**, *30*, 726-737; f) R. Romeo, Luigi M. Scolaro, Maria R. Plutino, A. Romeo, F. Nicolo, Alessandro D. Zotto, *Eur. J. Inorg. Chem.* **2002**, *2002*, 629-638; g) Q.-X. Wan, Y. Liu, Y.-Q. Cai, *Catal. Lett.* **2009**, *127*, 386-391; h) Z. Weng, S. Teo, T. S. A. Hor, *Organometallics* **2006**, *25*, 4878-4882; i) A. Caballero, F. A. Jalón, B. R. Manzano, G. Espino, M. Pérez-Manrique, A. Mucientes, F. J. Poblete, M. Maestro, *Organometallics* **2004**, *23*, 5694-5706; j) J. C. Jeffrey, T. B. Rauchfuss, *Inorg. Chem.* **1979**, *18*, 2658-2666; k) E. Poverenov, M. Gandelman, L. J. W. Shimon, H. Rozenberg, Y. Ben-David, D. Milstein, *Chem. Eur. J.* **2004**, *10*, 4673-4684; l) M. A. Rankin, G. Schatte, R. McDonald, M. Stradiotto, *Organometallics* **2008**, *27*, 6286-6299; m) L. J. Hounjet, M. Bierenstiel, M. J. Ferguson, R. McDonald, M. Cowie, *Dalton Trans.* **2009**, 4213-4226; n) V. T. Annibale, D. Song, *RSC Advances* **2013**, *3*, 11432-11449; o) J. McNulty, K. Keskar, *Organic & Biomolecular Chemistry* **2013**, *11*, 2404-2407.

[5] J. Andrieu, J.-M. Camus, P. Richard, R. Poli, L. Gonsalvi, F. Vizza, M. Peruzzini, *Eur. J. Inorg. Chem.* **2006**, *2006*, 51-61.

[6] a) J. McNulty, K. Keskar, R. Vemula, *Chem. Eur. J.* **2011**, *17*, 14727-14730; b) J. McNulty, K. Keskar, *Eur. J. Org. Chem.* **2012**, *2012*, 5462-5470.

[7] X. Bei, H. W. Turner, W. H. Weinberg, A. S. Guram, J. L. Petersen, *The Journal of Organic Chemistry* **1999**, *64*, 6797-6803.

[8] C. Kling, D. Leusser, T. Stey, D. Stalke, *Organometallics* **2011**, *30*, 2461-2463.

[9] C. Santelli-Rouvier, C. Coin, L. Toupet, M. Santelli, *J. Organomet. Chem.* **1995**, *495*, 91-96.

[10] a) S. Trofimenko, *J. Am. Chem. Soc.* **1966**, *88*, 1842-1844; b) S. Trofimenko, *Prog. Inorg. Chem.* **1986**, *34*, 115; c) J. C. Calabrese, S. Trofimenko, J. S. Thompson, *J. Chem. Soc., Chem. Commun.* **1986**, 1122-1123.

[11] S. Trofimenko, *Chem. Rev.* **1993**, *93*, 943-980.

[12] a) C. Pettinari, F. Marchetti, S. Orbisaglia, J. Palmucci, R. Pettinari, C. Di Nicola, B. W. Skelton, A. H. White, *Eur. J. Inorg. Chem.* **2014**, 546-558; b) S. Liang, M. P. Jensen, *Organometallics* **2012**, *31*, 8055-8058; c) B. E. Frauhiger, P. S. White, J. L. Templeton, *Organometallics* **2011**, *31*, 225-237; d) N. Tsoureas, A. Hamilton, M. F. Haddow, J. N. Harvey, A. G. Orpen, G. R. Owen, *Organometallics* **2013**, *32*, 2840-2856; e) Á. Beltrán, C. Lescot, M. Mar Díaz-Requejo, P. J. Pérez, P. Dauban, *Tetrahedron* **2013**, *69*, 4488-4492; f) A. Kunishita, T. L. Gianetti, J. Arnold, *Organometallics* **2011**, *31*, 372-380; g) A. Otero, J. Fernández-Baeza, L. F. Sánchez-Barba, J. Tejeda, M. Honrado, A. Garcés, A. Lara-Sánchez, A. M. Rodríguez, *Organometallics* **2012**, *31*, 4191-4202; h) M. Kumar, J. DePasquale, N. J. White, M. Zeller, E. T. Papish, *Organometallics* **2013**, *32*, 2135-2144; i) M. Imran, B. Neumann, H.-G. Stammler, U. Monkowius, M. Ertl, N. W. Mitzel, *Dalton Trans.* **2013**, *42*, 15785-15795; j) G. R. Owen, P. H. Gould, A. Moore, G. Dyson, M. F. Haddow, A. Hamilton, *Dalton Trans.* **2013**, *42*, 11074-11081; k) P. O. Shipman, C. Cui, P. Lupinska, R. A. Lalancette, J. B. Sheridan, F. Jäkle, *ACS Macro Letters* **2013**, *2*, 1056-1060; l) N. Xing, H. Shan, X. Tian, Q. Yao, L.-T. Xu, Y.-H. Xing, Z. Shi, *Dalton Trans.* **2013**, *42*, 359-363; m) J. Krzystek, D. C. Swenson, S. A. Zvyagin, D. Smirnov, A. Ozarowski, J. Telser, *J. Am. Chem. Soc.* **2010**, *132*, 5241-5253; n) R. Wanke, M. F. t. C. Guedes da Silva, S. Lancianesi, T. F. S. Silva, L. s. M. D. R. S. Martins, C. Pettinari, A. J. L. Pombeiro, *Inorg. Chem.* **2010**, *49*, 7941-7952; o) E. V. Mutseneck, S. Bieller, M. Bolte, H.-W. Lerner, M. Wagner, *Inorg. Chem.* **2010**, *49*, 3540-3552; p) N. Tsoureas, J. Nunn, T. Bevis, M. F. Haddow, A. Hamilton, G. R. Owen, *Dalton Trans.* **2011**, *40*, 951-958; q) M. N. McCain, S. Schneider, M. R. Salata, T. J. Marks, *Inorg. Chem.* **2008**, *47*, 2534-2542; r) K. Ruth, S. Tüllmann, H. Vitze, M. Bolte, H.-W. Lerner, M. C. Holthausen, M. Wagner, *Chem. Eur. J.* **2008**, *14*, 6754-6770; s) J. A. Camerano, M. A. Casado, M. A. Ciriano, C. Tejel, L. A. Oro, *Chem. Eur. J.* **2008**, *14*, 1897-1905; t) D. L. Reger, J. R. Gardinier, W. R. Gemmill, M. D. Smith, A. M. Shahin, G. J. Long, L. Rebbouh, F. Grandjean, *J. Am. Chem. Soc.* **2005**, *127*, 2303-2316; u) C. Pettinari, R. Pettinari, *Coord. Chem. Rev.* **2005**, *249*, 525-543; v) P. Braunstein, F. Naud, *Angew. Chem. Int. Ed.* **2001**, *40*, 680-699; w) F. T. Edelmann, *Angew. Chem. Int. Ed.* **2001**, *40*, 1656-1660.

[13] a) M. M. Meinholz, S. K. Pandey, S. M. Deuerlein, D. Stalke, *Dalton Trans.* **2011**, *40*, 1662-1671; b) M. M. Meinholz, M. Klemmer, E. Kriemen, D. Stalke, *Chem. Eur. J.* **2011**, *17*, 9415-9422; c) M. M. Meinholz, D. Stalke, *Z. Naturforsch., B: Chem. Sci.* **2011**, *66b*, 981-984; d) M. M. Meinholz, D. Stalke, *Z. Anorg. Allg. Chem.* **2011**, *637*, 2233-2238; e) J. T. E. Meyer, T. Schulz, S. K. Pandey, D. Stalke, *Inorg. Chem.* **2010**, *49*, 2743-2749.

[14] M. M. Meinholz, D. Stalke, *Eur. J. Inorg. Chem.* **2011**, 4578–4584.

[15] a) J. K. Brask, T. Chivers, *Angew. Chem. Int. Ed.* **2001**, *40*, 3960-3976; b) G. M. Aspinall, M. C. Copsey, A. P. Leedham, C. R. Russell, *Coord. Chem. Rev.* **2002**, *227*, 217-232; c) R. Fleischer, D. Stalke, *Coord. Chem. Rev.* **1998**, *176*, 431-450; d) A. Armstrong, T. Chivers, M. Parvez, G. Schatte, R. T. Boeré, *Inorg. Chem.* **2004**, *43*, 3453-3460; e) J. F. Bickley, M. C. Copsey, J. C. Jeffery, A. P. Leedham, C. A. Russell, D. Stalke, A. Steiner, T. Stey, S. Zacchini, *Dalton Trans.* **2004**, 989-995.

[16] a) P. R. Raithby, C. A. Russell, A. Steiner, D. S. Wright, *Angew. Chem. Int. Ed.* **1997**, *36*, 649-650; b) P. J. Bailey, A. J. Blake, M. Kryszczuk, S. Parsons, D. Reed, *J. Chem. Soc., Chem. Commun.* **1995**, 1647-1648; c) M. A. Beswick, S. J. Kidd, M. A. Paver, P. R. Raithby, A. Steiner, D. S. Wright, *Inorg. Chem. Commun.* **1999**, *2*, 612-614; d) L. T. Burke, J. C. Jeffery, A. P. Leedham, C. A. Russell, *J. Chem. Soc., Dalton Trans.* **2001**, 423-426.

[17] T. Chivers, M. Parvez, G. Schatte, *J. Organomet. Chem.* **1998**, *550*, 213-220.

[18] R. Fleischer, A. Rothenberger, D. Stalke, *Angew. Chem. Int. Ed.* **1997**, *36*, 1105-1107.

[19] T. Chivers, X. Gao, M. Parvez, *J. Am. Chem. Soc.* **1995**, *117*, 2359-2360.

[20] D. Stalke, *Chem. Commun.* **2012**, *48*, 9559-9573.

[21] a) W. Kutzelnigg, *Angew. Chem. Int. Ed.* **1984**, *23*, 272-295; b) A. E. Reed, F. Weinhold, *J. Am. Chem. Soc.* **1986**, *108*, 3586-3593; c) D. A. Bors, A. Streitwieser, *J. Am. Chem. Soc.* **1986**, *108*, 1397-1404; d) A. E. Reed, P. v. R. Schleyer, *J. Am. Chem. Soc.* **1990**, *112*, 1434-1445; e) U. Salzner, P. v. R. Schleyer, *J. Am. Chem. Soc.* **1993**, *115*, 10231-10236; f) T. Stefan, R. Janoschek, *J Mol Model* **2000**, *6*, 282-288.

[22] M. S. Schmøkel, S. Cenedese, J. Overgaard, M. R. V. Jørgensen, Y.-S. Chen, C. Gatti, D. Stalke, B. B. Iversen, *Inorg. Chem.* **2012**, *51*, 8607-8616.

[23] M. M. Labes, P. Love, L. F. Nichols, *Chem. Rev.* **1979**, *79*, 1-15.

[24] M. Goehring, G. Weis, *Angew. Chem.* **1956**, *68*, 678-678.

[25] a) O. Glemser, J. Wegener, *Angew. Chem. Int. Ed.* **1970**, *9*, 309-309; b) O. Glemser, S. Pohl, F.-M. Tesky, R. Mews, *Angew. Chem. Int. Ed.* **1977**, *16*, 789-790.

[26] W. Lidy, W. Sundermeyer, W. Verbeek, *Z. Anorg. Allg. Chem.* **1974**, *406*, 228-234.

[27] R. Mews, P. G. Watson, E. Lork, *Coord. Chem. Rev.* **1997**, *158*, 233-273.

[28] R. Fleischer, S. Freitag, D. Stalke, *Dalton Trans.* **1998**, 193-197.

[29] a) B. Walfort, A. P. Leedham, C. R. Russell, D. Stalke, *Inorg. Chem.* **2001**, *40*, 5668-5674; b) C. Selinka, D. Stalke, *Eur. J. Inorg. Chem.* **2003**, 3376-3382.

[30] a) D. Leusser, J. Henn, N. Kocher, B. Engels, D. Stalke, *J. Am. Chem. Soc.* **2004**, *126*, 1781-1793; b) J. Henn, D. Ilge, D. Leusser, D. Stalke, B. Engels, *J. Phys. Chem.* **2004**, *A108*, 9442-9452.

[31] a) T. Schulz, D. Stalke, *Eur. J. Inorg. Chem.* **2010**, 2185-2192; b) T. Schulz, S. Deuerlein, D. Stalke, *Eur. J. Inorg. Chem.* **2010**, 2178-2184.

[32] a) L. T. Byrne, L. M. Engelhardt, G. E. Jacobsen, W.-P. Leung, R. I. Papasergio, C. L. Raston, B. W. Skelton, P. Twiss, A. H. White, *J. Chem. Soc., Dalton Trans.* **1989**, 105-113; b) L. M. Engelhardt, G. E. Jacobsen, C. L. Raston, A. H. White, *J. Chem. Soc., Chem. Commun.* **1984**, 220-222; c) S. Deuerlein, Georg-August-Universität (Göttingen), **2007**.

[33] E. Carl, Georg-August-Universität (Göttingen), **2010**.

[34] a) R. Fleischer, D. Stalke, *Organometallics* **1998**, *17*, 832-838; b) D. Hänssgen, R. Steffens, *Z. Anorg. Allg. Chem.* **1983**, *507*, 178-182.

[35] R. Fleischer, B. Walfort, A. Gbureck, P. Scholz, W. Kiefer, D. Stalke, *Chem. Eur. J.* **1998**, *4*, 2266-2274.

[36] P. Rademacher, *Strukturen organischer Moleküle*, VCH, New York, **1987**.

[37] Cambridge Structural Database, release 5.34, **2012**.

[38] a) C. A. Nijhuis, E. Jellema, T. J. J. Sciarone, A. Meetsma, P. H. M. Budzelaar, B. Hessen, *Eur. J. Inorg. Chem.* **2005**, *2005*, 2089-2099; b) D. N. Woodruff, E. J. L. McInnes, D. O. Sells, R. E. P. Winpenny, R. A. Layfield, *Inorg. Chem.* **2012**, *51*, 9104-9109; c) C. Koch, A. Malassa, C. Agthe, H. Görls, R. Biedermann, H. Krautscheid, M. Westerhausen, *Z. Anorg. Allg. Chem.* **2007**, *633*, 375-382.

[39] a) A. Grirrane, A. Pastor, A. Galindo, E. Álvarez, C. Mealli, A. Ienco, A. Orlandini, P. Rosa, A. Caneschi, A.-L. Barra, J. F. Sanz, *Chem. Eur. J.* **2011**, *17*, 10600-10617; b) J. Zhang, S. Gao, X.-X. Zhang, Z.-M. Wang, C.-M. Che, *Dalton Trans.* **2012**, *41*, 2626-2631.

[40] a) B. Vendemiati, G. Prini, A. Meetsma, B. Hessen, Jan H. Teuben, O. Traverso, *Eur. J. Inorg. Chem.* **2001**, *2001*, 707-711; b) R. E. Cowley, J. r. m. Elhaïk, N. A. Eckert, W. W. Brennessel, E. Bill, P. L. Holland, *J. Am. Chem. Soc.* **2008**, *130*, 6074-6075; c) N. Muresan, C. C. Lu, M. Ghosh, J. C. Peters, M. Abe, L. M. Henling, T. Weyhermöller, E. Bill, K. Wieghardt, *Inorg. Chem.* **2008**, *47*, 4579-4590; d) B. M. Wile, R. J. Trovitch, S. C. Bart, A. M. Tondreau, E. Lobkovsky, C. Milsmann, E. Bill, K. Wieghardt, P. J. Chirik, *Inorg. Chem.* **2008**, *48*, 4190-4200.

[41] P. R. Edwards, C. E. Johnson, R. J. P. Williams, *J. Chem. Phys.* **1967**, *47*, 2074-2082.

[42] H. Andres, E. L. Bominaar, J. M. Smith, N. A. Eckert, P. L. Holland, E. Münck, *J. Am. Chem. Soc.* **2002**, *124*, 3012-3025.

[43] M. T. Mock, C. V. Popescu, G. P. A. Yap, W. G. Dougherty, C. G. Riordan, *Inorg. Chem.* **2008**, *47*, 1889-1891.

[44] M. P. Hendrich, W. Gunderson, R. K. Behan, M. T. Green, M. P. Mehn, T. A. Betley, C. C. Lu, J. C. Peters, *Proc. Natl. Acad. Sci. U.S.A.* **2006**, 17107–17112.

[45] a) S. Meyer, C. M. Orben, S. Demeshko, S. Dechert, F. Meyer, *Organometallics* **2011**, *30*, 6692-6702; b) H. Beinert, R. H. Holm, E. Munck, *Science* **1997**, *277*, 653–659.

[46] a) S. Chandra, K. B. Pandeya, G. L. Sawhney, J. S. Baijal, *Chem. Phys. Lett.* **1979**, *61*, 109-110; b) D. J. Evans, *Chem. Phys. Lett.* **1996**, *255*, 134-136.

[47] a) J. P. Fackler, T. Moyer, J. A. Costamagna, R. Latorre, J. Granifo, *Inorg. Chem.* **1987**, *26*, 836-841; b) S. Sproules, K. Wieghardt, *Coord. Chem. Rev.* **2010**, *254*, 1358-1382; c) S. Meyer, S. Demeshko, S. Dechert, F. Meyer, *Inorg. Chim. Acta* **2010**, *363*, 3088-3092.

[48] a) E. J. Hawrelak, W. H. Bernskoetter, E. Lobkovsky, G. T. Yee, E. Bill, P. J. Chirik, *Inorg. Chem.* **2005**, *44*, 3103-3111; b) J. Silver, B. Lukas, G. Al-Jaff, *Inorg. Chim. Acta* **1984**, *91*, 125-128; c) B. W. Fitzsimmons, C. E. Johnson, *Chem. Phys. Lett.* **1974**, *24*, 422-424; d) B. A. Shaevitz, G. Lang, C. A. Reed, *Inorg. Chem.* **1988**, *27*, 4607-4613; e) D. V. Naik, G. J. Palenik, *Chem. Phys. Lett.* **1974**, *24*, 260-262; f) E. König, G. Ritter, E. Lindner, I. P. Lorenz, *Chem. Phys. Lett.* **1972**, *13*, 70-72.

[49] C. Selinka, S. Deuerlein, T. Häuser, D. Stalke, *Inorg. Chim. Acta* **2004**, *357*, 1873-1880.

[50] a) G. W. Everett, R. H. Holm, *J. Am. Chem. Soc.* **1966**, *88*, 2442-2451; b) G. W. Everett, R. H. Holm, *Inorg. Chem.* **1968**, *7*, 776-785; c) S. A. Carabineiro, L. C. Silva, P. T. Gomes, L. C. J. Pereira, L. F. Veiros, S. I. Pascu, M. T. Duarte, S. Namorado, R. T. Henriques, *Inorg. Chem.* **2007**, *46*, 6880-6890.

[51] R. D. Jones, D. A. Summerville, F. Basolo, *Chem. Rev.* **1979**, *79*, 139-179.

[52] a) J. A. Wolny, M. F. Rudolf, Z. Ciunik, K. Gatner, S. Wolowiec, *J. Chem. Soc., Dalton Trans.* **1993**, 1611-1622; b) F. A. Cotton, G. Wilkinson, C. A. Murillo, M. Bochmann, in *Advanced inorganic chemistry, Vol. 6*, John Wiley & Sons, Inc., New York, **1999**; c) B. S. Jaynes, L. H. Doerrer, S. Liu, S. J. Lippard, *Inorg. Chem.* **1995**, *34*, 5735-5744; d) D. M. Jenkins, A. J. Di Bilio, M. J. Allen, T. A. Betley, J. C. Peters, *J. Am. Chem. Soc.* **2002**, *124*, 15336-15350.

[53] K. Chłopek, E. Bothe, F. Neese, T. Weyhermüller, K. Wieghardt, *Inorg. Chem.* **2006**, *45*, 6298-6307.

[54] M. M. Meinholz, Georg-August-Universität (Göttingen), **2011**.

[55] a) S. S. Al-Juaid, C. Eaborn, P. B. Hitchcock, M. S. Hill, J. D. Smith, *Organometallics* **2000**, *19*, 3224-3231; b) A. Asadi, C. Eaborn, M. S. Hill, P. B. Hitchcock, J. D. Smith, *J. Organomet. Chem.* **2005**, *690*, 944-951; c) H. Link, D. Fenske, *Z. Anorg. Allg. Chem.* **1999**, *625*, 1878-1884; d) S. Dehnen, C. Zimmermann, *Chem. Eur. J.* **2000**, *6*, 2256-2261; e) D. Zhang, Q. Yue, J. Wang, G. Shigeng, L. Weng, *Inorg. Chem. Commun.* **2009**, *12*, 1193-1196; f) P. L. Holland, T. R. Cundari, L. L. Perez, N. A. Eckert, R. J. Lachicotte, *J. Am. Chem. Soc.* **2002**, *124*, 14416-14424; g) Z. Moatazedi, M. J. Katz, D. B. Leznoff, *Dalton Trans.* **2010**, *39*, 9889-9896; h) K. J. Weese, R. A. Bartlett, B. D. Murray, M. M. Olmstead, P. R. Power, *Inorg. Chem.* **1987**, *26*, 2409-2413; i) A. Panda, M. Stender, R. J. Wright, M. M. Olmstead, P. Klavins, P. P. Power, *Inorg. Chem.* **2002**, *41*, 3909-3916; j) A. D. Sutton, T. Ngyuen, J. C. Fettinger, M. M. Olmstead, G. J. Long, P. P. Power, *Inorg. Chem.* **2007**, *46*, 4809-4814.

[56] K. W. Henderson, A. R. Kennedy, W. J. Kerr, P. H. Moran, *Acta Crystallogr. Sect. C* **1999**, *55*.

[57] a) J. M. Zadrozny, J. Liu, N. A. Piro, C. J. Chang, S. Hill, J. R. Long, *Chem. Commun.* **2012**, *48*, 3927-3929; b) W. Huang, T. Liu, D. Wu, J. Cheng, Z. W. Ouyang, C. Duan, *Dalton Trans.* **2013**, *42*, 15326-15331.

[58] a) J. M. Zadrozny, J. R. Long, *J. Am. Chem. Soc.* **2011**, *133*, 20732-20734; b) Y.-Y. Zhu, C. Cui, Y.-Q. Zhang, J.-H. Jia, X. Guo, C. Gao, K. Qian, S.-D. Jiang, B.-W. Wang, Z.-M. Wang, S. Gao, *Chemical Science* **2013**, *4*, 1802-1806.

[59] R. A. Layfield, *Organometallics* **2014**, *33*, 1084-1099.

[60] a) R. Boese, M. Düppmann, W. Kuchen, W. Peters, *Z. Anorg. Allg. Chem.* **1998**, *624*, 837-845; b) M. M. Khusniyarov , E. Bill, T. Weyhermüller, E. Bothe, K. Wieghardt, *Angew. Chem. Int. Ed.* **2011**, *50*, 1652-1655; c) Y. Matano, T. Shibano, H. Nakano, H. Imahori, *Chem. Eur. J.* **2012**, *18*, 6208-6216.

[61] J. Chen, J. Li, *Acta Crystallogr. Sect. E* **2012**, *68*, m357.

[62] a) M. Vázquez, Manuel R. Bermejo, M. Fondo, A. García-Deibe, Ana M. González, R. Pedrido, *Eur. J. Inorg. Chem.* **2002**, *2002*, 465-472; b) D. J. White, L. Cronin, S. Parsons, N. Robertson, P. A. Tasker, A. P. Bisson, *Chem. Commun.* **1999**, 1107-1108.

[63] a) R. Ahuja, M. Nethaji, A. G. Samuelson, *Inorg. Chim. Acta* **2011**, *372*, 220-226; b) B. Nohra, E. Rodriguez-Sanz, C. Lescop, R. Réau, *Chem. Eur. J.* **2008**, *14*, 3391-3403.

[64] a) A. M. Willcocks, T. P. Robinson, C. Roche, T. Pugh, S. P. Richards, A. J. Kingsley, J. P. Lowe, A. L. Johnson, *Inorg. Chem.* **2011**, *51*, 246-257; b) G. M. Chiarella, D. Y. Melgarejo, A. Rozanski, P. Hempte, L. M. Perez, C. Reber, J. P. Fackler Jr, *Chem. Commun.* **2010**, *46*, 136-138; c) A. Heine, D. Stalke, *Angew. Chem. Int. Ed.* **1993**, *32*, 121-122; d) P. Pyykkö, *Chem. Rev.* **1997**, *97*, 597-636.

[65] a) N. Schneider, V. César, S. Bellemin-Laponnaz, L. H. Gade, *J. Organomet. Chem.* **2005**, *690*, 5556-5561; b) F. A. Cotton, X. Feng, D. J. Timmons, *Inorg. Chem.* **1998**, *37*, 4066-4069.

[66] J. Cirera, P. Alemany, S. Alvarez, *Chem. Eur. J.* **2004**, *10*, 190-207.

[67] O. I. Guzyr, L. N. Markovskii, M. I. Povolotskii, H. W. Roesky, A. N. Chernega, E. B. Rusanov, *J. Mol. Struct.* **2006**, *788*, 89-92.

[68] A. Haaland, K. Hedberg, P. P. Power, *Inorg. Chem.* **1984**, *23*, 1972-1975.

[69] a) A. Haaland, *Angew. Chem. Int. Ed.* **1989**, *28*, 992-1007; b) S. Wingerter, H. Gornitzka, G. Bertrand, D. Stalke, *Eur. J. Inorg. Chem.* **1999**, *1999*, 173-178.

[70] M. Irwin, L. R. Doyle, T. Krämer, R. Herchel, J. E. McGrady, J. M. Goicoechea, *Inorg. Chem.* **2012**, *51*, 12301-12312.

[71] a) H. A. Jahn, E. Teller, *Proc. R. Soc. London, Ser. A.* **1937**, *161*, 220-235; b) M. A. Hitchman, *Comments Inorg. Chem.* **1994**, *15*, 197-254.

[72] a) M. A. Halcrow, *Chem. Soc. Rev.* **2013**, *42*, 1784-1795; b) M. Atanasov, B. Delley, D. Reinen, *Z. Anorg. Allg. Chem.* **2010**, *636*, 1740-1750.

[73] a) D. Devarajan, T. B. Gunnoe, D. H. Ess, *Inorg. Chem.* **2012**, *51*, 6710-6718; b) G. W. Roffe, H. Cox, *J. Phys. Chem. A* **2013**, *117*, 3017-3024.

[74] a) R. D. Shannon, C. T. Prewitt, *Acta Crystallogr. Sect. B* **1969**, *B25*, 925-946; b) R. D. Shannon, *Acta Crystallogr. Sect. A* **1976**, *A 32*, 751-767; c) A. F. Hollemann, N. Wiberg, *Lehrbuch der Anorganischen Chemie*, 102. ed., Walter de Gruyter, Berlin, **2007**.

[75] a) R. Fleischer, D. Stalke, *J. Organomet. Chem.* **1998**, *550*, 173-182; b) R. Fleischer, D. Stalke, *Inorg. Chem.* **1997**, *36*, 2413-2419; c) M. Westerhausen, W. Schwarz, *Z. Anorg. Allg. Chem.* **1993**, *619*, 1455-1461; d) M. Westerhausen, H. D. Hausen, W. Schwarz, *Z. Anorg. Allg. Chem.* **1992**, *618*, 121-130.

[76] W.-Y. Lee, L.-C. Liang, *Dalton Trans.* **2005**, 1952-1956.

[77] N. E. Mansfield, M. P. Coles, P. B. Hitchcock, *Dalton Trans.* **2005**, 2833-2841.

[78] S. Singh, H.-J. Ahn, A. Stasch, V. Jancik, H. W. Roesky, A. Pal, M. Biadene, R. Herbst-Irmer, M. Noltemeyer, H.-G. Schmidt, *Inorg. Chem.* **2006**, *45*, 1853-1860.

[79] a) C. Jones, *Coord. Chem. Rev.* **2010**, *254*, 1273-1289; b) Y. Ding, H. W. Roesky, M. Noltemeyer, H.-G. Schmidt, P. P. Power, *Organometallics* **2001**, *20*, 1190-1194; c) S. Nagendran, H. W. Roesky, *Organometallics* **2008**, *27*, 457-492.

[80] a) C. Jones, R. P. Rose, A. Stasch, *Dalton Trans.* **2008**, 2871-2878; b) S. P. Green, C. Jones, P. C. Junk, K.-A. Lippert, A. Stasch, *Chem. Commun.* **2006**, 3978-3980.

[81] W. D. Woodul, E. Carter, R. Müller, A. F. Richards, A. Stasch, M. Kaupp, D. M. Murphy, M. Driess, C. Jones, *J. Am. Chem. Soc.* **2011**, *133*, 10074-10077.

[82] A. E. Ayers, T. M. Klapötke, H. V. R. Dias, *Inorg. Chem.* **2001**, *40*, 1000-1005.

[83] S. S. Sen, M. P. Kritzler-Kosch, S. Nagendran, H. W. Roesky, T. Beck, A. Pal, R. Herbst-Irmer, *Eur. J. Inorg. Chem.* **2010**, *2010*, 5304-5311.

[84] a) S. Sinhababu, R. K. Siwatch, G. Mukherjee, G. Rajaraman, S. Nagendran, *Inorg. Chem.* **2012**, *51*, 9240-9248; b) Y. Ding, Q. Ma, I. Usón, H. W. Roesky, M. Noltemeyer, H.-G. Schmidt, *J. Am. Chem. Soc.* **2002**, *124*, 8542-8543; c) Y. Ding, Q. Ma, H. W. Roesky, I. Uson, M. Noltemeyer, H.-G. Schmidt, *Dalton Trans.* **2003**, 1094-1098.

[85] L. W. Pineda, V. Jancik, K. Starke, R. B. Oswald, H. W. Roesky, *Angew. Chem. Int. Ed.* **2006**, *45*, 2602-2605.

[86] a) N. D. Reddy, A. Jana, H. W. Roesky, P. P. Samuel, C. Schulzke, *Dalton Trans.* **2010**, *39*, 234-238; b) I. Saur, K. Miqueu, G. Rima, J. Barrau, V. Lemierre, A. Chrostowska, J.-M. Sotiropoulos, G. Pfister-Guillouzo, *Organometallics* **2003**, *22*, 3143-3149.

[87] a) T. Chlupaty, Z. Padelkova, A. Lycka, J. Brus, A. Ruzicka, *Dalton Trans.* **2012**, *41*, 5010-5019; b) D. Matioszek, N. Katir, N. Saffon, A. Castel, *Organometallics* **2010**, *29*, 3039-3046.

[88] P. B. Hitchcock, J. Hu, M. F. Lappert, J. R. Severn, *Dalton Trans.* **2004**, 4193-4201.

[89] A. Jana, G. Schwab, H. W. Roesky, D. Stalke, *Inorg. Chim. Acta* **2010**, *363*, 4408-4410.

[90] a) Y.-R. Zhong, M.-L. Cao, H.-J. Mo, B.-H. Ye, *Cryst. Growth Des.* **2008**, *8*, 2282-2290; b) V. Hathwar, S. M. Roopan, R. Subashini, F. N. Khan, T. N. Guru Row, *J. Chem. Sci.* **2010**, *122*, 677-685.

[91] a) F. Basuli, U. J. Kilgore, D. Brown, J. C. Huffman, D. J. Mindiola, *Organometallics* **2004**, *23*, 6166-6175; b) F. Bonnet, M. Visseaux, D. Barbier-Baudry, E. Vigier, M. M. Kubicki, *Chem. Eur. J.* **2004**, *10*, 2428-2434; c) L. Kakaliou, Scanlon, B. Qian, S. W. Baek, M. R. Smith, D. H. Motry, *Inorg. Chem.* **1999**, *38*, 5964-5977; d) P. B. Hitchcock, M. F. Lappert, D.-S. Liu, *J. Chem. Soc., Chem. Commun.* **1994**, 2637-2638; e) M. Rahim, N. J. Taylor, S. Xin, S. Collins, *Organometallics* **1998**, *17*, 1315-1323.

[92] M. Chen, J. R. Fulton, P. B. Hitchcock, N. C. Johnstone, M. F. Lappert, A. V. Protchenko, *Dalton Trans.* **2007**, 2770-2778.

[93] a) P. Braunstein, C. Graiff, F. Naud, A. Pfaltz, A. Tiripicchio, *Inorg. Chem.* **2000**, *39*, 4468-4475; b) L. Dahlenburg, C. Kühnlein, *J. Organomet. Chem.* **2005**, *690*, 1-13; c) M. S. Rahman, P. D. Prince, J. W. Steed, K. K. Hii, *Organometallics* **2002**, *21*, 4927-4933; d) H. Yang, M. Alvarez-Gressier, N. Lugan, R. Mathieu, *Organometallics* **1997**, *16*, 1401-1409; e) A. Bacchi, M. Balordi, R. Cammi, L. Elviri, C. Pelizzi, F. Picchioni, V. Verdolino, K. Goubitz, R. Peschar, P. Pelagatti, *Eur. J. Inorg. Chem.* **2008**, *2008*, 4462-4473; f) C. Slugovc, D. Doberer, C. Gemel, R. Schmid, K. Kirchner, B. Winkler, F. Stelzer, *Monatsh. Chem.* **1998**, *129*, 221-233.

[94] a) J. Li, L. Ackermann, *Tetrahedron* **2014**, *70*, 3342-3348; b) V. S. Thirunavukkarasu, S. I. Kozhushkov, L. Ackermann, *Chem. Commun.* **2014**, *50*, 29-39; c) M. Delgado-Rebollo, D. Canseco-Gonzalez, M. Hollering, H. Mueller-Bunz, M. Albrecht, *Dalton Trans.* **2014**, *43*, 4462-4473; d) P. S. Aparna, B. Prabha, P. Prakash, E. Jijy, R. Luxmi Varma, K. V. Radhakrishnan, *Tetrahedron Lett.* **2014**, *55*, 865-868; e) A. B. Chaplin, P. J. Dyson, *Organometallics* **2007**, *26*, 2447-2455; f) S. Gladiali, E. Alberico, *Chem. Soc. Rev.* **2006**, *35*, 226-236.

[95] M. A. Bennett, G. B. Robertson, A. K. Smith, *J. Organomet. Chem.* **1972**, *43*, C41-C43.

[96] a) R. García-Álvarez, S. E. García-Garrido, J. Díez, P. Crochet, V. Cadierno, *Eur. J. Inorg. Chem.* **2012**, *2012*, 4218-4230; b) D. Arquier, L. Vendier, K. Miqueu, J.-M. Sotiropoulos, S. Bastin, A. Igau, *Organometallics* **2009**, *28*, 4945-4957; c) K. Junge, B. Wendt, F. A. Westerhaus, A. Spannenberg, H. Jiao, M. Beller, *Chem. Eur. J.* **2012**, *18*, 9011-9018; d) L. J. Hounjet, M. Bierenstiel, M. J. Ferguson, R. McDonald, M. Cowie, *Inorg. Chem.* **2010**, *49*, 4288-4300.

[97] a) W. Schlenk, A. Thal, *Ber. Dtsch. Chem. Ges.* **1913**, *46*, 2840-2854; b) W. Schlenk, J. Holtz, *Ber. Dtsch. Chem. Ges.* **1917**, *50*, 262-274; c) W. Schlenk, in *Die Methoden der Organischen Chemie*, 2. Aufl. ed. (Ed.: J. Houben), G. Thieme, Leipzig, **1924**, p. 720; d) T. T. Tidwell, *Angew. Chem. Int. Ed.* **2001**, *40*, 331-337.

[98] E. Bill, in *Mfit*, Max-Planck Institute for Chemical Energy Conversion, Mülheim/Ruhr, Germany.

[99] a) T. Kottke, D. Stalke, *J. Appl. Crystallogr.* **1993**, *26*, 615-619; b) T. Kottke, D. Stalke, *Angew. Chem. Int. Ed.* **1993**, *32*, 580-582.

[100] T. Schulz, K. Meindl, D. Leusser, D. Stern, J. Graf, C. Michaelsen, M. Ruf, G. M. Sheldrick, D. Stalke, *J. Appl. Crystallogr.* **2009**, *42*, 885-891.

[101] COSMO, Bruker-AXS, Madison (WI), USA, **2011**.

[102] a) in *Bruker AXS Inst. Inc.*, Madison (WI), USA, **2012**; b) in *SAINT, v7.68A*, Bruker AXS, Madison (WI), USA, **2009**.

[103] G. M. Sheldrick, *SADABS-2012/1,* Göttingen, **2012**.

[104] G. M. Sheldrick, *TWINABS-2012/1*, Göttingen, **2012**.

[105] G. M. Sheldrick, *XPREP 2013/1*, Madison (WI), USA **2013**.

[106] G. M. Sheldrick, *Acta Crystallogr. Sect. A* **1990**, *46*, 467-473.

[107] G. M. Sheldrick, *Acta Crystallogr. Sect. A* **2008**, *64*, 112-122.

[108] C. B. Hübschle, G. M. Sheldrick, B. Dittrich, *J. Appl. Crystallogr.* **2011**, *44*, 1281-1284.

[109] G. M. Sheldrick, XP in SHELXTL v2008/2 ed., Madison (WI), USA, **2008**.

[110] P. Müller, R. Herbst-Irmer, A. L. Spek, T. R. Schneider, M. R. Sawaya, *Crystal Structure Refinement - A Crystallographer's Guide to SHELXL Vol. 8*, Oxford University Press, Oxford (England), **2006**.

[111] a) H. Flack, *Acta Crystallogr. Sect. A* **1983**, *39*, 876-881; b) H. D. Flack, G. Bernardinelli, *J. Appl. Crystallogr.* **2000**, *33*, 1143-1148.